La collana della Scuola di Alta Formazione Dottorale accoglie le migliori tesi di dottorato dell'Università degli Studi di Bergamo, insignite della dignità di stampa e sottoposte a procedura di *blind peer review*.

Electroconductive and stimuli-responsive coatings were synthesized for developing wearable smart textiles. Carbon nanotubes-based electroconductive cotton fabrics were efficient in environmental monitoring and electrical signals transmission for heart rate monitoring by photoplethysmography. Stimuli-responsive fabrics for sweat pH monitoring were realized using nitrazine yellow and alizarin red S. The results confirmed the dyestuffs immobilization on fabrics, by preserving the typical halochromic response, and that grafting or sol-gel techniques were efficient in reducing dye leaching after laundering cycles. Furthermore, sol-gel was also suitable for designing hybrid networks for controlled drug release, thus ensuring biocompatibility, drug reservoir and release of the encapsulated antioxidant molecule under the action of cutaneous stimuli. Two prototypes were developed to highlight the multidisciplinarity in smart technologies resulting in the integration of electronic devices with fabrics to realize intelligent textiles.

Valentina Trovato was awarded her Master's degree in "Chemistry" in 2013 from the University of Messina (IT). Between 2014 and 2015, she won a scholarship for "Nanomaterials and nanotechnologies for sustainable development and the cultural heritage" at the ISMN-CNR (IT), where she studied carbon nanotubes functionalization and applications through polymer coatings on textiles. She received her Ph.D. degree in "Engineering and Applied Sciences" at the University of Bergamo (IT) in 2020. Since 2020 she is holding a post-doctoral position at the Department of Engineering and Applied Sciences of the University of Bergamo, working on the development of several national and international research projects focused on wearable smart materials. sensors.

ISBN: 978-88-97413-56-1
DOI: 10.13122/978-88-97413-56-1

Valentina Trovato WEARABLE SMART TEXTILES

37

Collana della Scuola di Alta Formazione Dottorale
- 37 -

Valentina Trovato

WEARABLE SMART TEXTILES
Development of Electroconductive and Stimuli-Responsive Coatings

UNIVERSITÀ DEGLI STUDI DI BERGAMO

2021

Collana della Scuola di Alta Formazione Dottorale

Diretta da Paolo Cesaretti

Ogni volume è sottoposto a *blind peer review*.

ISSN: 2611-9927

Sito web: https://aisberg.unibg.it/handle/10446/130100

Valentina Trovato

DESIGN AND DEVELOPMENT
of electroconductive and stimuli-responsive coatings for wearable smart textiles

Università degli Studi di Bergamo

2021

Design and development of electroconductive and stimuli-responsive coatings for wearable smart textiles / Valentina Trovato.
– Bergamo : Università degli Studi di Bergamo, 2021.
(Collana della Scuola di Alta Formazione Dottorale; 37)

ISBN: 978-88-97413-56-1
DOI: 10.13122/978-88-97413-56-1

Progetto grafico: Servizi Editoriali – Università degli Studi di Bergamo
© 2018 Università degli Studi di Bergamo
via Salvecchio, 19
24129 Bergamo
Cod. Fiscale 80004350163
P. IVA 01612800167

https://aisberg.unibg.it/handle/10446/200568

Acknowledgements

I wish to thank the University of Bergamo for having offered me the opportunity to participate in the doctoral program on Engineering and Applied Science coordinated by Prof. Valerio Re. I am grateful to Prof. Giuseppe Rosace for providing me the possibility to work in his laboratory in the research field of smart textiles, thus allowing me to improve my skills, also thanks to the multidisciplinary nature of the developed research work. Furthermore, I would like to thank him for his expert guidance and assistance in each aspect of the research study, precious advice, stimulating discussions, and confidence in me.

I wish to thank all those with which the research activities were developed, particularly Dr. Maria Rosaria Plutino (ISMN-CNR), for her support of my research activities through precious suggestions and interesting discussions that helped me to improve my skills.

I also extend my thanks to my colleagues, Dr. Claudio Colleoni, for the practical help he gave me and stimulating discussions, and Dr. Angela Castellano, for support and precious suggestions.

I wish to thank all those who helped me, without which, I could not have completed my research activity.

Finally, I would particularly thank the cornerstones of my life, my family and Giovanni. I am grateful to my family for their immeasurable support, to have always believed in me and to have given me motivations to overcome difficulties and believe in myself.

I wish to thank Giovanni, the joy of my life and my great strength, for his unlimited support, comprehension, to have motivated me and for the precious help and advice both in life and in work.

Table of contents

Introduction

This thesis is focused on the study and development of both electroconductive and stimuli-responsive coatings for the design of wearable textiles.

In recent years, textile-based polymers have aroused great interest in the scientific community fostering the growth of a new research field focused on the enhancement and innovation of such materials by promoting functionalities beyond their conventional use, of protection against atmospheric agents, fashion and social identity. Properties like wearability, flexibility, lightness and breathability, made textile materials interesting as substrates for a new generation of sensor materials, called smart, or intelligent, textiles. In this regard, several research studies have been conducted to define the optimized strategy to obtain technical textile polymers characterized by particular functions. Among them are water repellency, flame retardancy, UV protection, wear and abrasion resistance, controlled release, electroconductivity, antimicrobial and halochromic properties. On the other side, smart fabrics are able to sense environmental stimuli, respond, and adapt intelligently thanks to specific functionality integrated into the textile structure. Accordingly, smart wearable materials can be obtained for several application fields, such as medicine, health, sport, automotive and aerospace, among many.

In particular, electrically conductive textiles can mainly consist of conductive fibers, yarns, fabrics, and final products made from these materials. These smart textiles should ensure fibrous performances, durability, launderability, and reusability. The most common materials used for developing smart textiles are organic polymers like polyaniline (PANI), polypyrrole (PPy) and poly(*3,4*-ethylenedioxythiophene) (PEDOT) as one of the polythiophenes (PTh) derivatives. These organic polymers conduct electricity and combine the electrical properties of metals with the mechanical characteristics of plastics. Smart textiles based on conductive organic polymers have been widely used for the development of protecting clothing, flexible fabric keyboards, medical textiles and several kinds of sensors. Recently, carbon nanotubes have been largely studied in this research field because of their interesting chemical-physical properties, particularly electrical conductivity.

Stimuli-responsive polymers provide changes in their properties depending on environmental variations. Nowadays, several examples of stimuli-responsive polymers to be integrated into textiles for developing smart fabrics are available, such as thermal and pH-responsive hydrogels, thermal, light, and moisture responsive polymers. Such stimuli-responsive textiles provide several kinds of uses ranging from comfort to smart controlled drug release, color-change, wound monitoring and protection against serious environmental variations.

Several technologies are available to integrate the most common functionalities in textile structures without losing the mechanical properties of the fabrics themselves, such as comfort and wearability. Among these technologies, the chemical approach is the most used, consisting of surface modification of the textile polymers through stable bonds (both physical or covalent) between electrically conductive or stimuli-responsive coatings and the textile surface itself.

In this research, both sol-gel technology and grafting polymerization approaches were used to obtain electrically conductive and stimuli-responsive coatings for textile applications. Among the former coatings, smart textiles for i) detecting environmental humidity percentage and temperature, and ii) heart rate monitoring through photoplethysmography, have been realized. Accordingly, carbon nanotubes coatings were incorporated on textiles, providing variations in their electrical resistance depending on the variable mentioned above. Among the stimuli-responsive coatings, halochromic textiles have been developed aimed at the colorimetric detection of sweat pH variation to assess the health status of the human body. In addition, controlled-release fabrics have also been realized to control the release from textiles of an antioxidant, anti-inflammatory molecule under cutaneous stimuli.

The sol-gel and grafting technologies were specifically chosen for developing electroconductive and stimuli-responsive smart coatings. With the sol-gel approach, it is possible to obtain organic-inorganic hybrid thin films doped with carbon nanotubes, halochromic, or active molecules highly adhering to the cotton surfaces. Similarly, the grafting polymerization is efficient in the stable immobilization of halochromic dye on textile surfaces. Both electrically conductive and stimuli-responsive coatings were thoroughly investigated through chemical-physical characterization techniques to study the chemical composition, morphology, and sensing properties.

Thanks to the obtained results, two prototypes have been developed, “ELECT” and “Health Belt”. The former is a T-shirt realized by the deposition of CNT-electroconductive tracks integrated with an electronic device for the monitoring of heart rate rhythm through electrocardiogram. The latter is a belt realized through a halochromic textile integrated with an electronic device for the monitoring of sweat pH. The developed prototypes highlight the multidisciplinarity in smart technologies resulting in the integration of electronic devices with fabrics to realize intelligent textiles.

Future perspectives can be focused on improving the described technologies for the development of both electrically conductive and stimuli-responsive coatings for textile applications. These can be higher performing due to technological developments and discoveries, both in the realization of the coating and in the electronics sector. Moreover, the total integration of electronics in the textile structure is an important challenge for the optimization of smart fabrics together with the

improvement of scientific research aimed at greater practical applications of the developed prototypes in areas such as wound monitoring and healing or surgery.

Chapter 1. Smart textiles: state of the art, methods and applications

The history of clothing follows the development of textiles contextually with human history. Thus, clothing and textiles reflect the materials and technologies available in different civilizations at different times. Simultaneously, the type and quality of clothing as well as of used fibers within a society reveal social customs and culture.

The wearing of clothing is exclusively a human characteristic, even if it is not precisely known when populations started wearing clothes. However, it is sure that animal skins and vegetation were adapted as protection from rain and cold, mainly as humans migrated to new climates. Other interesting examples of textiles employment in humans' life are assigned to specific dresses for marking the social identity as for the aristocracy, church, social orientation, and realizing for developing the worldwide diffused market, the fashion. Nowadays instances of textiles use are greatly enhanced, overcoming their protection action. Such enhancement resulted from scientific progress, such as the advancement of electronics and nanotechnologies and the fascinating, unique properties of textiles. These interesting properties refer to mechanical strength, hardness, flexibility, breathability, biocompatibility (in textile polymers of natural origin), simplicity of processing and the possibility of being subjected to washing cycles. For these reasons, textiles polymers provide promising advantages compared to conventionally planar and bulk structures. Indeed, smart textiles can stably accommodate several kinds of deformations (e.g., twisting and bending) thanks to the fibers which are made of, and they are soft and close-fitting to any surface. These properties are critical for wearable and sensing applications, and they are challenging for the planar and bulky counterparts, which are losers in flexibility, comfort, and wearability. Further, the low-weight of smart textiles is an advantage for the integration of microelectronics, as well as breathability (as a consequence of the fibers assemblage creating voids) of fabrics is a relevant feature for wearability and comfort.

In this regard, textile polymers became the protagonist of a new generation of materials [1] because of their innovative ability to interact with the surrounding environment due to the integration with electronic devices, such as batteries, sensors, displays, and so on.

Recent developments in technological and scientific fields, such as nanotechnology, chemistry, computer science, engineering, electronics, and textile technology, allow progress in polymeric materials processing and engineering. Such progress was also enhanced by the request of both modern companies and society to obtain real-time information on health status and environmental pollution, thus leading to the development of an innovative and multidisciplinary field, the so-called smart textiles, also known as intelligent textiles and electronic textiles (E-Textiles) [2].

This kind of textiles materials can be categorized according to several definitions [3]. An exhaustive interpretation has been provided by L. Van Langenhove and C. Hertleer [4], who suggested that smart textiles are:

> "textiles that are able to sense stimuli from the environment, to react to them and adapt to them by integration of functionalities in the textile structure. The stimulus and response can have an electrical, thermal, chemical, magnetic or other origin".

The first scientific research on smart textiles has been launched in the medical and military field [5] and, more recently, in the sports field [6], health care [7], professional workwear and many others. Therefore, as physical substrates and like a source of information, the textile fabrics have been extensively studied. Several kinds of smart textiles [8] have been produced recently, such as sensors, energy harvesting devices, and antennas, to be integrated into garments to create flexible and wearable devices. In particular, scientific research aimed at integrating textile electrodes (but also sensors and actuators) into garments began at the end of the 20th century with the main objective of long-term monitoring or correcting specific physiological parameters related to human health's status in a non-invasive manner.

Today's smart textiles market is still growing thanks to the progress in the industrial and scientific fields that allows for manipulating textile materials at a nanometric level or incorporating microelectronic components in them. Compared to conventional bulk sensors, this innovative typology designed with textile polymers is undoubtedly more comfortable to be wear and easier to be integrated into garments.

The potentiality of smart textiles as wearable and intelligent technology for everyday life applications has made them one of the most interesting front-ends between biology and technology. The development of smart textiles is usually based on multidisciplinary research merging know-how coming from several scientific areas besides the textile one, such as medicine, biotechnology, electronics, and telecommunications. In this regard, the combination of computer technology and intelligent textiles paves the way for introducing a new type of functionality, such as the possibility for fabrics to perform computational operations [9]. Some iconic products of smart textiles are represented by electrocardiography T-shirts, electromyography pants, electroencephalogram caps, and many others. All these examples are based on collecting different types of inputs or stimuli (electrical, mechanical, acoustic, optical) and electrical responses. In particular, in healthcare, interactive electronic tissues have been developed to detect different parameters, such as blood pressure, time, distance, calories and movement in sportswear [10].

From the economic point of view, the ability of smart textiles to remotely monitoring various physiological and biochemical parameters could lead to advantages in terms of health costs thanks to

their use for the early diagnosis of many diseases. Furthermore, the monitoring of these parameters during sports activities (training or competition) could also be fundamental for athletes to obtain optimal performance.

In the following paragraphs, an overview concerning state of the art, the most relevant applications of smart textiles, their classifications, commonly technology available for their design, and future perspectives are examining.

1.1 Smart textiles: state of the art

It was 1989 when, for the first time, in Japan, smart materials were defined. But the birth of real smart materials was identified by the discovery of shape memory materials (the 1960s) and intelligent polymeric gels (the 1970s), while intelligent materials were introduced in textiles in the 1990s with a shape memory ancestor consisting of silk thread [11]. So, in the early 1990s, smart textiles made known their benefits, and in this regard, several examples of smart clothing (or smart garments) are available. They are clothes built (at least in part) with smart textiles consisting of knitted or woven fabrics with integrated specific functionality for sensing, processing and actuation (e.g., gestures, wearer's postures, vitals tracking). Among the first examples of smart clothing, the sensor jacket [12] deserves to be mentioned. This first smart clothing was able to measure the wearer's upper body posture through knitted stretch sensors placed over the joints. Following the interesting information provided by the monitoring of posture, a lot of research was conducted to integrate smart textiles with motion sensors. The linear correlation between the resistance of textile strain sensors and the flexing angle of joints was studied [13, 14], thus highlighting the potentiality of conductive textiles in the measurements of joint angles. A representative example was fulfilled by Munro et al. in preventing injuries for athletes by employing conductive polymers connected with acoustic feedback when reached a proper degree of knee flexing to keep legs in an optimal position [15]. Strain sensors were also used to investigate football kicking actions in a non-invasive way, just not interfering with athletes' movements [16].

However, smart clothing was designed not only for the detection and analysis of activities but also for the evaluation of the wearer's physiological status. The earliest approaches date back to the end of the 1990s with the "Georgia Tech Wearable Motherboard" project [17, 18] that allowed developers to plugin different sensors into a single garment. However, it had to wait until 2005 to observe the development of the first example of clothing with wearable sensors intended for the healthcare sector [7]. Other examples are the "European MyHeart project" [19], in which underwear was realized for the assessment of cardiovascular diseases (e.g., electrocardiogram - ECG) and respiration, and the "SimpleSkin shirt" [20], able to provide both physical and physiological sensing.

The increased importance of assessing cardiorespiratory activities has aroused much interest in the scientific community, and a lot of research was conducted to integrate electrodes in garments. For example, Cho et al. demonstrated the good performance of embroidered and knitted ECG combined electrodes [14]. Employing belt-worn sensors, made by polyvinylidene fluoride film and conductive fabrics as sensing elements, for the analysis of the respiratory cycle and the consecutive cardiac inter-beat intervals (RR-intervals or RR-signals), Choi and Jiang developed a system for monitoring sleep conditions [21].

Together with scientific development, the designing and construction principles of intelligent textiles are continuously up-to-date. In this regard, several studies have been conducted dealing with the strategies of textiles integration and components attachments depending on movement and body shape, as well as prediction of errors due to skin contact, strain sensing and loose-fitting in orientation [22].

Nowadays, textiles can be employed as substrates for application in the most modern and diffused market segments such as health, transpiration, energy, security or digital, thus giving them a significant added value. As well as the market of technical, nonwoven and composites textiles, estimated at $ 5.3, $ 3.4 and $ 10.5 (for 1kg) respectively, also the market of smart textiles is constantly growing [11]. The smart textiles market has grown rapidly by starting from 2014 with a market figure of $ 79 Million, and in 2019, this value reached $ 1.3 billion. It was estimated that the smart textiles market would get profits of $ 2.9 billion in 2021 in a very rapid way [23].

Currently, a simultaneous increase in the "Internet of Things" (IoT), with which it is possible to merge physical and virtual worlds creating smart environments, has been observed. The expansion of technology and rising investments are anticipated to drive the overall market over the next years. In 2020, it can be count as 30 billion devices connected, 10% of which will be clothing [11]. So, the market for smart textiles will be higher than the statistics. These predictions indicate significant changes in the way of life that we are already living in, and they are very encouraging for textile industries.

For example, Google's Project Jacquard [24], thanks to new conductive yarns, allows the introduction of touch and gesture interactivity into any textiles using industrial and standard looms. In this regard, innovative techniques to integrate the conductive yarns with tiny circuits with the dimension of a jacket button are continuously studied to obtain complimentary and discrete engineered components. Furthermore, miniaturized electronics can capture touch interactions among many functions, thus deducing gestures through machine-learning algorithms.

Smart textiles, useful for the design of intelligent clothing wearable as conventional clothes, are also feasible because of the availability of new fibers and textiles materials, as well as miniaturized electronic components.

1.2 Classification of smart textiles

Based on the definition of smart textiles previously provided, specific actions of these fabrics concern detecting, reacting and adapting to stimuli. Thanks to these abilities, smart textiles can also be considered adaptive, intelligent, interactive and reactive fabrics [2]. Following a general scheme, smart textiles [25] are characterized by several elements: sensor, actuator, communication elements, power supply, generation, interconnections, storage and data processing. Therefore, it is possible to make a first classification of smart textiles according to the action they can perform [26]:

- *Passive smart textiles;*
- *Active smart textiles;*
- *Very smart textiles*.

The passive smart textiles represent the first generations of these materials, sensors-based and able to sense in a passive mode, specific user's or environmental parameters [27]. The most representative examples of passive smart textiles are optical fibers, halochromic, antimicrobial, anti-static and anti-odor fabrics [28].

The second generation of intelligent textiles is represented by active smart textiles that are both sensors and actuators. They can both sensing and automatically react to external stimuli through actuators on a textile, flexible or miniaturized basis. Examples of active textiles are thermoregulated, vapor absorbing, and heat evolving fabric, but also water-resistant and vapor permeable (hydrophilic/ nonporous), heat storage and electrically heated suits [28, 29].

Finally, the third generation of smart textiles, the very smart, can sense, react and adapt their response to given situations.

Sensors can be compared to the nervous system and, for this reason, they are the core of passive smart materials. Similarly, essential elements for active smart textiles are actuators together with sensors. Actuators can act from a central control unit [30] or autonomously. Thus, the core of very smart textiles is a unit working as a brain with cognition, reason, and activity capability. They are the most representative example of the previous mentioned "multidisciplinarity" because they were designed to merge the scientific knowledge coming from traditional textiles and clothing technology, with those from other fields, among that sensor and actuator technology, nanotechnology, chemistry, medicine, material science and biology [29].

Such sensing elements can be integrated into textiles at any level, and in particular, fabrics can be modified according to specific physical/chemical treatments to act as sensors, actuators or transducers.

According to the previous definitions, a sensor can be defined as a device able to transform physical inputs in signals of different types. This definition is often also adopted for a transducer that converts a signal in one form of energy to another one. The main difference with a generic sensor is that the conversion that a transducer provides on the physical input is electrical, while actuators convert electrical energy into physical manifestations. Furthermore, sensors can be classified according to their application, thus referring to the physical/chemical phenomena measured. On the other hand, transducers can be electrochemical, optical, electromagnetic, colorimetric, piezoelectric and mechanical.

In this panorama, hybrid technologies are still developed, considering the convergence of conventional scientific sectors. In this regard, new processes have been developed to achieve ever stronger synergies between textiles and electronics. According to the term "textilification" [31], it is possible to preserve specific requirements of textiles fabrics (such as flexibility, comfort, washability) and, at the same time, to transfer in them functions from certain technology by realizing a functionality (e.g., antenna), by textile processes (e.g., weaving) or by integrating with technological components (e.g., LED). More in detail, techniques that enable the creation of smart textiles are mainly related to the type of application and can be summarized in two common approaches whose main aspects are reported in Table 1 [32]. The first one concerning the introduction of transducers and filiform material electrically conductive in textiles and the second one is based on connecting transducers and circuit components to fabrics.

Approach	Materials employed	Advantages	Disadvantages
Introduction of transducers and filiform material electrically conductive in textiles	Flexible conductive materials (e.g., conductive polymers/fibers, optical fibers, stainless steel wires, carbon nanotubes, piezoelectric materials)	Wearable textiles with intrinsic properties of fabrics	Lack of: - Sensibility - Computational functions
Connection of transducers and circuit components to fabrics	Electronic devices	Complementary to the first approach	*Limitation of: - comfort - textiles flexibility

Table 1: a) Approaches for the development of smart textiles: advantages and disadvantages (* referred to rigid and non-washable electronic components)

A detailed classification based on the applications foresees three main categories of smart textiles [26]:

- Portable and wearable electronic products developed through the incorporation of piezoelectric, thermoelectric devices and organic solar cells;
- Materials with high electrochemical performance, mainly used as flexible feeding systems;
- Chromatic devices integrated into the fabrics, intending to develop wearable sensors.

As already mentioned, smart textiles find applications in various fields, including medicine, diagnostics, health care, fitness, wellness and the environment [33, 34] thanks to the advantages deriving from the high number of "sensing molecules" and electronic devices available for the integration with fabrics. Different types of sensors can be integrated into fabrics, such as ECG (electrocardiography), EMG (electromyography) and EEG (electroencephalography), thermocouples, luminescent elements, but also carbon electrodes, useful for detecting biomedical and environmental components and/or parameters (e.g., oxygen, salinity, moisture or contaminants) [28].

1.3 Stimuli-responsive coatings for smart textiles

As already mentioned, through the combination of knowledge from conventional scientific fields, such as textile technology, chemistry, and electronics, it is possible to introduce specific functionalities in textile fabrics to design active coatings.

It is useful to clearly distinguish between functional and smart coating. The former is defined as conventional coating with properties of decoration and protection with additional functionalities such as self-cleaning, antimicrobial, anti-wrinkle, flame retardant, thermal insulation, softening, soil

release properties [35]. On the other hand, an advanced functional coating can be considered an active (or smart) coating able to sense the environmental changes and respond appropriately depending on those external stimuli by changing its physical or chemical properties irreversibly or reversibly [36]. For their definition, active coatings are generally sensors, transducers, or actuators [37, 38], thus performing, besides response, the tracing of performance, for example, through remote monitoring.
Moreover, active coatings can be doped with intelligent elements or molecules able to respond to the environment, such as chromic molecules, conductive materials, phase-change materials, memory materials and many others.
So, doped smart coatings can sense and react to heat, humidity, pressure changes, light, chemicals, bioactivity changes according to a lot of response modalities depending on the nature of the intelligent element or molecule. The response could consist of shape adaption, color change, surface cleaning, energy release, textiles structure dimensional changes, drug release, and many others.
Several examples of active materials or molecules are available in the literature, such as polymers or resins with specific properties. Among these, nanoparticles for self-cleaning, pigments for color changes, memory polymer, phase-changes materials for thermoregulation, antimicrobial agents for medical textiles, microelectronic devices for wearable electronics [39].
Depending on the applications, several types of wearable sensors can be designed by starting from active coatings or materials to obtain deformation, pressure, temperature, heat flow, humidity, temperature and gas wearable sensors. For example, deformation sensors for rate monitoring [40], posture [13] or body movements [41] can be obtained by using deformation-sensitive fibers, combining conventional fibers with sensitive ones, coating conventional fibers with metals, or by using conductive polymeric composites (e.g., carbon nanotubes inserted in textile polymers). Swallow and Thompson in 2001 [42] created a "sensory fabric" made up of two conductive fabric layers with a non-conductive mesh sandwiched in between: applying pressure on the upper conductive fabric, it will make contact with the bottom conductive fabric through the holes of the mesh thus providing a variation in the measured electrical resistance. Smart textiles for monitoring body temperature should follow the most common body deformation, so they should comply with wearability criteria. In this regard, the most critical limit is represented by the electronic devices used, which are commonly flexible, thus allowing compliance to these criteria. In particular, depending on the materials used and the principle on which they are based, thermistors, thermocouples and silicone-based sensors can be obtained. To monitor or improve the thermal comfort of a garment, smart textiles capable of measuring the amount of thermal energy crossing the two sides of the fabric and acting as heat (or thermal) flow sensors can be obtained. The latter provides information on the heat exchange between body and environment. Moisture sensors are usually made up of metal electrodes deposited

on a substrate coated with a conductive polymer, salt or other chemical products: with increasing humidity (which consists of the absorption of vapor water molecules by the sensor and consequent dissociation of functional groups), the resistance of the material decreases. This type of smart textiles can be useful for the analysis of body fluids (sweat, urine or tears), as well as gas sensors can be used to detect odors (volatile compounds) related to body fluids (urine, sweat in specific body parts, breath composition).

Besides the choice of suitable textile polymers to realize smart textiles, in-depth studies were also carried out to select conductive materials and coatings to be used and for electronic devices to improve the comfort of the sensors. The main features of wearable electronics are miniaturization, low-consumption work capacity, and, when possible, the use of biocompatible materials to minimize the impact on the wearer's daily activities. In particular, electronic devices can be integrated into textiles according to three approaches based on the employment of i) sensors, electronic elements (e.g., resistors, diodes, transistors, LEDs, thermoresistors, thermocouples, conventional batteries) or electroconductive fibers/yarns; ii) miniaturized circuits; iii) manufacture of electronic components (conductors, diodes, transistors, sensors and actuators, photovoltaic cells, LEDs, batteries) directly on the textile substrate, thanks to the use of nanotechnologies. An example is provided by the manufacture of miniaturizable silicon sensors thanks to Si technology, which are also easily functionalizable for the detection of contaminants (bacteria [43], heavy metals [44], pesticides [45]).

Most of the detection mechanisms of smart textiles are based on electrical signals and make use of electroconductive fabrics, but optical detection methods have also been used, based for example, on the use of polymeric optical fibers (POF) thanks to their strengths and more compatibility with textile materials compared to conventional optical fibers [46]. In particular, optical detection methods can be used for monitoring vital signals [47] thanks to the use of very sensitive photodetectors (silicon photomultipliers - SiPMs), whose most recent examples are biosensing applications [48], photoplethysmography measurements (PPG) [49].

Electric transduction methods have attracted considerable interest thanks to the possibility of miniaturizing microelectronic devices such as MOSFETs (metal-oxide-semiconductor field-effect transistors) or MOS diodes.

All electronic devices require energy, obtainable through piezoelectric elements [50], which store energy from movement or photovoltaic elements [51].

Human interfaces to active systems can be grouped mainly into two categories: input devices and display devices. Input devices may include capacitive patches that act as buttons or shape-sensitive fabric [52] capable of recording movement or bending, pressure, and stretching or compression. Signaling and visualization devices can include electroluminescent yarns [53] or threads that are

processed to integrate organic light-emitting diodes (OLEDs) [54]. Textile-based antennas are a relatively simple application of smart textiles: they are conductive yarns of specific lengths sewn or woven into non-conductive textile polymers [55].
Similarly, there is a wide range of data transmission elements starting from USB connections with conductive wires in flexible tape [56] up to the integration of antennas in clothing [4] and wireless technologies (Bluetooth, WiFi, etc.).

1.4 Development of smart textiles

Recently, besides their conventional uses, textile fabrics have aroused much interest in technical applications for functional properties that they can provide, such as water repellency, fire resistance, abrasion resistance, and their advanced use like smart textiles. Indeed, fabric samples became the ideal substrate for this kind of application thanks to their extensive employment in daily life but also intrinsic properties, among which breathability, washability, high flexibility, mechanical stability, reusability, large surface area, and lightweight.

1.4.1 Textile polymers and their features

Compared to other bulk materials, textile fabrics are characterized by unique properties, making them interesting for innovative and advanced applications. Textile fabrics can have different natures depending on the fibers they are made, natural or artificial. The main textile properties depend on the fibers' ones, which can provide a well-defined elasticity, heat, resistance and other features to the final fabrics.
Starting from the constituent fibers, they can be natural, regenerated, or synthetic. Natural fibers are produced from plants, animals or insects, mainly represented by cellulose (e., g. cotton) or proteins (e., g. wool and silk). On the other side, regenerated and synthetic fibers are also known as human-made or manufactured fibers. More in detail, regenerated fibers are produced from natural polymers to develop new materials by chemical processes. The most important cotton-like regenerated fibers examples are viscose and acetate. Synthetic fibers are produced through the polymerization of small molecules (monomers) into larger ones (polymer) in an industrial process. There are many different synthetic fibers, but polyester and polyamide are widely used among them.
Furthermore, fibers can be classified into nanofibers, microfibers, or conventional textile fibers depending on their diameter, respectively, < 500 nm, 3 – 10 μm and 10 – 50 μm.
The most important natural fiber is cotton, and it consists of cellulose, the most abundant polymer. Compared to synthetic fibers, the flexibility, lightweight, absorption potential, renewable nature, biodegradability, and high porosity [57] of cellulose fibers make the cotton fabric commonly used in

several application areas such as clothing. In particular, the porosity (total volume of the pores in one fabric and its distribution plotted against the pore radius) significantly affects the wettability of the fabric [58]. Moreover, thanks to the high density of hydroxyl groups on the cotton surface, it is possible to obtain ease surface modification and distribute active materials on fabrics through high adhesion [59]. Besides unique properties, cotton fabrics are characterized by hydrophilicity, strength, sensitivity to UV light, and low antimicrobial activity that limit their applications for areas like self-cleaning, functional textile, medicine, and personal healthcare. However, through functionalization, it is possible to provide added values to cotton fabrics and allow their use in biological and medical protection.

Synthetic fibers are a large part of the textile industry. Many different kinds of synthetic fibers are widely used in textile productions, among which polyamide, also known as nylon, and polyester that surpassed cotton production. Polyethylene terephthalate (PET), as polyester-based polymer, is a cheap fiber characterized by interesting mechanical properties [60, 61], with some drawbacks. It is s a hydrophobic synthetic fiber [62] with very low moisture, thus limiting some applications and the adverse electrostatic properties of the end-product [63].

1.4.2 Technologies for the development of smart coatings

Two strategies can be followed to give or improve functional or intelligent properties to polymer fabrics. The first one is based on developing new fibers, which is an expensive approach that often needs the relearning of product manufacture and new equipment for different materials. The second approach is the surface modification of conventional fibers or fabrics according to cheap processes with minimum changes to the textile processes [64].

The latter approach is the most interesting in the field of textile engineering and for the development of smart textiles. A definition provided by Kosa [65] stated that a “coating” is:

> “the application of a semi liquid material such as rubber, polyvinyl chloride, or polyurethane to one or both sides of a textile material. Once the coating has been dried (and cured, if necessary), it forms a bond with the fabric”.

The development of higher advanced coatings has led to not only functional fabrics but also engineered textiles able to interact with and respond to the environment.

Active coating for smart textiles can be prepared according to different techniques, most of which are conventional, while some of them are recent and innovative, such as nanotechnologies. In general, all these techniques are based on the bond of specific chemical moieties on textile surfaces and, at the same time, they differ for the modifying material, substrate to be modified, type of modification and other parameters.

In a coating process, the wettability of the fabric and the adhesion of the coating to the fabric sample are crucial. In particular, the wettability of the textiles by the coating affects the wicking of the treated fabrics; the adhesion of the coating is essential for a stable bond with fabric surfaces. Coating adhesion with textiles fabrics consists of intermolecular forces between the two interfaces, ionic or covalent bonds or weak interactions (dipole-dipole, hydrogen bond, induced dipole-dipole interactions or dispersive) [66].

An important aspect of being addressed is the optimization of the coating process because it can affect several textile parameters such as comfort, breathability and the hand of the treated fabric. Moreover, the coating adhesion can be influenced by both the fabrics surface and the presence of contaminants. In this regard, the homogeneity and good coating distribution on fabric surfaces are essential for obtaining both functional and smart textiles with excellent performance. For these reasons, textile fabrics are pretreated according to specific treatments. Among the latter, the most common are represented by: i) water/solvent scouring to remove residual spin finishes or dirt, oil, grease or stains; ii) plasma ablation or caustic etch to improve wettability; iii) bonding coat to improve the coating adhesion to the substrate. The next step, after substrate preparation, is the synthesis of the coating that can be represented by the mixture of functional substances in solvents or emulsions, often through the use of stabilizing additives useful to keep the coating solution stable for the time required for the application. After coating application, the post-processing step could be required, such as curing (cross-linking) through thermal treatment or different energy sources like gas, infrared oven or ultraviolet light [67, 68].

Several technologies are available to develop smart coatings, mainly consisting of sol-gel, plasma, electrospinning, physical and chemical vapor deposition, among many.

1.4.2.1 Sol-gel technique

The sol-gel technique represents an environmentally friendly and promising technology for introducing specific functionality on textile fabrics through the deposition of a thin layer with particular physical properties, chemical stability and optical transparency [69]. Indeed, through the sol-gel process, it is possible to obtain UV-protection, halochromic, antimicrobial, hydrophilic, self-cleaning and flame-retardant coating [32, 69–88].

Sol-gel coatings also provide durability to textile fabrics thanks to their protection action over fibers' mechanical and chemical properties [89–91]. They are considered particularly suitable for textile applications thanks to their no cytotoxic effects on human skin cells [92]. Furthermore, sol-gel represents a versatile and easy synthetic process to realize glass materials and ceramics, thus providing several advantaged with respect to other conventional methods such as the possibility to

control both porosity and composition at the molecular scale, low process temperature, possibility to obtain a final product with high purity up to atomic scale, as well as the possibility to synthesize complex composition materials and coatings over complex geometries [93].

The main reactions involved in this process are hydrolysis and condensation reactions of metal alkoxide precursors. The most employed precursors for developing hybrid organic-inorganic coatings are Si-based although their lower reactivity than that of other metal alkoxides. Other inorganic precursors like Ti, Al, Zr, Sn, V salts, or organometallic substrates in which the metal is linked to organic moieties that can be hydrolyzed and then condensed are available [94–96]. The sol-gel process is characterized by several advantages compared to other conventional techniques like high purity of the obtained product, low-temperature process conditions and ease removal of the solvent during the handling period.

The sol-gel synthesis is based on the transition of a system from a colloidal liquid (sol) into a solid gel and consists of two main reaction steps: hydrolysis of metal alkoxides and subsequent condensation reactions. During the first step, hydroxyl groups were produced by the hydrolysis of metal alkoxides, thus leaving alkoxyl groups, while the condensation reactions between hydrolyzed metal alkoxides were induced by heat treatment, thus generating a hybrid organic-inorganic three-dimensional (3D) porous network. Organic and inorganic precursors can interact between them according to weak (e., g. hydrogen, ionic, van der Waals interactions) or covalent bonds, classified as Class I and II, respectively [91, 97, 98]. In particular, the covalent interaction leads to the supramolecular Hybrid Organic-Inorganic Materials (HOIM), which the most common precursor for textile applications is represented by the organofunctional alkoxysilane (Class II). Such precursors are characterized by a general formula R'_n-Si$(OR)_{4-n}$ in which R is methyl, propyl or butyl functionalities, while R' is an alkyl or organofunctional group. The schematic representation of the hydrolysis of the three R groups of the silica alkoxide precursor and further condensation to provide the 3D network is reported in Scheme 1a and 1b, respectively. The hydrolysis in water can be catalyzed by acids or bases and followed by condensation reactions leading to the formation of the Si-O-Si linkages (Scheme 1a). Often sol-gel precursors bring also an organic functional group besides the alkoxysilane one, such as vinyl, epoxy or methacrylate functionality [91, 97].

Depending on the catalyst employed for hydrolysis and polymerization reactions, linear or randomly branched polymers and highly branched clusters such as spherical nanoparticles can be obtained for acidic or alkali medium [99]. It was also observed that hydrolysis reactions are faster in the acidic than in the alkaline medium, while the condensation rate is higher in alkali catalyzed reactions.

Another important parameter to be controlled is the temperature of the process. Indeed, it influences the mechanisms of hydrolysis and condensation reactions, and in particular, their kinetics. On the

other hand, the temperature of the process affects the evaporation, whose rate plays a crucial role in the definition of the morphology of the hybrid networks, thus leading to final products characterized by fractures or cracks or with different density if evaporation is too fast.

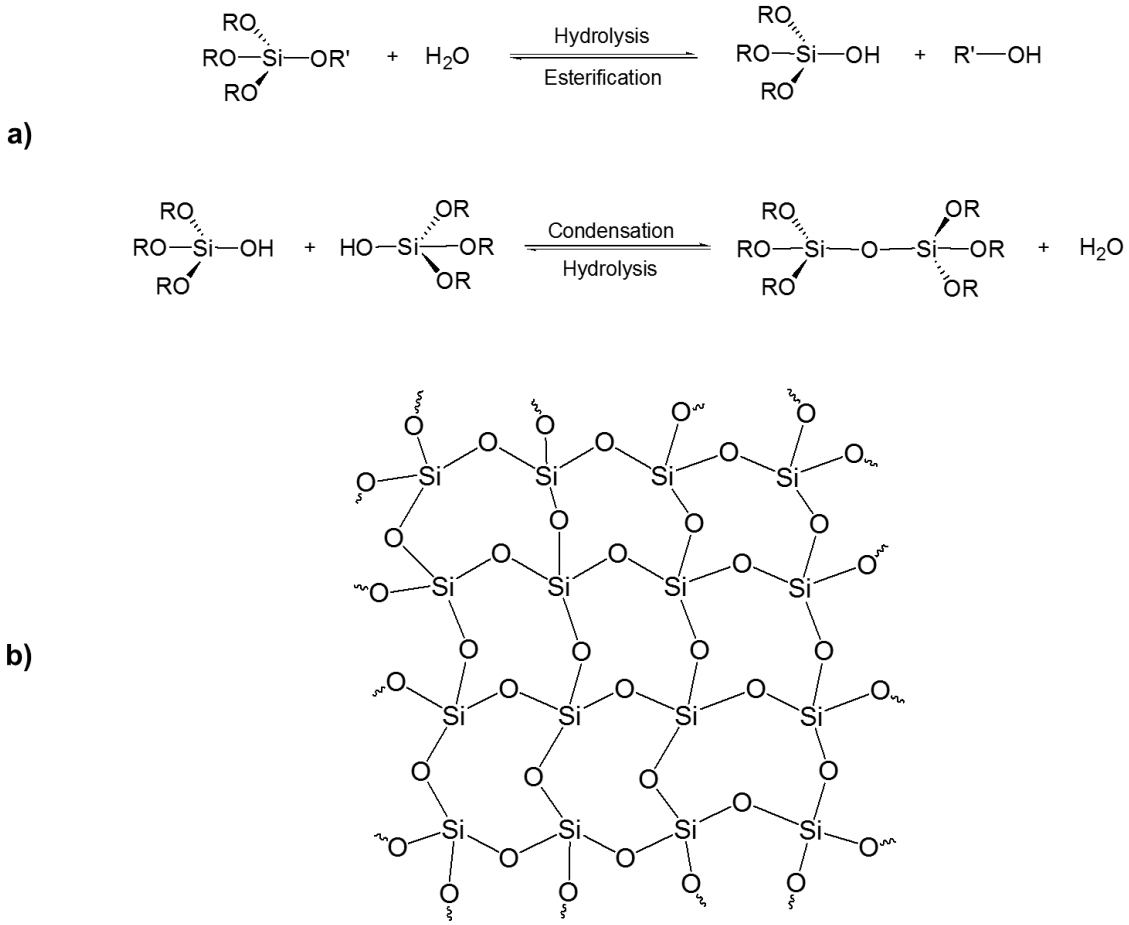

Scheme 1: a) Hydrolysis and condensation reactions of a generic silica precursor catalyzed by acids or alkali; b) Three-dimensional silica network resulting from condensation reactions. Reproduced with permission from Valentina Trovato et al [69], Copyright © 2018, Springer Nature

Different porous materials (e.g., polycrystalline powder, dry gel, coating film, or glass) can be obtained by tailoring pH, temperature, time, catalyst and solvent [100]. Several parameters influence the thermodynamics of both synthetic steps, among which electrophilicity of the metal, the strength of nucleophile and stability of the leaving group, while the kinetics of the processes depend on the molecular complexity of the metal precursor. On the other side, both the chemical structure and the nature of the metal precursors affect the properties of the obtained hybrid material. The latter can also be obtained by doping the silica 3D network with different organic or inorganic functionalities, thus realizing hybrid materials useful for sensing applications [69].

The sol-gel process represents a suitable wet method for the deposition of nanoparticles and hybrid organic-inorganic materials. The widely employed application processes are based on dip-coating, padding or spray, thus obtaining functional or smart textiles with features strictly related to the metal oxide precursors or the doped molecules. Sol-gel process, as well as other process technologies, provides surface modifications of textile materials through the bonding of coating chemical moieties to the surface of materials themselves. The bond between the coating and the substrate can be based on covalent linkages, on molecular attractions (such as Van der Waals forces, hydrogen bonding, dipole-dipole interactions) with a functional molecule (entrapped in the matrix or held in- or on- the surface of a substrate by steric factors), and finally based on retention of the molecule by the substrate through adhesive and cohesive forces between the molecule to the substrate, and the molecule to itself, respectively [66].

1.4.2.2 Grafting polymerization

Grafting polymerization technologies have been widely studied for textiles functionalization because they allow the introduction of covalent linkages between the polymeric textile surfaces and the functional matrix. The grafting processes need active sites on the surface of materials (e.g., textile fabrics) to which reactive species will be closely placed in contact for the covalent graft on their surface. These active sites on the textile surface consist of free radicals created by other free radicals coming from reactive molecules such as vinyl or acryl groups of other reactive functional species (e.g., hydroxyl, carboxyl, and many others) through radical initiators (chemical grafting) or radiation (radiation-induced grafting). Similarly, active sites on a substrate can be generated by a high-energy system of ions, radicals, and metastable molecules in plasma-induced grafting. Also the ultraviolet light is employed as an energy source for activation of the substrate in light-induced grafting. On the other side, the employment of radical initiators (e.g., potassium persulfate) is a low-cost approach than other ones.

The common mechanism refers to as a "grafting from" [101]. It starts from the generation of free radical sites on the substrate polymer chain (e.g., cellulose), whereby the active monomers (e.g., vinyl monomers) can react with the radicals to propagate on the surface to obtain permanent linkages of the monomers themselves on the substrate. Accordingly, covalent bonds are formed between monomers and polymers, thus providing new functionalities with high durability to the treated polymeric materials. In Scheme 2, the main steps of the graft polymerization of a generic vinyl monomer on cellulose polymers through a radical initiator are reported. Following the thermal heating, in water solution, the radical initiator (potassium persulfate in Scheme 2) leads to the formation of sulfate ion radicals ($SO_4^{-\cdot}$) due to the decomposition of persulfate ions (Scheme 2a).

Such radicals can react with water molecules to produce OH˙ radicals (Scheme 2b). Both persulfate and hydroxyl free radicals attack the double bond of vinyl monomers in solution, thereby generating other radicals (Scheme 2c), able to initiate homo- and co-polymerization reactions [102, 103]. Then, the solution containing the radical species and the formed polymers can be used to wet cotton fabrics, thus allowing the free radical species in solution to attack the textile polymer producing macroradicals by the direct abstraction of hydrogen atoms from the cellulose molecules and initiating grafting reactions on polymer surface (Scheme 2d and 2e). Subsequently, the graft polymerization between vinyl monomers and cellulose macroradicals is promoted by further propagation reactions (Scheme 2f). Finally, the grafting process ends through coupling or disproportionation reactions between the cellulose chain and the initiator [102, 103]. According to the described mechanism, the formation of functional polymer chains covalently bonded with the cotton surface occurs, thus providing durable functional material for technical and smart applications, such as flame retardant, halochromic, hydrophilic, antibacterial, controlled release systems.

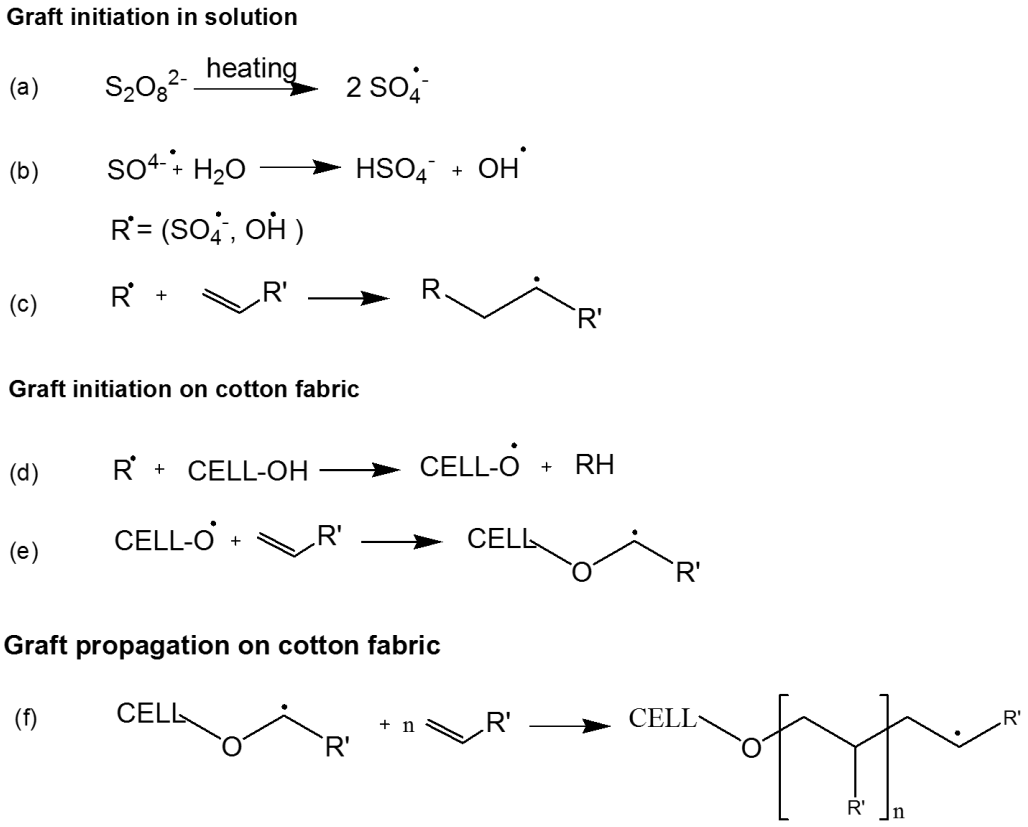

Scheme 2: Schematic representation of graft initiation and propagation of radical reactions [103]

1.4.2.3 Plasma

Plasma treatments have been widely investigated for their potentiality in developing hydrophilic/hydrophobic, flame-retardant, antibacterial, electroconductive surface treatments for

textiles. This technique leads to several advantages over other surface treatments, such as low-energy cost, physical and chemical range and being environmentally friendly [64].

Plasma is defined as the fourth state of matter and is characterized in terms of the average electron temperature and the charge density within the system [64]. The process consists of the exciting gaseous state characterized by atoms, molecules, ions and metastables and electrons in such a way that the concentration of positively and negatively charged species is almost the same. Ionized gas systems are characterized by physical and chemical properties, notably different from those of neutral conditions.

Hot and cold plasma are the two main phenomena commonly employed. The latter, held at low temperature, is generally used in material modification and the electron temperatures are 10 or 100 times higher than the gas temperature [104]. This technology is used to modify polymer surfaces, and the definition of low temperature comes from the density and temperature of electrons. Indeed, due to the very low density and heat capacity of electrons, they reach a very high temperature, over several tens of thousand Kelvin (not implying hot plasma), maintaining though the gas temperature at 100 K. Due to its composition, a gaseous mixture consisting of electrons, equally charged ions, molecules and atoms, different reactions can co-occur in the plasma system.

The main processes are two, plasma polymerization and ablation, and they provide opposite effects. Indeed, the former leads to the deposition of materials contrary to ablation that involves the removal of materials. Not only the condition of discharge (e.g., energy density) but also the plasma gas determines the dominant process [104]. In particular, plasma polymerization is provided if the plasma gas has high proportions of carbon and hydrogen atoms (e.g., methane, ethylene and ethanol).

Generally, the plasma polymeric films are highly cross-linked, insoluble and often very thin [105]. On the other side, two principles are at the base of the ablation, the physical sputtering and the chemical etching. The former can be represented by the sputtering of materials by chemically nonreactive plasma (e.g., argon gas plasma), while an example of the chemical etching occurs in chemically reactive types of plasma gas, including inorganic and organic molecular gases (e.g., O_2, N_2 and CF_4) which are chemically reactive but do not deposit polymers in the pure gas plasma. Plasma ablation represents a competitive way compared to polymer formation to treat solid surface materials [104].

The plasma treatment provides many free radicals on the treated textile fiber surface that have a crucial role in the formation of both functional groups and bonds between the fiber and the deposited material. The atmosphere exposure, in particular to oxygen, generates a decrease in the extent of such bonding, thus extinguishing the radical species. Accordingly, the time lapse between plasma treatment and composite fabrication should be as short as possible.

Therefore, the plasma treatment is a chemical modification of the surface achieved by some reactive functions. During plasma treatment, a thin film at the surface of the material is produced. In particular, it is commonly desired the formation of covalent bonding between the plasma species and the material surface instead of physically adsorbed coatings [106].

Compared with conventional technologies and finishing processes, plasma treatment presents advantages relative to the reduction in the use of chemicals, water, and energy. Through plasma technologies, it is possible to achieve a wide range of the most common functionalities on textiles.

1.4.2.4 Physical and chemical vapor deposition

Among the conventional process techniques for textile surface modification, vapor deposition is one of the most diffused. They are represented by the physical (PVD) and the chemical (CVD) vapor deposition. The PVD is based on physical processes to vaporize a solid target material according to several approaches, among which sputtering, laser bombardment, vacuum evaporation and many others, differing in the way the energy is put in the target material [107]. PDV is prevalently used in the metallization of films and fabrics to obtain conductive materials for electromagnetic interference shielding and for the realization of gold sputter coatings of samples for scanning electron microscopy (SEM). In general, PVD is a vapor coating in which a solid target material is converted and has atoms or molecules removed from it on an atomic or molecular scale. The vapor is first created and then deposited and condensed on the surface to be modified. Hence, the first step occurs in a vacuum chamber with vaporization of the target material, which is hotter than the substrate material. Then, the evaporated molecules condense on the substrate surface without interfering with other molecules [108]. Three main streams characterize the PVD process, vacuum evaporation, ion implantation, and sputter coating, which differ in the energy of their depositing materials. The coating materials in vacuum evaporation, sputter coating and ion implantation techniques have low (a few tenths of electronvolts), moderate (tens to hundreds of electronvolts) and high energy, respectively [64]. The applied energy is influential in the interactions of coatings materials with substrates and the growth of the film [64].

On the other side, CVD uses reactive gases that can react on, or near, the heated surface of a material, then diffuse on the surface and chemically attach by evacuating from the chamber by-products or unreacted precursors gases. Contrary to PVD, CVD does not need a high vacuum, but the substrate must be hotter than the gas steam, which could consist of volatile gas. By controlling the temperature process of CVD, it is possible to expand the window of precursor gases and, when they require very high temperature to volatilize, additional energy sources can be employed, such as plasma, thus

obtaining plasma-enhanced or plasma-assisted CVD. Even CVD is widely used for the realization of conductive or metalized textiles and fibers.

It is possible to produce uniform conformal conductive coating by the CVD method using polypyrrole [109], and further, such technology allows to realize superhydrophobic, wear and corrosion resistance coated surfaces.

1.4.2.5 Electrospinning

According to electrospinning, it is possible to deposit uniform coatings of nanofibers on different substrates. In this approach, a high voltage is introduced to the nozzle and a substrate, thus producing an interconnected membrane-like network of mat fibers. By starting from a solvent solution or a melt form, electrospun fibers are obtained by tailoring several environmental parameters and solution properties that affect the transformation of the starting polymer solutions into nanofibers [110–112]. According to this technique, it is possible to obtain fibers with a diameter between 10 and 500 nm and several polymers, such as polyurethane, nylon, polyacrylonitrile, polylactic acid, and polyvinyl alcohol, are applied by providing ultrathin fibers with different properties [110–112].

An electric field is applied between the tip of a nozzle, through which the polymer solution flows, and a collector plate, thus generating electrostatic forces between them. The polymer solution is distorted by the electric field from a spherical drop shape to a conical one (Taylor cone). When the electrostatic forces overcome the surface tension of the polymer solution at the nozzle, a jet stream is drawn from the tip of the latter. The jet becomes unstable because of interactions between the external electric field charges and solvent evaporation, thus providing bending and splaying. These two processes cause elongation of the jet, and the so produced nanofibres are randomly deposited on the collector plate as a non-woven structure.

Electrospinning is employed not only for the synthesis of nanofibers but also to coat nanofiber surfaces to obtain electrodes with a high ratio of surface area to volume. In particular, the tailoring of the processing time achieves the thickness control of the coating and, an increase in the coating thickness leads to an insignificant decrease in sensor sensitivity [113].

According to the electrospinning process, it is possible to realize coating with specific functionalities for interesting textile applications, thus obtaining halochromic fabrics or abrasion-resistance textiles, among many. The latter is realized by the coating of monofilaments via electrospinning, and subsequent twisting improves abrasion resistance as a result of the cohesion phenomenon [114].

1.5 Future perspectives of smart textiles

Smart textiles applications can be considered related to some features that are at the basis of wearable sensor systems. In particular, the development of organic solar cells, thermoelectric and piezoelectric devices to be incorporated into textiles allows overcoming the non-portability and non-wearability of conventional planar power systems. Electrochemical storage devices, lithium-ion batteries, and supercapacitors have been fabricated into fabrics to take advantage of the electricity and obtain high electrochemical performances as flexible powering systems. Moreover, several powered functionalities, like actuating and chromatic devices, have been introduced into textiles providing high performances.

It was supposed that smart textiles would develop in two different ways that proceed in parallel [11]. The first kind of smart textiles is defined as "low-cost", mainly produced for the general public and integrated into clothes and home textiles. The second type is dedicated to superior applications and characterized by high costs and significant added value.

The smart textiles sector has been growing rapidly during the last years, but nowadays, few products are available on the market mainly because they are not yet been fully developed, particularly for reliability. However, thanks to the research activities, several products are available and ready for scale-up to make them more reliable and robust.

In a future perspective, thanks to scientific developments, available technologies can be even more improved for realizing higher-performing electrically conductive and stimuli-responsive fabrics. Important challenges are the total integration of electronics in the textile structure, as well as the scientific improvements for advanced practical applications of prototypes in surgery, wound monitoring and healing, among many.

1.6 Aim of the thesis

According to the premises made in the preceding paragraphs, the following chapters are focused on the study and development of both electroconductive and stimuli-responsive coatings for the design of wearable textiles. In this research study, both sol-gel technology and grafting polymerization approaches were used to obtain the aforementioned active coatings for textile applications.

Among electrically conductive coatings, smart textiles for the detection of environmental humidity and temperature level, and also for heart rate monitoring through photoplethysmography, have been realized. With this aim, carbon nanotubes coatings were incorporated on textiles, which can provide variations in their electrical resistance depending on each variable. More in detail, Chapter 3 deeply describes the following research studies:

- Carbon nanotubes-based conductive textiles for environmental detection;

- Carbon nanotubes-based conductive textiles for heart rate monitoring.

As a function of changes in the surrounding environment, stimuli-responsive polymers provide variations in their properties. By integrating thermal and pH-responsive hydrogels, thermal-, light- and moisture-responsive polymers in textiles, among many, smart fabrics for several uses such as comfort, wound monitoring, color-change, smart controlled drug release, and protection against extreme environmental conditions can be obtained. In this thesis, halochromic textiles for colorimetric detection of sweat pH variations to assess the health status of the human body have been developed.

Controlled release fabrics have also been realized to control the release from textiles of an antioxidant, anti-inflammatory molecule under cutaneous stimuli. In this regard, Chapter 4 is focused on the development of halochromic textiles and specifically on the following research:

- Halochromic textiles for human sweat pH monitoring by grafting of nitrazine yellow through glycidyl methacrylate on cotton fabrics;
- Halochromic textiles for human sweat pH monitoring by sol-gel immobilization of alizarin red S on cotton and polyester fabrics.

Chapter 5 deals with the development of controlled drug release textiles, particularly with the sol-gel encapsulation of an anti-inflammatory/antioxidant molecule for textile applications.

To improve readiness, the references related to the discussed research studies were reported at the end of each chapter.

Investigations conducted through characterization techniques reveal the potentiality of the developed systems, and thanks to the obtained results, two prototypes have been realized in collaboration with the Microelectronics Laboratory of the University of Bergamo, "ELECT" and "Health Belt". The former is a T-shirt achieved by the deposition of CNT-electroconductive tracks integrated with an electronic device to monitor heart rate rhythm through an electrocardiogram. The latter is a belt realized through a halochromic textile integrated with an electronic device to monitor sweat pH. The developed prototypes highlight the importance of integrating electronic devices with fabrics for the realization of smart textiles and the necessity to use and greatly improve the multidisciplinarity in smart technologies.

References

1. Gorgutsa S, Bélanger-Garnier V, Ung B, et al (2014) Novel Wireless-Communicating Textiles Made from Multi-Material and Minimally-Invasive Fibers. Sensors 14:19260–19274. https://doi.org/10.3390/s141019260
2. Choi K, Park H, Jeong E-S, Peksoz S (2011) Scientometric Analysis of Research in Smart Clothing: State of the Art and Future Direction. pp 500–508
3. Cherenack K, van Pieterson L (2012) Smart textiles: Challenges and opportunities. J Appl Phys 112:091301. https://doi.org/10.1063/1.4742728
4. Van Langenhove L, Hertleer C (2004) Smart clothing: a new life. Int J Cloth Sci Technol 16:63–72. https://doi.org/10.1108/09556220410520360
5. Gu JF, Gorgutsa S, Skorobogatiy M (2010) Soft capacitor fibers using conductive polymers for electronic textiles. Smart Mater Struct 19:115006. https://doi.org/10.1088/0964-1726/19/11/115006
6. Lam Po Tang S, Stylios GK (2006) An overview of smart technologies for clothing design and engineering. Int J Cloth Sci Technol 18:108–128. https://doi.org/10.1108/09556220610645766
7. Paradiso R, Loriga G, Taccini N (2005) A Wearable Health Care System Based on Knitted Integrated Sensors. IEEE Trans Inf Technol Biomed 9:337–344. https://doi.org/10.1109/TITB.2005.854512
8. Lee J, Kwon H, Seo J, et al (2015) Conductive Fiber-Based Ultrasensitive Textile Pressure Sensor for Wearable Electronics. Adv Mater 27:2433–2439. https://doi.org/10.1002/adma.201500009
9. Libertino S, Plutino MR, Rosace G (2018) Design and development of wearable sensing nanomaterials for smart textiles. p 020016
10. Harifi T, Montazer M (2017) Application of nanotechnology in sports clothing and flooring for enhanced sport activities, performance, efficiency and comfort: a review. J Ind Text 46:1147–1169. https://doi.org/10.1177/1528083715601512
11. Koncar V (2016) Introduction to smart textiles and their applications. In: Smart Textiles and their Applications. Elsevier, pp 1–8
12. Farringdon J, Moore AJ, Tilbury N, et al Wearable sensor badge and sensor jacket for context awareness. In: Digest of Papers. Third International Symposium on Wearable Computers. IEEE Comput. Soc, pp 107–113

13. Shyr T-W, Shie J-W, Jiang C-H, Li J-J (2014) A Textile-Based Wearable Sensing Device Designed for Monitoring the Flexion Angle of Elbow and Knee Movements. Sensors 14:4050–4059. https://doi.org/10.3390/s140304050
14. Cho G, Jeong K, Paik MJ, et al (2011) Performance Evaluation of Textile-Based Electrodes and Motion Sensors for Smart Clothing. IEEE Sens J 11:3183–3193. https://doi.org/10.1109/JSEN.2011.2167508
15. Munro BJ, Campbell TE, Wallace GG, Steele JR (2008) The intelligent knee sleeve: A wearable biofeedback device. Sensors Actuators B Chem 131:541–547. https://doi.org/10.1016/j.snb.2007.12.041
16. Helmer RJN, Farrow D, Ball K, et al (2011) A pilot evaluation of an electronic textile for lower limb monitoring and interactive biofeedback. Procedia Eng 13:513–518. https://doi.org/10.1016/j.proeng.2011.05.123
17. Rajamanickam R, Park S, Jayaraman S (1998) A Structured Methodology for the Design and Development of Textile Structures in a Concurrent Engineering Framework. J Text Inst 89:44–62. https://doi.org/10.1080/00405009808658682
18. Gopalsamy C, Park S, Rajamanickam R, Jayaraman S (1999) The Wearable Motherboard?: The first generation of adaptive and responsive textile structures (ARTS) for medical applications. Virtual Real 4:152–168. https://doi.org/10.1007/BF01418152
19. Van Langenhove L (2007) Smart textiles for medicine and healthcare: materials, systems and applications. Woodhead Publishing
20. Schneegass S, Hassib M, Zhou B, et al (2015) SimpleSkin: towards multipurpose smart garments. In: Proceedings of the 2015 ACM International Joint Conference on Pervasive and Ubiquitous Computing and Proceedings of the 2015 ACM International Symposium on Wearable Computers - UbiComp '15. ACM Press, New York, New York, USA, pp 241–244
21. Choi S, Jiang Z (2008) A wearable cardiorespiratory sensor system for analyzing the sleep condition. Expert Syst Appl 35:317–329. https://doi.org/10.1016/j.eswa.2007.06.014
22. Dunne LE, Simon C, Gioberto G (2015) E-textiles in the apparel factory: leveraging cut-and-sew technology toward the next generation of smart garments. In: Fundamentals of Wearable Computers and Augmented Reality, Second edi. CRC Press, pp 619–638
23. (2019) General Introduction. In: Smart textiles for in situ monitoring of composites. pp 1–10
24. Poupyrev I, Gong N-W, Fukuhara S, et al (2016) Project Jacquard. In: Proceedings of the 2016 CHI Conference on Human Factors in Computing Systems. ACM, New York, NY, USA, pp 4216–4227

25. Schwarz A, Van Langenhove L, Guermonprez P, Deguillemont D (2010) A roadmap on smart textiles. Text Prog 42:99–180. https://doi.org/10.1080/00405160903465220
26. Stoppa M, Chiolerio A (2014) Wearable electronics and smart textiles: A critical review. Sensors (Switzerland) 14:11957–11992. https://doi.org/10.3390/s140711957
27. Kandi SG, Tehran MA, Rahmati M (2009) New method for obtaining proper initial clusters to perform FCM algorithm for colour image clustering. J Text Inst 100:237–244. https://doi.org/10.1080/00405000701757545
28. Sarif Ullah Patwary MS (2015) Smart Textiles and Nano-Technology: A General Overview. J Text Sci Eng 05: https://doi.org/10.4172/2165-8064.1000181
29. Castano LM, Flatau AB (2014) Smart fabric sensors and e-textile technologies: a review. Smart Mater Struct 23:053001. https://doi.org/10.1088/0964-1726/23/5/053001
30. Langereis GR, Bouwstra S, Chen W (2013) Sensors, actuators and computing systems for smart textiles for protection. In: Smart Textiles for Protection. Elsevier, pp 190–213
31. Persson N-K, Martinez JG, Zhong Y, et al (2018) Actuating Textiles: Next Generation of Smart Textiles. Adv Mater Technol 3:1700397. https://doi.org/10.1002/admt.201700397
32. Caldara M, Colleoni C, Guido E, et al (2012) Development of a textile-optoelectronic pH meter based on hybrid xerogel doped with Methyl Red. Sensors Actuators B Chem 171–172:1013–1021. https://doi.org/10.1016/j.snb.2012.06.024
33. Diamond D, Coyle S, Scarmagnani S, Hayes J (2008) Wireless Sensor Networks and Chemo-/Biosensing. Chem Rev 108:652–679. https://doi.org/10.1021/cr0681187
34. Farré M, Kantiani L, Pérez S, et al (2009) Sensors and biosensors in support of EU Directives. TrAC Trends Anal Chem 28:170–185. https://doi.org/10.1016/j.trac.2008.09.018
35. Paul R (2015) Functional finishes for textiles: an overview. In: Paul R (ed) Functional Finishes for Textiles. Woodhead Publishing, pp 1–14
36. Baghdachi J (2009) Smart Coatings. pp 3–24
37. Tao X (2001) Smart Fibers, Fabrics and Clothing: Fundamentals and Applications. Elsevier Publishing Ltd
38. Mattila HR (2006) Intelligent textiles and clothing. Woodhead Publishing Limited
39. Ielo I, Giacobello F, Sfameni S, et al (2021) Nanostructured Surface Finishing and Coatings: Functional Properties and Applications. Materials (Basel) 14:2733. https://doi.org/10.3390/ma14112733
40. AL-Khalidi FQ, Saatchi R, Burke D, et al (2011) Respiration rate monitoring methods: A review. Pediatr Pulmonol 46:523–529. https://doi.org/10.1002/ppul.21416

41. Yamada T, Hayamizu Y, Yamamoto Y, et al (2011) A stretchable carbon nanotube strain sensor for human-motion detection. Nat Nanotechnol 6:296–301. https://doi.org/10.1038/nnano.2011.36
42. Swallow SS, Thompson AP (2001) Sensory Fabric for Ubiquitous Interfaces. Int J Hum Comput Interact 13:147–159. https://doi.org/10.1207/S15327590IJHC1302_4
43. Santangelo MF, Libertino S, Turner APF, et al (2018) Integrating printed microfluidics with silicon photomultipliers for miniaturised and highly sensitive ATP bioluminescence detection. Biosens Bioelectron 99:464–470. https://doi.org/10.1016/j.bios.2017.07.055
44. Biswas P, Karn AK, Balasubramanian P, Kale PG (2017) Biosensor for detection of dissolved chromium in potable water: A review. Biosens Bioelectron 94:589–604. https://doi.org/10.1016/j.bios.2017.03.043
45. Gubanova O, Andrianova M, Saveliev M, et al (2017) Fabrication and package of ISFET biosensor for micro volume analysis with the use of direct ink writing approach. Mater Sci Semicond Process 60:71–78. https://doi.org/10.1016/j.mssp.2016.12.007
46. Cochrane C, Hertleer C, Schwarz-Pfeiffer A (2016) Smart textiles in health. In: Smart Textiles and their Applications. Elsevier, pp 9–32
47. Zheng Y-L, Ding X-R, Poon CCY, et al (2014) Unobtrusive Sensing and Wearable Devices for Health Informatics. IEEE Trans Biomed Eng 61:1538–1554. https://doi.org/10.1109/TBME.2014.2309951
48. Santangelo MF, Sciuto EL, Lombardo SA, et al (2016) Si Photomultipliers for Bio-Sensing Applications. IEEE J Sel Top Quantum Electron 22:335–341. https://doi.org/10.1109/JSTQE.2015.2504979
49. Agro D, Canicatti R, Tomasino A, et al (2014) PPG embedded system for blood pressure monitoring. In: 2014 AEIT Annual Conference - From Research to Industry: The Need for a More Effective Technology Transfer (AEIT). IEEE, pp 1–6
50. Edmison J, Jones M, Nakad Z, Martin T Using piezoelectric materials for wearable electronic textiles. In: Proceedings. Sixth International Symposium on Wearable Computers,. IEEE, pp 41–48
51. Bedeloglu A (Celik), Demir A, Bozkurt Y, Sariciftci NS (2010) A Photovoltaic Fiber Design for Smart Textiles. Text Res J 80:1065–1074. https://doi.org/10.1177/0040517509352520
52. Pacelli M, Loriga G, Taccini N, Paradiso R (2006) Sensing Fabrics for Monitoring Physiological and Biomechanical Variables: E-textile solutions. In: 2006 3rd IEEE/EMBS International Summer School on Medical Devices and Biosensors. IEEE, pp 1–4

53. Dias T, Monaragala R (2012) Development and analysis of novel electroluminescent yarns and fabrics for localized automotive interior illumination. Text Res J 82:1164–1176. https://doi.org/10.1177/0040517511420763
54. Janietz S, Gruber B, Schattauer S, Schulze K (2012) Integration of OLEDs in Textiles. Adv Sci Technol 80:14–21. https://doi.org/10.4028/www.scientific.net/AST.80.14
55. Salonen P, Hurme L A novel fabric WLAN antenna for wearable applications. In: IEEE Antennas and Propagation Society International Symposium. Digest. Held in conjunction with: USNC/CNC/URSI North American Radio Sci. Meeting (Cat. No.03CH37450). IEEE, pp 700–703
56. Ghahremani Honarvar M, Latifi M (2017) Overview of wearable electronics and smart textiles. J Text Inst 108:631–652. https://doi.org/10.1080/00405000.2016.1177870
57. Pasta M, La Mantia F, Hu L, et al (2010) Aqueous supercapacitors on conductive cotton. Nano Res 3:452–458. https://doi.org/10.1007/s12274-010-0006-8
58. Kálmán F, Borsa J, Madarász R, Rusznák I (1989) Iodine sorption, porosity, and wettability of carboxymethylcellulose of low degree of substitution. Colloid Polym Sci 267:349–352. https://doi.org/10.1007/BF01413629
59. Hu L, Pasta M, La Mantia F, et al (2010) Stretchable, Porous, and Conductive Energy Textiles. Nano Lett 10:708–714. https://doi.org/10.1021/nl903949m
60. Küçük M, Öveçoğlu ML (2018) Surface modification and characterization of polyester fabric by coating with low temperature synthesized ZnO nanorods. J Sol-Gel Sci Technol 88:345–358. https://doi.org/10.1007/s10971-018-4817-5
61. Khoddami A, Soleimani MI, Gong H (2011) Effects of finishing on the mechanical and thermal properties of fabrics from wool and hollow polyester fibres. Text Res J 81:2006–2016. https://doi.org/10.1177/0040517511407381
62. Zaman M, Liu H, Xiao H, et al (2013) Hydrophilic modification of polyester fabric by applying nanocrystalline cellulose containing surface finish. Carbohydr Polym 91:560–567. https://doi.org/10.1016/j.carbpol.2012.08.070
63. Wang CX, Lv JC, Ren Y, et al (2015) Surface modification of polyester fabric with plasma pretreatment and carbon nanotube coating for antistatic property improvement. Appl Surf Sci 359:196–203. https://doi.org/10.1016/j.apsusc.2015.10.060
64. Hu J (2016) Active coatings for smart textiles. Woodhead Publishing Series in Textiles: Number 176
65. Kosa (1999) Dictionary of fiber & textile technology, p36

66. Mittal KL (1976) Adhesion Measurement of Thin Films. Electrocompon Sci Technol 3:21–42. https://doi.org/10.1155/APEC.3.21
67. Benkreira H (1993) Classification of coating flows. In: Benkreira H (ed) Thin film coating. The Royal Society of Chemistry, Cambridge, pp 49–57
68. Shim E (2010) Coating and laminating processes and techniques for textiles. In: Smith W (ed) Smart textiles coatings and laminates. Woodhead Publishing in Association with the Textile Institute, Cambridge and CRC Press, Boston, New York, Washington, DC, pp 10–40
69. Trovato V, Colleoni C, Castellano A, Plutino MR (2018) The key role of 3-glycidoxypropyltrimethoxysilane sol–gel precursor in the development of wearable sensors for health monitoring. J Sol-Gel Sci Technol. https://doi.org/10.1007/s10971-018-4695-x
70. Wang E, Chow K-F, Kwan V, et al (2003) Fast and long term optical sensors for pH based on sol–gels. Anal Chim Acta 495:45–50. https://doi.org/10.1016/S0003-2670(03)00904-8
71. Ismail WNW (2016) Sol–gel technology for innovative fabric finishing—A Review. J Sol-Gel Sci Technol 78:698–707. https://doi.org/10.1007/s10971-016-4027-y
72. Mahltig B, Haufe H, Böttcher H (2005) Functionalisation of textiles by inorganic sol–gel coatings. J Mater Chem 15:4385. https://doi.org/10.1039/b505177k
73. Camlibel NO, Arik B (2017) Sol-Gel Applications in Textile Finishing Processes. In: Recent Applications in Sol-Gel Synthesis. InTech
74. Štular D, Simončič B, Tomšič B (2017) Stimuli-responsive Hydrogels for Textile Functionalisation: A Review. TEKSTILEC 60:76–96. https://doi.org/10.14502/Tekstilec2017.60.76-96
75. Abidi N, Hequet E, Tarimala S, Dai LL (2007) Cotton fabric surface modification for improved UV radiation protection using sol–gel process. J Appl Polym Sci 104:111–117. https://doi.org/10.1002/app.24572
76. Mahltig B, Textor T (2006) Combination of silica sol and dyes on textiles. J Sol-Gel Sci Technol 39:111–118. https://doi.org/10.1007/s10971-006-7744-9
77. Mahltig B, Fiedler D, Böttcher H (2004) Antimicrobial Sol-Gel Coatings. J Sol-Gel Sci Technol 32:219–222. https://doi.org/10.1007/s10971-004-5791-7
78. Poli R, Colleoni C, Calvimontes A, et al (2015) Innovative sol–gel route in neutral hydroalcoholic condition to obtain antibacterial cotton finishing by zinc precursor. J Sol-Gel Sci Technol 74:151–160. https://doi.org/10.1007/s10971-014-3589-9
79. Colleoni C, Guido E, Migani V, Rosace G (2015) Hydrophobic behaviour of non-fluorinated sol–gel based cotton and polyester fabric coatings. J Ind Text 44:815–834. https://doi.org/10.1177/1528083713516664

80. Colleoni C, Esposito F, Guido E, et al (2017) Ceramic coatings for water-repellent textiles. IOP Conf Ser Mater Sci Eng 254:122002. https://doi.org/10.1088/1757-899X/254/12/122002
81. Mahltig B, Textor T (2008) Nanosols and Textiles. World Scientific Publishing Co. Pte. Ltd, Singapore
82. Alongi J, Colleoni C, Malucelli G, Rosace G (2012) Hybrid phosphorus-doped silica architectures derived from a multistep sol–gel process for improving thermal stability and flame retardancy of cotton fabrics. Polym Degrad Stab 97:1334–1344. https://doi.org/10.1016/j.polymdegradstab.2012.05.030
83. Vasiljević J, Hadžić S, Jerman I, et al (2013) Study of flame-retardant finishing of cellulose fibres: Organic–inorganic hybrid versus conventional organophosphonate. Polym Degrad Stab 98:2602–2608. https://doi.org/10.1016/j.polymdegradstab.2013.09.020
84. Kappes RS, Urbainczyk T, Artz U, et al (2016) Flame retardants based on amino silanes and phenylphosphonic acid. Polym Degrad Stab 129:168–179. https://doi.org/10.1016/j.polymdegradstab.2016.04.012
85. Guido E, Alongi J, Colleoni C, et al (2013) Thermal stability and flame retardancy of polyester fabrics sol–gel treated in the presence of boehmite nanoparticles. Polym Degrad Stab 98:1609–1616. https://doi.org/10.1016/j.polymdegradstab.2013.06.021
86. Grancaric AM, Colleoni C, Guido E, et al (2017) Thermal behaviour and flame retardancy of monoethanolamine-doped sol-gel coatings of cotton fabric. Prog Org Coatings 103:174–181. https://doi.org/10.1016/j.porgcoat.2016.10.035
87. Colleoni C, Massafra MR, Rosace G (2012) Photocatalytic properties and optical characterization of cotton fabric coated via sol–gel with non- crystalline TiO_2 modified with poly(ethylene glycol). Surf Coatings Technol 207:79–88. https://doi.org/10.1016/j.surfcoat.2012.06.003
88. Rosace G, Castellano A, Trovato V, et al (2018) Thermal and flame retardant behaviour of cotton fabrics treated with a novel nitrogen-containing carboxyl-functionalized organophosphorus system. Carbohydr Polym 196:348–358. https://doi.org/10.1016/j.carbpol.2018.05.012
89. Yin Y, Wang C (2012) Organic–inorganic hybrid silica film coated for improving resistance to capsicum oil on natural substances through sol–gel route. J Sol-Gel Sci Technol 64:743–749. https://doi.org/10.1007/s10971-012-2911-7
90. Schmidt H, Jonschker G, Goedicke S, Mennig M (2000) the sol-gel process as a basic technology for nanoparticle--dispersed inorganic-organic composites. J Sol-Gel Sci Technol 19:39–51. https://doi.org/10.1023/A:1008706003996

91. Vasiljević J, Tomšič B, Jerman I, Simončič B (2017) Organofunctional Trialkoxysilane Sol-Gel Precursors for Chemical Modification of Textile Fibres. TEKSTILEC 60:198–213. https://doi.org/10.14502/Tekstilec2017.60.198-213
92. Plutino MR, Colleoni C, Donelli I, et al (2017) Sol-gel 3-glycidoxypropyltriethoxysilane finishing on different fabrics: The role of precursor concentration and catalyst on the textile performances and cytotoxic activity. J Colloid Interface Sci 506:504–517. https://doi.org/10.1016/j.jcis.2017.07.048
93. Colleoni C (2012) Sol-gel synthesis and hybrid thin film deposition for innovative textile finishing – Study, characterization and environmental impact evaluation. Tesi di Dottorato in Tecnologie per l'energia e l'ambiente. Dipartimento di Ingegneria Industriale - Università degli studi di Bergamo. ISBN: 978-88-974-13-19-6
94. Serra A, Ramis X, Fernández-Francos X (2016) Epoxy Sol-Gel Hybrid Thermosets. Coatings 6:8. https://doi.org/10.3390/coatings6010008
95. Wen J, Wilkes GL (1996) Organic/Inorganic Hybrid Network Materials by the Sol−Gel Approach. Chem Mater 8:1667–1681. https://doi.org/10.1021/cm9601143
96. Schubert U, Huesing N, Lorenz A (1995) Hybrid Inorganic-Organic Materials by Sol-Gel Processing of Organofunctional Metal Alkoxides. Chem Mater 7:2010–2027. https://doi.org/10.1021/cm00059a007
97. Sanchez C, Julián B, Belleville P, Popall M (2005) Applications of hybrid organic–inorganic nanocomposites. J Mater Chem 15:3559. https://doi.org/10.1039/b509097k
98. Boury B, Corriu RJP (2002) Auto-organisation of hybrid organic–inorganic materials prepared by sol–gel chemistry. Chem Commun 795–802. https://doi.org/10.1039/b109040m
99. Izumi K, Tanaka H, Uchida Y, et al (1993) Hydrolysis of trifunctional alkoxysilanes and corrosion resistance of steel sheets coated with alkoxysilane-derived films. J Mater Sci Lett 12:724–727. https://doi.org/10.1007/BF00626699
100. Sanchez C, Rozes L, Ribot F, et al (2010) ?Chimie douce?: A land of opportunities for the designed construction of functional inorganic and hybrid organic-inorganic nanomaterials. Comptes Rendus Chim 13:3–39. https://doi.org/10.1016/j.crci.2009.06.001
101. Jenkins DW, Hudson SM (2001) Review of vinyl graft copolymerization featuring recent advances toward controlled radical-based reactions and illustrated with chitin/chitosan trunk polymers. Chem Rev 101:3245–3273. https://doi.org/10.1021/cr000257f
102. Rosace G, Massafra MR (2008) Marking of Cellulose Yarn by Vinyl Monomer Grafting. Text Res J 78:28–36. https://doi.org/10.1177/0040517507082187

103. Rosace G, Colleoni C, Trovato V, et al (2017) Vinylphosphonic acid/methacrylamide system as a durable intumescent flame retardant for cotton fabric. Cellulose 24:3095–3108. https://doi.org/10.1007/s10570-017-1294-x
104. Luo S, Van Ooij WJ (2002) Surface modification of textile fibers for improvement of adhesion to polymeric matrices: a review. J Adhes Sci Technol 16:1715–1735. https://doi.org/10.1163/156856102320396102
105. Rakowski W (2008) Plasma treatment of wool today. Part 1 - Fibre properties, spinning and shrinkproofing. J Soc Dye Colour 113:250–255. https://doi.org/10.1111/j.1478-4408.1997.tb01909.x
106. Brétagnol F, Valsesia A, Ceccone G, et al (2006) Surface Functionalization and Patterning Techniques to Design Interfaces for Biomedical and Biosensor Applications. Plasma Process Polym 3:443–455. https://doi.org/10.1002/ppap.200600015
107. Meirowitz RE (2016) Coating processes and techniques for smart textiles. In: Active Coatings for Smart Textiles. Elsevier, pp 159–177
108. Wei Q, Xu Y, Wang Y (2009) Textile surface functionalization by physical vapor deposition (PVD). In: Surface Modification of Textiles. Elsevier, pp 58–90
109. Wilson J (2009) Textile surface functionalization by chemical vapour deposition (CVD). In: Wei Q (ed) Surface Modification of Textiles. Boca Raton, Boston, New York, Washington, DC, pp 126–138
110. Deitzel J., Kleinmeyer J, Harris D, Beck Tan N. (2001) The effect of processing variables on the morphology of electrospun nanofibers and textiles. Polymer (Guildf) 42:261–272. https://doi.org/10.1016/S0032-3861(00)00250-0
111. Bhardwaj N, Kundu SC (2010) Electrospinning: A fascinating fiber fabrication technique. Biotechnol Adv 28:325–347. https://doi.org/10.1016/j.biotechadv.2010.01.004
112. Huang Z-M, Zhang Y-Z, Kotaki M, Ramakrishna S (2003) A review on polymer nanofibers by electrospinning and their applications in nanocomposites. Compos Sci Technol 63:2223–2253. https://doi.org/10.1016/S0266-3538(03)00178-7
113. Wang N, Burugapalli K, Song W, et al (2013) Electrospun fibro-porous polyurethane coatings for implantable glucose biosensors. Biomaterials 34:888–901. https://doi.org/10.1016/j.biomaterials.2012.10.049
114. Zhou F-L, Gong R-H, Porat I (2010) Nano-coated hybrid yarns using electrospinning. Surf Coatings Technol 204:3459–3463. https://doi.org/10.1016/j.surfcoat.2010.04.021

Chapter 2. Materials, methods and characterizations

In this chapter, materials, methods, and instrumentations employed for physical-chemical characterizations of both synthesized coating products and textiles substrates used for developing smart textiles will be reported and deeply described. Paragraph 2.1. is divided into subparagraphs dealing with studies developed in the PhD research studies carried out:

2.1.1. Carbon nanotubes-based conductive textiles for environmental detection;
2.1.2. Carbon nanotubes-based conductive textiles for heart rate monitoring;
2.1.3. Halochromic textiles for human sweat pH monitoring by grafting of nitrazine yellow through glycidyl methacrylate on cotton fabrics;
2.1.4. Halochromic textiles for human sweat pH monitoring by sol-gel immobilization of alizarin red S on cotton and polyester fabrics;
2.1.5. Controlled drug release textiles by sol-gel encapsulation of active molecules.

Common materials and methods employed for all research will be reported before the detailed description of each paragraph.
Depending on the nature of the synthesized coatings, they have been applied to textile fabrics according to specific methodologies deeply reported in Paragraph 2.2. and divided for coating typology (conductive, halochromic, controlled drug release), while specific conditions of application, drying and curing will be reported later, after the synthetic procedure in the corresponding chapter of the research study.
A subparagraph schedule will be followed for some specific characterization techniques (e.g., morphological one), while techniques employed for all research will be reported without further specifications.

2.1 Materials

All chemicals reported in the following subparagraphs were used as received, without further purifications.
In all research studies conducted, cotton or polyester fabrics were employed as substrates.
100% plain-weave cotton fabric, scoured and bleached, with mass per unit area 331 g/m^2, supplied by Mascioni S.p.A (Cuvio, Italy) was employed in all research studies.

Besides the cotton described before, another cotton fabric, with the same characteristics, except for the mass per unit area of 119 g/m^2 (kindly supplied by Albini S.p.A., Albino, Italy), was employed in the research study dealing with the controlled release of *N*-palmitoyl-(*4*-nitro-phenyl)-amine (PNPA). In this research, the two cotton samples were named CO_H and CO_L (H = heavy, L = light), respectively.

Polyester sample, with a mass per unit area of 213 g/m^2, was kindly supplied by Cittadini S.p.A (Paderno Franciacorta, Italy).

Before all experiments, to purify textiles fabrics from impurities, the textile substrates were washed in non-ionic detergent for 20 minutes at 40°C and pH 7. After washing, the samples were rinsed with deionized water several times and put in a convection oven to be dried. As the last step, the washed and dried fabrics were left in a climatic chamber for at least 24 h. The fabric conditioning was performed under standard atmospheric pressure at 20 (± 1) °C and 65 (± 2)% relative humidity.

2.1.1 Carbon nanotubes-based conductive textiles for environmental detection

Pristine multiwalled carbon nanotubes (P_MWCNTs) were used as starting conductive materials to develop a conductive coating with environmental monitoring textiles applications. P_MWCNTs were synthesized according to an optimized procedure [1] and then oxidized following an established method [2] later described in Chapter 3. The conductive coating was realized using *1,2,3,4*-butanetetracarboxylic acid (BTCA), Sodium hypophosphite monohydrate (SHP), both purchased from Aldrich, poly(vinyl alcohol) (PVA) and MIROX®FC, kindly supplied by KemPaTex S.r.l. (Italy) and Bozzetto Group S.p.A. (Italy), respectively.

2.1.2 Carbon nanotubes-based conductive textiles for heart rate monitoring

For the realization of conductive coating for heart rate monitoring textiles, two kinds of vertically aligned carbon nanotubes (VACNTs), previously synthesized [3], characterized by two different lengths (1.5 mm and 3.0 mm, sample s-CNTs and l-CNTs, respectively) were employed.

For CNT dispersion and immobilization on cotton substrates, Ethanol (bought from Carlo Erba), the commercial products Geniosil® GF 94 (N-[*3*-(triethoxysilyl)propyl]ethylenediamine, named EDAES), Invadine® PBN (1-3 wt%) and thickener CT were employed and purchased from Wacker Chemie AG, Huntsman Chemicals and F.T.R. S.p.A, respectively.

2.1.3 Halochromic textiles for human sweat pH monitoring by grafting of nitrazine yellow through glycidyl methacrylate on cotton fabrics

The functionalization of nitrazine yellow (NY) through glycidyl methacrylate (GMA) and the immobilization on cotton fabrics to obtain smart textiles for sweat pH detection was performed through thermal-induced grafting by the radical initiator potassium persulfate (KPS).

For this approach, the following chemicals were employed. NY, GMA (≥ 97.0%), KPS, ethanol (≥ 99.8%) were bought from Sigma Aldrich (Italy), NaOH was acquired from Carlo Erba (Italy), while Boron trifluoride diethyl etherate (BF_3OEt_2), as the catalyst, was purchased from Fluka (Italy). For the pH-sensing study in the range between 4 and 8, both in solution and on treated textiles, McIlvane buffers were used and prepared by mixing Sodium phosphate dibasic dihydrate and Citric acid (acquired from Carlo Erba, Italy) in water solutions.

2.1.4 Halochromic textiles for human sweat pH monitoring by sol-gel immobilization of alizarin red S on cotton and polyester fabrics

Alizarin red S (ARS) was used in a sol-gel synthesis to obtain a pH-sensing coating to be applied on both cotton and polyester fabrics. In this synthesis, (3-Glycidyloxypropyl)trimethoxysilane was used and purchased from Acros Organics. ARS and HCl (37 %) were bought from Sigma Aldrich (Italy), NaOH was acquired from Carlo Erba, and Boron trifluoride diethyl etherate (BF_3OEt_2), as the catalyst, was purchased from Fluka (Italy).

For the pH-sensing study in the range between 2and 8, both in solution and on treated textiles, phosphate buffers were used and prepared by mixing ortho-Phosphoric acid 85%, Sodium phosphate monobasic dihydrate and Sodium phosphate dibasic dodecahydrate (bought from Carlo Erba).

2.1.5 Controlled drug release textiles by sol-gel encapsulation of active molecules

Following the sol-gel synthesis, a system for the controlled release of a molecule of pharmacological interest, *N*-palmitoyl-(*4*-nitro-phenyl)-amine (PNPA), was realized. This molecule was previously synthesized according to an optimized procedure [4]. *3*-glycidyloxypropyltriethoxysilane (GPTES) and methanol are the chemicals employed for the development of the controlled release system, and they were bought from Wacker and Aldrich, respectively.

2.2 Application methods

As already explained, depending on the nature of the synthesized coatings, different application techniques were employed. Below, a detailed summary of the application methodology used in the research studies conducted is reported.

2.2.1 Application technology for conductive coatings

The obtained CNT-conductive viscous pastes were deposited on one side of cotton fabrics using the knife-over-roll technique to achieve a very thin layer of conductive materials on the fabric surface.
For such an application, an in-house developed coater has been employed. It consists of a flat and movable knife blade under which textiles are laid out. In particular, the blade height and movement rate determine both the quantity and the thickness of the coatings applied on fabrics. For both studies, a multi-layer approach was performed. At least two consecutive coating layers were applied on textiles: each layer was dried after application and textiles were cured after the last layer application. This approach aimed to obtain the thickest and homogeneous layer after every application step and avoid dispersion of CNTs between textile fibers, otherwise not possible with other technologies, thus promoting an efficient electrical contact point between layers and a proper electrical interconnection between CNTs.

2.2.2 Application technology for halochromic coatings

In this paragraph, two different application technologies will be described for the deposition of the developed halochromic coatings on textile fabrics.
As already mentioned, the solution of functionalized NY molecule was applied on cotton fabrics according to the thermal-induced grafting approach.
The application procedure of the modified NY solution was carried out through the exhaustion method in Labomat Mathis equipment (Werner Mathis AG). For grafting, a sample of cotton fabrics with dimensions 21 cm x 29 cm was put in a canister with the radical initiator (KPS) and the NY solution and set under N_2 atmosphere for 30 minutes at room temperature to remove oxygen trapped in the fabric and dissolved in the solution. Finally, the described equipment was heated to 70°C for 60 minutes to make the grafting happen and dried in a convection oven at 70°C for 30 minutes.
The ARS sol-gel solution was applied on both cotton and polyester fabrics (21 cm x 29 cm) through a two-roll laboratory padder (Werner Mathis, Zurich, Switzerland) at a nip pressure of 3 bar. Both sample fabrics were dried (90°C for 5 minutes) and then cured (120°C for 3 minutes and 170°C for 3 minutes for cotton and polyester fabrics, respectively) in a convection oven.

2.2.3 Application technology for controlled drug release coating

Solutions synthetized for controlled drug release were applied on both light and heavy cotton fabrics (10 cm x 10 cm) by a two-roll laboratory padder (Werner Mathis, Zurich, Switzerland). Nip pressure

of 2 bar was employed, and treated textiles were dried at 80°C for 5 minutes and finally cured at 100°C for 1 minute in a convection oven.

2.3 Add-on and washing fastness

Treated textiles samples were weighed before and after coating applications to calculate the total dry solid add-on (wt%) according to Equation 1:

$$Add-on\ (\%) = \frac{W_T - W_{UT}}{W_{UT}} \cdot 100 \qquad \text{(Eq. 1)}$$

In this equation, WT and WUT are the dry weights of treated and untreated fabrics, respectively.

The washing fastness of treated fabric samples, as well as the leaching of sol-gel immobilized and pure dyes, was assessed according to the International ISO Standard 105C01, after 1 and 5 washing cycles, in a Labomat Mathis equipment (Werner Mathis AG). Eventually, modifications to this standard will be specified later in the corresponding chapters.

The weight loss after washing cycles (WLW, wt%) was calculated according to the following Equation 2:

$$WLW\ (\%) = \frac{W_{TW} - W_T}{W_T} \cdot 100 \qquad \text{(Eq. 2)}$$

Where WT and WTW are the dry weights of treated and washed treated cotton fabrics, respectively. WLW (wt%) was calculated with respect to the unwashed samples.

For both add-on (wt%) and WLW (wt%) calculations, all samples were weighted three times using a Mettler balance (accuracy 10^{-4} g) with a standard deviation lower than 2% after conditioning in a climatic chamber for at least 24 h under standard atmospheric pressure (20 (± 1)°C and 65 (± 2)% relative humidity).

2.4 NMR characterizations

The chemical structure of solutions realized for the development of both pH-sensing and controlled drug release fabrics were studied according to Nuclear Magnetic Resonance (NMR) analysis.

2.4.1 NMR characterizations of halochromic solutions

All starting materials and sol-gel solutions were fully characterized by NMR spectroscopy. ^{1}H and $^{13}C\{^{1}H\}$ NMR spectra were recorded in deuterated water (D_2O) on a Bruker 300 or Varian 500 gradient shimming spectrometers, equipped with a 5 mm probe and operating at 300.13 and 75.46MHz and 500.1 and 125.7 MHz, respectively. All chemical shifts are reported in parts per million (δ/ppm), downfield to tetramethylsilane (Me_4Si) as an internal standard (δ = 0.0 ppm), or

referenced to the residual protiated solvent signal such as in acetone-d_6 (^{1}H NMR: 2.05 ppm and ^{13}C NMR: 29.9 and 206.7 ppm); coupling constants J are given in Hertz. The purity of all starting materials, and reaction products characterization were determined by ^{1}H NMR assignment. ^{1}H and ^{13}C{^{1}H} NMR resonances were assigned by means of bidimensional homo- and heteronuclear NMR gradient experiments (gCOSY, ROESY, gHSQC and gHMBC). Gradient selected COSY, and ^{1}H-^{13}C Heteronuclear single and multiple bond correlations (HSQC and HMBC, respectively) spectra were acquired using the standard sequences as supplied by the VNMR software package. Two-dimensional Rotating frame nuclear Overhauser Effect Spectroscopy (ROESY) experiments were performed by employing a standard pulse sequence with a typical mixing time of 200 ms.

2.4.2 NMR characterizations of controlled drug release solutions

A Bruker ARX-300, equipped with a 5 mm gradient probe and operating at 300.1 MHz for ^{1}H nucleus, was employed, and both mono and bidimensional NMR spectra were acquired at 298.2 (±0.1) K in methanol.

All chemical shifts are shown in parts per million (δ/ppm), downfield to tetramethylsilane (Me_4Si) as an internal standard (δ = 0.0 ppm), or referenced to the residual protiated solvent signal such as in methanol-d_4 (^{1}H NMR: 3.30 ppm).

^{1}H NMR signals were assigned by means of bidimensional homonuclear NMR gradient experiments (gCOSY, gNOESY), acquired using standard Bruker pulse sequences.

2.5 FTIR characterizations

The chemical composition of synthesized coatings and their adhesive properties toward textiles fabrics were evaluated through Fourier Transform Infrared spectroscopy (FTIR). In particular, infrared spectroscopy in Attenuated Total reflection mode (ATR) is a characterization technique with a penetration depth of only a few micrometers useful for studying the surface functional groups of textile fabric substrates [5]. With this aim, both coatings and treated fabrics were analyzed and spectra compared with starting precursors and untreated fabrics FTIR curves, respectively.

Synthesized solutions were analyzed as xerogel, obtained by depositing few drops of solutions on a glass slide followed by drying and curing processes in a convection oven [6]. This procedure aims to obtain a solid residue suitable for FTIR evaluation without the interference of fabrics' highly intense absorption curves.

A Thermo Avatar 370, equipped with an attenuated total reflection accessory (ATR), was employed for infrared spectroscopic analysis. As internal reflectance element was used a diamond crystal and FTIR spectra were performed ranging from 4000 to 550 cm^{-1} with a resolution of 4 cm^{-1} and 32 scans.

Spectra of starting chemical material and sols were reported in Transmittance, while the spectra of fabrics in Absorbance after normalization at a specific wavenumber referred to a peak of untreated textile samples specified later for each study.

2.6 Morphological characterizations

Morphological characterizations were performed on both coatings and textiles, and different instrumentations were employed. In the below paragraphs, instrumentations for transmission electron microscopy (TEM), scanning electron microscopy (SEM) and atomic force microscopy (AFM) were reported for each research study.

2.6.1 Carbon nanotubes-based conductive textiles for environmental detection

Multiwalled carbon nanotubes (MWCNTs) were analyzed through SEM and TEM characterization techniques before study the uncoated and coated cotton fabrics. An FEI Quanta FEG 450 instrument, operating at 20 or 5kV, and a JEOL JEM 2010, operating at 200kV and equipped with a Gatan 794 MultiScan CCD camera were used for SEM and TEM characterizations, respectively.

The morphology of the untreated and treated fabrics has been studied, besides through SEM technique, also by AFM. The morphological measurement of textile samples was performed on a Multimode 8 AFM microscope equipped with a Nanoscope V controller and a type J piezoelectric scanner (Bruker, USA) in Peak- Force imaging mode, employing SNL-A probes with a nominal spring constant of 0.35 N/m (Bruker, USA). Background interpolation and surface roughness parameter calculations were performed with Gwyddion 2.45 [7]. Reported root means squared area roughness (Sq) values are the average of at least five different regions, with the standard deviation of these measures as the uncertainty.

2.6.2 Carbon nanotubes-based conductive textiles for heart rate monitoring

Vertically aligned carbon nanotubes (VACNTs) were analyzed by high-resolution transmission electron microscopy (HRTEM) to study morphology, the number of walls, and diameters of the nanotubes employed for the realization of conductive textiles for heart rate monitoring.

VACNTs were dispersed in isopropanol through gentle sonication for an hour. Then one drop of the CNT dispersion was placed on a 300 mesh Cu lacey carbon grid (from SPI) and analyzed through a JEOL-JEM 2100 electron microscope with a LaB6 emitter operating at 200 kV.

High-resolution scanning electron microscopy (HRSEM) was used to study the morphology of both the uncoated and coated cotton fabrics with CNT coatings. An FEI Magellan 400 Extreme High-resolution (XHR) SEM scanning electron microscope was used to collect HRSEM images.

2.6.3 Halochromic textiles for human sweat pH monitoring by grafting of nitrazine yellow through glycidyl methacrylate on cotton fabrics

Untreated and treated cotton fabrics with pure nitrazine yellow and grafted textiles with nitrazine yellow modified through glycidyl methacrylate were investigated through scanning electron microscopy to study changes in cotton surface morphology after the grafting process.

A Leica Electron Optics 435 VP instrument (UK) equipped with an accelerator voltage of 10 kV was employed for the characterizations of each cotton fabric sample.

2.6.4 Controlled drug release textiles by sol-gel encapsulation of active molecules

The sol-gel network for the controlled release of *N*-palmitoyl-(*4*-nitro-phenyl)-amine (PNPA) was analyzed according to SEM and AFM characterization techniques to evaluate the morphology of the hybrid system. An FEI Quanta FEG 450 microscope was used for SEM and EDS (Energy Dispersive X-Ray) analyses by fixing samples on aluminum sample holders using a graphitic adhesive. Operating voltage of 5 kV and 20 kV, both in low vacuum, were used for SEM and EDS analyses, respectively.

AFM analyses were conducted on untreated and treated cotton samples to investigate the deepness of the applied coatings and their morphologies. A stand-alone SMENA head by NTMDT, equipped with a Bruker silicon probe model NCHV and working in semi-contact mode, was used. The samples were fixed on metallic stubs using a small piece of double-sided scotch tape and studied at room temperature.

2.7 XPS measurements

Textiles substrates, both untreated and treated with alizarin red S functionalized through sol-gel technique, were analyzed in terms of surface chemical composition through X-ray Photoelectron Spectroscopy (XPS). XPS measurements were performed by an ESCALAB MkII (VG Scientific – UK) spectrometer, equipped with a standard Al excitation source and 5-channeltron detection system. The spectra were collected at 20 eV pass energy, and the binding energy (BE) scale was calibrated, positioning the C 1s peak of adventitious carbon at BE = 285.0 eV. More experimental details have been reported elsewhere [8].

2.8 UV-Vis analyses

UV-vis spectroscopy was employed to assess the color change of dye solutions in different pH range, using the same procedure and instrument for both studies involving nitrazine yellow and alizarin red S dyestuffs. Specific information dealing with the pH range studied for each dye and the buffer system used to obtain the dye solution at different pH were previously reported in the corresponding paragraph above and will be further reported in Chapter 4. Both NY and ARS buffer solutions were obtained by diluting a similar amount of dye or immobilized dye in an aqueous pH buffer solution.

Thermo Nicolet Evolution UV-vis 500 spectrophotometer was used for the acquisition of absorbance spectra of each sample in the range between 400-800 nm for NY dyestuff and between 300 nm and 650 nm for ARS, with a resolution of 0.5 nm and by employing quartz cells with a path length of 1 cm.

UV-vis diffuse reflectance spectroscopy was used to characterize the optical absorption properties and pH-response of fabrics treated with both dye and functionalized dye (for both grafted NY and sol-gel immobilized ARS). Each washed treated textile (50 mm x 70 mm) was soaked in 20 ml of buffer solution for 5 minutes and then dried in a convection oven. Finally, fabrics were characterized by a double beam UV-vis scanning spectrophotometer (Thermo Nicolet Evolution UV–Vis 500) equipped with a diffuse reflectance accessory (RSA-PE150 Labsphere). Reflectance spectra were collected in the spectral region between 380 nm and 770 nm with a 10-nm interval.

The reflectance values R (%) for each sample was the result of the average of three acquisitions (experimental error: max 2 %), and they were used to calculate the corresponding Kubelka-Munk values, according to the following equation:

$$\frac{K(\lambda)}{S(\lambda)} = \frac{(1 - R_\infty)}{2R_\infty} \qquad \text{(Eq. 3)}$$

In Eq. 3, K and S are the adsorption and scattering coefficients, respectively, while R_∞ is the absolute reflectance of an effectively infinitely thick layer. Eq. 3 was also employed for the definition of color strength of textiles, thus evaluating the dye fixation ratio of treated samples, according to equation 4:

$$F_{dye} = \frac{\left(\frac{K}{S}\right)_{TW}}{\left(\frac{K}{S}\right)_{T}} \cdot 100 \qquad \text{(Eq. 4)}$$

In the latter equation, $(K/S)_T$ and $(K/S)_{TW}$ are the color strength values at the maximum absorbance wavelength of treated samples, before and after washing cycles, respectively.

The pH response and the repeatability of pH sensing properties of treated textiles were evaluated through the measurements of CIE (International Commission of Illumination) color space coordinates, L* (lightness), a* (position between green and red) and b* (position between yellow and

blue) using a D65/10 illuminant. Negative and positive values can be obtained for each coordinate, thus referring to a specific color region: negative values for a* and b* represent green and blue colors, respectively, while positive values for a* and b* represent the red and yellow color region, respectively [9, 10].

A useful parameter to define the total color difference between two samples was obtained through the ΔE*, calculated according to Equation 5:

$$\Delta E^{*} = \sqrt{(\Delta L^{*})^2 + (\Delta a^{*})^2 + (\Delta b^{*})^2} \quad \text{(Eq. 5)}$$

where ΔL*, Δa*, Δb* represent brightness, redness and yellowness difference between two samples [10]. If ΔE* is greater than 5, the color difference between the two samples is detectable by the naked eye; if ΔE* is greater than 12, the color belongs to a different space [11, 12].

ΔE* was also employed to assess the repeatability of the NY pH-sensors. To evaluate if the developed pH-sensors were able to give a consistent response after several cycles, each washed fabric sample was soaked in pH 4 solutions, dried and then soaked in pH 8 solution and dried again (1 cycle). After each cycle, measurements were carried out 4 times, and ΔE* was calculated as the difference between the color space coordinates at pH 4 and 8.

2.9 Thermo-gravimetric analyses

The thermal behavior and stability of the CNT-doped coating for the environmental application were studied through Thermo-gravimetric analysis. A NETZSCH STA 409PC instrument, using Al_2O_3 pans, was used for these characterizations. TGA analyses were performed in the temperature range between RT and 1000°C with a heating rate of 10°C/min. Ar and Air atmosphere were used to characterize MWCNT and textile samples with a flux of 100 ml/min and 30 ml/min, respectively.

2.10 Controlled drug release tests

As mentioned before, two different cotton textiles were treated with the sol-gel system designed for PNPA controlled release, CO_H and CO_L. Both treated fabrics were subjected to in vitro diffusion analyses through Franz diffusion cells following an optimized experimental protocol here described [13]. Strat-M® membranes (25 mm discs, Cat. No. SKBM02560, Merck Millipore, Darmstadt, Germany) were used for in vitro diffusion tests and placed between the donor and the receptor slot of each Franz cell. All the experiments were performed at 37 ± 0.5°C, and the two treated cotton samples were positioned on the Strat-M® membrane by pointing the GPTES layer towards the acceptor chamber. After sample positioning, the Frans cell donor and receptor slots were fixed together and filled with 0.5 and 5.5 mL of phosphate buffer at pH 7.4 (10^{-3} M), respectively. UV-Vis analyses of

the content of the receptor slot were carried at different times (1, 2, 4, 6 and 24 h), thus replacing the analyzed solution with phosphate buffer. The same procedure was performed for the in vitro test of a control sample consisting of a standard PNPA solution.

All in vitro diffusion tests were repeated three times, and the obtained results were reported as the diffused amount (%).

2.11 Evaluation of the stiffness of the carbon nanotubes-based conductive textiles for heart rate monitoring

The stiffness of the CNT conductive textiles realized for heart rate monitoring was investigated to evaluate the comfort of cotton fabric after treatment. The stiffness is mainly affected by weave structure and mass per unit area of the fabric and yarn count and was measured as bending length (L_B) according to DIN 53362 as described below. A strip of fabric (10 cm x 2.5 cm) was moved together with a measurement bar over the edge of a standing bar. If the fabric was bent from its weight over the 41.5° line, the bending length was determined on the measurement bar as the length of the textile moved over the edge of the standing bar.

The measurements were repeated five times, and the average values were reported with a standard deviation lower than ±5%.

2.12 Resistance measurements

The electrical properties of treated cotton fabrics were performed through resistance measurements. Such measures were used to calculate sheet resistance (R_s) values according to Equation 6:

$$R_S = R\,\frac{W}{L}\,\left[\frac{\Omega}{\text{sq}}\right] \qquad \text{(Eq. 6)}$$

in which R is the measured electrical resistance, and W/L is the width-to-length ratio of the sample. According to this relation, it is possible to evaluate the conductive properties of treated textiles by referring to the resistance over a fixed aspect ratio sample area [14].

Indeed, following literature data [15], the thickness contribution can be neglected, and the resistance measurements are approximated on the surface, thus referring to “surface resistance”.

The treated fabric was placed horizontally on plexiglass support and held in place by two metal electrodes fixed on it to perform resistance measurements. These electrodes, which generate a uniform electrical contact with the sample surface, are connected to a Source Measurement Unit (Agilent B2961A Low Noise Power Source). Three resistance measurements were performed for

each treated textile at different applied voltages and distances, and only the average R_s values are reported.

2.12.1 Humidity sensing

The humidity sensing performances of CNT-coated cotton fabrics were assessed through electrical resistance measurements. Both uncoated and coated cotton fabrics were put in a climatic chamber and connected through alligator clips at the extremities (clips distance of 42 mm) with instruments placed outside the chamber. Due to the width of samples (4 mm), the total resistance of 10.5 squares was measured. A tester (Fluke 79) and a Source-Measure Unit (Agilent Power Source B2961A) were used to measure the resistance of samples as a function of relative humidity (% RH) and temperature. At the same time, the humidity and temperature parameters were collected by employing a high accuracy (±1.8% RH, ±0.2°C) humidity and temperature sensor (Sensirion SHT25), directly connected via a USB cable to a PC. The relative humidity percentage values ranging from 56.1% and 92.0%, while the temperature was varied from 4.3°C to 29.3°C. The response and recovery times, two parameters qualifying the dynamic response of a sensor, defined as the times taken to reach, by room conditions, the % RH value imposed in the climatic chamber and to recover the restored room conditions, respectively, were measured. The repeatability of the sensing properties was measured for four exposure cycles performed in the established % RH and temperature range.

2.13 Photoplethysmography

Photoplethysmography (PPG) is an optical technique widely employed to evaluate hearth rhythm as an alternative to electrocardiogram (ECG).

Several advantages support the use of PPG systems compared to ECG, such as ease of use, low cost, fast response, comfort for patients, no electrical interference, and no need for electrodes.

Changes of blood volume in the microvascular bed of tissue, via reflection from or transmission through the tissue, are optically detected by PPG sensors. Two components characterize the PPG waveform, the DC and the AC. The former depends on the structure of the tissue and the average blood volume of arterial and blood, while the latter reveals variations in the blood volume occurring during the systolic and diastolic phases of the heart cycle. Moreover, a PPG system operates in transmission or reflectance mode. In the first case, the light traveling through the tissue is detected by a photodetector (PD) placed at the opposite side of the source. In the second case, the PD detects the light reflected from the tissue and the blood vessels.

The most commonly employed light in the PPG system operating in reflection mode is green because it exhibits the most significant changes compared to the red and infrared lights.

CNT-conductive textiles realized for heart rate monitoring were tested as a transmission element in photoplethysmography (PPG). The PPG signals were collected from five volunteers from the fingertip.

The PPG measurements were carried out using the setup made up as follows:

- power supply: the system is powered by a 3.7 V, 155 mAh Lithium polymer battery and is scaled down to the 3.3 V operating voltage through a Low Dropout voltage regulator (ADP166 by Analog Devices);
- led: the light source is a bright green LED from Kingbright (AM2520ZGC09);
- photodetector: the reflected light is measured through a low-cost analog-output ambient light photosensor (APDS-9008 by Avago);
- analog Front-end for filtering and amplification of the analog signal.

The described setup is connected to an oscilloscope (LeCroy) through CNT-textiles strips in turn connected to the electronic through alligator clips.

2.14 Development of prototypes

As a result of scientific research conducted on the development of both conductive and halochromic textiles, two examples of prototypes, “ELECT” and “Health Belt”, will be discussed in Chapters 3 and 4, respectively, and here materials and methods employed for their realization are provided.

A long-sleeved T-shirt (polyester 70%, polyamide 24% and elastane 6%) was chosen for the development of “ELECT”. The CNT-conductive paste was spread according to the knife-over-roll technique on the chest side of the T-shirt by obtaining symmetric tracks to form an “X". The conductive paste was also spread on the inner side of the T-shirt only in correspondence with the end extremities of the tracks realized on the opposite shirt side to ensure direct contact with the skin and between the conductive tracks themselves. In the center of the realized “X” form, a box (3 cm x 3 cm x 1 cm) containing the electronic device was fixed and connected to the conductive tracks. The electronic device consists of:

- STM32F411 microcontroller (CPU);
- power supply: the system is powered by a 3.7 V, 155 mAh Lithium polymer battery and is scaled down to the 3 V operating voltage with a high-efficiency step-down power management circuit;

- ECG Analog Front-end for filtering and amplification of the analog signal. An integrated circuit, ADS1298R, featuring 8 low-power and low-noise differential amplifier was employed;
- SPBT2632C2A Bluetooth V3 Class 2 module with antenna enabling a high data wireless communications capable of streaming up to 4 ECG traces at 500 Hz through the Serial Port Profile (SPP);
- LIS2DH12 3D accelerometer for activity detection and recognition.

An elastic cotton textile was employed to realize “Health Belt”. A cotton fabric (3 cm x 3 cm) treated according to the sol-gel technique for the immobilization of halochromic dyestuffs (as reported in previous paragraphs) was fixed on one side of the belt. The sensing cotton fabric was directly connected with the electronic devices placed in a box (3 cm x 3 cm x 1 cm) on the opposite side of the belt. The main components of electronics are a color sensor, a skin thermometer, embedded processing devices, and a Bluetooth module. More in detail, the electronic device consists of:

- White LED;
- RGB photodiode;
- low-power ARM Cortex-M4 microcontroller (STM32F411VE);
- Li-poly type battery (110 mAh capacity);
- SPBT2632C2A Bluetooth V3 module.

References

1. Donato MG, Galvagno S, Lanza M, et al (2009) Influence of carbon source and Fe-catalyst support on the growth of multi-walled carbon nanotubes. J Nanosci Nanotechnol 9:3815–3823. https://doi.org/10.1166/jnn.2009.NS73
2. Milone C, Hameed a RS, Piperopoulos E, et al (2011) Catalytic Wet Air Oxidation of p-Coumaric Acid over Carbon Nanotubes and Activated Carbon. Ind Eng Chem Res 50:9043–9053. https://doi.org/Doi 10.1021/Ie200492g
3. Teblum E, Itzhak A, Shawat-Avraham E, et al (2016) Differential preheating of hydrocarbon decomposition and water vapor formation shows that single ring aromatic hydrocarbons enhance vertically aligned carbon nanotubes growth. Carbon N Y 109:727–736. https://doi.org/10.1016/j.carbon.2016.08.086
4. Saturnino C, Popolo A, Ramunno A, et al (2017) Anti-Inflammatory, Antioxidant and Crystallographic Studies of N-Palmitoyl-ethanol Amine (PEA) Derivatives. Molecules 22:616. https://doi.org/10.3390/molecules22040616
5. Rosace G, Massafra MR (2008) Marking of Cellulose Yarn by Vinyl Monomer Grafting. Text Res J 78:28–36. https://doi.org/10.1177/0040517507082187
6. Brancatelli G, Colleoni C, Massafra MR, Rosace G (2011) Effect of hybrid phosphorus-doped silica thin films produced by sol-gel method on the thermal behavior of cotton fabrics. Polym Degrad Stab 96:483–490. https://doi.org/10.1016/j.polymdegradstab.2011.01.013
7. Nečas D, Klapetek P (2012) Gwyddion: an open-source software for SPM data analysis. Open Phys 10:. https://doi.org/10.2478/s11534-011-0096-2
8. Ingo GM, Kaciulis S, Mezzi A, et al (2004) Surface characterization of titanium nitride composite coatings fabricated by reactive plasma spraying. Surf Interface Anal 36:1147–1150. https://doi.org/10.1002/sia.1862
9. Agarwal A, Raheja A, Natarajan TS, Chandra TS (2012) Development of universal pH sensing electrospun nanofibers. Sensors Actuators B Chem 161:1097–1101. https://doi.org/10.1016/j.snb.2011.12.027
10. Devarayan K, Kim B-S (2015) Reversible and universal pH sensing cellulose nanofibers for health monitor. Sensors Actuators B Chem 209:281–286. https://doi.org/10.1016/j.snb.2014.11.120
11. Aghaei Z, Emadzadeh B, Ghorani B, Kadkhodaee R (2018) Cellulose Acetate Nanofibres Containing Alizarin as a Halochromic Sensor for the Qualitative Assessment of Rainbow

Trout Fish Spoilage. Food Bioprocess Technol 11:1087–1095. https://doi.org/10.1007/s11947-017-2046-5

12. Tassanawat S, Phandee A, Magaraphan R, et al (2007) pH-Sensitive PP/Clay Nanocomposites for Beverage Smart Packaging. In: 2007 2nd IEEE International Conference on Nano/Micro Engineered and Molecular Systems. IEEE, pp 478–482
13. Parisi O, Scrivano L, Amone F, et al (2018) Interconnected PolymerS TeChnology (IPSTiC): An Effective Approach for the Modulation of 5α-Reductase Activity in Hair Loss Conditions. J Funct Biomater 9:44. https://doi.org/10.3390/jfb9030044
14. Banaszczyk J, Schwarz A, De Mey G, Van Langenhove L (2010) The Van der Pauw method for sheet resistance measurements of polypyrrole-coated para-aramide woven fabrics. J Appl Polym Sci 117:2553–2558. https://doi.org/10.1002/app.32186
15. Fang X-Y, Yu X-X, Zheng H-M, et al (2015) Temperature- and thickness-dependent electrical conductivity of few-layer graphene and graphene nanosheets. Phys Lett A 379:2245–2251. https://doi.org/10.1016/j.physleta.2015.06.063

Chapter 3. Conductive textiles

In this chapter, two scientific research for the development of carbon nanotubes-based conductive textiles for both environmental and heart rate monitoring are deeply reported. Before describing the experimental part and discussing the main results, an introduction dealing with conductive textiles, main conductive polymers, and technologies commonly employed for the design of E-textiles will be provided. Materials, general methods, and instrumentation for characterization were previously reported in Chapter 2.

The research study on carbon nanotubes-based conductive textiles for environmental detection was realized with the valuable contribution of Prof. C. Milone, Dr. E.Piperopoulos, Dr. M. R. Plutino, Prof. G. Rosace, Prof. V. Re, Dr. C. Colleoni, Dr. M. Caldara, Dr. M. Brucale, Dr. E. Mastronardo, Prof. G. De Luca, Prof. L. M. Bonaccorsi, Prof. A. Pistone.
The research study on carbon nanotubes-based conductive textiles for heart rate monitoring was realized with the valuable contribution of Dr. E. Teblum, Dr. Y. Kostikov, Dr. A. Pedrana, Prof. V. Re, Prof. G. D. Nessim, and Prof. G. Rosace.
"ELECT" was realized with the valuable contribution of Prof. V. Re, Prof. G. Rosace and Dr. A. Pedrana.

Part of this chapter was published on:

- *Rosace G, Trovato V, Colleoni C, et al (2017) Structural and morphological characterizations of MWCNTs hybrid coating onto cotton fabric as potential humidity and temperature wearable sensor. Sensors Actuators B Chem 252:428–439. https://doi.org/10.1016/j.snb.2017.05.175*
- *Trovato V, Teblum E, Kostikov Y, et al (2020) Sol-gel approach to incorporate millimeter-long carbon nanotubes into fabrics for the development of electrical-conductive textiles. Mater Chem Phys 240:122218. https://doi.org/10.1016/j.matchemphys.2019.122218*

3.1 Introduction

In recent years, electrically conductive textiles have aroused a great interest in the scientific community due to their high impact on the market for the wide range of innovative applications, among which the antistatic or electromagnetic shielding materials [1], smart textiles [2], or flexible electronics [3-6].

The interest in textiles as a substrate or structural materials for conductive devices comes from their properties, thoroughly described in Chapter 1, such as lightness, low cost, softness, stretchability, washability.

An important challenge in the development of conductive textiles is introducing electrical functionality in textile fibers by maintaining all these properties. Designed conductive fabrics can store energy, sense different stimuli (e.g., posture, temperature, strain, humidity, physiological signals [7]), even simultaneously [8], and are also employed for signal processing or transmission electronics [9]. The field of E-textiles covers several application areas, from healthcare, sport, environment, and as a support of high-risk professionals.

Electrically conductive textiles include conductive yarns, fabrics, fibers, and products built from them. Both flexibility and the possibility to control the shape and size of textile-based conductive materials provide several advantages over the conventional bulky and planar structures. Contrary to traditional electronic devices, which are rigid and (even they can be thin and flexible films) usually deform or fail under severe deformations, electronic textiles-based materials stably support complex and severe deformation thanks to their fibers compositions, thus closely accommodating on curved surfaces.

In the next paragraphs, an overview dealing with the most common conductive materials and technologies employed for the realization of conductive fabrics will be described.

3.1.1 Conductive polymers

Different approaches are used for developing conductive textiles, and the first examples consist of knitting or wovening of metals or conductive metal oxide fibers with conventional ones [3]. Unfortunately, the low flexibility and poor comfort of such materials are conflicting with the main properties of wearable conductive textiles. In this regard, different alternative technologies were used for their development, such as dip drying, dip coating [10], in-situ polymerization [11], electroless plating [12], chemical plating [13], layer-by-layer deposition [14]. High process cost and the long time required of some of these techniques are other disadvantages as well as the pollution by heavy metals. To develop smart conductive materials, other materials, such as the conductive polymers (CP) [15], are used to overcome the latter issue. They are organic polymers able to exhibit both conductive or semi-conductive behavior [16] that combine the mechanical properties of plastics with the electrical features of metals [17]. Nowadays, greater than 25 conductive polymers are available [18, 19], and the interest in their employment as functional materials for conductive textiles comes from their excellent properties such as lightweight, cost-effective, flexibility, biocompatibility, ease of manufacturability and, electrical properties. The most significant applications are fuel cells, supercapacitors, energy storage, energy conversion, antistatic packaging, conducting inks, intelligent membrane, electrostatic discharge (ESD), electromagnetic interference (EMI) and many others [20,

21]. Several applications of conductive textiles are available in different fields: fashion, functional clothing, health monitoring in sport and fitness, sportswear, clinical applications, security (e.g., uniforms for firefighters), non-clothing applications (e.g., automotive and home textiles). On the market, there are different types of smart textiles based on conductive polymers, such as medical fabrics, protective clothing, touch screen displays, flexible fabric keyboards and sensors for various application areas.

Conductive polymers can be classified into intrinsic (ICPs) and extrinsic (ECPs). The ICPs are conjugated polymers and synthetic metals with interesting optical and electrical properties characterized by conductivity values ranging from 10^{-10} to 10^{+5} S cm^{-1} [20–22]. The most important representative ICPs are polypyrrole (PPy), polyaniline (PANI) and poly(*3,4*-ethylenedioxythiophene) (PEDOT), characterized by environmental stability and high electrical conductivity, easily synthesized but with poor mechanical properties [23, 24]. These materials present limited stability after repeated cycling due to degradation in the mechanical strength, and their oxidation leads to radical cations that provide further chemical reactions that contribute to CPs instability [25].

ECPs, also known as conductive polymer composites (CPCs), derive from the blending of insulating polymer (thermoplastic or thermosetting) with conductive fillers. The latter are mainly represented by: (i) metal powders and their compounds (aluminum zinc oxide – AZO, and indium tin oxide – ITO), (ii) ICPs and (iii) carbon (carbon black – CB and carbon nanotubes – CNTs). ECPs show conductive values lower than ICPs ones, ranging from 10^{-5} to 10^{3} S cm^{-1} depending on applications [23, 24, 26, 27], and they also exhibit good thermal conductivity and mechanical properties and corrosion resistance. Several parameters influence the conductivity of a polymer, such as the density of the charge carriers, their mobility and direction, the presence of doping elements and the temperature [26]. Two factors are responsible for the conduction properties of polymers: (i) alternation of conjugated single and double bonds (sigma "σ" and pi-greco "π", respectively) responsible for localized and strong chemical bonds and of less strongly localized and weaker bonds, respectively, (ii) p-doping and n-doping (removal or addition of electrons from/into polymers, oxidation and reduction, respectively).

Conductive polymers are characterized by π-conjugation, and when π orbitals are overlapped, they provide valence bands, while the overlapping of π* orbitals leads to conductive bands. Due to the oxidation of conductive polymers, electrons can be removed from the valence bands leading to the formation of a delocalized charge on conductive polymers that provide the most stable geometry form. On the other side, the most common dopants are represented by anions, cations or larger

polymer particles (e.g., ClO^{4-}, Na^{+}, polyelectrolytes, poly(vinyl sulfonic acid), poly(styrene sulfonic acid), which can be introduced in the polymer during synthesis, or retrofitted.

Several approaches are available to realize conductive polymers by starting from conventional fibers, yarns or fabrics, occurring through modification of such conventional polymers according to grafting, curing and blending. The grafting approach was described in Chapter 1 as an efficient technique for surface modification. According to it, monomers are covalently bonded on a polymer chain through chemical, radiation, photochemical, enzyme grafting and plasma-induced techniques. According to curing, monomers are polymerized to form a coating on the surface of a substrate by physical interactions. Blending is a technique that allows obtaining a physical mixture of polymers.

3.1.2 Conductive materials and technologies for developing electrically conductive fabrics

As already mentioned, electrically conductive fabrics can be produced by several technologies based on the production of conductive fibers or yarns, insertion of yarns during or after fabric manufacturing, embroidery techniques, coating techniques, and many others [3, 20, 28–30].

Conductive yarns and fibers can be classified as intrinsic (naturally conductive) and extrinsic (treated conductive) [16]. The intrinsic conductive yarns and fibers consist of materials showing high electrical conductivity. Some examples are metallic fibers, carbon fibers, and fibers or yarn entirely made by ICPs.

Metallic fibers are highly conductive, but at the same time, they are brittle and heavier than conventional fibers. They can be produced from electrically conductive materials (nickel, titanium, aluminum, stainless steel, ferrous alloys) according to shaving, bundle-drawing processes or can be shaved off the edge of a thin metal sheet. Moreover, the metallic fibers can be used to realize very thin threads or yarns to be knitted or woven into textiles [3, 20, 30].

Carbon fibers or yarns are of great interest for their properties such as electrical conductivity, low density, heat resistance and strength, allowing their use as reinforcement in composites, ESD and sorption materials. They consist of fibrous carbon materials (carbon content greater than 90%) obtained by heat treatment (1000 – 1500°C) of organic matter. Depending on the production conditions and on the presence of impurities, carbon fibers with different structures and different electrical conductivity could be obtained (from conductor to semiconductor products) [16].

Three approaches are employed to obtain fibers or yarns entirely built of ICPs: melt spinning, wet spinning or electrospinning. Because of the decomposition of ICPs thermoplastic materials at a temperature lower than their melting point, melt spinning represents not an excellent approach to

obtain ICPs fibers. Similarly, instability and low concentration problems are important limitations of electrospinning [20, 31].

Differently, extrinsic conductive fibers or yarns are the results of the combination of conductive fillers and non-conductive materials such as polyethylene, polystyrene, and polypropylene. The most common techniques employed to introduce the conductive fillers in the insulating polymers are melt and wet spinning. In particular, the latter allows obtaining fibers or yarns with enhanced mechanical and electrical properties compared with those derived by the melt spinning approach [16]. Generally, CB particles (20-100 mm) are introduced into melts or thermoplastics polymers and then melt-spun into conductive polymer fibers or yarns. More than 10 wt% of CB is used for realizing conductive fibers, while CB in the range between 10 and 40 wt% is introduced in polymers to obtain yarns. The latter amount negatively influences the yarn conductivity because the increase in CB concentration causes the mechanical degradation of developed yarns. Contrary, the CB-based yarns present the advantage of low-cost thanks to the wide availability of CB and the ease of the synthetic procedure.

CNTs, thanks to their one-dimensional structure and unique physical properties (widely described later), are considered better fillers than CB. Through the spinning approaches mentioned above, they result in CNT-based yarns or fibers with improved mechanical properties compared to original yarns or fibers.

Following a similar strategy, insulating fibers and yarns can be made conductive by coating conductive fillers. Both the manufactory process and the conductive fillers employed influence the final conductive fibers/yarns/textiles [31, 32].

Common metals employed as conductive fillers are gold, aluminum, copper, and silver, while physical vapor deposition, metal-paint brushing, electroless plating, and polymer-metal lamination are examples of available coating techniques for the realization of conductive textiles. The coating of fibers or yarns with metals presents several disadvantages, mainly based on the leaching of the metals or their mechanical abrasion from fabrics. On the other side, the coating of CNTs and CB, as well as of ICPs, on fibers or yarns is usually performed through the dipping-and-drying technique. The coating of ICPs on polymers can also be carried out through chemical/vapor polymerization, and such conductive materials influence the mechanical properties of the obtained conductive polymers. Indeed important parameters to be considered are ICPs and yarn type, ICPs concentration, coating uniformity and thickness [16]. Thanks to surface pretreatments, materials with low surface energy can be made conductive on the surface with good coating adhesion (polyolefins, fluoropolymers, and silicones) [33]. Some examples concern the coating of fabrics in polyethylene terephthalate (PET) with a Cu-Ni-P alloy by electrochemical plating [34].

Not only yarns or fibers are coated with conductive materials to obtain the equivalent conductive polymers, but also the surface of the textile, thus achieving flexible conductive fabrics. The most common techniques are represented by printing approaches (knife-over-roll, inkjet printing, roll to roll, screen printing), spraying, vapor deposition, sputtering of thin films, electrodeposition, and electroless plating. Moreover, masking techniques, dip-coating, soft lithography, imprint and embossing make it possible to deposit a thick conductive layer on textile surfaces. Several parameters should be controlled for the optimal coating deposition, including uniformity of the application, coating viscosity and porosity, tension and flexural rigidity of the textile substrate. Other important parameters to be addressed are the coating adhesion, degree of moisture resistance and air permeability. As an example, metal fiber fabrics are different if compared with metal-coated textile materials. The latter benefit of both substrate and manufacturing technique, thus showing lightweight, breathability and electrical conductivity depending on both the coating thickness and chosen metals. The coating of conductive polymers on textiles provide several properties in the final conductive fabrics: (i) uniformity in the coating deposition, (ii) possibility to functionalize different textiles forms, (iii) thickness of the treated fabric ranging from 0.1 mm to a few mm, surface resistivity between 10 Ω and billion Ω, (iv) lightweight, flexibility and durability of final conductive textile-based materials.

A complex process to obtain conductive textiles by starting from conductive yarns is their insertion in textile fabrics by knitting, weaving and braiding approaches [32, 35]. An example is provided by the roll-to-roll mechanism for aluminum, developed for the production of textile sensors (poly(*3,4*-ethylenedioxythiophene)-poly(styrenesulfonate), PEDOT:PSS) to monitor the structural health of fabric-reinforced composite materials [36].

Another interesting technique used in textile industries simultaneously with the previously described ones, in particular, to obtain interconnections between sensors and electronic output systems, is embroidery. It allows attaching conductive patterns to a textile structure with high precision, creating circuit layouts and integrating yarns or fibers with different electrical properties [3, 37]. Essential features of each technique are reported in Table 2.

	Conductive fibers/yarns	Insertion of conductive yarns	Coating	Embroidery
Advantages	Possibility to adjust the processes parameters.	Conductivity establishment depending on yarns types; Complex integration on fabric.	Less expensive than conductive fibers; Possibility to apply uniform coatings with good adhesion on various textile forms; Lightweight, flexibility and durability of the coatings.	Potential to treat different textile; Possibility to specify the circuit layout and stitching pattern.
Disadvantages	Washability; Differences in conductivity.	High manufacturing costs.	High thickness for a certain application.	A large amount of wires is needed to be used.

Table 2: Techniques for the development of conductive fabrics: advantages and disadvantages [16]

3.2 Overview of conductive textiles integration into clothing

Although most smart textiles are based on electrically conductive fabrics and appear as the result of the integration of electronic devices and remote communication systems with fabrics, almost half of this market probably comes from companies that are not protagonists in today's electronics market. As mentioned in the previous paragraphs, there are many commercially available smart textiles based mainly on health, sports and fitness, wellness and automotive products. In the last 20 years, wearable sensors have been widely studied, particularly for their potential in the biomedical field [38], for their use as an in-between interface and potential means of monitoring both the environmental and operator's physiological parameters. Currently, wearable systems are available for continuous monitoring, but sensors for in-situ human health monitoring are still under development [39]. Indeed, the applications in the medical-health field are the most interesting as they are driven by the increase in population and life expectancy and concern, for example, monitoring, diagnoses, surgical and therapeutic treatments. Among the several medical sensors, wearable Body Sensor Networks (BSN) are a promising emerging technology for real-time and non-invasive detection of vital signs. In the

fitness and wellness fields, discreet and real-time monitoring of some physiological, biomedical and biomechanical parameters is of great interest, an example of which will be described later (ELECT). In 2000, the Georgia Institute of Technology created a shirt for monitoring heart rate, ECG, temperature, breathing, and other vital parameters [40]. Similarly, the "Sensatex Smart Shirt" (Sensatex, Inc.) can collect data from different parts of the body and transmit it to a device for processing, transmission, data visualization and then transfer through wireless technology to the data processing software [40]. Another example is provided by the "Numetrex sports top", featuring silver-coated nylon fibers and cotton-coated Lycra, capable of detecting the heart rate through tissue pressure in contact with the body thanks to the presence of sensors [41]. Takamatsu [37] has developed a wearable device for ECG recording consisting of PEDOT:PSS electrodes on polyester fabric that have shown low impedance in contact with the skin. Carvalho [42] described a shirt used for health and sports monitoring in high-risk environments. The electrode areas were knitted with a polyamide yarn with a thin silver coating (less than 10 nm), while the ECG connections were made on the back of the shirt and connected to a specific acquisition circuit. Edema ApS has produced a device (Edema Stocking) to measure the variations of the volume of the lower limbs allowing to obtain information regarding the retention of liquids and the efficiency of the treatment for drainage through objective scientific measurements [16]. Intelligent socks integrated with textile sensors capable of detecting foot pressure have also been developed [16]. In particular, the conductive fibers present in the sock transmit the data to an anklet capable of sending information via Bluetooth to an application for mobile devices. In this case, the production of reliable textile sensors capable of supporting washing cycles is essential for developing useful smart textiles. Paul et al. [43] have realized textile electrodes suitable for biopotential monitoring using the screen-printing technique to create conductive tracks. The latter ensured the electrical connection with the skin's surface by using different pastes for electrode networks: a polyurethane, a silver conductor and a conductive rubber.
In strictly healthcare applications, a T-shirt (WarmX©) was designed for use in extreme cold weather conditions. It is characterized by two heated areas around the kidneys, both in the back and front, made of silver-coated polyamide and fed by a 12 V battery that can be removed for washing [41]. A similar example is provided by the intelligent 3-in-1 jacket, known as the "Life Tech jacket", useful for survival in extreme conditions [16]. For the protection of the knees, an intelligent knee brace was designed, consisting of a single-sided polymer-coated textile sensor at the height of the patella integrated into an electronic circuit (3 V). The latter acts as a deformation sensor when the knee is bent: at a minimum resistance threshold based on the knee bending angle, an acoustic signal is emitted to warn the user that the desired bending angle has been reached [44]. Relevant research in the medical

field was carried out by Binkey in 2003, which considered necessary the presence of reliable instruments for clinical assistance and new therapies for patients with Parkinson's disease, one of the most widespread and neurological disorders responsible for motor dysfunctions. These tools are based on the possibility of obtaining a model of the patient status during several days and of correlating it to the time and the drug doses [45]. In this regard, an integrated shirt with specific sensors and interconnections was designed. It is made with PPy-coated fibers, able to read and record the posture and movements of the subject based on the principle of deformation sensors, worn in a non-invasive and systematic manner [46]. Similar smart textiles, capable of recording variations in electrical resistance following the movements of the arms, fingers, and torso, can be used in rehabilitation, sports medicine and virtual reality fields, as showed by Danilo De Rossi in 2003 with the body and the glove integrating carbon-based rubber sensors [47].

In the surgical field, an example is provided by Shim, which in 2008 integrated cotton threads (20 Ω/cm) in E-textiles using a polyelectrolyte-based coating with CNTs. This type of wires can be used for the detection of albumin (key blood protein) with high selectivity and sensitivity and therefore for applications in extreme situations, such as high-risk surgical, to detect bleeding where other methods are not available [48].

3.3 Development of carbon nanotubes-based conductive textiles for environmental and biomedical applications

As already explained in the first paragraph of this chapter, conductive textiles can be obtained according to several technologies, including the incorporation in textile materials of metal or conductive polymers. Another research field focused on the design of conductive fabrics has grown up during the last years and based on the employment of carbon nanotubes as a source of conductive properties.

Carbon nanotubes are of great interest thanks to their chemical-physical properties. They were recently employed as nanoscale modifiers to enhance the mechanical and electrical properties of conventional polymers [49, 50]. Moreover, CNTs are used in different areas of biomedical fields (e.g., drug and gene delivery, phototherapy, bioimaging, biosensing [51]) thanks to their transport capabilities. Indeed CNTs can be functionalized with molecules characterized by anticancer or cytotoxic activity [52, 53].

The use of CNTs for the realization of conductive coatings for textiles applications must satisfy several aspects, among which the homogeneous dispersion of nanotubes in the coating matrix, thus ensuring the electrical contact between them. This aspect represents an important challenge to be

addressed due to the chemical inertness of CNTs that tends to agglomerate according to van der Waals attractions, thus preventing their homogeneous dispersion. Strategies such as functionalization of external walls or open ends can be employed to enhance the interface between the CNTs and the employed solvent [49, 54–58] to overcome agglomeration issues of nanotubes.

An interesting approach that leads to ceramic carbon composite with high electrical conductivity is represented by the sol-gel technique [59–63]. In particular, according to the silanization of carbon nanotubes, it is possible to enhance the interfacial adhesion between the nanotubes and the matrix without the disadvantages resulting from the employment of strong acids [64]. The latter, employed for oxidation CNTs, reduces the aspect ratio of nanotubes. The most commonly employed sol-gel precursors are represented by *3*-aminopropyltriethoxysilane [62] or *3*-glycidoxypropyltrimethoxysilane [55]. According to reduction or oxidation processes carried out on the nanotubes surfaces, hydroxyl groups, able to react with the functionalities of the sol-gel precursors (silanol, epoxy, alkoxy, amine), are introduced [64].

In the following paragraphs, an overview of the main properties of CNTs will be provided. Moreover, two research studies dealing with the design of CNT-based conductive textiles for environmental and biomedical applications will be widely described.

3.3.1 Carbon nanotubes: state of the art

After their discovery in 1991 by Iijima, and thanks to their anisotropic properties [65], carbon nanotubes (CNTs) have aroused scientific interest during the last two decades. Among many materials, CNTs are fascinating for their chemical and physical properties such as semiconducting or metallic behavior, thermal conductivity, strength greater than 100 times of steel, high melting point, chemical inertness, elevated aspect ratio, ultra-lightweight, structural flexibility, high mechanical properties.

CNTs are carbon allotropes, such as graphite and diamond, with a tubular structure consisting of rolled-up sheet graphene (a sheet of carbon atoms arranged in hexagonal rings). The wrapped graphene sheet is characterized by the chiral vector, a pair of indices (n, m) representing the number of unit vectors along with two directions in the honeycomb crystal lattice of graphene. Depending on the chiral vector, CNTs are called “chiral” or, if m = 0 and m = n, "zig-zag" or "armchair", respectively. If CNTs are characterized by only one rolled-up graphene sheet, they are single-wall carbon nanotubes (SWCNTs); if more rolled-up graphene sheets are organized concentrically, carbon nanotubes are defined as multi-walled (MWCNTs). Commonly, SWCNTs are characterized by small diameters in the range between 0.4 and 4 nm and, depending on their chirality, they can be metallic

or semiconducting [66]. The numbers of walls in MWCNTs could range between 2 (double-wall) and 100 with an average diameter ranging from 1 to 100 nm and an intertubes distance of 0.34 nm, which is the same distance of two parallel graphene sheets. Commonly, MWCNTs are metallic because at least one of the walls will be metallic.

Depending on the synthetic strategy employed to obtain CNTs, they can present some defects, missing or added atoms, even if crystalline carbon nanotubes are ideally without defects. "Bamboo" is one common defect of MWCNTs, and it consists of different walls capping at different lengths and appear as stacked. Carbon nanofibers, graphite platelets arranged in various orientations, are another type of filament formation that can be confused with MWCNTs.

As already mentioned, the anisotropic properties of CNTs have been made them attractive for several applications such as thermal [67, 68], mechanical [69] and electrical [70, 71]. Structural composites represent typical examples of developed products, heat sinks, and microelectronic interconnects.

The electrical properties of MWCNTs have not been thoroughly investigated as for SWCNTs because of their more complex structure and the interaction between shells that entail different features. Experimental studies [72] demonstrated that shell-to-shell interactions play a crucial role in lowering MWCNTs resistance. On the other hand, both metallic and semiconducting SWCNTs have been widely studied for IC interconnects and fields emission applications [73], and as channels in transistor devices [74, 75], respectively. More in detail, for metallic SWCNTs, both valence and conduction bands touch at a specific point, while for semiconducting SWCNTs, these bands do not touch.

Carbon nanotubes are considered promising materials for developing CNT-polymer composites thanks to their mechanical properties [76]. Compared to other conventional materials, CNTs are characterized by interesting mechanical properties. Indeed, it was demonstrated that CNTs have the highest tensile strength and. Young's modulus, comparable with which of graphene sheet of around 1000 GPa, and they are stiffer than diamond.

As well as diamond and graphite, SWCNTs exhibit exceptionally low heat capacity and high thermal conductivity. Literature data report thermal conductivity of 3500 $Wm^{-1}K^{-1}$ for SWCNTs with a diameter of 1.7 nm and a length of 2.6 μm [77]. Based on these data, models of thermal conductivity depending on nanotube diameter and temperature are available. The high thermal conductivity of CNTs represents an important benefit for the development of future electrical applications, such as microprocessors, because of the importance of thermal management and dissipation.

3.3.2 Carbon nanotubes-based conductive textiles for environmental detection

Thanks to their electrical and physical-chemical properties, CNTs are also employed for sensing applications. In this regard, chemical sensors featuring high versatility and sensitivity can be designed for the evaluation of environmental changes at room temperature [78, 79]. The field of humidity sensing is of great interest for several applications such as in greenhouses industries, storage depots, food processing [80] and in recent years, they have been realized through miniaturization.

A conductive textile-based sensor to monitor the humidity and temperature of the surrounding environment was designed through the development of a hybrid functional MWCNTs-based coating [8]. A stable dispersion of functionalized MWCNTs was obtained through the aid of poly(vinyl alcohol) (PVA), *1,2,3,4*-butanetetracarboxylic acid (BTCA), and a polyacrylic resin, specifically chosen to preserve the electrical contact points between CNTs, thus ensuring their conduction properties although their immobilization in the polymer matrix. Several characterization techniques were used to assess the physical-chemical properties of the obtained conductive cotton textiles, while different levels of simultaneous environmental humidity and temperature were detected through electrical resistance measurements.

3.3.2.1 Experimental part

In this research study, pristine MWCNTs (P-MWCNTs), previously synthesized according to an optimized procedure showed by Donato et al. [81], were oxidizing following the method described by Milone et al. [82] to introduce hydrophilic functionalities (e.g., carboxylic and hydroxy groups) in nanotube structure. According to this oxidation procedure, 3 g of P-MWCNTs were soaked into a mixture of HNO_3 (67%) and H_2SO_4 (98%), (v/v 1:1, 300 ml) and kept at 60°C. The mixture was ultrasonicated for 6 h and, after this time, the solution was cooled down to room temperature. The cold mixture was further diluted with deionized water, filtered under vacuum with Millipore 0.2 μm filter paper and rinsed with deionized water until pH 7 to remove residual acid. Functionalized multi-walled carbon nanotubes (F-MWCNTs) were obtained as a black powder after drying and then employed in the following described procedure for the development of CNT-based conductive coating for textile applications.

100 mg of F-MWCNTs were mixed with 10 ml of deionized water. The mixture was ultrasonicated and then heated at 80°C. Then, 50 mg of PVA, 20 mg of BTCA and a catalytic amount of SHP were added separately and subsequently under vigorous stirring. Finally, at the homogeneous colloidal phase, 130 mg of acrylic thickener (MIROX® FC) were added, thus obtaining a paste (F-MWCNTs paste) to be applied on cotton surfaces by the knife-over-roll technique (previously explained in

Chapter 2). The coating application was made twice on the cotton sample with dimensions 20 cm x 30 cm, and the coated fabric was cured at 120°C for 5 min after both the first and the second layer to obtain a multi-layer architecture.

3.3.2.2 Results and discussions

In this paragraph, results and discussion of characterization analyses will be provided and scheduled depending on the chemical-physical technique employed.

3.3.2.2.1 Coating composition

As already explained before, to obtain a conductive coating for textile applications, MWCNTs were synthesized and then mixed with proper organic chemicals.

To improve the dispersion of MWCNTs in the polymeric matrix, they were oxidized as described in the previous paragraph. During this synthetic step, hydrophilic groups, such as COOH and OH, were introduced in the pristine nanotube structures (Scheme 3).

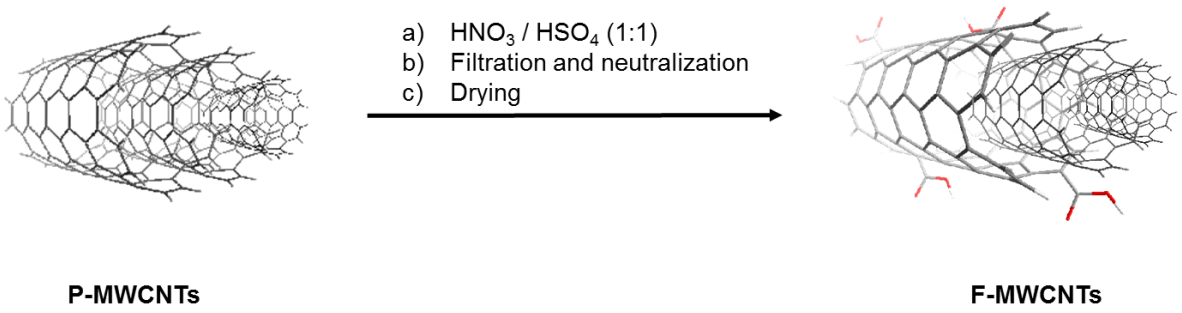

Scheme 3: Schematic representation of oxidation of P-MWCNTs

The obtained F-MWCNTs were then mixed with a polycarboxylic acid (BTCA), a polymer (PVA) and an acrylic thickener (MIROX® FC) as schematically reported in Scheme 4.

All these chemicals were specifically chosen for their properties and chemical structures with the aim to both disperse and immobilize nanotubes on cotton surfaces by preserving their mutual electrical connection.

More in detail, the water-soluble polymer PVA was chosen for its emulsifying, film-forming and adhesive properties thanks to the high density of OH groups in its structure [83]. On the other hand, the BTCA was selected for the presence of four carboxylic functionalities that ensure, thanks to the SHP catalytic action, to link both PVA and F-MWCNTs through OH groups and to lead to esterification reactions with cellulose [84]. For such reasons, BTCA plays a key role in the formation

of the coating, thus providing a stable immobilization of the coating on cotton surfaces [85]. Finally, the acrylic thickener was employed to obtain a viscous paste that was applied to cotton fabrics according to the knife-over-roll technique.

Depending on the chemical structure of the employed chemicals and according to previous evidence [86], a dispersion mechanism of F-MWCNTs within the polymer matrix was hypothesized and schematically reported in Scheme 4.

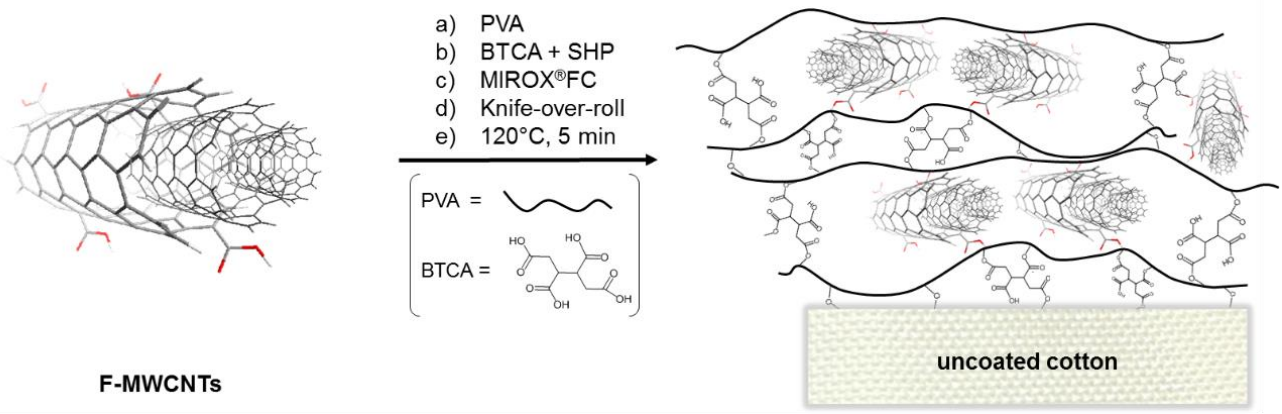

Scheme 4: Schematic representation of reaction steps for the development of MWCNT coating and application on cotton fabrics with its hypothesized chemical structure [87] Copyright © 2018, IEEE

The long PVA chains, spaced by BTCA, generate the orderly arrangement of carbon nanotubes. Moreover, BTCA acts as a cross-linker towards PVA chains, F-MWCNTs, and cellulose.

The amount of F-MWCNTs with the polymeric paste was 33.0% while, the add-on (wt%) on the cotton sample was measured at 3.8 %.

Thanks to the application technique employed, the knife-over-roll, the obtained paste was spread uniformly on textiles sample.

3.3.2.2.2 Morphological studies

Following the oxidation treatment, both pristine and functionalized carbon nanotubes were analyzed through TEM and SEM techniques to study structural modification as a consequence of the acid treatments.

TEM images show long, highly entangled carbon filaments formed by the P-MWCNTs (Figure 1, above). These filaments are characterized by external diameters in the range from 5 to 20 nm and, the typical CNT walls morphology of smooth graphene layers is observed from higher magnification images. On the other hand, a slight length reduction of nanotubes, as well as a sidewall degradation

with the comparison of edges and steps at external sheets, are observed in TEM figures of F-MWCNTs (Figure 1, below).

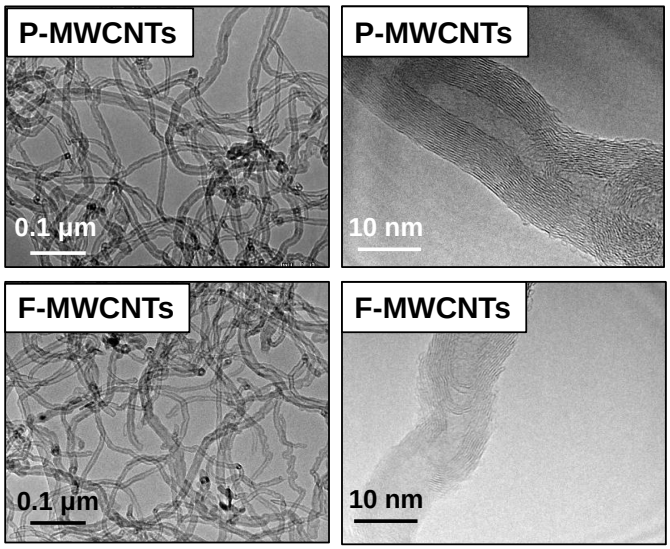

Figure 1: TEM images of pristine (above) and functionalized (below) carbon nanotubes at different magnifications. Adapted under the terms of the Creative Commons CC BY-NC-ND license [8]. Copyright 2017, the Authors, Published by Elsevier

Similarly, SEM figures of both pristine and functionalized carbon nanotubes were acquired and shown in Figure 2, in which the presence of agglomerated MWCNTs bundles is evident after the functionalization process.

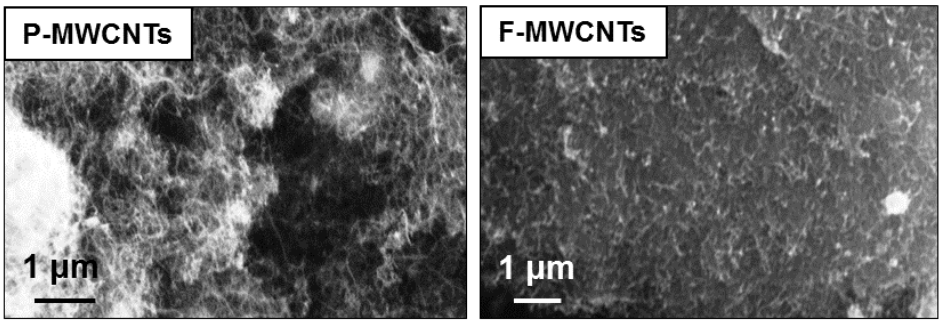

Figure 2: SEM images of pristine (on the left) and functionalized (on the right) carbon nanotubes

SEM images of both uncoated and coated cotton samples confirm the presence of MWCNTs coating on cotton surfaces due to the evident differences here below explained. The coating entirely and homogeneously covered the uncoated cotton fabric (Figure 3A and 3B**), which is characterized by

smooth fibers typical of cellulose, as shown in Figure 3B*. Moreover, the coating exhibits a highly rough and porous structure and results in a high coverage degree of cellulose surface (Figure 3A). In the same SEM figure, it is possible to observe MWCNTs well exposed to environmental humidity, which, thanks to the porous structure of the coating, are easily reached by environmental vapor molecules. The latter influences the dielectric constant of the coating and, as a consequence, the electrical resistance of carbon nanotubes, which changes for different relative humidity levels. Furthermore, the thickness of the applied coating was evaluated by SEM analysis, and it is uniform, even in section, and in the range between 99 and 138 μm (Figure 3C).

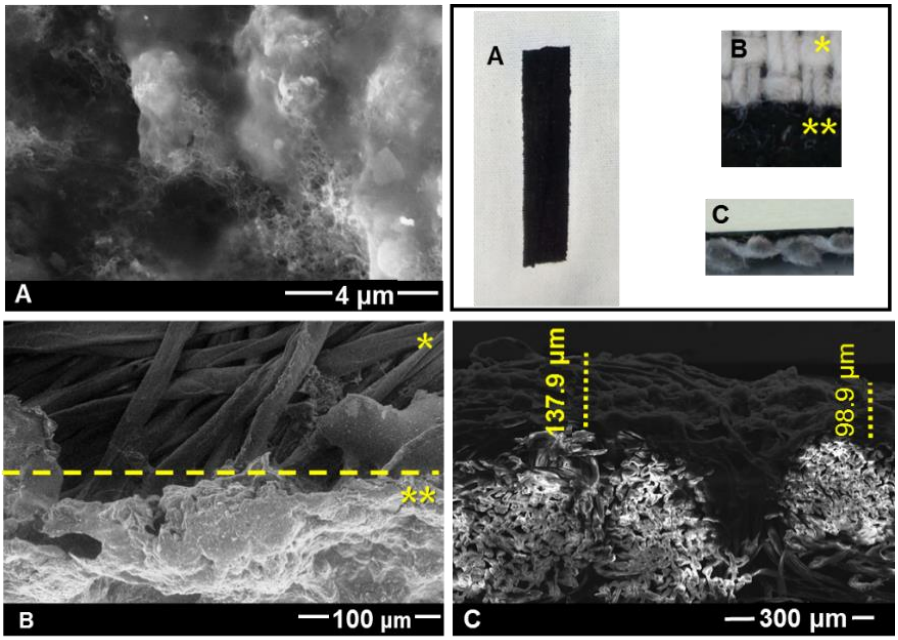

Figure 3: SEM images of cotton fabrics coated with F-MWCNTs paste (A-C) and corresponding images [87] Copyright © 2018, IEEE

Another morphological analysis was performed through PeakForce AFM imaging (Figure 4). The uncoated cotton sample reveals the presence of cavities and grooves randomly depth from 10 to 100 nm, corresponding to the interstitial zones in which individual fibers adjoin [88]. Sq values calculated on 1 μm^2 randomly selected zones of the untreated cotton sample are largely influenced by these mostly stochastic variations (S_q of untreated cotton = 42 ± 28 nm). Despite the above, the morphological alteration induced by the processing of the treated sample is so marked that it is possible to quantitatively assert its difference with respect to the untreated sample (S_q of treated cotton = 185 ± 42 nm). Through optical and AFM microscopy, it is possible to observe the micrometric and nanometric constituent fibers of the untreated sample (Figure 4a and 4c). Differently,

through optical microscopy, the presence of dark granular material covering the majority of the micrometric fibrils in the treated sample is evident (Figure 4b). The typical texture, characterized by nanometric fibers, in pristine cotton is no longer discernible after functionalization, as revealed by AFM microscopy (Figure 4d).

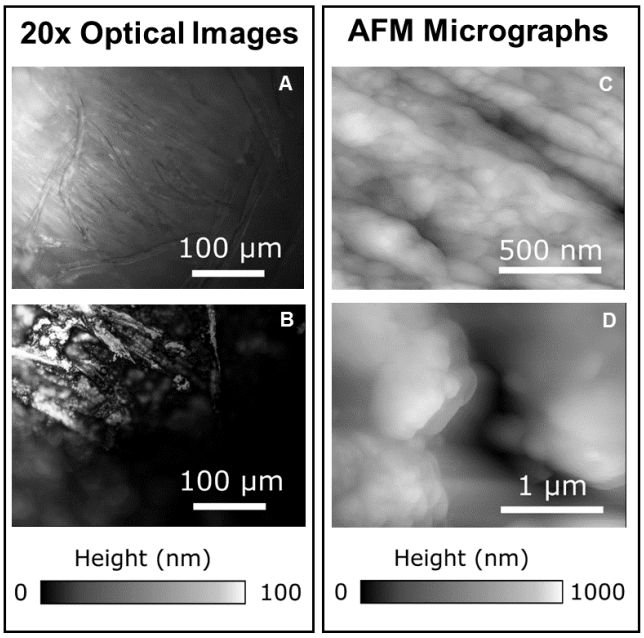

Figure 4: Optical images (on the left) and AFM micrograph (on the right) of uncoated (a and c) and coated cotton fabrics with F-MWCNTs paste (b and d)

3.3.2.2.3 ATR-FTIR characterization

ATR-FTIR spectroscopy was employed to study the chemical composition of the applied coating and to confirm its presence on cotton surfaces. ATR-FTIR Transmittance spectra of polymeric MWCNT paste, uncoated and coated cotton fabrics are compared in Figure 5. As evident, spectra of uncoated and coated cotton fabrics result completely different due to the presence of the coating that leads to the disappearance of the main characteristic absorption bands of cellulose, reported in Table 3. While, other peaks in the FTIR spectra of coated cotton at 1634 cm^{-1}, 1713 cm^{-1} and 1150 cm^{-1} are associated with C=C, C=O and C-O stretching of COOH functionalities of carbon nanotubes, respectively [89].

FTIR bands	Literature data
O-H stretching	3500 – 3100 cm^{-1}
C-H stretching	3000 – 2800 cm^{-1}
C-H wagging and deformation mode	1400 - 1200 cm^{-1}
asymmetric stretching of C-O-C in-plane ring stretching C-O stretching	1200 - 800 cm^{-1}

Table 3: Main absorption bands of cellulose [90]

As observable from spectra in Figure 5, the main absorption bands of cellulose in the analyzed spectral region, result overlapped by the FTIR peaks of MWCNTs paste: 1320 cm^{-1}, 1055 cm^{-1} and 1030 cm^{-1} (C-H wagging, asymmetric in-plane ring stretch, and C-O stretch, respectively) [90].

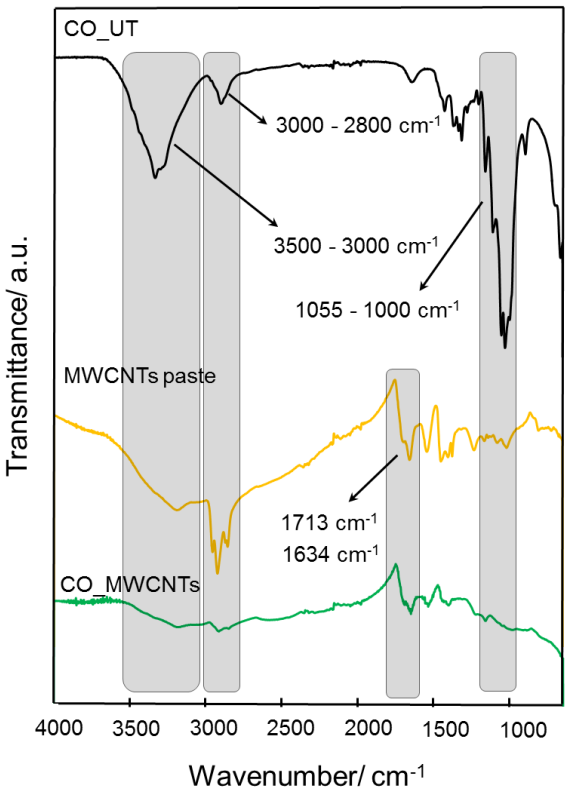

Figure 5: ATR – FTIR spectra of uncoated cotton (black curve), F-MWCNTs paste (yellow curve) and coated cotton (green curve)

3.3.2.2.4 Thermo-gravimetric analysis

The thermo-gravimetric analysis of both uncoated and coated cotton fabrics was performed to obtain information about the thermal properties and stability of coated samples.

TGA analysis in the inert atmosphere was realized starting from F-MWCNTs to obtain information about organic functional groups [91,92] (Figure 6). During the first step of a multistep process, up to 150°C, the evaporation of absorbed water by the F-MWCNTs sample was observed. For temperatures ranging from 150 to 350°C (second step), the decarboxylation of COOH groups occurs, while between 350 and 600°C the degradation of anhydrides and lactones takes place. In the final step, above 600°C, the decomposition of phenols, carboxyl groups, quinones, pyrans, and ethers occurs as confirmed by the weight loss.

The mass loss at 900°C of F-MWCNTs is significantly different from P-MWCNTs one due to the presence of carboxylic, carbonyl and hydroxyl groups in their structure and, as evident from Figure 6, such functionalities make carbon nanotubes more reactive and less stable, thus leading to a weight loss of about 12 wt% compared to the 4 wt% of P-MWCNTs.

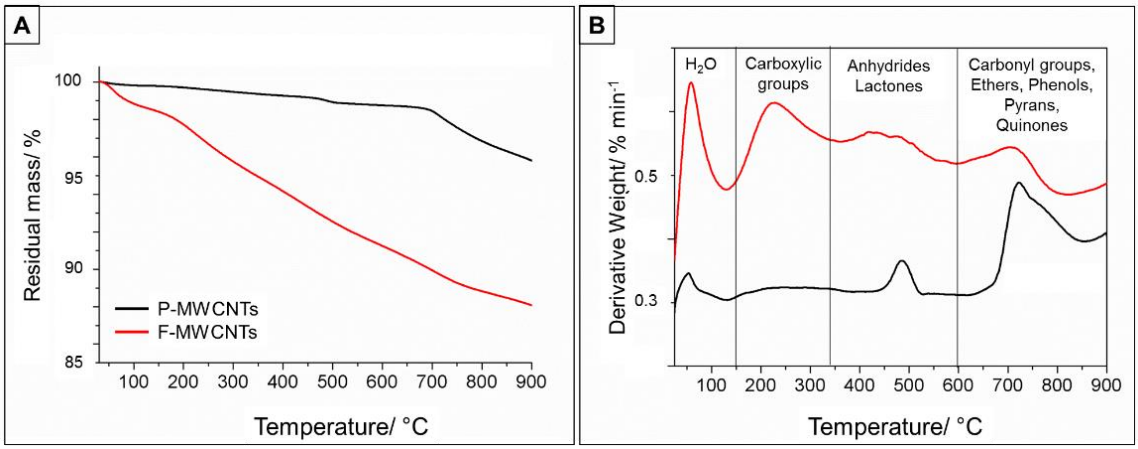

Figure 6: TGA (A) and dTGA (B) of pristine (black curve) and functionalized multiwalled carbon nanotubes. Reproduced under the terms of the Creative Commons CC BY-NC-ND license [8]. Copyright 2017, the Authors, Published by Elsevier

The thermal stability of coated fabrics was studied by TGA analysis in the air atmosphere and compared with the thermal behavior of F-MWCNTs, F-MWCNTs paste and paste without carbon nanotubes. As observable from Figure 7, the F-MWCNTs curve is characterized by a slight weight loss for temperatures lower than 600°C correspondings to the decomposition of surface functional groups, while they completely oxidize between 600 and 800°C in accordance with literature data [93]. On the other hand, a multistep decomposition behavior is observed for both reference paste and F-MWCNTs paste for temperature ranging from 200 to 600°C with a residual mass of 10% attributable

to the inorganic SHP. Moreover, the presence of F-MWCNTs reduces the paste decomposition rate without affecting the range of stability.

Two degradation steps are observed for the uncoated cotton fabric, which also showed a significant weight loss for temperature between 300 and 380°C corresponding to two alternative pathways: (i) the decomposition of glycosyl units to char; (ii) the depolymerization of such units to volatile products containing levoglucosan [94]. The complete oxidation of char occurred in the range of 450 – 520°C. The presence of the coating on cotton fabrics did not provide the first degradation step of cellulose significantly, but it affects the second one by lowering its rate. The residual mass lower than 1% corresponds to the presence of SHP in the coating. So, the presence of F-MWCNTs in the coating paste does not significantly affect the overall thermal stability of the cotton sample even if they induce the start of paste degradation at lower temperatures than the uncoated cotton.

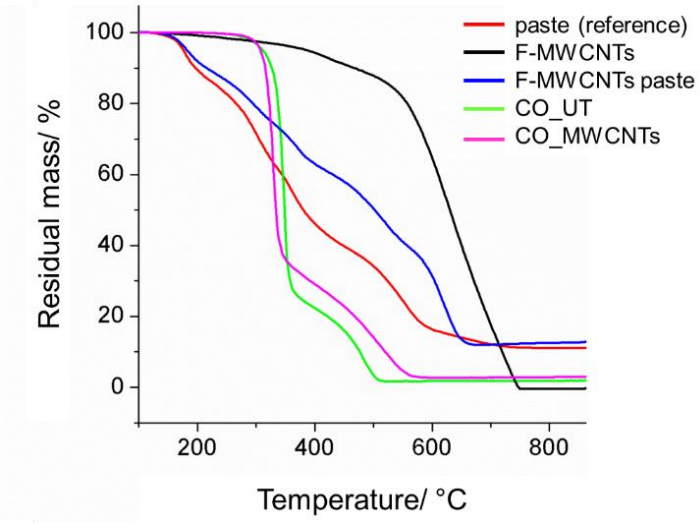

Figure 7: TGA analysis of the reference paste (red curve), functionalized carbon nanotubes (black curve), F-MWCNTs (blue curve), uncoated cotton (green curve) and coated cotton (magenta curve). Reproduced under the terms of the Creative Commons CC BY-NC-ND license [8]. Copyright 2017, the Authors, Published by Elsevier

3.3.2.2.5 Sensing studies

Preliminary resistance measurements were carried out on both uncoated and coated cotton fabrics with the F_MWCNTs paste to assess the electrical conductivity properties and the potential application of the designed fabric as humidity sensors. According to these measurements, the uncoated cotton sample reveals its insulting nature due to the electrical resistance measured over 10 MΩ and so no dependence with temperature and relative humidity percentage (% RH) was observed for this sample. On the other side, the presence of carbon nanotubes-doped coating influences the electrical resistance of the cotton fabrics measured at 1.16 x 10^4 Ω/sq. This behavior could be

explained by taking into account the carbon nanotubes arrangement inside the polymeric matrix, according to which they are tightly electrostatically attached to PVA chains and stacked in a crosslinked and large structure, thus providing the conductivity of the coating.

Many parameters influence the electrical resistance of CNT-based coatings, such as resistance between nanotubes, the resistance between nanotubes and cross-linkers used, the resistance of water absorbed in an established region and many others [95]. Furthermore, the concentration of CNTs, the distance and the swelling (reversible or not) of all components could influence the resistance previously cited and so the resistance of the coating itself.

The chemical composition and the observed electrical properties of the realized coating, together with the already mentioned properties, make possible the employment of the F-MWCNTs coating for humidity sensing. This application is also due to the high density of polar functional groups on both the functionalized carbon nanotubes and the polymeric matrix that makes the coated cotton fabric able to bind water molecules and interact with environmental humidity [95]. The hole transport as like p-type semiconductors affects the interaction of water molecules with F-MWCNTs and thus the resistance variations [96, 97]. In particular, two phenomena, physisorption and chemisorption affect the reversible interaction of carbon nanotubes with gases and so, their sensing properties. Generally, in humidity sensors, the chemisorption of water molecules on the hydroxyl groups present on the outermost coating surface occurs and then such molecules are physisorbed. Depending on the environmental %RH, a certain amount of water molecules can be adsorbed by MWCNTs. The overall resistance of the coated cotton sample was reduced by the physisorbed water layer that also enables charge transport through the sample itself. Furthermore, a strong response of the coating towards water vapors can be deduced by the presence of several carboxylic groups in the carbon nanotube structure according to hydrogen bonding and dipole-dipole interactions, thus increasing their absorption efficiency. The p-type semiconductor behavior of F-MWCNTs was suggested by the increase in the electrical resistance of the coating due to the absorbed water molecules that donate electrons to the valence band thus depleting the concentration of holes in carbon nanotubes.

Furthermore, variations in resistance values are dependent on the swelling of the film generated by few nanometers rearrangements of macromolecules in the coating that affects the nanotubes junctions and so the contact resistance between nanotubes in the matrix. Moreover, when a gap occurs between MWCNTs junctions, electrons characterized by potential energy lower than the gap energy, which consists of a distance between CNTs higher than a few tens of nanometers, cannot move freely around the coating [98]. So, the resistance of the carbon nanotube-doped film is influenced by both phenomena and, more in detail, for higher RH level a higher amount of water molecules are adsorbed

and, as a consequence, a higher number of electrons are transferred by generating the swelling of the coating and finally, the increase of the resistance.

According to these explanations, the obtained coated cotton fabric could be used as a humidity and temperature sensor by evaluating the electrical resistance changes under controlled conditions. With this aim, the surface resistance of coated textile versus both humidity and concomitant temperature variations are reported in Figure 8 in which, each R_s value refers to a combination of % RH and T (°C) in the climatic chamber. As clearly evident, the coated sample shows R_s values similar in the RH range between 55 and 75 %, while these values are strongly dependent on humidity levels above 75 % RH, indeed R_s are almost doubled in the range 75 - 90 %RH.

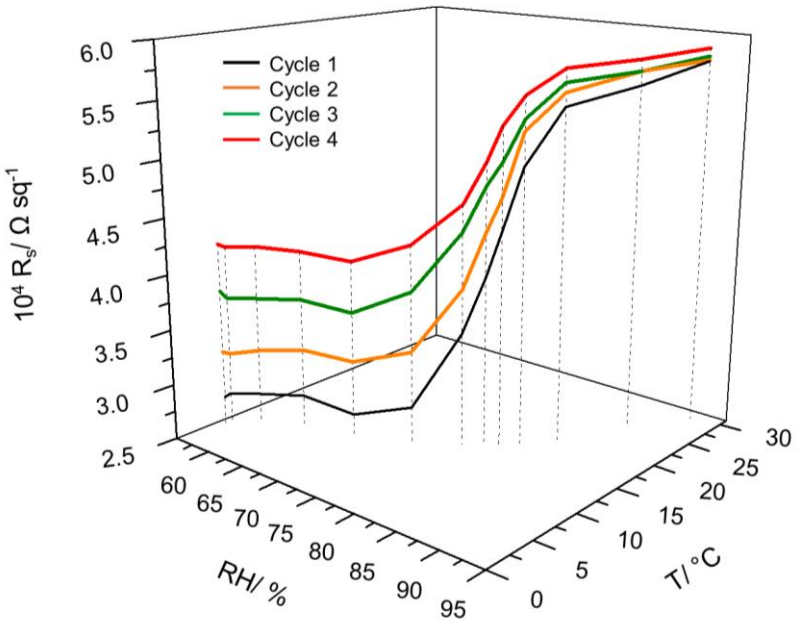

Figure 8: Surface resistance values as a function of relative humidity percentage (RH %) and temperature (°C) at different exposure cycles (1 to 4). Adapted under the terms of the Creative Commons CC BY-NC-ND license [8]. Copyright 2017, the Authors, Published by Elsevier

This trend could be justified by the following explanation: the higher the %RH values, the more water vapor molecules can be physically absorbed into the coating, thus increasing the resistance values. In the studied %RH range, the observed resistance dependence from humidity, and so the decrease of conductivity of the coating, can be due to the adsorption of water molecules that decreases the density of the nanoparticles, causing the coating swelling (Figure 9). Due to the definition of relative humidity, according to which it is the ratio of the partial pressure of water vapor present in the gas, to its saturation vapor pressure, at a given temperature [99], the resistance changes as a function of humidity may also be used as temperature sensing. Indeed, as demonstrated by values reported in

Figure 8, the R_s is not significantly affected by the temperature up to 10 °C, while these resistance values strongly increase with the relative humidity in the temperature range between 10 and 20°C. Moreover, in the studied temperature range, the relative humidity percentage can be directly deduced from the resistance values of the coated cotton.

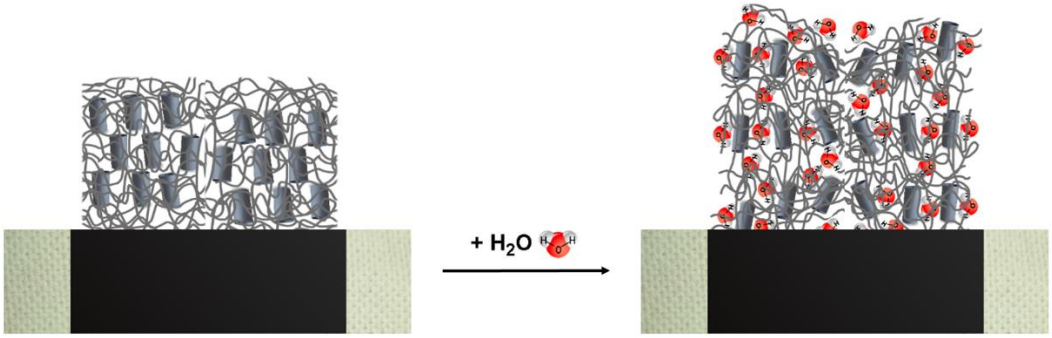

Figure 9: Schematic representation of the coating swelling as a consequence of the RH % increase. Adapted under the terms of the Creative Commons CC BY-NC-ND license [8]. Copyright 2017, the Authors, Published by Elsevier

The designed sensor has shown a clear response-recovery behavior and good repeatability for humidity/temperature sensing. More in detail, the response time of the sensing coating was measured in 4 s, a time shorter than the recovery time estimated in 30 s, as observed for conventional humidity sensors. Resistance measurements were performed for four consecutive cycles, and the sensor showed that both response and recovery times returned to baseline after being exposed to humidity and temperature variation. A sensitivity decrease of about 50% after the last cycle was observed and ascribed to the cotton fabric for its intrinsic properties that largely influence the physisorption of water by both the carbon nanotubes-doped coating and by the cotton fabric itself. Two exponential contributions, characterized by two different time constants, affect the resistance variations. More in detail, the cotton fabric is characterized by a much higher time constant that dominates the response time of the whole system. With the aim of decreasing the response time, no hydrophilic textile fabrics could be employed instead of cotton textiles.

The experimental findings in the humidity range from 60 to 90% demonstrated the potential application of the realized cotton sensor in the microclimate control system in greenhouses for growing plants [100]. In these systems, water stress could be generated for %RH lower than 60, while serious problems, like the rapid development of fungus diseases, can occur if the humidity values are greater than 95 %RH.

3.3.2.3 Conclusions

According to a simple synthetic strategy, oxidized MWCNTs were used for the realization of a nanostructured coating for textile applications in sensing fields. The obtained coated textiles were characterized by flexibility and less-resistance properties than uncoated cotton, making them attractive in the realization of flexible electronics compared to conventional rigid materials. The developed coating is characterized by good homogeneity and alignment of CNTs, further preserving their conductive properties. Indeed, the functionalization of carbon nanotubes led to improved dispersion of CNTs in the polymer matrix, otherwise not possible through the employed chemical precursors, thus allowing the useful contact points between tubes for the maintenance of their electrical properties. For these features, the conductive coating was tested as a sensitive element for the development of environmental humidity and temperature sensors by evaluating its resistance variations.

With this aim, a circuit mask was printed on a cotton sample with quite good precisions, and the obtained coated textiles confirm the potential employment as flexible, adaptable material in the realization of innovative and wearable sensors. In the future, further investigations will be carried out to assess the washing fastness of the CNT-doped coating and the reversibility of the sensing performances.

3.3.3 Carbon nanotubes-based conductive textiles for heart rate monitoring

Essential components of wearable sensors are represented by signal transmission elements and control units, functions that can be performed by conductive fabrics. For this reason, the integration of electronics components with textiles is an important challenge that has aroused the interest of the scientific community. Further, the development of wearable sensors for several applications was simplified by integrating electronic devices with conductive textiles with several advantages, particularly in the health monitoring field. Thanks to the flexibility and comfort of fabrics, smart textiles are attracting for the design of wearable health monitoring devices compared to the conventional bulk counterpart.

Health monitoring is of great interest for the detection of biomedical signals in several application fields, among which medical, fitness and sports ones are the most representative. In particular, heart rate monitoring (HRM) is employed for the evaluation of exercise intensity in sport and training as well as to avoid the effect of overtraining [95]. On the other hand, HRM is used to assess the patients' conditions in healthcare quickly. In particular, the evaluation of heart rate is simple compared with other techniques as well as cheap and adaptable to several situations. Examples of HRM refer to large

instruments in the 1900s until wearable devices (such as watches) of recent years. In this regard, several athletes widely use HRM to monitor their training and plan the intensity.

Heart rate (HR) is measured by devices consisting of electrocardiogram (ECG), but an attractive and non-invasive optical technique for the same kind of evaluation is photoplethysmography (PPG). Not only HR can be evaluated according to it but also other clinical parameters, such as heart rate variability, cardiac output, oxygen saturation, endothelial functions, arterial compliance, and many others [101].

In the research study described in the following paragraphs, wearable CNT-conductive strips were built to realize a signal transmission element for application in the PPG technique for assessing HRM [63]. Very long and no-functionalized carbon nanotubes, previously synthesized through chemical vapor deposition (CVD) [102], were mixed with an amino-functionalized sol-gel precursor (EDAES), a thermo-degradable surfactant (Invadine PBN©) and a polyurethane thickener with the aim of both preserving their high aspect ratio and electrical properties, and of obtaining a paste to spread on cotton fabrics.

The designed conductive fabrics were characterized according to different chemical-physical techniques to assess the coating chemical structure, morphology, and in particular, to evaluate the electrical properties of the CNT-based coatings and eventually changes in textiles comfort after treatment. More in detail, the tested electrical properties of the CNT-based textiles ensure their employment as a signal transmission element in the PPG technique for heart rhythm monitoring.

3.3.3.1 Experimental part

As already explained in Chapter 2, VACNTs with two different lengths (1.5 mm and 3.0 mm, sample s-CNTs and l-CNTs, respectively) were synthesized according to the CVD technique [103–105] and employed in this research study for the development of CNT-conductive textiles for heart rate monitoring.

The conductive coatings were synthesized by following the below procedure, in which both carbon nanotubes are generically named CNTs.

A low amount of CNTs (0.2 mg/ml, 0.5 mg) was separately mixed with EDAES (68 μl) and Ethanol (132 μl) under vigorous stirring. Then, both mixtures were added with Invadine® PBN until reaching the final volume of 2.5 ml and further stirred and ultrasonicated for at least 2 h. As the last synthetic step, a suitable amount of thickener CT (291 mg) was added to both CNT dispersions, thus obtaining two viscous pastes (s-CNT_paste and l-CNT_paste) [8]. In Scheme 5, a schematic representation of the synthetic strategy is provided.

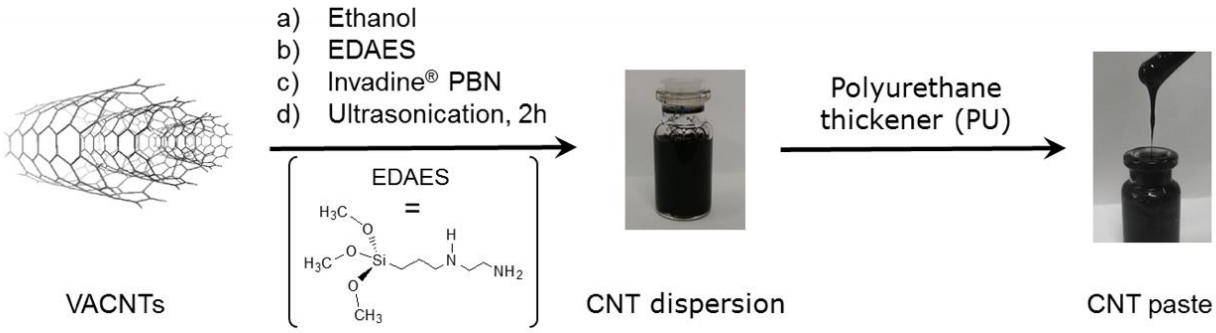

Scheme 5: Schematic representation of the synthetic strategy employed for the dispersion of carbon nanotubes and development of the CNT paste

To evaluate the stability of both CNT dispersions, they were left for 48 h without stirring. After this time, no sign of agglomeration was observed, so both s-CNT_paste and l-CNT_paste have been applied separately on cotton fabrics by knife-over-roll technique as described in Chapter 2: the treated samples (CO_s and CO_l, respectively) were dried (70 °C for 5 minutes) after each layer deposition and finally cured 120°C for 2 minutes (Scheme 6).

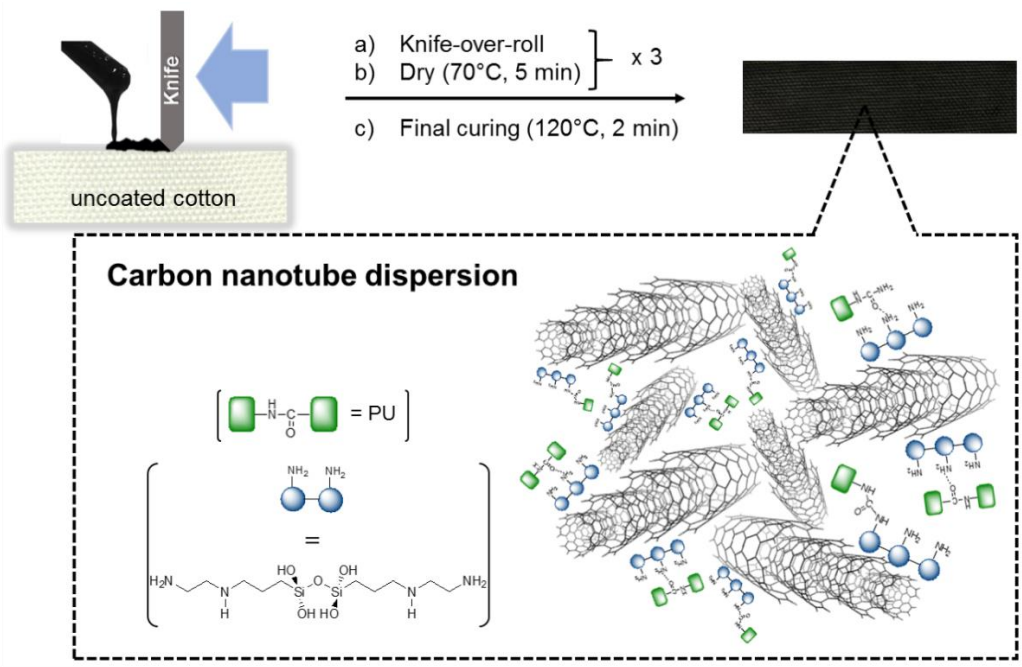

Scheme 6: Schematic representation of the coating deposition on cotton fabrics according to the knife-over-roll technique and mechanism of CNT dispersion into the coating. Adapted under the terms of the Creative Commons CC BY-NC-ND license [63]. Copyright 2019, the Authors, Published by Elsevier

3.3.3.2 Results and discussions

In this paragraph, results and discussion of characterization analyses will be provided and scheduled depending on the chemical-physical technique employed.

3.3.3.2.1 Morphological studies

Before studying the morphology of the uncoated and coated cotton samples, this kind of study was performed on VACNTs employed for the realization of conductive pastes. With this aim, both CNTs were dispersed in ethanol solution to obtain HRTEM images (Figure 10), which evidenced the presence of two and four walls in sample s-CNT and l-CNT, respectively. More in detail, images show outside diameters of approximatively 7 nm and 10 nm for sample s-CNTs and l-CNTs, respectively. These two diameters are due to the different growth duration (30 mins and 60 mins, respectively) performed for both CNT samples [106] that also lead to two different nanotubes lengths, 1.5 mm and 3.0 mm for sample s-CNT and l-CNT, respectively.

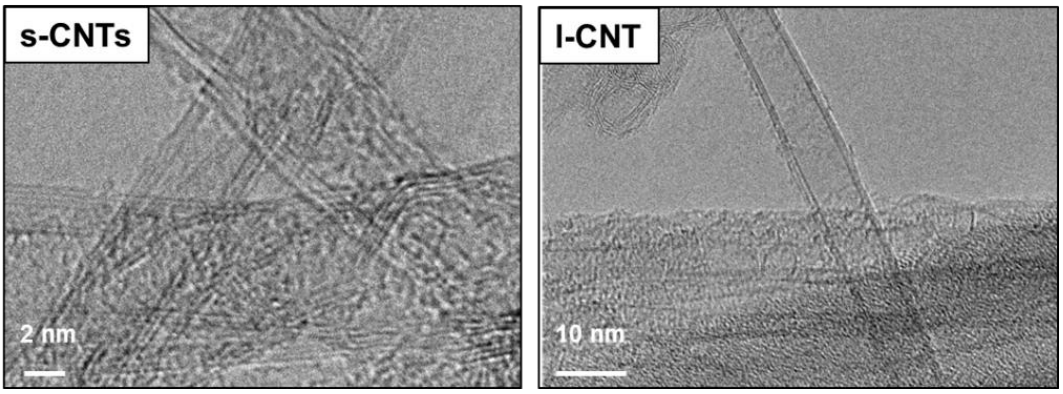

Figure 10: HRTEM images of s-CNTs and l-CNTs characterized by 1.5 mm and 3.0 mm length, respectively. Adapted under the terms of the Creative Commons CC BY-NC-ND license [63]. Copyright 2019, the Authors, Published by Elsevier

The morphology of textiles coated with the two CNT pastes was studied according to HRSEM analysis (Figure 11). HRSEM images at different magnifications of CO_s and CO_l evidenced the complete degree of coverage of the smooth cotton surfaces by CNT pastes. The same images highlight the morphology of the deposited films, which results rough and, as expected for the presence of CNTs, made up by several "microfibers". The distribution of CNTs and coatings was evaluated through higher magnification HRSEM images (Figure 11): nanotubes appear well dispersed in both pastes and the latter homogeneously distributed on the cotton surface.

Depending on the observed morphological features of treated cotton samples, a high mutual interconnection between CNTs is expected and, as a consequence, coatings with good electrical conductivity.

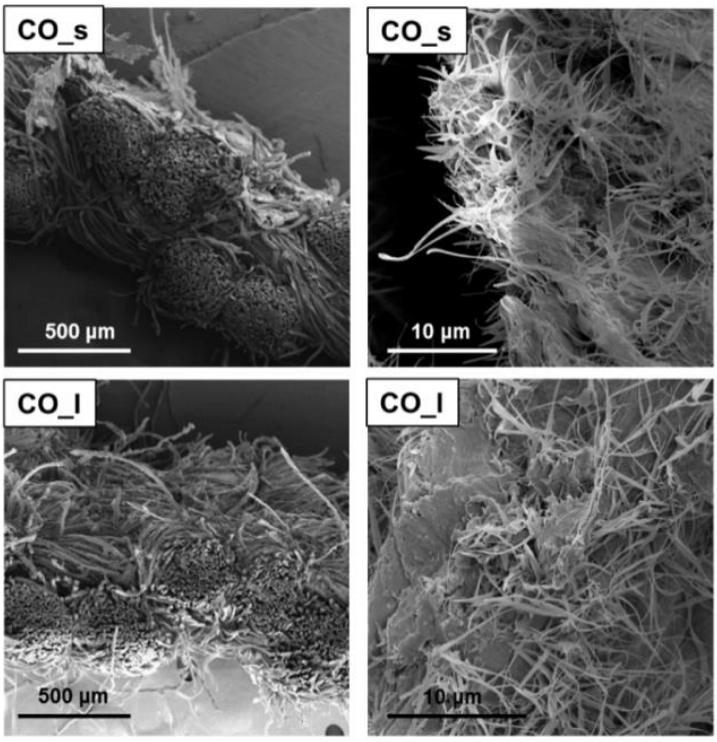

Figure 11: HRSEM images of cotton fabrics coated with s-CNT paste (above) and with l-CNT (below) at different magnifications

3.3.3.2.2 ATR-FTIR analysis

As already explained in Chapter 2, before analyzing uncoated and coated cotton fabrics through FTIR spectroscopy, the same characterization has been conducted on the xerogel of both s-CNT paste and l-CNT_paste to study the chemical composition of both films. Spectra of synthesized films, uncoated (CO_UT) and coated cotton fabrics (CO_s and CO_l) are reported in Figure 12 to investigate and confirm the presence of each CNT paste on the surface of cotton fabrics. All these spectra were expressed in absorbance and, more in detail, spectra of cotton samples were reported after normalization at 1202 cm^{-1}.

From the curve of uncoated cotton (Figure 12, black curve), it is possible to observe the main absorption bands of cellulose [107], previously summarized in Table 3. Many of these bands result overlapped by FTIR peaks of CNT coatings, as evidenced in Figure 12. Such differences distinctly consist in the presence of the CNT coatings on cotton surfaces and are referred to C=O stretching of urethane groups and its interaction with N-H groups (1725 and 1693 cm^{-1}, respectively), C-N

stretching and N-H bending (1537 cm^{-1}), CH_2 and CH_3 bending (1466 cm^{-1} and 1342 cm^{-1}), C-N stretching (1279 and 1240 cm^{-1}), C-H bending (841 cm^{-1}) and N-H bending (769 cm^{-1}) [108, 109]. Moreover, the NH stretching bands of both polyurethane thickener and EDAES overlap the OH stretching peaks of cellulose. Similarly, both the C-H stretching and the bands between 1400 – 800 cm^{-1} of cellulose result increased due to the sum effect of the C-H stretching of the polyurethane thickener.

An interesting evaluation can be made from the FTIR curves of both CNT pastes. Indeed, these spectra reveal a different profile than those of coated textiles. The most evident difference is referred to the C=O stretching consisting of a unique and split in two transmittance bands for the paste containing the longer and the shorter CNTs, respectively. The former, the peaks at 1698 cm^{-1}, can be assigned to the formation of urea linkages between the polyurethane thickener and EDAES, while the FTIR split in two of coating containing the shorter CNTs is assigned to carbonyl groups of free urethane (1726 cm^{-1}) and the coordination of some C=O to NH groups via hydrogen bonding (1712 cm^{-1}) [108, 110], (Figure 12, yellow curve on the left). In both curves of CNT pastes, the presence of the sol-gel matrix is confirmed by the unique observable peak referred to the Si-O-Si symmetric stretching (810 cm^{-1}). Other peaks of sol-gel matrix or absorption bands of CNTs are not visible in both coatings due to the masking effect of the polyurethane thickener that is characterized by highly intense bands.

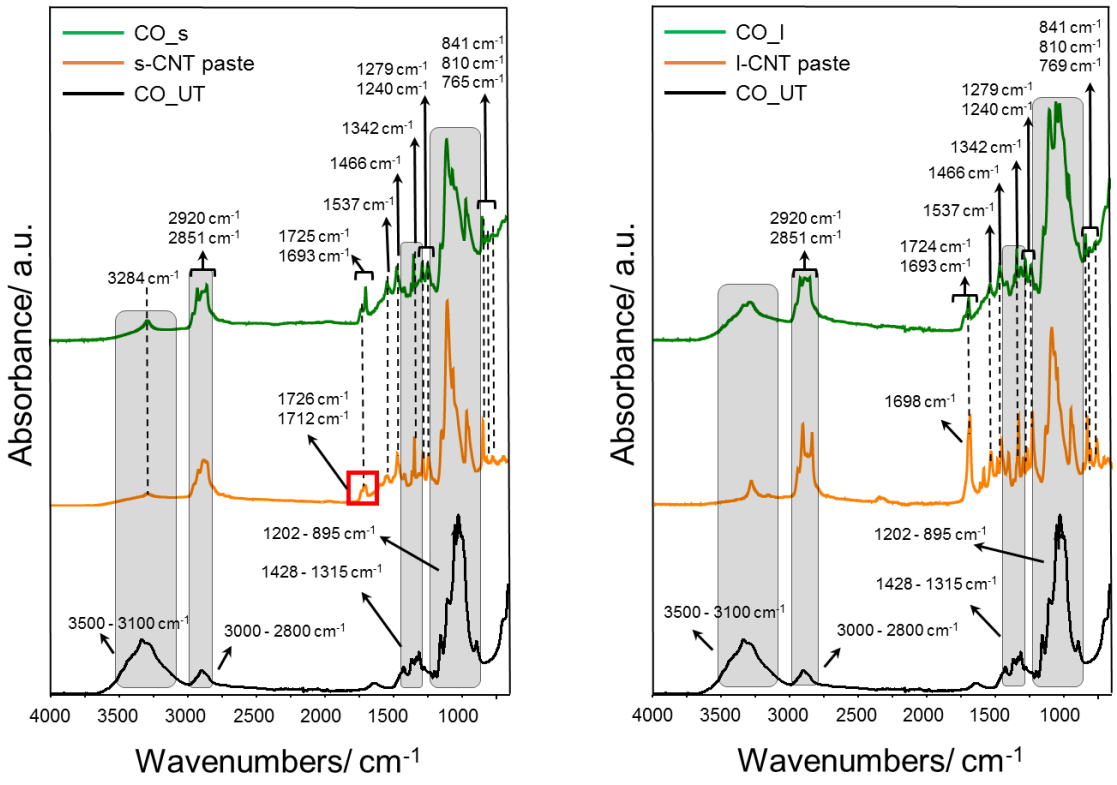

Figure 12: ATR -FTIR spectra of uncoated cotton (black curve), s-CNTs paste (yellow curve on the left), l-CNTs paste (yellow curve on the right) and cotton fabrics coated with both s-CNTs paste (green curve on the left) and l-CNTs paste (green curve on the right)). Adapted under the terms of the Creative Commons CC BY-NC-ND license [63]. Copyright 2019, the Authors, Published by Elsevier

3.3.3.2.3 Dispersion mechanism of CNTs in the polymeric coating

According to the experimental findings from both morphological and FTIR characterizations, it was possible to suppose and discuss the dispersion mechanism of both CNTs in the polymeric coatings. The first evaluation can be done by choice of precursors. Indeed amino-terminated silane represents a versatile and easy way for obtaining homogeneous dispersion based on sol-gel technology.

The chosen sol-gel precursor monomer can diffuse in gaps among bounded CNTs during the hydrolysis step, and a silica matrix on the nanotubes surfaces is formed by the hydrolyzed ethoxide groups of EDAES [111]. More in detail, through the absorption peak assigned to the Si-O-Si network (810 cm^{-1}), it was possible to confirm the condensation of precursor silanols and so the formation of a self-assembled silica network monolayer on CNT surfaces, promoted during the curing process of both coatings.

For pH< ca. 10.5, the protonation of NH_2 groups occurs [112], and such positively charged amine groups of EDAES can be considered aligned away from the underlying CNT surfaces, thus generating

a Coulombic charge repulsion among functionalized nanotubes, finally resulting in a well-dispersed sol (Scheme 6).

Furthermore, both the waterborne wetting agent and the polyurethane thickener were specifically chosen. The former was employed to improve the uniformity in the distribution of CNTs into the polymeric matrix. This high-performance wetting agent, thanks to its chemical composition consisting of a mixture of ethoxylated aliphatic ether-alcohols and ethoxylated fatty alcohols, can disperse CNTs efficiently, without altering the interconnection between them. Acting as a thermo-degradable anionic surfactant, it does not leave any residue after curing, thus not interfering with CNT connections and so with their electrical conductivity. So, thanks to its capability, employing the thermo-degradable surfactant, it was possible to disperse CNTs avoiding the addition of further solvents and, as a consequence, to use a low percolation threshold, thus preserving the electrical properties of carbon nanotubes [113]. Moreover, to address the latter point, a gentle-bath sonication (up to 2h) was used during coatings synthesis to preserve the aspect ratio of nanotubes.

As observed before, HRSEM images show homogeneous coatings on the surface of treated cotton fabrics characterized by a well-distribution of CNTs inside it due to the combination of both amino-functionalized sol-gel precursor thermo-degradable surfactant.

Finally, the polyurethane thickener was specifically chosen for its capability to react with amine functionalities of sol-gel precursor through urethane moieties to form urea linkages, as confirmed by the FTIR band at 1698 cm^{-1}, and for its emulsifying and adhesive properties.

3.3.3.2.4 Surface resistance measurement and electrical properties of CNT coatings

To study the conductive properties of CNT coatings, surface resistance measurements of the treated cotton samples were carried out, and the results are showed in this paragraph.

Before analyzing such results, a brief explanation of an important parameter to be controlled in the evaluation of the electrical conductivity of CNT polymer coatings, the percolation limit of CNTs, is provided. This parameter refers to the minimum content of nanotubes needed to obtain a conductive network that spans the whole system [114–116]. It is influenced by several parameters, among which: the typology of nanotubes (if single or double-walled), their nature (depending on the ratio of amorphous carbon or of metallic/semi-metallic tubes), aspect ratio (length/diameter), morphology and dispersion degree in a polymer matrix [117]. In this research study, only the influence of the CNT length on the electrical conductivity of the composite was investigated as a parameter of the percolation threshold.

According to literature, carbon nanotubes featuring a high aspect ratio, well dispersed in a polymer matrix, are more suitable than those with a low aspect ratio for the realization of conductive materials due to their higher electrical conductivity provided by the lower number of contacts needed to reach percolation [113, 118, 119]. The conductivity of a CNT coating is strictly affected by the CNTs length since it exists an inverse proportionality between aspect ratio and percolation limit. In literature, both the increase and the decrease in percolation threshold with increasing CNT length are reported [120–123].

The CNTs employed in this research study are characterized by a high aspect ratio (about $2 \cdot 10^5$ and $3 \cdot 10^5$ for s-CNTs and l-CNTs, respectively), and this feature makes them attractive for the realization of conductive coating with a low percolation threshold in the range between 0.0025 – 4 wt% [124]. Preliminary laboratory tests establish the percolation limit of both CNTs at 0.14 w/w %, in agreement with literature data referred to conductive composite realized with CNTs with high aspect ratio [120, 125, 126].

Electrical resistance measurements conducted on both coated cotton samples (CO_s and CO_l) were used to calculate the average surface resistance ($\overline{R}_s$) obtaining $9.46 \cdot 10^2$ Ω/sq and $2.61 \cdot 10^4$ Ω/sq for CO_s and CO_l, respectively.

Contrary to the extremely high resistance of uncoated cotton, which exceeds the full range of the instruments (>10 MΩ), the average resistance values of both coated samples promise good electrical conductivity. The electrical properties observed for coated textiles highlight the capability of synthesized coatings, characterized by low amounts of CNTs, to make insulator fabrics conductive thanks to the formation of a highly continuous CNT network [127].

Parameters such as CNT dispersion, length reduction, damage, density, adhesion, and cohesion, influence the sheet resistance of CNT pastes [128]. Due to the capability of CNTs to percolate through insulating fabrics, it is possible to employ electrical resistance to study the dispersion of nanotubes in a polymeric paste. Contrary to literature data [118, 125] that report higher electrical conductivity of CNT composite for longer CNT, in this research study, shorter nanotubes provided the more conductive electrical polymeric composite, thus measuring lower resistance values for CO_s.

This behavior was investigated by considering the dispersion of CNT in the polymeric matrix because this parameter is considered the main factor controlling the electrical percolation when the CNT aspect ratio is greater than 100 [126].

Below, digital images of s-CNT paste and l-CNT paste are reported with the aim of investigating the CNT distribution within both coatings at the macroscale (Figure 13). As evident, according to van der Waals interactions, bundles of nanotubes are formed and appear as “sticks” randomly oriented

inside the polymer matrix. The electrical behavior of such conductive sticks should be described according to the percolation theory of their random distribution [129].

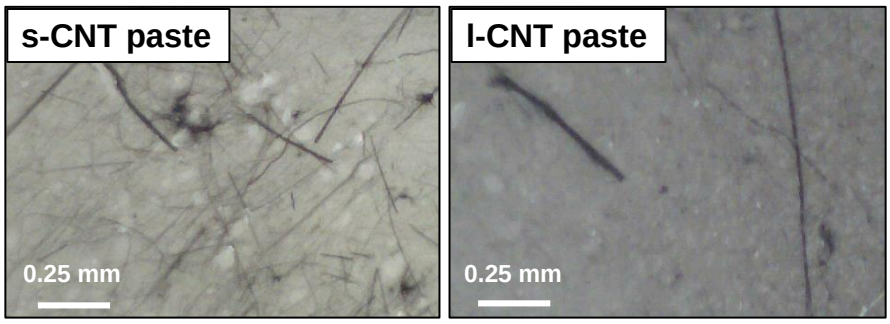

Figure 13: Optical images of pastes containing shorter (s-CNT paste) and longer (l-CNT paste) carbon nanotubes

More in detail, s-CNT, thanks to their lower tube length, which contributes to preventing re-aggregation [130], are organized in bundles highly interconnected between them, resulting in a uniform nanotube distribution and a high number of electric contact points. On the other hand, l-CNT, due to their higher tube length, provide a high number of van der Waals interactions and, as a consequence, a high degree of aggregation between them that results in an evident non-uniform distribution of tubes.

These observations and explanations are in agreement with the measured resistance values of coated fabrics: the shorter CNTs, thanks to the high number of electric contact points, provide higher electrical conductivity than that shown by the coating containing the longer CNTs.

3.3.3.2.5 Evaluation of coatings adhesion

Among several properties, the adhesion of the conductive coating on textile fabrics represents an essential property of E-textiles. To test the adhesion of both CNT coatings on cotton fabrics, the coated textiles underwent one washing cycle by following the standard described in Chapter 2 using only distilled water. Understandably, the stress of washing cycles can damage the coating, thus affecting its integrity and continuity by increasing its sheet resistance. The effects of the laundry cycle were evaluated through resistance measurements to assess any influences on the electroconductive properties of coated fabrics. The surface resistance values were confirmed after one washing cycle for the CO_s sample, while the cotton coated with l-CNT paste reveals R_s value almost doubled.

According to these experimental findings, the longer carbon nanotubes can not stably interact within the coating, thus providing leaching after washing.

3.3.3.2.6 Evaluation of the stiffness of the CNT-based conductive textiles

The physical properties of cotton materials could be altered or influenced by the CNT conductive coating on their surface. As a representative characteristic of these physical properties, the stiffness was studied because it exhibits particular sensitivity for the presence of the coating layer, and it could be considered an index of textile comfort. The coating is expected to alter the mobility of textile fibers, thus providing a higher stiffness of the coated fabrics. Generally, a slight increase in stiffness was measured for coated samples compared to uncoated materials (reference sample). The stiffness was measured in terms of bending length and according to the standard described in Chapter 2 (DIN 53362:1970). The sample length to achieve the bending angle of 41.58 was touched at 55 mm and 60 mm for CO_s and CO_l, respectively. On the contrary, such length for the reference sample was 50 mm.

According to these results, the stiffness of both CO_s and CO_l was not significantly affected by the presence of the coatings.

3.3.3.2.7 Evaluation of conductive properties of coated textiles in PPG analysis

PPG technique was employed for the evaluation of five volunteers' heart rhythm according to the setup described in Chapter 2, and results are reported in Figure 14.

The PPG signal obtained using commercial metal wires as elements of electrical signal transmission, compared with that obtained by substituting the metal wires with the CNT-cotton strips is reported in Figure 14a and 14b, respectively. The comparison between the first two graphs reveals that the realized conductive textiles are reliable in the detection of both systolic and diastolic peaks, thus providing a quite similar signal to that obtained by the use of metal wires. Interesting information can be obtained from the amplitude of systolic peaks that are strictly related to pulsatile changes in blood volume caused by arterial blood flow around the measurements site [131, 132]. In this regard, in Figure 14c, a Premature Ventricular Contraction (PVC) is shown in the PPG plot, and it refers to an irregular beat because of the interruption of the normal heart rhythm. PVC is felt like a "flip-flop" or "missed beats" in the chest [132].

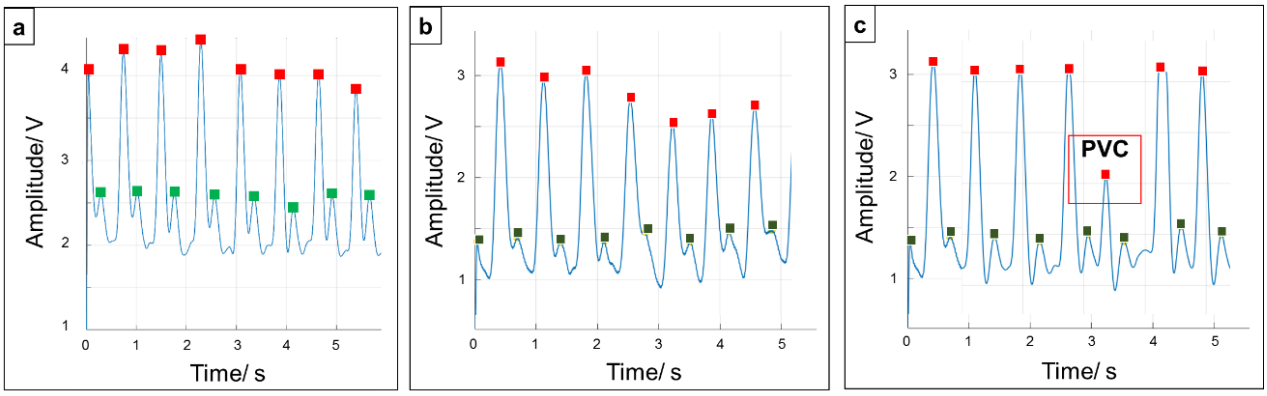

Figure 14: PPG signal obtained by using commercial metal wires (a), CNT-cotton strips as elements of signal transmission and referred to a normal heart rhythm (b) and an abnormal heart rhythm (c)

Both the normal and abnormal heart rate data collected (Figure 14b and 14c, respectively) confirm the potentiality of the carbon nanotubes coated textiles in the PPG technique thanks to their reliability in the transmission of acquired signals by optoelectronic system, clearly distinguishing between systolic and diastolic peaks and evidencing variation even in the systolic peaks in PVC.

3.3.3.3 Conclusions

In the synthetic strategy designed for the realization of homogeneous and stable CNT-coatings for biomedical signal transmission in the PPG system, the simultaneous employment of EDAES and the thermo-degradable surfactant led to a homogeneous distribution of nanotubes in the coatings without interfering with the electrical properties of CNTs. Indeed, experimental findings demonstrated the formation of a conductive-CNT network firmly linked, which made the originally insulating cotton fabric electrically conductive. The presence of these coatings on cotton fabrics did not significantly affect the samples comfort. In particular, a correlation was found between the aspect ratio and the decrease in electrical resistance: at the value of percolation, the shorter nanotubes have proven to be able to make the treated fabric more conductive, showing a value of $9.46 \cdot 10^2$ Ω/sq, while the surface resistance of the longer ones was $2.61 \cdot 10^4$ Ω/sq. The surface resistance obtained for both samples demonstrated the effect of the no-functionalized high aspect ratio tubes in low concentration on the conduction properties of a polymer matrix. Due to the influence of parameters like length and functionalization of carbon nanotubes on the conduction properties of CNT-doped coatings, future studies will be developed on the effect of the chemical functionalization of high aspect ratio carbon nanotubes on conduction properties.

The developed CNT-cotton strips revealed reliability in the transmission of electrical signals for heart rate long-term monitoring by providing a signal reasonably fitted with that obtained from the use of commercial metal wires.

Moreover, further investigations will be carried out to assess the durability of the coatings after several washing cycles and the potentially harmful effects of the released nanotubes on human health. Coated textiles were found to make the transmission of biomedical data reliable and efficient for the development of wearable smart textiles for sports, healthcare, and military applications, also due to their properties consisting of comfort and non-invasive compared to the conventional conductive systems in long term monitoring applications.

3.4 Development of prototypes: “ELECT”

As described in Chapter 2, "ELECT" (Figure 15) is a smart textile obtained by the integration of ELEctro ConducTive carbon nanotubes tracks with an electronic device developed for real-time monitoring of heart rate through ECG and suitable for several kinds of clothing. The conductive tracks, as well as electrodes, made through the sol-gel technology, can transmit electrical signals thanks to the presence of CNTs. For ECG measurements, the cardiac electrical signals are amplified and digitized through an Analog Front End. Afterwards, the signals are processed for transmission or storage on the onboard memory. The system is powered by a rechargeable Lithium polymer battery. Using a specific app communicating through a standard Bluetooth Serial Port Profile (SPP), it is possible to display the collected data simply and rapidly. "ELECT", thanks to the advantages deriving from the printing technique used for the deposition of conductive tracks (which maintains the flexibility of the treated fabric) and to the miniaturization of the integrated electronics, can be used comfortably and straightforwardly in wellness, healthcare, medical and fitness fields for remote cardiac real-time monitoring in a non-invasive way.

Figure 15: “ELECT”, smart textile for the heart rate monitoring through ECG

References

1. Rosace G (2015) Radiation protection finishes for textiles. In: Functional Finishes for Textiles. Elsevier, pp 487–512
2. Smith WC (2010) Overview of textile coating and lamination. In: Smith WC (ed) Smart textile coatings and laminates. Woodhead Publishing Limited, pp 3–9
3. Stoppa M, Chiolerio A (2014) Wearable Electronics and Smart Textiles: A Critical Review. Sensors 14:11957–11992. https://doi.org/10.3390/s140711957
4. Review AC, Heo JS, Eom J, et al (2018) Recent Progress of Textile-Based Wearable Electronics : and Applications. 1703034:1–16. https://doi.org/10.1002/smll.201703034
5. Tao X (2001) Smart technology for textiles and clothing - introduction and overview. In: Tao X (ed) Smart fibres, fabrics and clothing. Woodhead Publishing Limited, pp 1–6
6. Li Z, Luo G, Wei F, Huang Y (2006) Microstructure of carbon nanotubes/PET conductive composites fibers and their properties. Compos Sci Technol 66:1022–1029. https://doi.org/10.1016/j.compscitech.2005.08.006
7. Giovanelli D, Farella E (2016) Force Sensing Resistor and Evaluation of Technology for Wearable Body Pressure Sensing. J Sensors 2016:1–13. https://doi.org/10.1155/2016/9391850
8. Rosace G, Trovato V, Colleoni C, et al (2017) Structural and morphological characterizations of MWCNT s hybrid coating onto cotton fabric as potential humidity and temperature wearable sensor. Sensors Actuators B Chem 252:428–439. https://doi.org/10.1016/j.snb.2017.05.175
9. Castano LM, Flatau AB (2014) Smart fabric sensors and e-textile technologies: a review. Smart Mater Struct 23:053001. https://doi.org/10.1088/0964-1726/23/5/053001
10. Atwa Y, Maheshwari N, Goldthorpe IA (2015) Silver nanowire coated threads for electrically conductive textiles. J Mater Chem C 3:3908–3912. https://doi.org/10.1039/C5TC00380F
11. Zhang Y, Dong A, Wang Q, et al (2014) Conductive Cotton Prepared by Polyaniline In Situ Polymerization Using Laccase. Appl Biochem Biotechnol 174:820–831. https://doi.org/10.1007/s12010-014-1094-9
12. Iwai Y, Sameshima S, Yonezawa S, Katayama S (2015) Fabrication of conductive cotton by electroless plating method with supercritical carbon dioxide. J Supercrit Fluids 100:46–51. https://doi.org/10.1016/j.supflu.2015.02.027

13. Jiang SQ, Newton E, Yuen CWM, Kan CW (2006) Chemical Silver Plating on Cotton and Polyester Fabrics and its Application on Fabric Design. Text Res J 76:57–65. https://doi.org/10.1177/0040517506053827
14. Parsons GN, Atanasov SE, Dandley EC, et al (2013) Mechanisms and reactions during atomic layer deposition on polymers. Coord Chem Rev 257:3323–3331. https://doi.org/10.1016/j.ccr.2013.07.001
15. Wallace GG, Campbell TE, Innis PC (2007) Putting function into fashion: Organic conducting polymer fibres and textiles. Fibers Polym 8:135–142. https://doi.org/10.1007/BF02875782
16. Grancarić AM, Jerković I, Koncar V, et al (2018) Conductive polymers for smart textile applications. J Ind Text 48:612–642. https://doi.org/10.1177/1528083717699368
17. Tamburri E, Orlanducci S, Toschi F, et al (2009) Growth mechanisms, morphology, and electroactivity of PEDOT layers produced by electrochemical routes in aqueous medium. Synth Met 159:406–414. https://doi.org/10.1016/j.synthmet.2008.10.014
18. Benhamou SM, Hamouni M (2014) Determination of reflection loss, absorption loss, internal reflection and shielding effectiveness of a double electromagnetic shield of conductive polymer. J Mater Environ Sci 5:1982–1987
19. Balint R, Cassidy NJ, Cartmell SH (2014) Conductive polymers: Towards a smart biomaterial for tissue engineering. Acta Biomater 10:2341–2353. https://doi.org/10.1016/j.actbio.2014.02.015
20. Ala O, Fan Q (2009) Applications of Conducting Polymers in Electronic Textiles. Res J Text Appar 13:51–68. https://doi.org/10.1108/RJTA-13-04-2009-B007
21. Bajgar V, Penhaker M, Martinková L, et al (2016) Cotton Fabric Coated with Conducting Polymers and its Application in Monitoring of Carnivorous Plant Response. Sensors 16:498. https://doi.org/10.3390/s16040498
22. Ding Y, Invernale MA, Sotzing GA (2010) Conductivity Trends of PEDOT-PSS Impregnated Fabric and the Effect of Conductivity on Electrochromic Textile. ACS Appl Mater Interfaces 2:1588–1593. https://doi.org/10.1021/am100036n
23. Cochrane C, Koncar V, Lewandowski M, Dufour C (2007) Design and Development of a Flexible Strain Sensor for Textile Structures Based on a Conductive Polymer Composite. Sensors 7:473–492. https://doi.org/10.3390/s7040473
24. Cristian I, Nauman S, Cochrane C, Koncar V (2011) Electro-Conductive sensors and heating elements based on conductive polymer composites in woven fabric structures. In: Vassiliadis S (ed) Advances in Modern Woven Fabrics Technology. InTech, pp 3–22

25. Kim BC, Ko JM, Wallace GG (2008) A novel capacitor material based on Nafion-doped polypyrrole. J Power Sources 177:665–668. https://doi.org/10.1016/j.jpowsour.2007.11.078
26. Li Y, Wang S, Zhang Y, Zhang Y (2005) Electrical properties and morphology of polypropylene/epoxy/glass fiber composites filled with carbon black. J Appl Polym Sci 98:1142–1149. https://doi.org/10.1002/app.22105
27. Harel Y, Azoubel S, Magdassi S, Lellouche J-P (2013) A dispersability study on poly(thiophen-3-yl-acetic acid) and PEDOT multi-walled carbon nanotube composites using an analytical centrifuge. J Colloid Interface Sci 390:62–69. https://doi.org/10.1016/j.jcis.2012.09.006
28. Wang H, Zhou H, Gestos A, et al (2013) Robust, electro-conductive, self-healing superamphiphobic fabric prepared by one-step vapour-phase polymerisation of poly(3,4-ethylenedioxythiophene) in the presence of fluorinated decyl polyhedral oligomeric silsesquioxane and fluorinated alkyl silane. Soft Matter 9:277–282. https://doi.org/10.1039/C2SM26871J
29. Safarova V, Gregr J (2010) Electrical Conductivity Measurement of Fibers and Yarns. 7th Int Conf 2–9
30. Diamond D, Coyle S, Scarmagnani S, Hayes J (2008) Wireless Sensor Networks and Chemo-/Biosensing. Chem Rev 108:652–679. https://doi.org/10.1021/cr0681187
31. Xue P, Park KH, Tao XM, et al (2007) Electrically conductive yarns based on PVA/carbon nanotubes. Compos Struct 78:271–277. https://doi.org/10.1016/j.compstruct.2005.10.016
32. Kaushik V, Lee J, Hong J, et al (2015) Textile-Based Electronic Components for Energy Applications: Principles, Problems, and Perspective. Nanomaterials 5:1493–1531. https://doi.org/10.3390/nano5031493
33. Baćani M, Babić D, Novak M, et al (2009) Equilibrium doping of polyaniline by dodecylbenzenesulfonic acid. Synth Met 159:2584–2589. https://doi.org/10.1016/j.synthmet.2009.09.016
34. Gan X, Wu Y, Liu L, et al (2008) Electroless plating of Cu–Ni–P alloy on PET fabrics and effect of plating parameters on the properties of conductive fabrics. J Alloys Compd 455:308–313. https://doi.org/10.1016/j.jallcom.2007.01.054
35. Knittel D, Schollmeyer E (2009) Electrically high-conductive textiles. Synth Met 159:1433–1437. https://doi.org/10.1016/j.synthmet.2009.03.021

36. Jerkovic I (2015) E-glass/polypropylene sensor yarns developed by roll to roll coating procedure. In: Proceedings of the 5th ITMC International Conference, Casablanca & Marrakesh, Morocco
37. Takamatsu S, Lonjaret T, Crisp D, et al (2015) Direct patterning of organic conductors on knitted textiles for long-term electrocardiography. Sci Rep 5:15003. https://doi.org/10.1038/srep15003
38. Yang Y-L, Chuang M-C, Lou S-L, Wang J (2010) Thick-film textile-based amperometric sensors and biosensors. Analyst 135:1230. https://doi.org/10.1039/b926339j
39. Ledet EH, D'Lima D, Westerhoff P, et al (2012) Implantable Sensor Technology: From Research to Clinical Practice. J Am Acad Orthop Surg 20:383–392. https://doi.org/10.5435/JAAOS-20-06-383
40. Postolache G, Carvalho H, Catarino A, Postolache OA (2017) Smart Clothes for Rehabilitation Context: Technical and Technological Issues. pp 185–219
41. Van Langenhove L (2007) Smart textiles for medicine and healthcare: materials, systems and applications. Woodhead Publishing
42. Carvalho H, Catarino AP, Rocha A, Postolache O (2014) Health monitoring using textile sensors and electrodes: An overview and integration of technologies. In: 2014 IEEE International Symposium on Medical Measurements and Applications (MeMeA). IEEE, pp 1–6
43. Paul G, Torah R, Beeby S, Tudor J (2014) The development of screen printed conductive networks on textiles for biopotential monitoring applications. Sensors Actuators A Phys 206:35–41. https://doi.org/10.1016/j.sna.2013.11.026
44. Wallace GG, Steele J, Innes P, et al (2001) Sensors in fabrics with audio feedback: A training tool for enhanced performance and rehabilitation
45. Binkley PF, Frontera W, Standaert DG, Stein J (2003) Predicting the potential of wearable technology. IEEE Eng Med Biol Mag 22:23–27. https://doi.org/10.1109/MEMB.2003.1213623
46. Park S, Mackenzie K, Jayaraman S (2002) The wearable motherboard. In: Proceedings of the 39th conference on Design automation - DAC '02. ACM Press, New York, New York, USA, p 170
47. Rossi D De, Carpi F, Lorussi F, et al (2003) Electroactive Fabrics and Wearable Biomonitoring Devices. 3:3–8

48. Shim BS, Chen W, Doty C, et al (2008) Smart electronic yarns and wearable fabrics for human biomonitoring made by carbon nanotube coating with polyelectrolytes. Nano Lett 8:4151–4157. https://doi.org/10.1021/nl801495p
49. Liu Y, Wang X, Qi K, Xin JH (2008) Functionalization of cotton with carbon nanotubes. J Mater Chem 18:3454. https://doi.org/10.1039/b801849a
50. Spitalsky Z, Tasis D, Papagelis K, Galiotis C (2010) Carbon nanotube-polymer composites: Chemistry, processing, mechanical and electrical properties. Prog Polym Sci 35:357–401. https://doi.org/10.1016/j.progpolymsci.2009.09.003
51. Biju V (2014) Chemical modifications and bioconjugate reactions of nanomaterials for sensing, imaging, drug delivery and therapy. Chem Soc Rev 43:744–764. https://doi.org/10.1039/C3CS60273G
52. Caruso A, Sinicropi MS, Lancelot J-C, et al (2014) Synthesis and evaluation of cytotoxic activities of new guanidines derived from carbazoles. Bioorg Med Chem Lett 24:467–472. https://doi.org/10.1016/j.bmcl.2013.12.047
53. Saturnino C, Caruso A, Longo P, et al (2015) Crystallographic Study and Biological Evaluation of 1,4-dimethyl-N-alkylcarbazoles†. Curr Top Med Chem 15:973–979. https://doi.org/10.2174/1568026615666150317222444
54. Paredes JI, Burghard M (2004) Dispersions of Individual Single-Walled Carbon Nanotubes of High Length. Langmuir 20:5149–5152. https://doi.org/10.1021/la049831z
55. Babooram K, Narain R (2009) Fabrication of SWNT/Silica Composites by the Sol−Gel Process. ACS Appl Mater Interfaces 1:181–186. https://doi.org/10.1021/am8001296
56. Mondal S, Hu JL (2007) A novel approach to excellent UV protecting cotton fabric with functionalized MWNT containing water vapor permeable PU coating. J Appl Polym Sci 103:3370–3376. https://doi.org/10.1002/app.25437
57. Li G, Wang H, Zheng H, Bai R (2010) A facile approach for the fabrication of highly stable superhydrophobic cotton fabric with multi-walled carbon nanotubes-azide polymer composites. Langmuir 26:7529–7534. https://doi.org/10.1021/la904337z
58. Byrne MT, Gun'ko YK (2010) Recent Advances in Research on Carbon Nanotube-Polymer Composites. Adv Mater 22:1672–1688. https://doi.org/10.1002/adma.200901545
59. Tsionsky M, Gun G, Glezer V, Lev O (1994) Sol-Gel-Derived Ceramic-Carbon Composite Electrodes: Introduction and Scope of Applications. Anal Chem 66:1747–1753. https://doi.org/10.1021/ac00082a024

60. Sampath S, Lev O (1996) Inert Metal-Modified, Composite Ceramic−Carbon, Amperometric Biosensors: Renewable, Controlled Reactive Layer. Anal Chem 68:2015–2021. https://doi.org/10.1021/ac951094b
61. del Mar Cordero-Rando M, Hidalgo-Hidalgo de Cisneros JL, Blanco E, Naranjo-Rodríguez I (2002) The Sonogel-Carbon Electrode As a Sol−Gel Graphite-Based Electrode. Anal Chem 74:2423–2427. https://doi.org/10.1021/ac010782u
62. Bottini M, Tautz L, Huynh H, et al (2005) Covalent decoration of multi-walled carbon nanotubes with silica nanoparticles. Chem Commun 758. https://doi.org/10.1039/b412876a
63. Trovato V, Teblum E, Kostikov Y, et al (2020) Sol-gel approach to incorporate millimeter-long carbon nanotubes into fabrics for the development of electrical-conductive textiles. Mater Chem Phys 240:122218. https://doi.org/10.1016/j.matchemphys.2019.122218
64. Kathi J, Rhee KY (2008) Surface modification of multi-walled carbon nanotubes using 3-aminopropyltriethoxysilane. J Mater Sci 43:33–37. https://doi.org/10.1007/s10853-007-2209-2
65. Hoenlein W, Kreupl F, Duesberg GS, et al (2003) Carbon nanotubes for microelectronics: status and future prospects. Mater Sci Eng C 23:663–669. https://doi.org/10.1016/j.msec.2003.09.153
66. Kataura H, Kumazawa Y, Maniwa Y, et al (1999) Optical properties of single-wall carbon nanotubes. Synth Met 103:2555–2558. https://doi.org/10.1016/S0379-6779(98)00278-1
67. Berber S, Kwon Y-K, Tománek D (2000) Unusually High Thermal Conductivity of Carbon Nanotubes. Phys Rev Lett 84:4613–4616. https://doi.org/10.1103/PhysRevLett.84.4613
68. Tong T, Zhao Y, Delzeit L, et al (2007) Dense Vertically Aligned Multiwalled Carbon Nanotube Arrays as Thermal Interface Materials. IEEE Trans Components Packag Technol 30:92–100. https://doi.org/10.1109/TCAPT.2007.892079
69. Coleman JN, Khan U, Blau WJ, Gun'ko YK (2006) Small but strong: A review of the mechanical properties of carbon nanotube–polymer composites. Carbon N Y 44:1624–1652. https://doi.org/10.1016/j.carbon.2006.02.038
70. Bernholc J, Brenner D, Buongiorno Nardelli M, et al (2002) Mechanical and Electrical Properties of Nanotubes. Annu Rev Mater Res 32:347–375. https://doi.org/10.1146/annurev.matsci.32.112601.134925
71. Baughman RH (2002) Carbon Nanotubes--the Route Toward Applications. Science (80-) 297:787–792. https://doi.org/10.1126/science.1060928
72. Li HJ, Lu WG, Li JJ, et al (2005) Multichannel Ballistic Transport in Multiwall Carbon Nanotubes. Phys Rev Lett 95:086601. https://doi.org/10.1103/PhysRevLett.95.086601

73. Naeemi A, Meindl JD (2007) Design and Performance Modeling for Single-Walled Carbon Nanotubes as Local, Semiglobal, and Global Interconnects in Gigascale Integrated Systems. IEEE Trans Electron Devices 54:26–37. https://doi.org/10.1109/TED.2006.887210
74. Avouris P, Appenzeller J, Martel R, Wind SJ (2003) Carbon nanotube electronics. Proc IEEE 9:1772–1784. https://doi.org/10.1109/JPROC.2003.818338
75. Avouris P (2002) Molecular Electronics with Carbon Nanotubes. Acc Chem Res 35:1026–1034. https://doi.org/10.1021/ar010152e
76. Thostenson ET, Ren Z, Chou T-W (2001) Advances in the science and technology of carbon nanotubes and their composites: a review. Compos Sci Technol 61:1899–1912. https://doi.org/10.1016/S0266-3538(01)00094-X
77. Pop E, Mann D, Wang Q, et al (2006) Thermal Conductance of an Individual Single-Wall Carbon Nanotube above Room Temperature. Nano Lett 6:96–100. https://doi.org/10.1021/nl052145f
78. Liu L, Ye X, Wu K, et al (2009) Humidity Sensitivity of Multi-Walled Carbon Nanotube Networks Deposited by Dielectrophoresis. Sensors 9:1714–1721. https://doi.org/10.3390/s90301714
79. Trovato V, Teblum E, Kostikov Y, et al (2021) Electrically conductive cotton fabric coatings developed by silica sol-gel precursors doped with surfactant-aided dispersion of vertically aligned carbon nanotubes fillers in organic solvent-free aqueous solution. J Colloid Interface Sci 586:120–134. https://doi.org/10.1016/j.jcis.2020.10.076
80. Daoud WA, Xin JH, Szeto YS (2005) Polyethylenedioxythiophene coatings for humidity, temperature and strain sensing polyamide fibers. Sensors Actuators B Chem 109:329–333. https://doi.org/10.1016/j.snb.2004.12.067
81. Donato MG, Galvagno S, Lanza M, et al (2009) Influence of carbon source and Fe-catalyst support on the growth of multi-walled carbon nanotubes. J Nanosci Nanotechnol 9:3815–3823. https://doi.org/10.1166/jnn.2009.NS73
82. Milone C, Hameed a RS, Piperopoulos E, et al (2011) Catalytic Wet Air Oxidation of p-Coumaric Acid over Carbon Nanotubes and Activated Carbon. Ind Eng Chem Res 50:9043–9053. https://doi.org/Doi 10.1021/Ie200492g
83. Carvalho RA, Maria TMC, Moraes ICF, et al (2009) Study of some physical properties of biodegradable films based on blends of gelatin and poly(vinyl alcohol) using a response-surface methodology. Mater Sci Eng C 29:485–491. https://doi.org/10.1016/j.msec.2008.08.030

84. Alimohammadi F, Parvinzadeh Gashti M, Shamei A (2013) Functional cellulose fibers via polycarboxylic acid/carbon nanotube composite coating. J Coatings Technol Res 10:123–132. https://doi.org/10.1007/s11998-012-9429-3

85. Alimohammadi F, Gashti MP, Shamei A (2012) A novel method for coating of carbon nanotube on cellulose fiber using 1,2,3,4-butanetetracarboxylic acid as a cross-linking agent. Prog Org Coatings 74:470–478. https://doi.org/10.1016/j.porgcoat.2012.01.012

86. de Lannoy CF, Jassby D, Davis DD, Wiesner MR (2012) A highly electrically conductive polymer-multiwalled carbon nanotube nanocomposite membrane. J Memb Sci 415–416:718–724. https://doi.org/10.1016/j.memsci.2012.05.061

87. Trovato V, Rosace G, Colleoni C, et al (2018) Carbon nanotubes textile coating for the development of wearable sensors. In: 2018 7th International Conference on Modern Circuits and Systems Technologies (MOCAST). IEEE, pp 1–4

88. Rosace G, Guido E, Colleoni C, et al (2017) Halochromic resorufin-GPTMS hybrid sol-gel: Chemical-physical properties and use as pH sensor fabric coating. Sensors Actuators B Chem 241:85–95. https://doi.org/10.1016/j.snb.2016.10.038

89. Pistone A, Piperno A, Iannazzo D, et al (2013) Fe_3O_4–MWCNTPhCOOH composites for ammonia resistive sensors. Sensors Actuators B Chem 186:333–342. https://doi.org/10.1016/j.snb.2013.06.027

90. Chung C, Lee M, Choe EK (2004) Characterization of cotton fabric scouring by FT-IR ATR spectroscopy. Carbohydr Polym 58:417–420. https://doi.org/10.1016/j.carbpol.2004.08.005

91. Pistone A, Ferlazzo A, Lanza M, et al (2012) Morphological Modification of MWCNT Functionalized with HNO3/H2SO4 Mixtures. J Nanosci Nanotechnol 12:5054–5060. https://doi.org/10.1166/jnn.2012.4928

92. Villa A, Plebani M, Schiavoni M, et al (2012) Tuning hydrophilic properties of carbon nanotubes: A challenge for enhancing selectivity in Pd catalyzed alcohol oxidation. Catal Today 186:76–82. https://doi.org/10.1016/j.cattod.2011.09.041

93. Santangelo S, Messina G, Faggio G, et al (2011) Evaluation of crystalline perfection degree of multi-walled carbon nanotubes: correlations between thermal kinetic analysis and micro-Raman spectroscopy. J Raman Spectrosc 42:593–602. https://doi.org/10.1002/jrs.2766

94. Alongi J, Colleoni C, Rosace G, Malucelli G (2012) Thermal and fire stability of cotton fabrics coated with hybrid phosphorus-doped silica films. J Therm Anal Calorim 110:1207–1216. https://doi.org/10.1007/s10973-011-2142-0

95. Yoo K-P, Lim L-T, Min N-K, et al (2010) Novel resistive-type humidity sensor based on multiwall carbon nanotube/polyimide composite films. Sensors Actuators B Chem 145:120–125. https://doi.org/10.1016/j.snb.2009.11.041
96. Liu L, Ye X, Wu K, et al (2009) Humidity Sensitivity of Carbon Nanotube and Poly (Dimethyldiallylammonium Chloride) Composite Films. IEEE Sens J 9:1308–1314. https://doi.org/10.1109/JSEN.2009.2030381
97. Varghese OK, Kichambre PD, Gong D, et al (2001) Gas sensing characteristics of multi-wall carbon nanotubes. Sensors Actuators B Chem 81:32–41
98. Zamborini FP, Leopold MC, Hicks JF, et al (2002) Electron Hopping Conductivity and Vapor Sensing Properties of Flexible Network Polymer Films of Metal Nanoparticles. J Am Chem Soc 124:8958–8964. https://doi.org/10.1021/ja025965s
99. Chen Z, Lu C (2005) Humidity Sensors: A Review of Materials and Mechanisms. Sens Lett 3:274–295. https://doi.org/10.1166/sl.2005.045
100. Garcia-Mier L, Jimenez-Garcia SN, Chapa-Oliver AM, et al (2014) Strategies for sustainable plant food production: facing in the current agricultural challenges-agriculture for today and tomorrow. In: Guevara-Gonzalez R, Torres-Pacheco I (eds) Biosystems Engineering: Biofactories for food production in the century XXI. Springer International Publishing, pp 1–50
101. Achten J, Jeukendrup AE (2003) Heart Rate Monitoring. Sport Med 33:517–538. https://doi.org/10.2165/00007256-200333070-00004
102. Nessim GD (2010) Properties, synthesis, and growth mechanisms of carbon nanotubes with special focus on thermal chemical vapor deposition. Nanoscale 2:1306. https://doi.org/10.1039/b9nr00427k
103. Teblum E, Itzhak A, Shawat-Avraham E, et al (2016) Differential preheating of hydrocarbon decomposition and water vapor formation shows that single ring aromatic hydrocarbons enhance vertically aligned carbon nanotubes growth. Carbon N Y 109:727–736. https://doi.org/10.1016/j.carbon.2016.08.086
104. Nessim GD, Seita M, O'Brien KP, et al (2009) Low Temperature Synthesis of Vertically Aligned Carbon Nanotubes with Electrical Contact to Metallic Substrates Enabled by Thermal Decomposition of the Carbon Feedstock. Nano Lett 9:3398–3405. https://doi.org/10.1021/nl900675d

105. Nessim GD, Al-Obeidi A, Grisaru H, et al (2012) Synthesis of tall carpets of vertically aligned carbon nanotubes by in situ generation of water vapor through preheating of added oxygen. Carbon N Y 50:4002–4009. https://doi.org/10.1016/j.carbon.2012.04.043
106. Nessim GD, Hart AJ, Kim JS, et al (2008) Tuning of Vertically-Aligned Carbon Nanotube Diameter and Areal Density through Catalyst Pre-Treatment. Nano Lett 8:3587–3593. https://doi.org/10.1021/nl801437c
107. Schramm C, Rinderer B (2015) Non-formaldehyde, crease-resistant modification of cellulosic material by means of an organotrialkoxysilane and metal alkoxides. Cellulose 22:2811–2824. https://doi.org/10.1007/s10570-015-0664-5
108. Ruanpan S, Manuspiya H (2018) Synthesized amino-functionalized porous clay heterostructure as an effective thickener in waterborne polyurethane hybrid adhesives for lamination processes. Int J Adhes Adhes 80:66–75. https://doi.org/10.1016/j.ijadhadh.2017.10.005
109. Mishra AK, Chattopadhyay DK, Sreedhar B, Raju KVSN (2006) FT-IR and XPS studies of polyurethane-urea-imide coatings. Prog Org Coatings 55:231–243. https://doi.org/10.1016/j.porgcoat.2005.11.007
110. Queiroz DP, de Pinho MN, Dias C (2003) ATR−FTIR Studies of Poly(propylene oxide)/Polybutadiene Bi-Soft Segment Urethane/Urea Membranes. Macromolecules 36:4195–4200. https://doi.org/10.1021/ma034032t
111. Hemraj-Benny T, Wong SS (2006) Silylation of Single-Walled Carbon Nanotubes. Chem Mater 18:4827–4839. https://doi.org/10.1021/cm061185x
112. Bharathi S, Fishelson N, Lev O (1999) Direct Synthesis and Characterization of Gold and Other Noble Metal Nanodispersions in Sol−Gel-Derived Organically Modified Silicates. Langmuir 15:1929–1937. https://doi.org/10.1021/la980490x
113. Backes EH, Sene TS, Passador FR, Pessan LA (2017) Electrical, Thermal and Mechanical Properties of Epoxy/CNT/Calcium Carbonate Nanocomposites. Mater Res 21:e20170801. https://doi.org/10.1590/1980-5373-mr-2017-0801
114. Dietrich S, Amnon A (1994) Introduction to Percolation Theory. Taylor & Francis
115. Torquato S (2002) Motivation and Overview. In: Random Heterogeneous Materials: Microstructure and Macroscopic Properties. Springer-Verlag, New York, pp 1–19
116. Kyrylyuk A V., van der Schoot P (2008) Continuum percolation of carbon nanotubes in polymeric and colloidal media. Proc Natl Acad Sci 105:8221–8226. https://doi.org/10.1073/pnas.0711449105

117. Aguilar JO, Bautista-Quijano JR, Aviles F (2010) Influence of carbon nanotube clustering on the electrical conductivity of polymer composite films. Express Polym Lett 4:292–299. https://doi.org/10.3144/expresspolymlett.2010.37

118. Ayatollahi MR, Shadlou S, Shokrieh MM, Chitsazzadeh M (2011) Effect of multi-walled carbon nanotube aspect ratio on mechanical and electrical properties of epoxy-based nanocomposites. Polym Test 30:548–556. https://doi.org/10.1016/j.polymertesting.2011.04.008

119. Russ M, Rahatekar SS, Koziol K, et al (2013) Length-dependent electrical and thermal properties of carbon nanotube-loaded epoxy nanocomposites. Compos Sci Technol 81:42–47. https://doi.org/10.1016/j.compscitech.2013.03.011

120. Bauhofer W, Kovacs JZ (2009) A review and analysis of electrical percolation in carbon nanotube polymer composites. Compos Sci Technol 69:1486–1498. https://doi.org/10.1016/j.compscitech.2008.06.018

121. Celzard A, McRae E, Deleuze C, et al (1996) Critical concentration in percolating systems containing a high-aspect-ratio filler. Phys Rev B 53:6209–6214. https://doi.org/10.1103/PhysRevB.53.6209

122. Bai JB, Allaoui A (2003) Effect of the length and the aggregate size of MWNTs on the improvement efficiency of the mechanical and electrical properties of nanocomposites—experimental investigation. Compos Part A Appl Sci Manuf 34:689–694. https://doi.org/10.1016/S1359-835X(03)00140-4

123. Martin CA, Sandler JKW, Shaffer MSP, et al (2004) Formation of percolating networks in multi-wall carbon-nanotube–epoxy composites. Compos Sci Technol 64:2309–2316. https://doi.org/10.1016/j.compscitech.2004.01.025

124. Lisunova MO, Mamunya YP, Lebovka NI, Melezhyk AV (2007) Percolation behaviour of ultrahigh molecular weight polyethylene/multi-walled carbon nanotubes composites. Eur Polym J 43:949–958. https://doi.org/10.1016/j.eurpolymj.2006.12.015

125. Singh BP, Saini K, Choudhary V, et al (2014) Effect of length of carbon nanotubes on electromagnetic interference shielding and mechanical properties of their reinforced epoxy composites. J Nanoparticle Res 16:2161. https://doi.org/10.1007/s11051-013-2161-9

126. Li J, Ma PC, Chow WS, et al (2007) Correlations between Percolation Threshold, Dispersion State, and Aspect Ratio of Carbon Nanotubes. Adv Funct Mater 17:3207–3215. https://doi.org/10.1002/adfm.200700065

127. Shrivastava NK, Khatua BB (2011) Development of electrical conductivity with minimum possible percolation threshold in multi-wall carbon nanotube/polystyrene composites. Carbon N Y 49:4571–4579. https://doi.org/10.1016/j.carbon.2011.06.070
128. Floweri O, Kim J, Seo Y, et al (2015) Characterisation of carbon nanotube pastes for field emission using their sheet resistances. Appl Surf Sci 353:54–62. https://doi.org/10.1016/j.apsusc.2015.05.188
129. Hu L, Hecht DS, Grüner G (2004) Percolation in Transparent and Conducting Carbon Nanotube Networks. Nano Lett 4:2513–2517. https://doi.org/10.1021/nl048435y
130. Huang YY, Terentjev EM (2012) Dispersion of Carbon Nanotubes: Mixing, Sonication, Stabilization, and Composite Properties. Polymers (Basel) 4:275–295. https://doi.org/10.3390/polym4010275
131. Asada HH, Shaltis P, Reisner A, et al (2003) Mobile monitoring with wearable photoplethysmographic biosensors. IEEE Eng Med Biol Mag 22:28–40. https://doi.org/10.1109/MEMB.2003.1213624
132. Chua CP, Heneghan C (2006) Continuous Blood Pressure Monitoring using ECG and Finger Photoplethysmogram. In: 2006 International Conference of the IEEE Engineering in Medicine and Biology Society. IEEE, pp 5117–5120

Chapter 4. Halochromic textiles

In this chapter, two scientific research for the development of halochromic textiles to monitor human sweat pH are deeply reported. Before describing the experimental part and discussing the main results, an introduction dealing with optical sensors, halochromic fabrics, and the main technologies employed for their development will be provided. Materials, general methods, and instrumentations for characterizations were previously reported in Chapter 2.

The research on halochromic textiles for human sweat pH monitoring by grafting of nitrazine yellow through glycidyl methacrylate on cotton fabrics was realized with the valuable contribution of Prof. G. Rosace, Dr. M. R. Plutino, Dr. A. Vitali, Prof. A. Ferri, Prof. P. Bongiovanni.
The research on halochromic textiles for human sweat pH monitoring by sol-gel immobilization of alizarin red S on cotton and polyester fabrics was realized with the valuable contribution of Prof. G. Rosace, Dr. M. R. Plutino, Dr. A. Mezzi.
"Health Belt" was realized with the valuable contribution of Prof. V. Re, Prof. G. Rosace and Dr. A. Pedrana.

Part of this chapter was published on:

- *Trovato V, Vitale A, Bongiovanni R, et al (2021) Development of a Nitrazine Yellow-glycidyl methacrylate coating onto cotton fabric through thermal-induced radical polymerization reactions: a simple approach towards wearable pH sensors applications. Cellulose. https://doi.org/10.1007/s10570-021-03733-w*

4.1 Introduction

Several application fields, among which environmental, food monitoring, biomedical or biotechnological arouse advantages from the use of pH-sensors able to provide information about different processes and how to explain them [1–3]. In recent years, the development of intelligent textiles able to detect the pH of several microenvironments (both in environmental and biomedical fields) was of significant importance for the definition of both acidic or alkaline conditions to monitor the degree of pollution or for diagnostic or medical tests [4, 5] among many examples. An attractive application deals with the detection and monitoring of sweat pH because of the chemical and biological composition of human sweat that allows obtaining information about health status, thanks to the investigation of the body hydration level of both patients and athletes.

Potentiometric and amperometric systems are the first examples of pH-sensors that often suffered drift and instability and sometimes needed constant recalibrations [6]. Conversely, the design of fabrics acting as optical pH sensors through the immobilization of pH sensing dye in the textile structure and the integration of an optoelectronic circuit are of great interest because such systems can overcome the already mentioned disadvantages of conventional pH sensors.

Generally, optical sensors are chemical sensors in which electromagnetic radiation generates an analytical signal in a transduction element. The change of specific optical parameters is used to evaluate the interaction of radiation with the sample, which is related to the concentration of a specific analyte [7]. The main components of optical chemical sensors are generally a sensing element (e.g., indicator dye) and a transduction component. The sensing element gives an optical signal proportional to the magnitude of a specific parameter (e.g., concentration of an analyte). It usually consists of a thin layer able to interact with the analyte itself through catalyzing a reaction or participating in the chemical equilibrium with the analyte. The optical signal obtained by the sensing element is further converted and processed (e.g., amplification, filtering, recording) into a measurable signal [7–9].

Optical principles like fluorescence, luminescence, reflectance, and absorbance are at the base of optical sensors. Through these kinds of sensors, it is possible to investigate a wide range of the spectral region, UV, Visible, and Near Infrared (NIR) and to measure the intensity of light and other properties (lifetime, scattering, diffraction, refractive index, polarization) [10].

As already mentioned, optical pH sensors are characterized by several advantages compared to conventional electrochemical pH electrodes. Indeed, they feature a longer lifetime, selectivity, sensitivity, low-cost, fast and reversible response, safety, ease of miniaturization, mechanical robustness, high photostability, high extinction coefficient, proper pK_a [11], no suffering from electromagnetic interference, no needing of reference cells. Moreover, they are characterized by a high signal-to-noise ratio (SNR), thus allowing their employment for analyses with a single control instrument at a central site [12–14].

Besides the disadvantages, optical pH sensors suffer from interferences or intrinsic nature of the components because, as examples, both ambient light and some sweat components could influence the long-term stability (e.g., leaching or photobleaching of the indicator dye) and the selectivity of the sensors itself. Moreover, to ensure an analytical signal, the mass transfer of the analyte from the sample into the indicator is necessary [11].

Several approaches are available to develop optical pH sensors and, the immobilization of an indicator dyestuff on a fabric surface allows obtaining robust and reversible optical sensors. Generally, the indicator dye is immobilized into a polymer matrix that should ensure the proton diffusion (it should

be hydrophilic) and should be thermally, chemically and mechanically stable. Among several techniques aimed at immobilizing an indicator into a polymer matrix, the sol-gel method and the grafting copolymerization are interesting routes with lower environmental effects than conventional approaches [15]. The sol-gel technique could provide some limiting factors, such as the molecule diffusion into the dried silica xerogel that leads to longer response times and the covalent dye immobilization that reduces the dye sensitivity. However, this approach, as well as grafting co-polymerization, represent efficient and straightforward ways to realize optical pH sensors.

4.2 Chromic and halochromic textiles

Due to the increasing attention received in the last years, chromic materials that reversibly change color depending on external stimuli have been widely investigated [16]. Several examples are common in daily life, such as photochromic lenses for spectacles or thermochromic temperature indicators [17]. Textiles-based chromic materials are nowadays innovative with high potentiality in sensor fields thanks to the optical, easily detectable, and non-destructive signal they can provide.

Depending on the external stimulus nature leading to the color variation, chromism is classified as photochromism (color change induced by light), thermochromism (color change induced by heat), ionochromism (color change induced by ions) [18]. Among the latter cited, the halochromic materials (or textiles-based) are of great interest because they change color depending on pH variations, thus providing several applications like protective clothing, medical bandages, sportswear, and many others [18]. Moreover, the interest in halochromic textiles over the conventional optical pH sensors is also due to their advantages coming from the technology employed for their realization, the indicator dye involved, and in particular from their substrate, the textile fabric, which further provides a wide range of advantages over the use of conventional materials. In the following paragraphs, an overview of the importance of human sweat pH-monitoring, the most important approaches used for the development of halochromic textile-based sensors will be described.

4.2.1 Human sweat pH

The importance of halochromic textile-based sensors derives from the wide range of information that can be obtained from monitoring the human sweat pH, water pH [19, 20], and soil pH [21, 22].

In particular, the human sweat pH is relevant for the assessment of several pathologies, and by monitoring it in real-time during physical activities, it is possible to evaluate the body hydration level and define approaches for rehydration and re-mineralization.

Human sweat pH ranging from 2 to 8.2, with an average value of 5.3 and, at least 61 different chemical constituents have been identified in its composition [23]. The composition and concentration of each component are strictly related with body region, age, diet, activity level [24–28], gender [24, 29], season, degree of acclimation, and sampling technique [30]. Human sweat is composed of 99.0 – 99.5% of water and 0.5 - 1.0% of solids (half organic and half inorganic), and main components are primary electrolytes, ionic constituents, organic acids and carbohydrates, amino acids, nitrogen substances, vitamins, and miscellaneous constituents. In Table 4, the most relevant components for each mentioned class are reported.

Thanks to its chemical composition, the human sweat pH can be correlated to the health status and level of hydration or mineralization of the human body. In particular, the detection of the Sodium electrolyte is important for the relationship between body pH and its concentration in the body itself [25, 31]. Indeed, it was demonstrated that an increase in Sodium electrolyte concentration provides high pH values. The ingestion of sodium bicarbonate also leads to a rise in both blood and sweat pH [31], as well as the increase in sweat rate provides a raise in pH values [28].

Different pathogenesis of skin diseases like irritant contact dermatitis, acne vulgaris, atopic dermatitis, ichthyosis, and Candida albicans infections can be detected by variations in sweat pH [32]. In addition, the latter leads to the growth of some bacteria because of the more favorable environment generated by some pH values.

Sweat constituents	Main substances	Average concentration (M)
Primary electrolytes	Sodium	3.1×10^{-2}
	Chloride	2.3×10^{-2}
	Calcium	5.2×10^{-3}
	Potassium	6.1×10^{-3}
	Magnesium	8.2×10^{-5}
	Phosphate	3.1×10^{-4}
	Bicarbonate	3.0×10^{-3}
Ionic constituents	Sulfate	4.2×10^{-4}
	Sulfur	2.3×10^{-3}
	Fluorine	1.1×10^{-5}
	Phosphorous	1.3×10^{-5}
	Bromine	2.3×10^{-6}
	Cadmium	1.8×10^{-8}
	Copper	9.4×10^{-7}
	Iodine	7.1×10^{-8}
	Iron	9.8×10^{-6}
	Lead	1.2×10^{-7}
	Manganese	1.1×10^{-6}
	Nickel	4.2×10^{-7}
	Zinc	1.3×10^{-5}

Organic acids and carbohydrates	Lactic acid	1.4×10^{-2}
	Pyruvic acid	1.8×10^{-4}
	Butyric acid	2.4×10^{-6}
	Acetic acid	1.3×10^{-4}
	Hexanoic acid	9.0×10^{-7}
	Propionic acid	3.5×10^{-6}
	Isobutyric acid	8.0×10^{-7}
	Isovaleric acid	1.1×10^{-6}
	Glucose	1.7×10^{-4}
Amino acids	Alanine	3.6×10^{-4}
	Arginine	7.8×10^{-4}
	Aspartic acid	3.4×10^{-4}
	Citrulline	4.0×10^{-4}
	Glutamic acid	3.7×10^{-4}
	Glycine	3.9×10^{-4}
	Histidine	5.2×10^{-4}
	Isoleucine	1.7×10^{-4}
	Leucine	2.1×10^{-4}
	Lysine	1.5×10^{-4}
	Ornithine	1.5×10^{-4}
	Phenylalanine	1.3×10^{-4}
	Threonine	4.5×10^{-4}
	Tryptophan	5.5×10^{-5}
	Tyrosine	1.7×10^{-4}
	Valine	2.5×10^{-4}
Nitrogenous substances	Ammonia	5.2×10^{-3}
	Urea	1.0×10^{-2}
	Uric acid	5.9×10^{-5}
	Creatinine	8.4×10^{-5}
	Creatine	1.5×10^{-5}
Vitamins and miscellaneous constituents	Thiamine (B1)	5.0×10^{-3}
	Riboflavin (B2)	2.0×10^{-2}
	Nicotinic acid or niacin (B3)	4.1×10^{-1}
	Pantothenic acid (B5)	1.3×10^{-1}
	Pyridoxine (B6)	1.0×10^{-8}
	Pyridoxal or folic acid (B9)	1.6×10^{-8}
	Ascorbic acid	1.0×10^{-5}
	dehydroascorbic acid	1.1×10^{-5}
	Inositol	1.6×10^{-6}
	Choline	2.6×10^{-5}
	p-aminobenzoic acid	7.1×10^{-8}

Table 4: Sweat constituents and their average concentration (M) [23, 33].Adapted with permission from Christopher J. Harvey et al [33], Copyright 2010, Published by Elsevier Ltd

4.2.2 Techniques for the development of halochromic textile-based sensors

Generally, halochromic functionalities can be introduced in textiles by the conventional dyeing method characterized by low-cost and simplicity [34, 35] and mainly represented by exhaustion and direct dyeing process.

According to the exhaustion method, a dye molecule is totally or partially dissolved in a water solution, then adsorbed by the textile fabric surface to further diffuse into the fiber. The diffusion of the dye into the fabric fiber is strictly dependent on the dye molecular structure and fiber nature, and their mutual interaction. The temperature also plays a relevant role in this process. Indeed, the process ranging from low to elevated temperatures ensures the diffusion of the dye molecules into the fiber thanks to the exceeding of the glass transition temperature of the textile polymer. For example, cotton fabrics can be dyed through direct dyeing processes (at neutral pH and in the presence of salt) that lead to weak interactions (hydrogen bonds, van der Waals and hydrophobic mainly) between the dye and the fiber, thus providing low washing fastness of the dyed cotton. Post-treatments with fixation agents are commonly employed to improve the dye fixation on cotton fibers, leading to complexes with low dye diffusion capability [36]. On the other side, polyester fabrics are commonly dyeing through disperse dyes, which are non-ionic, hydrophobic, and with low solubility. However, to be absorbed by fibers, a small amount of dye molecules is dissolved in water in the monomolecular form, and the dyeing process is carried out at elevated temperatures in acidic conditions. As well as for cotton, also the dyeing by the diffusion process of polyester leads to weak interactions between fibers and dye [36].

Conventional dyeing presents several disadvantages in developing halochromic sensors, among which long dyeing time, elevated temperature, low exhaustion and fixation levels, a low affinity of the dye and fibers, dye leaching, and slow response rate of the incorporated dye. Several alternative methods are available aimed at textiles functionalization with lower process time and energy and consisting of the covalent linkage between dye molecules and fabrics, thus ensuring a lower dye leaching compared with conventional dyeing techniques [37].

A stable chromic or halochromic functionality in textile fabrics can be obtained by introducing the dye during the manufacturing process of textiles, as for electrospinning [17]. The electrospinning approach is an interesting route to produce advanced fiber materials by incorporating halochromic functionality in nanofibers, thus combining the intrinsic properties of nanofibers and pH-sensing functionality. Such nanofibers can be produced by starting from polymer solutions, and according to this technique, it is possible to use different polymers and additives and to control fibers diameters (ranging from nanometers to microns) [38]. An alternative in the electrospinning approach is the

addition of the dye molecule or additive before starting the process, followed by the nanofiber formation. Both the addition of the dye or of the additives could cause a minor effect or instability in the electrospinning process [39].

Moreover, halochromic functionality can be incorporated in textile polymers by other already mentioned application techniques, such as printing (e.g., knife-over-roll) or coating, or by sol-gel approach. The latter, widely explained in Chapter 1, represents an innovative, environmentally friendly approach for functionalizing halochromic molecules, thus leading to stable bonds with textile surfaces. The most common silica precursor employed for the development of halochromic textiles are silica epoxy derivatives, *3*-glycidoxypropyltrimethoxysilane (GPTMS) or its ethoxy derivative (GPTES) [12, 37, 40–44]. The interest in these molecules derives from their chemical structures, both epoxy and methoxy/ethoxy groups that ensure a dual functionality. Through the epoxy ring-opening, the dye molecules can be stably immobilized, while the condensation of hydroxyl groups of methoxy or ethoxy functionalities leads to the formation of a 3D polymeric structure by ensuring the crosslinking with cellulose surface. In particular, it was demonstrated that a specific dye molecule can be entrapped into the silica-based network not only by covalent bonds but also through weak interactions [44]. Indeed, through hydrogen bonds or polar interactions, weak linkages are established within the silica polyethylene oxide network (PEO) that lead to more significant leaching of the dye as a consequence of washing cycles. While, according to covalent bonds, the chemical structure of the halochromic molecule is modified to form a more stable link with the silica network than weak interactions.

Another interesting approach to obtain halochromic textile sensors consists of the grafting of the cellulose surface. Grafting polymerization reactions are carried out in the presence of a radical initiator, which acts on C=C bonds of monomers like acrylic or vinyl derivatives or containing oxidizable functionalities (e.g., OH) according to free-radical reactions [45]. Thus, grafting represents an efficient and widely employed route for the stable functionalization of textiles surfaces.

4.2.3 Halochromic dyes

Halochromic dyes are mainly classified in phthalides, fluorans, triarylmethanes, and azo dyes [18]. The color change of these dyes is due to protonation or de-protonation of the molecule itself, processes that cause a different electron configuration. More in detail, due to protonation or de-protonation, a halochromic dye changes color from one color to another (or from colorless to a color compound, like phthaleins) according to a ring-opening of the dye molecule or on tautomerism. The

latter is common in hydroxyazo dyes, which consists of an azo/hydrazone tautomerism, in aminoazo dyes, or of ammonium or azonium tautomerism [46].

The color change can be the result of a hypsochromic (blue shift) or a bathochromic (red shift) shift of the absorption peaks.

Generally, the most common pH indicators are employed as pH-sensitive dyes to develop halochromic textile-based sensors. Typical examples are methyl red, nitrazine yellow, alizarin red S, and the non-toxic litmus and resorufin [41, 44]. To be stably immobilized on textiles surfaces by simultaneously providing efficient pH sensing properties, some of these molecules are covalently linked to the polymer matrix, thus modifying the microenvironment around the chromophore group. In some cases, both the UV-Vis spectra and the pH-response can be slightly different from the pure dye. Recently, wearable pH-meter textiles, based on the halochromic properties of nitrazine yellow were proposed by UV-curing [47], or thermal grafting [48] of glycidyl methacrylate monomers for promoting the in-situ grafting of polymer network on cellulose surface.

4.3 Halochromic textiles for human sweat pH monitoring by grafting of nitrazine yellow through glycidyl methacrylate on cotton fabrics

Due to the biological interest of nitrazine yellow (NY) as an azo pH indicator, it was employed for the design of a halochromic textile-based sensor. Indeed, this dye detects the pH variation ranging from acidic to alkaline values with the colorimetric change between yellow and blue, respectively. As already mentioned, the dye leaching from textile after washing cycles is a crucial issue to be addressed, and in this regard, a synthetic two-step procedure was designed for the efficient immobilization of this halochromic dye on cotton fabrics.

The first reaction step consists of the immobilization of nitrazine yellow molecules through epoxy ring-opening of a bifunctional precursor, the glycidyl methacrylate (GMA). Then, the same modified NY solution was immobilized on cellulose fabric during the second reaction step according to the grafting copolymerization approach. In the following paragraphs, the experimental part and main results will be discussed.

4.3.1 Nitrazine yellow

1-((*2,4*-dinitrophenyl)diazenyl)-*4*-hydroxynaphthalene-*2,7*-disulfonic acid disodium salt, hereafter nitrazine yellow (NY), is a pH-sensitive azo dye that provides the main color change in the neutral pH range between 6.0 and 7.0. Even if it is considered potentially responsible for skin irritation and life-threatening diseases [49], it is widely employed in hematological and histological analyses and cell biology.

The color change of NY is mainly based on tautomerism, the latter provided by the two NY isomers, the *ortho*- and *para*-hydroxyazo isomers [50]: the donation of the proton in the *ortho* or *para* position (with respect to the azo functionality) leads to the azo-hydrazone tautomerism [51, 52]. It was found that the acidic and neutral pH is related to the hydrazone NY form (more planar), leading to the formation of dye aggregates that are not rapidly able to turn into the azo form (in alkaline medium), thus providing the green color variation between the two transitions [51, 53].

Even if the most accepted tautomeric form of NY is the *ortho* one, several studies [40, 50], based on NMR explanations, have demonstrated that the isomer providing the deprotonation responsible for the color change is the *para*-hydroxyazo isomer, as reported in Scheme 7. The research study described in the following paragraphs demonstrates and confirms the real structure of NY as the *para* isomer.

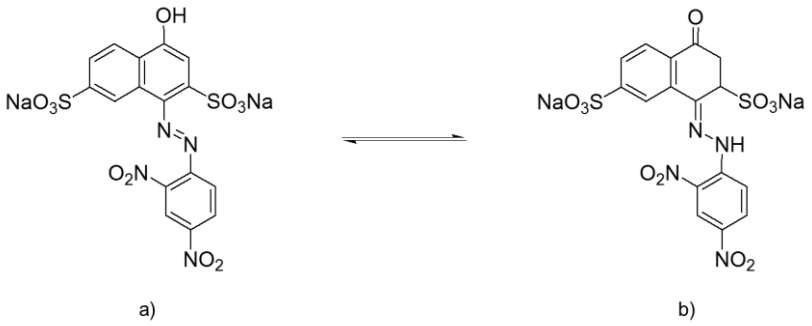

Scheme 7: Nitrazine yellow chemical structure and its tautomerism: azo (a) and hydrazone (b) forms

4.3.2 Synthesis of the functionalized NY dyestuff: experimental part

0.0015 mols of NY (0.8133 g) were dissolved in distilled water (80 ml) at room temperature. After few seconds of ultrasonication treatment, 0.0601 mols of glycidyl methacrylate (GMA) (8 ml) were added drop by drop to the obtained NY solution (GMA:NY molar ratio of 40.01:1), thus resulting in a 0.3 M GMA final concentration. The so-obtained G-N solution was stirred for 15 minutes and then an aqueous solution of the Lewis acid catalyst, BF_3OEt_2 (10% w/w GMA, 0.745 ml of catalyst in 70 ml of water) was added drop by drop. After 26.5 h, the reaction was neutralized (until pH 5) with 41.3 ml of NaOH 0.2 M solution. Finally, to remove insoluble dye residue, the G-N solution was filtered.

The same concentration of NY was employed to obtain a reference water solution of pure NY dyestuff.

4.3.3 Synthesis of the functionalized NY dyestuff: results and discussion

In the following subparagraphs, a detailed discussion of the most important experimental findings according to characterization techniques described in Chapter 2 is reported.

4.3.3.1 Chemical composition of G-N sol and NMR characterization

The catalyst action of the Lewis acid BF_3OEt_2 was largely explained in previous research studies [40, 41]. Indeed, BF_3 can provide the epoxy ring-opening through the interaction between the boron and oxygen atoms of the epoxy functionality thanks to the empty boron orbitals that ensure the hosting of the electron pair of oxygen. According to this interaction, the primary carbon of the epoxy ring is the most susceptible center for nucleophilic attack by other GMA molecules. It was demonstrated that the presence of NY molecules provides a decrease in the rate of the epoxy-ring opening reaction may be due to the formation of fluoboric and boric acids as a consequence of the water dissolution of the BF_3OEt_2 [41]. Indeed, the dyestuff can react with the formed acids, thus leading to a lower amount of pure Lewis acid available to react with epoxy groups with respect to similar reactions performed in the absence of NY. Moreover, it was demonstrated that the SO_3^- group is an efficient nucleophilic substituent in the epoxy ring-opening reaction of epoxy-derivatives [41]. According to this explanation, the schematic reaction between NY dyestuff and GMA bifunctional precursor using BF_3OEt_2 is reported in Scheme 8.

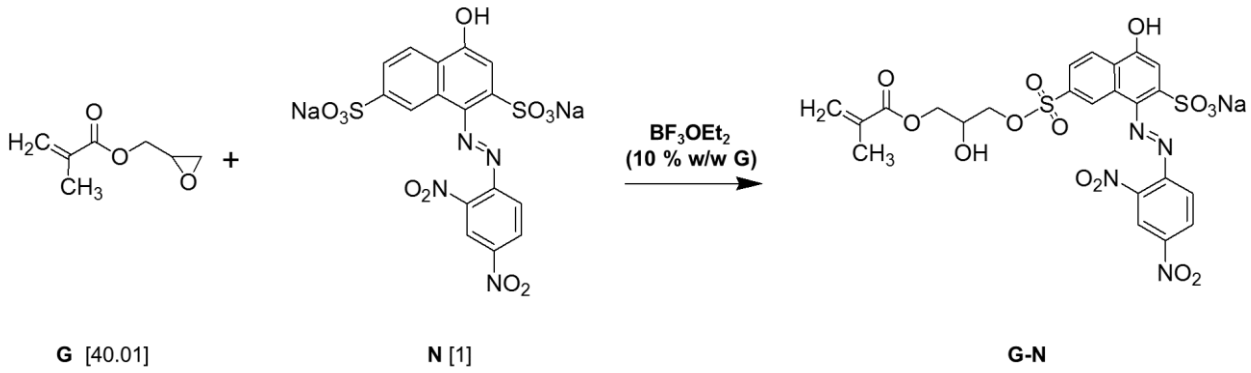

Scheme 8: Schematic representation of covalent functionalization of NY with GMA precursor. Adapted with permission from Trovato et al. [48], Copyright © 2021, under exclusive licence to Springer Nature B.V. part of Springer Nature

Figure 16 shows the ^{1}H NMR spectra of the starting NY, as recorded in DMSO-d_6 and deuterated water (up and down, respectively). In this latter case, a pair of signals, in a ratio of 1:0.3 for each type of protons, is detectable. These two resonances patterns could be ascribed to the equilibrium between the more thermodynamically stable *trans*-isomer and the corresponding *cis*-diazo species.

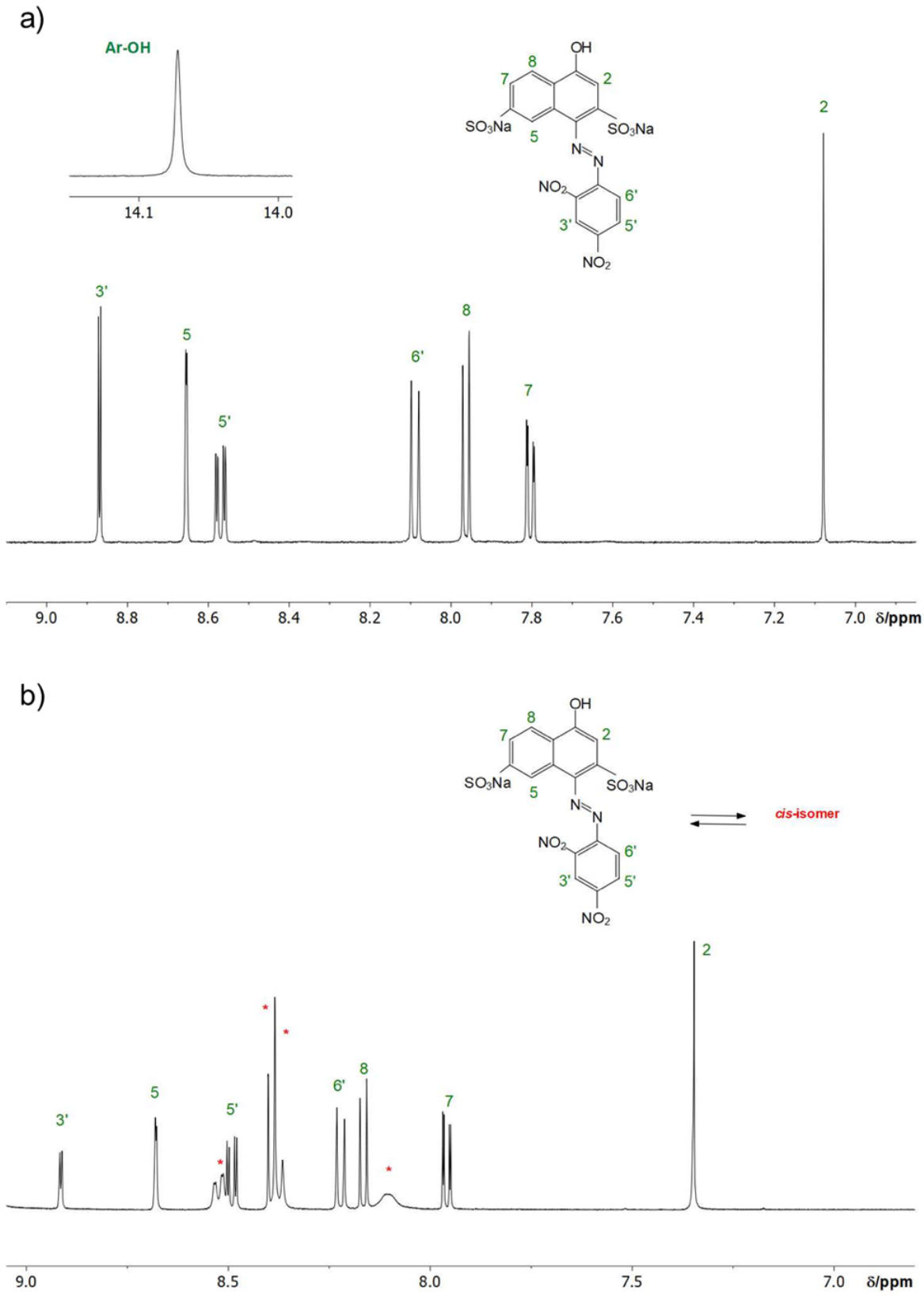

Figure 16: ^{1}H NMR spectrum of NY in (a) DMSO-d_6 and (b) D_2O, showing the presence of two *cis*- and *trans*-diazo isomers (500 MHz, 298 K). Adapted with permission from Trovato et al. [48], Copyright © 2021, under exclusive licence to Springer Nature B.V. part of Springer Nature

In Figure 17 and 18, a typical ^{1}H NMR comparison between the acrylic monomer (GMA) and the starting chromophore (NY), respectively, and the reaction crude (G-N) is reported (in D_2O at 298 K, 500 MHz).

As clearly shown in the protons assignment reported either in the aliphatic and aromatic regions of the ^{1}H NMR spectra (Figure 17 and 18), the epoxy ring-opening reaction has occurred with ester bond formation between the GMA and the NY.

In particular, in the G-N derivative, there is a general upper field shift of all aliphatic protons, except H_e proton that shows a downfield shift, maybe due to the resonance cone effect of the bonded aromatic dye NY.

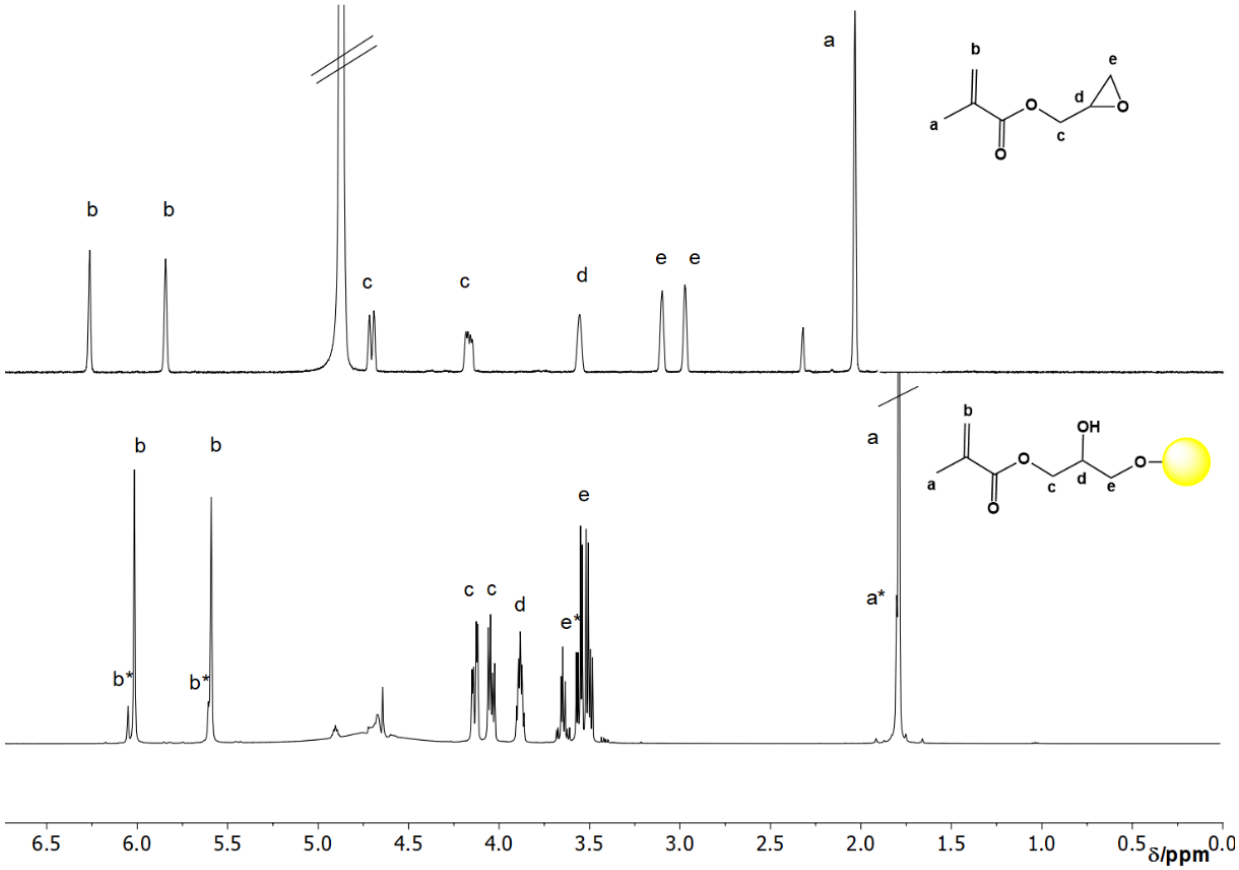

Figure 17: Aliphatic section of ^{1}H NMR spectrum of the (up) GMA in D_2O and (down) G-N derivative in D_2O (500 MHz, 298 K). Adapted with permission from Trovato et al. [48], Copyright © 2021, under exclusive licence to Springer Nature B.V. part of Springer Nature

The aromatic region of the ^{1}H NMR spectrum recorded on a water reaction mixture containing the G-N derivative (Figure 18), as dissolved in the deuterated solvent (20:80 = water: D_2O), shows the presence of at least two different species: (i) a slight major species assigned to the stable *trans*-isomer for the new diazo reaction product; (ii) its minor cis isomer (ratio 1:0.8 = trans:cis). This trans to cis

increased isomerism may be due to the presence of water employed as the reaction solvent and temperature reaction. All the aromatic protons show a general down- and up-field resonances shift due to ester bond formation in the newly formed G–N derivative.

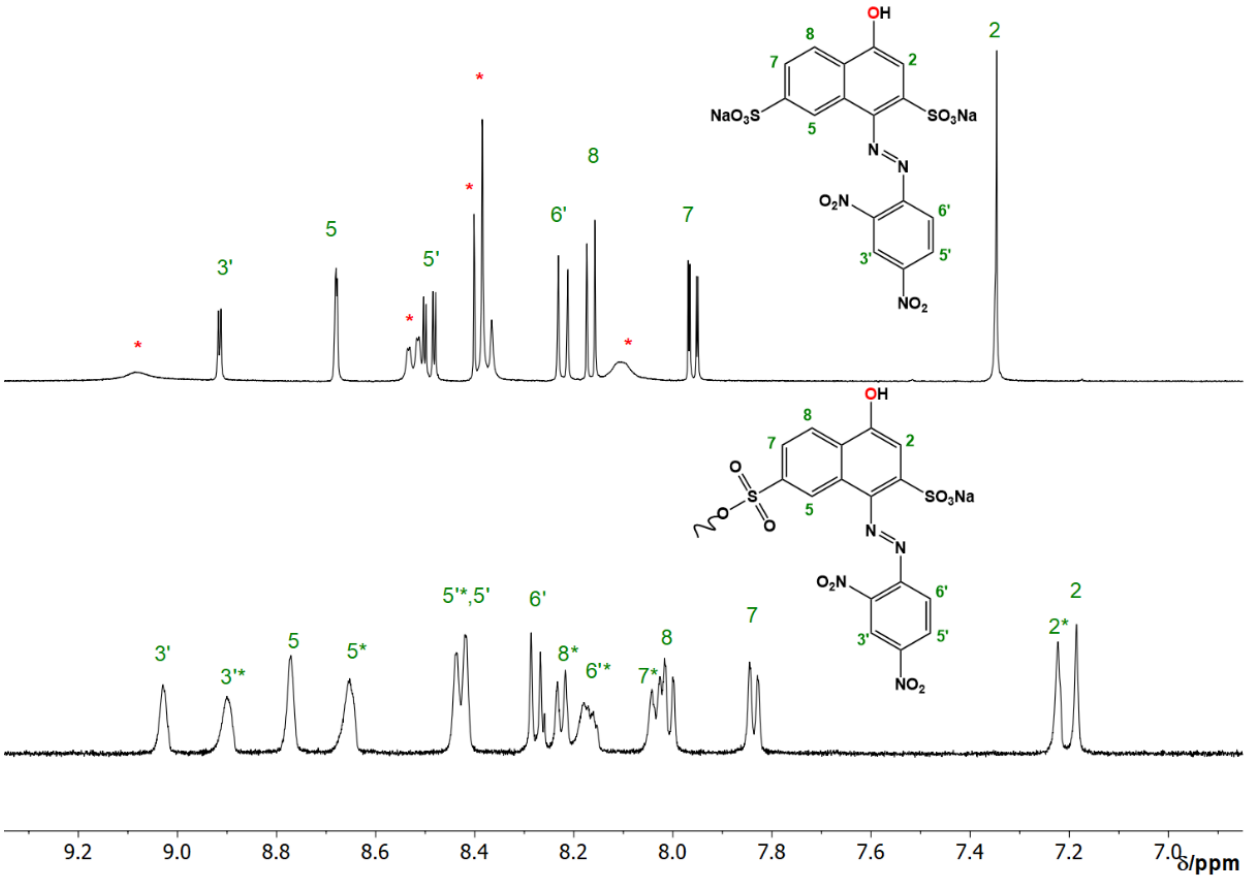

Figure 18: Aromatic section of ^{1}H NMR spectrum of the (up) NY in D_2O and (down) G-N derivative in D_2O (500 MHz, 298 K). Adapted with permission from Trovato et al. [48], Copyright © 2021, under exclusive licence to Springer Nature B.V. part of Springer Nature

As previously shown [40], these experimental findings suggest that the sulfonate group acts as an efficient nucleophilic substituent in the epoxide ring-opening reaction of GMA. Even if the substitution reaction could occur by the attack of two suitable sulfonate groups, namely at the C_3 and C_6 carbons of the NY, an adverse higher steric hindrance effect in the *cis*- and *trans*-isomer of the final G–N derivative by the attack at the C_6 carbon must be taken into account. These reasonings led us to confirm the proposed structure shown in Scheme 8.

4.3.3.2 ATR- FTIR characterization of NY solutions

To study the effectiveness of the covalent functionalization of the NY dyestuff through the catalyzed epoxy ring-opening of GMA molecules, xerogel of pure GMA (hereafter G), NY powder, and

solution of modified NY (hereafter G-N), obtained as described in Chapter 2, were analyzed through ATR - FTIR spectroscopy.

The ATR - FTIR curve of GMA (Figure 19, cyano curve) clearly shows the presence of both the epoxy and acrylic functionalities. The former is characterized by the absorption peaks assigned to asymmetric and symmetric C-H stretching (3059 and 3000 cm^{-1}, respectively), ring breathing (1254 cm^{-1}), and asymmetric and symmetric ring deformation (907 and 842 cm^{-1}, respectively) [40, 41, 54]. The addition of the catalyst led to the GMA epoxy-ring opening, as confirmed by the reduction in the intensity of these bands, as evident in the curve of G-N (Figure 19, yellow curve). Moreover, in the spectrum of G-N, the absorption bands relative to the presence of the acrylic functionality were confirmed by the observed peaks assigned to C=C stretching (1637 cm^{-1}) and wagging (942 cm^{-1}) (Figure 19, yellow curve) [55].

Other main peaks in the G-N spectrum refer to both ester C=O stretching (1716 cm^{-1}) and NY chemical structure. As evidenced in (Figure 19, black curve), the spectrum of NY is characterized by the peak at 1608 cm^{-1} assigned to N=N asymmetric stretching [43], while the C-N-N bending, as well as naphthalene ring deformation and C-SO_3 symmetric stretching, are visible at 911 cm^{-1}. Other peaks relative to NY structure refer to SO_2 stretching and S bonded with benzene ring (1242 cm^{-1}, 1196 cm^{-1}, 1131 cm^{-1}, 1042 $cm^{-1,}$ and 1024 cm^{-1}), C-H stretching of substituted ring (816 cm^{-1} and 768 cm^{-1}) [43] and C-H and O-H bending (835 cm^{-1}) [40].

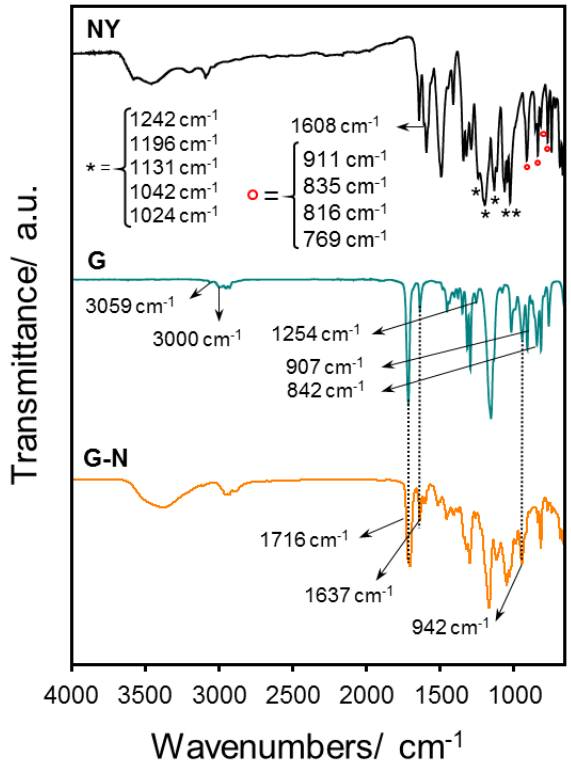

Figure 19: ATR-FTIR spectra of NY powder (black curve), G (cyano curve), and G-N (yellow curve) xerogels

4.3.3.3 pH-response of NY and G-N solutions

UV-Vis spectroscopy was employed to assess the pH properties of G-N solutions compared to those of NY solutions. Both NY and G-N solution at pH ranging from 4 to 8 were obtained by adding to McIlvane buffer solutions (Na_2HPO_4/Citric Acid) a specific and equal amount of NY or G-N solutions.

As clearly evident from (Figure 20), the presence of McIlvane buffer in both NY and G-N solutions leads to a color change from yellow to blue at acidic and alkaline pH, respectively, thus confirming that the pH-response of G-N solutions is in accordance with NY halochromic properties.

UV-Vis spectra of both NY and G-N buffer solutions reveal one maximum absorbance peak at 463 nm and 590 nm in acidic and alkaline media, respectively. In Figure 21, absorbance values at these two wavelengths were reported as a function of pH for both NY and G-N solutions.

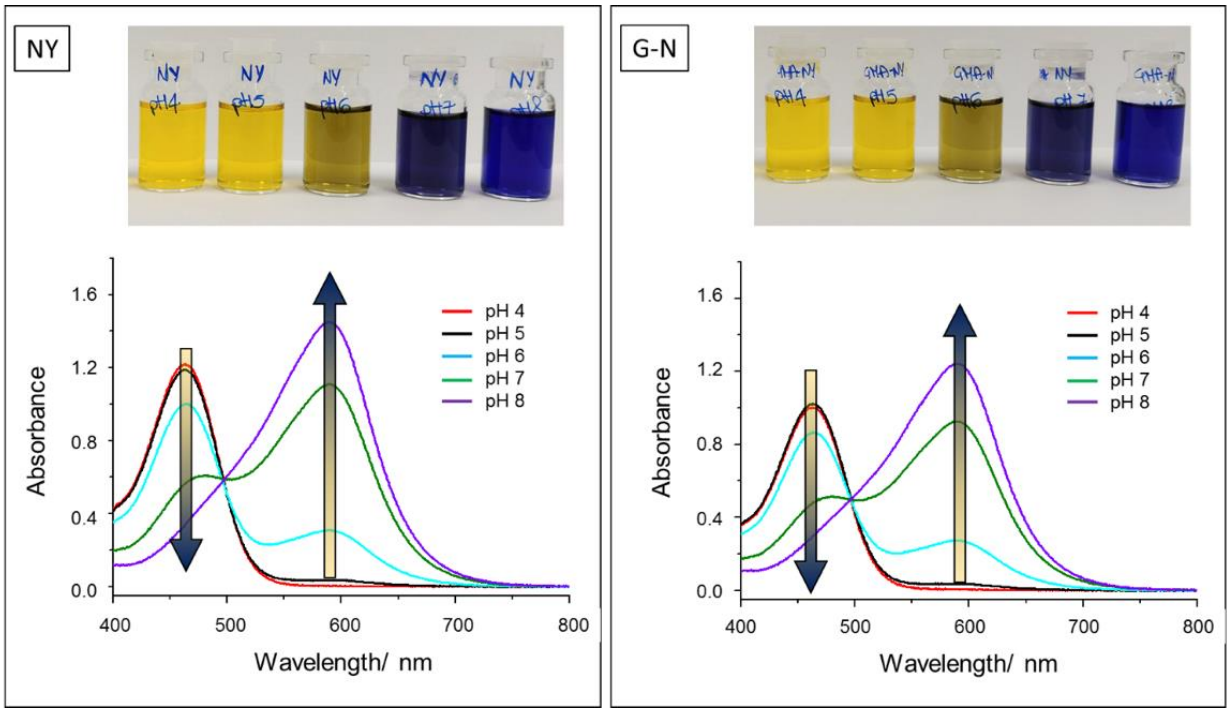

Figure 20: UV-Vis spectra of pure NY and G-N solutions at different pH with the corresponding images of solutions. Adapted with permission from Trovato et al. [48], Copyright © 2021, under exclusive licence to Springer Nature B.V. part of Springer Nature

As confirmed by spectra (Figure 21), the NY halochromic response occurs mainly between pH 6 and 8. G-N solutions exhibit similar behavior despite the covalent linkages of NY with GMA molecules through epoxy ring-opening.

Furthermore, at each pH, G-N solutions provide lower absorbance values compared to that of NY solutions, maybe due to the presence of different chemical bonds surrounding the dyestuff chromophore in the G-N solution.

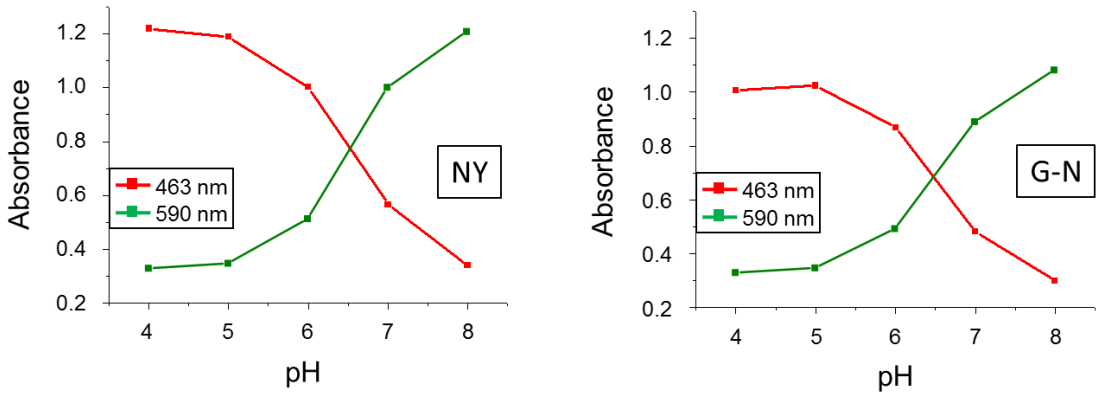

Figure 21: UV-Vis spectra of pure NY and G-N solutions at maxima wavelengths as a function of different pH. Adapted with permission from Trovato et al. [48], Copyright © 2021, under exclusive licence to Springer Nature B.V. part of Springer Nature

4.3.4 Radical polymerization of G-N solution on cotton fabrics: experimental part

As already mentioned, the second synthetic step is the grafting of the obtained G-N solution on cotton fabrics. This procedure was carried out through the exhaustion method and in the presence of a radical initiator, potassium persulfate (hereafter KPS). First, 90 ml of G-N solution and KPS (12 % w/w GMA, 0.4671 g) were put into a canister of Labomat Mathis equipment together with cotton fabric. Then, to reduce the presence of oxygen molecules entrapped between cotton fibers and dissolved in the G-N solution that could interfere with radical polymerization reactions, the whole system was put under N_2 atmosphere for at least 30 minutes at room temperature. Successively, the system was heated up to 70°C for 60 minutes to ensure the grafting reactions. After this time, the treated cotton fabric was dried for 30 minutes at 70°C in a convection oven, thus obtaining the sample CO_G-N (Scheme 9). Finally, a similar procedure was performed with the NY solution, without the presence of the radical initiator, to obtain a reference treated cotton sample (CO_N).

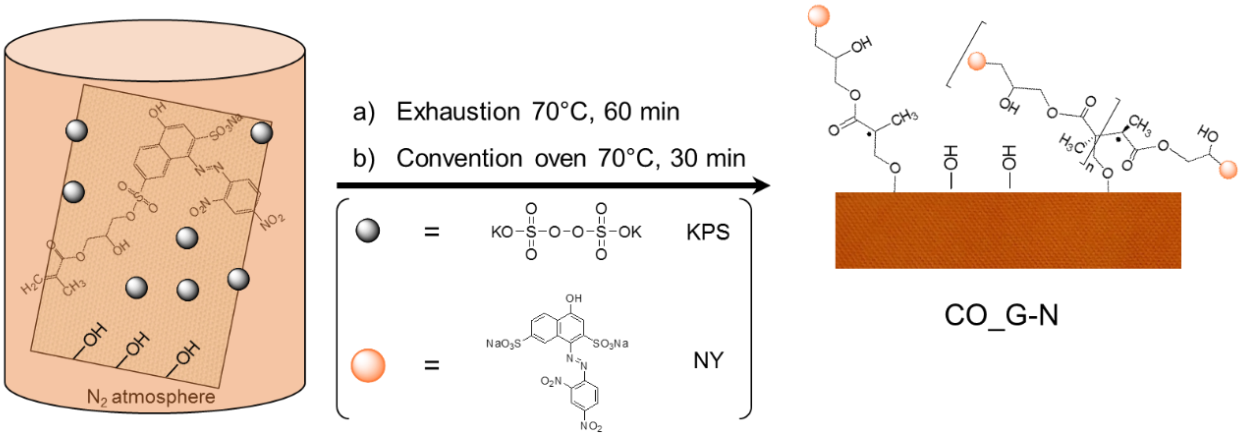

Scheme 9: Schematic representation of the application of G-N sol on cotton fabrics by exhaustion process

4.3.5 Radical polymerization of G-N solution on cotton fabrics: results and discussion

In the following subparagraphs, a detailed discussion of the most important experimental findings according to characterization techniques described in Chapter 2 is reported.

4.3.5.1 Chemical composition of the G-N solution for grafting polymerization

As already mentioned, after the first synthetic step, the NY dye results covalently bonded to GMA molecules through the catalyzed epoxy ring-opening while the C=C moiety remains unreacted. The latter was employed for the grafting reactions of the modified NY dyestuff (G-N) on cotton fabrics initiated by KPS. The latter is one of the most employed initiators for grafting C=C monomers on macromolecules with oxidizable functional groups according to free-radical reactions [45]. The "grafting from" [56] mechanism of radical polymerization was deeply described in Chapter 1 and here summarized for better clarity.

The first step of the grafting reaction consists of the decomposition of persulfate ions in water solution by thermal treatment. As a consequence, sulfate ions radicals are formed [57], as well as hydroxyl radicals. All these radicals lead to the formation of other radicals through the attack on the C=C bonds of GMA, thus creating branched structures (initiation reactions of homo- and co-polymerization) [58]. Successively, the direct abstraction of hydrogen atoms of the cellulose chain occurs through grafting and propagation reactions by all formed radicals. In the end, reactions of coupling or disproportionation stop the propagation [58].

4.3.5.2 Washing fastness of grafted G-N coating on cotton fabrics

Several examples are reported in the scientific literature dealing with the dye leaching from textiles of halochromic dyestuff according to conventional dyeing technique [12, 59]. As a solution to this issue, alternative textile dyeing methods like covalent grafting or dye-complexation provide good dye fastness. The effectiveness of the radical polymerization, performed to link the NY dye to cellulose substrates covalently, was demonstrated by both add-on (wt%) and weight loss % (WLW, wt%) after washing cycles, both calculated according to Eq. 1 and 2 reported in Chapter 2, respectively. CO_N and CO_G-N samples were washed 1 and 5 times following the procedure described in Chapter 2, and the measured add-on (wt%) and WLW (wt%) are reported in Table 5. The effectiveness of the grafting polymerization is confirmed by the high add-on obtained for sample CO_G-N than that of CO_N, which establishes a weak linkage degree of pure dyestuff with cotton fabrics. Moreover, WLW (wt%) values relative to CO_N after 1 and 5 washing cycles are not reported in Table 5 due to the high dye leaching that does not lead to significant weight loss value, thus confirming the low efficiency of the conventional exhaustion dyeing technique. Contrary, the CO_G-N sample provides WLW (wt%) after 1 and 5 washing cycles quite stable (Table 5): after 5 washing cycles, the WLW (wt%) was only 0.72 % higher than that obtained after 1 washing cycle.

The washing fastness of the cotton fabrics grafted with the G-N solution was also confirmed by the diffuse reflectance data used to calculate the F_{dye} (Eq. 4, Chapter 2). Indeed the dye fixation ratio of CO_G-N samples is greater than that of CO_N fabrics. The latter, contrary to WLW (wt%), was successfully obtained thanks to the high sensitivity of UV-Vis spectroscopy that allows detecting spectroscopic variation between unwashed and washed CO_N fabrics although the very low amount of dye after washing cycles.

Sample	Add-on (%)	WLW %	F_{dye}
CO_N	1.02	1W -	0.82
		5W -	0.53
CO_G-N	6.82	1W 3.92	5.07
		5W 4.64	4.39

Table 5: Data referred to the add-on (%), WLW (%), and F_{dye} after 1 and 5 washing cycles relative to cotton dyed with pure NY and with G-N solutions with corresponding images. Adapted with permission from Trovato et al. [48], Copyright © 2021, under exclusive licence to Springer Nature B.V. part of Springer Nature

4.3.5.3 ATR - FTIR characterization of grafted G-N fabrics and durability of the coating

Before studying the grafting of the G-N solution on cotton fabrics, the xerogel of G-N with KPS (G-N + K) was obtained following the same procedure described in Chapter 2. By comparing the ATR - FTIR curves of the G-N xerogel and G-N + K (Figure 22), the strong intensity decrease of absorption bands referred to C=C groups in the G-N + K curve is noticeable, thus confirming the occurrence of grafting polymerization reactions.

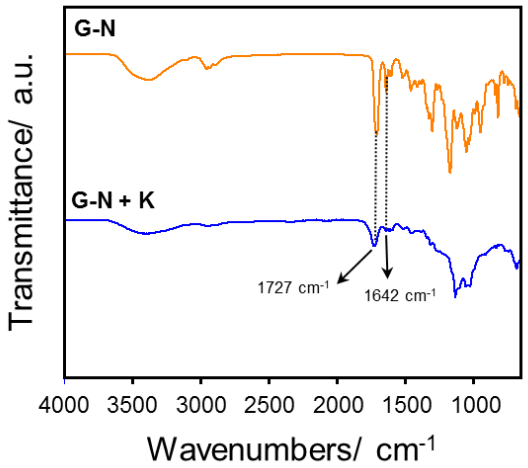

Figure 22: Comparison between ATR - FTIR spectra of G-N before (yellow curve) and after the addition of the radical initiator (KPS) (blue curve)

To assess the effectiveness of G_N graft polymerization on textile fabrics and the washing fastness of treated textiles, ATR - FTIR characterization was performed on untreated (CO), G-N treated (CO_G-N), and NY dyed (CO_N) cotton fabrics even after 1 and 5 washing cycles (_1w and _5w, respectively).

As clearly evident in spectra reported in Figure 23, the typical absorption bands of cellulose moiety are still present in all spectra of treated cotton fabrics, although the presence of both NY dye and G-N coating (Figure 23A and 23B, respectively). These peaks are highlighted in the FTIR curve of CO_UT, and the FTIR characterization of cotton is deeply described in Chapter 3. The graft co-polymerization of G-N solution on cotton fabrics was studied by monitoring the peaks referred to the C=C functional group of GMA. As shown by the curve of CO_G-N (Figure 23B, solid red curve), the C=C wagging (942 cm^{-1}) is no longer present, thus confirming that the grafting reaction on textile fibers took place. On the other side, the C=C stretching (1634 cm^{-1}) is still visible in the CO_G-N spectrum, maybe because of the presence of NY. Indeed such a band was also found in the CO_N spectrum.

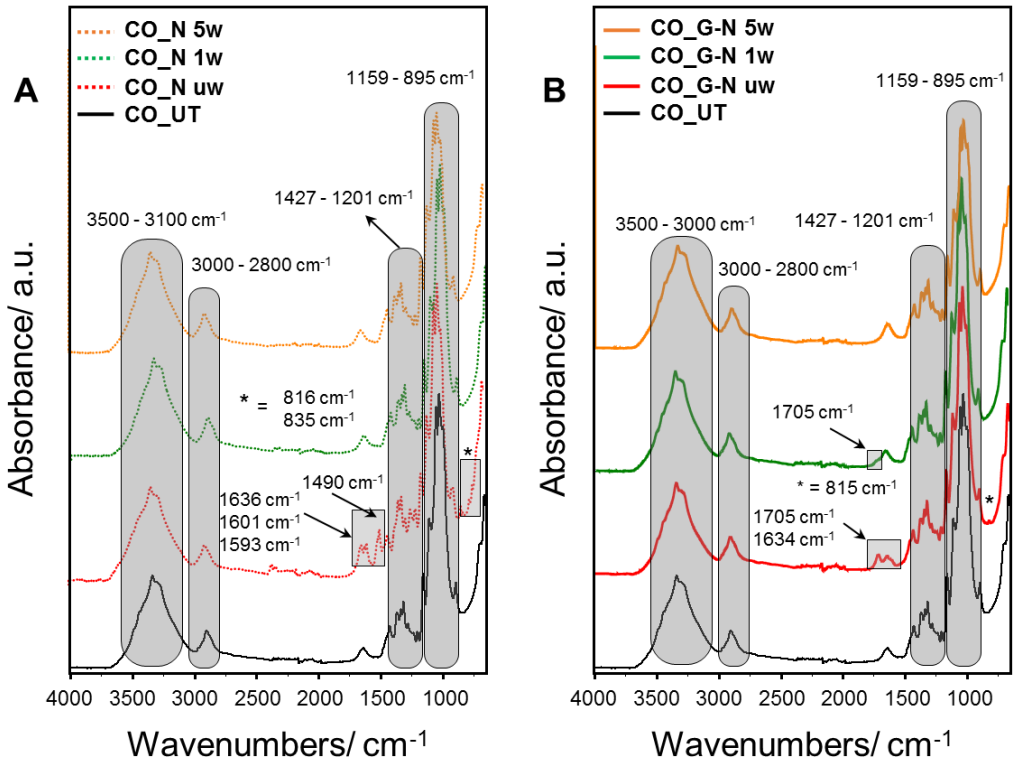

Figure 23: ATR-FTIR spectra of untreated cotton fabric (CO_UT) and cotton fabrics treated with pure NY (A, dashed curve) and G-N sol (B, solid curve), before and after 1 and 5 washing cycles. Adapted with permission from Trovato et al. [48], Copyright © 2021, under exclusive licence to Springer Nature B.V. part of Springer Nature

The durability of the G-N coating on cotton surfaces was established after 1 and 5 washing cycles according to ATR - FTIR characterizations. The FTIR curve of CO_G-N_1w (Figure 23B, solid green curve) reveals the presence of the coating through the peaks relative to the C=O group (1705 cm^{-1}) as a small shoulder in the broad peak assigned to the adsorbed water of cellulose (1640 cm^{-1}). While both the reduced intensity of the C=O stretching band and the absence of peaks at 1634 and 942 cm^{-1} (C=C stretching and C=C wagging, respectively) are coherent with the obtained weight loss of 3.9 % after 1 washing cycle, thus indicating that the unreacted monomer was removed from the cotton surface. However, the durability of the coating was further demonstrated by both the negligible weight loss after 5 washing cycles that were measured in 4.6 %, as well as by the F_{dye} obtained (5.07 and 4.39 after 1 and 5 washing cycles, respectively) with respect to un-washed CO, and by the quite unchanged color of CO_G-N_5w compared to CO_G-N_1w visible at naked eye.

The comparison between ATR - FTIR spectra of CO_N fabric (Figure 23A), as the reference sample, and CO_G-N (Figure 23B) highlight the effectiveness of the co-polymerization on fabric surfaces. Indeed, peaks assigned to the NY dyestuff (1636, 1601, 1593, 1490, 835, and 816 cm^{-1}) are evident in the curve of CO_N, but they are no longer present in the FTIR spectra of CO_N after 1 and 5 washing cycles (CO_N_1w and CO_N_5w, respectively). The latter evidence is in agreement with the F_{dye} values obtained after 1 and 5 washing cycles (0.82 and 0.53, respectively), thus confirming the poor durability of cotton fabrics dyed with pure NY according to the exhaustion method.

4.3.5.4 SEM characterizations

According to SEM images (Figure 24), the untreated and treated cotton fabrics result in slightly different morphology. Untreated cotton is characterized by fiber with the typical smooth and clean surface. Similarly, the cotton fabric dyed with NY reveals the same morphology of cotton due to the presence of only the dyestuff that does not provide significant changes. Differently, the SEM images of CO_G-N samples evidence the presence of a thin coating along the surface of the fibers and the increase of the surface roughness. Moreover, some agglomerates entrapped between the fibers are evident and maybe due to the high add-on (wt%). The same agglomeration is no longer observable after washing cycles while the presence of a uniform and thin homogeneous coating are still noticeable on the surface of the fibers.

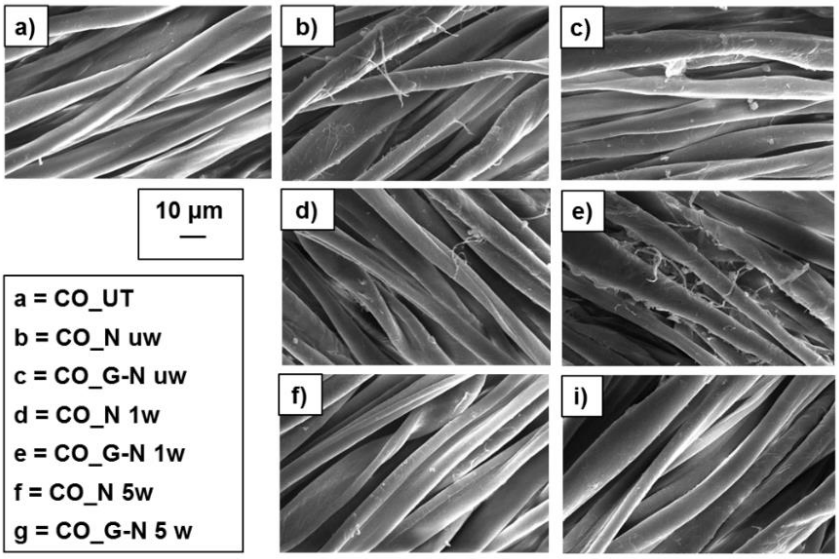

Figure 24: SEM images of untreated and treated cotton sample

4.3.5.5 Diffuse reflectance measurements: textile pH-response

The halochromic dye behavior is influenced by the interaction of the dye with textile fibers, as clearly evidenced by the color of both NY and G-N buffer solutions and the color of the corresponding treated textiles [51].

With this premise, UV-Vis reflectance spectroscopy in CIELAB color space was employed to study the pH-response of treated cotton samples after washing cycles. Both CO_N and CO_G-N, after 1 and 5 washing cycles, were soaked separately in pH buffer solutions ranging from 4 to 8, and the R% values were obtained for each sample and used in the Kubelka-Munk equation (Eq. 3, Chapter 2). The Kubelka-Munk diffuse reflectance UV-Vis spectra for each sample are reported in Figure 25.

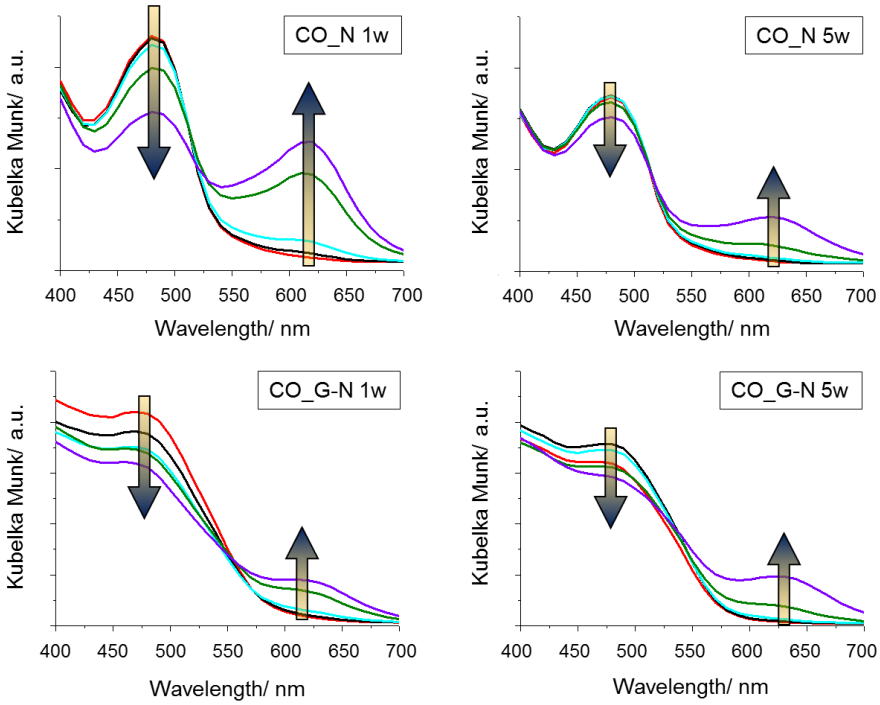

Figure 25: Kubelka-Munk diffuse reflectance UV-Vis spectra for cotton fabrics treated with NY and G-N solutions after 1 and 5 washing cycles. Adapted with permission from Trovato et al. [48], Copyright © 2021, under exclusive licence to Springer Nature B.V. part of Springer Nature

CO_N and CO_G-N samples show a slightly different halochromic behavior due to the covalent immobilization of GMA. Compared to the buffer solution (Figure 20), the G-N grafted cotton samples reveal the typical color transition of NY, thus differing from the solution for the bathochromic shift of the maxima absorbance peaks. More in detail, for NY samples, the acidic maximum shifted from 463 nm to 480 nm in the NY solution and CO_N, respectively (Figure 25). Similarly, the alkaline maximum shifted from 590 nm (in NY solution) to 615 nm and 620 nm for cotton samples (for CO_N_1w and CO_N_5w, respectively) (Figure 25).

According to a similar trend, CO_G-N_1w is characterized by a red shift of acidic maximum to 470 nm and the alkaline maximum to 620 nm. On the other side, CO_G-N_5w reveals a red shift of acidic maximum to 480 nm and a shift of the alkaline maximum to 680 nm. The observed higher bathochromic shift in the alkaline medium is due to the characteristic halochromic response of NY dye in the pH range between 6 and 8, although its covalent immobilization with GMA precursor provides changes in the surroundings of the chromophore. The observed halochromic behavior of G-N grafted cotton fabrics is coherent with that found in other research studies dealing with the sol-gel covalent immobilization of NY for halochromic textiles [40, 51]. As clearly evident in Figure 25, increasing pH, a less intensity variation, both in the decrease and increase in the maxima absorbance

peaks, is observed for CO_N_5w. Conversely, no changes in the intensity of both acidic and alkaline maxima absorbance are found for CO_G-N after 1 and 5 washing cycles. The latter evidence confirms the efficiency in the pH-response of the G-N grafted coating on cotton fabrics even after 5 washing cycles.

Moreover, according to the obtained Kubelka-Munk curves, both treated cotton fabrics (CO_N and CO_G-N) show color changes as a function of the pH ranging from yellow to blue as previously observed from the solutions reported in Figure 20.

The time response of the halochromic textiles results slightly different in acidic (faster response) and alkaline media (slower response), although the pH-response time was fully established within 5 minutes.

ΔE* color changes with respect to pH 4 as a function of pH variations are reported in Figure 26 for both washed CO_N and CO_G-N samples. All samples reveal a distinct color variation between pH 4 and 8, although a less bluish color was observed for CO_N than CO_G-N textiles. Lower ΔE* for CO_N samples at each pH value was obtained. More in detail, CO_N_5w samples provide ΔE* values significantly lower than that of CO_N_1w and CO_G-N samples between pH 6 and 8. Contrary, CO_G-N_5w samples provide ΔE* values almost similar compared to those obtained for CO_G-N_1w. These experimental findings confirm both the good washing fastness of the G-N grafted cotton fabrics and the consistent halochromic response of the G-N solution with the NY dyestuff.

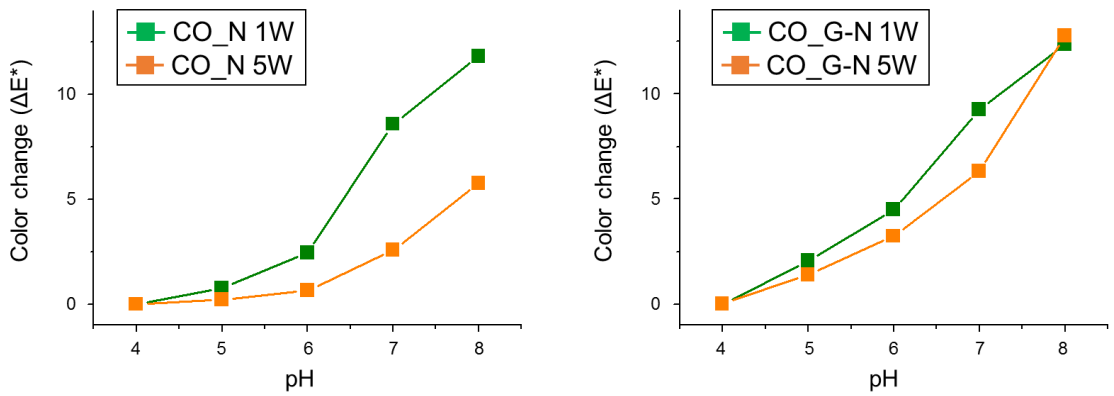

Figure 26: ΔE* color change with respect to pH 4 of both CO_N and CO_G-N after 1 and 5 washing cycles as a function of pH variations. Adapted with permission from Trovato et al. [48], Copyright © 2021, under exclusive licence to Springer Nature B.V. part of Springer Nature

4.3.5.6 Repeatability of the pH-sensing response of G-N grafted textiles

The pH-sensing response of the G-N grafted textiles after repeated exposure to acidic and alkaline environments is an important parameter for the development of halochromic sensors for different application fields such as medical, protective garments, fitness, and healthcare.

CIELAB color space analysis, as described in Chapter 2, was performed on textile samples for assessing the repeatability of the pH-sensing response of both CO_N and CO_G-N after 1 and 5 washing cycles. Each fabric was soaked in a buffer solution (pH 4 or 8) for 5 minutes, dried, and ΔE* was measured as the difference between color space values of the sample after soaking in pH 4 and 8 buffer solutions (1 cycle), respectively, and the cycle was repeated for 4 times.

ΔE* values confirmed the reversible color change from yellow (pH 4) to blue (pH 8), and vice-versa. Data reported in Figure 27 highlights the capability of CO_G-N samples to give high color changes after repeated cycles and even after 5 washing cycles compared to CO_N. The latter provide similar color changes and ΔE* values after the first and last exposure cycles.

According to the obtained results, both the reversibility and the repeatability of the pH-sensing response of G-N grafted cotton samples were demonstrated, thus confirming the potentiality of the designed wearable pH-sensors for repeated applications instead of disposable use.

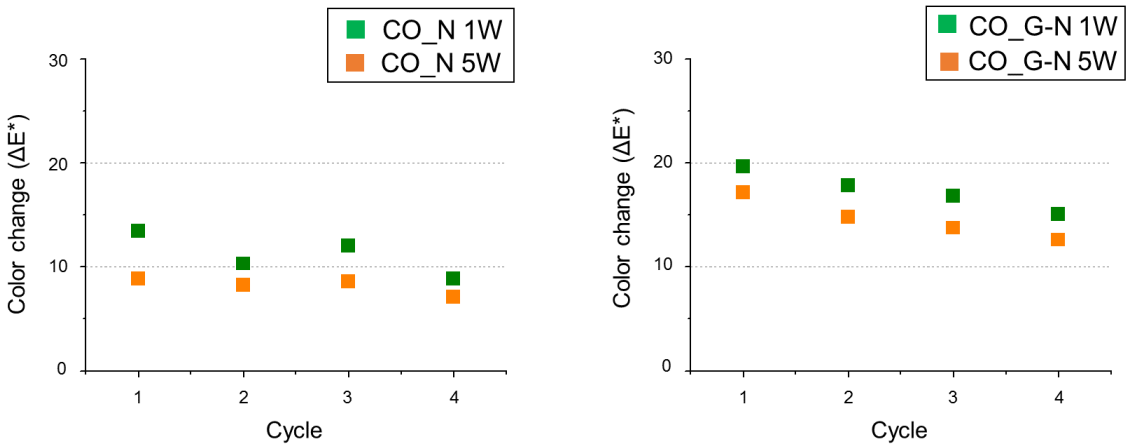

Figure 27: ΔE* color change of treated textiles after 1 and 5 washing cycles for each pH value with respect to pH 4. Adapted with permission from Trovato et al. [48], Copyright © 2021, under exclusive licence to Springer Nature B.V. part of Springer Nature

4.4 Halochromic textiles for human sweat pH monitoring by sol-gel immobilization of alizarin red S on cotton and polyester fabrics

Several halochromic dyes can be immobilized into the fabric structure to design halochromic textile-based sensors. Alizarin red S is another molecule of great interest among many available dyes, both in biomedical and diagnostic fields.

To develop halochromic textiles characterized by pH-response in a more broad range compared to nitrazine yellow, two fabrics with different nature, cotton and polyester textiles, were functionalized with alizarine red S. The latter is a halochromic dye characterized by color variations from yellow to purple for acidic and alkaline solutions, respectively. Through sol-gel reactions, the dye was covalently immobilized on cotton and polyester substrates, and the halochromic properties of the modified dye were thoroughly investigated and compared to reference fabrics dyeing with pure alizarin red S.

4.4.1 Alizarin red S

The *1,2*-dihydroxy- *9,10*-anthraquinone sulphonic acid sodium salt, hereafter alizarin red S (ARS), is an anthraquinone dye of great interest thanks to its chelation properties that make it a widely employed colorimetric reagent for cations. The capability of ARS to form chelates with metal ions is due to its chemical structure characterized by two hydroxy groups in positions 1 and 2 with respect to the quinoid oxygen. The presence of the sulfonate group also provides improved reactivity to the ARS molecule. The color changes of ARS depending on pH variations are due to the already mentioned hydroxy groups. As reported in the literature, the pKa values of ARS are 5.5 and 11.0 [60]. For pH lower than 5, ARS is present in the neutral form, for pH values between 5 and 9, the dye exists in the mono-anionic form, while the dianionic structure is available for pH greater than 9 (Scheme 10).

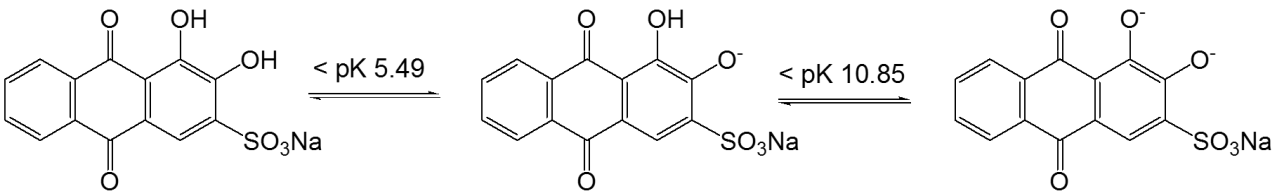

Scheme 10: Alizarin red S chemical structure depending on pH variations

Several studies have been conducted dealing with the stability of complexes with copper, lead, chromium and, other metal ions [61]. Thanks to its capability to provide sharp color changes after

forming complexes with different metal ions, ARS is also used for metal separation from wastewater [60, 62].

During the last years, it is also employed as a staining agent for Calcium in biological samples in the spectrophotometric determination of pH and textile dyeing [63–65]. Moreover, ARS is also used in carbohydrate detection in biological fluids thanks to its color changes and fluorescence intensity in response to the binding of boronic acids.

4.4.2 Synthesis of the hybrid alizarin red S – GPTMS halochromic sol and application on textile fabrics: experimental part

GPTMS (9.9 ml, 0.045 mol) and HCl 0.1 M (2.5 ml) were consecutively added to 50 ml of water, and the resulting mixture was left under vigorous stirring for at least 30 minutes. Then, ARS (ARS: GPTMS molar ratio 1:30, 0.5133 g, 0.0015 mol) and a small amount of water (10 ml) was added to the obtained GPTMS sol. The new GPTMS- ARS (hereafter, G-A) mixture was left under stirring until the dye was homogeneously dispersed. In the next step, a water solution (60 ml) of the BF_3OEt_2 catalyst (9.8 % w/w GPTMS, 0.9 ml) was added drop by drop to the G-A sol. The solution was monitored for 40 h by FTIR spectroscopy. The acidic G-A solution was added with NaOH 5 M (2 ml) until pH 5. Then, ethanol (14.7 ml) was added, and finally, the solution was filtered to eliminate no dissolved dye residue. A schematic representation of the reaction is reported in Scheme 11.

Scheme 11: Schematic representation of the covalent immobilization of ARS through GPTMS catalyzed epoxy ring-opening

The same amount of ARS (0.5133 g, 0.0015 mol) was dissolved in a hydroalcoholic solution (150 ml), thus obtaining the pure ARS solution (ARS) as a reference.

Both ARS and G-A solutions were applied separately on cotton and polyester fabrics according to the pad-cure method described in Chapter 2, thus obtaining CO_ARS, CO_G-A, PL_ARS, and PL_G-A, respectively. All treated samples were washed 1 and 5 times in a Labomat Mathis by following the Standard procedure described in Chapter 2, thus obtaining for each textile, the sample coded as "1w" and "5w".

4.4.3 Results and discussion

In the following subparagraphs, a detailed discussion of the most important experimental findings according to characterization techniques described in Chapter 2 is reported.

4.4.3.1 NMR spectra of ARS and functionalized ARS with GPTMS

As previously shown [43], NMR spectroscopy may be used to confirm the epoxy ring-opening that brings from the starting GPTMS and the ARS dye towards the formation of the sol-gel derivative GPTMS-ARS with an ester bond formation.

In Figure 28, displaying the aromatic region of the ^{1}H NMR spectrum of G-A (upper side), compared with the starting ARS dye (lower side), it is evident that a general upper shift of the proton signals belonging to the dye fragment after the reaction occurred.

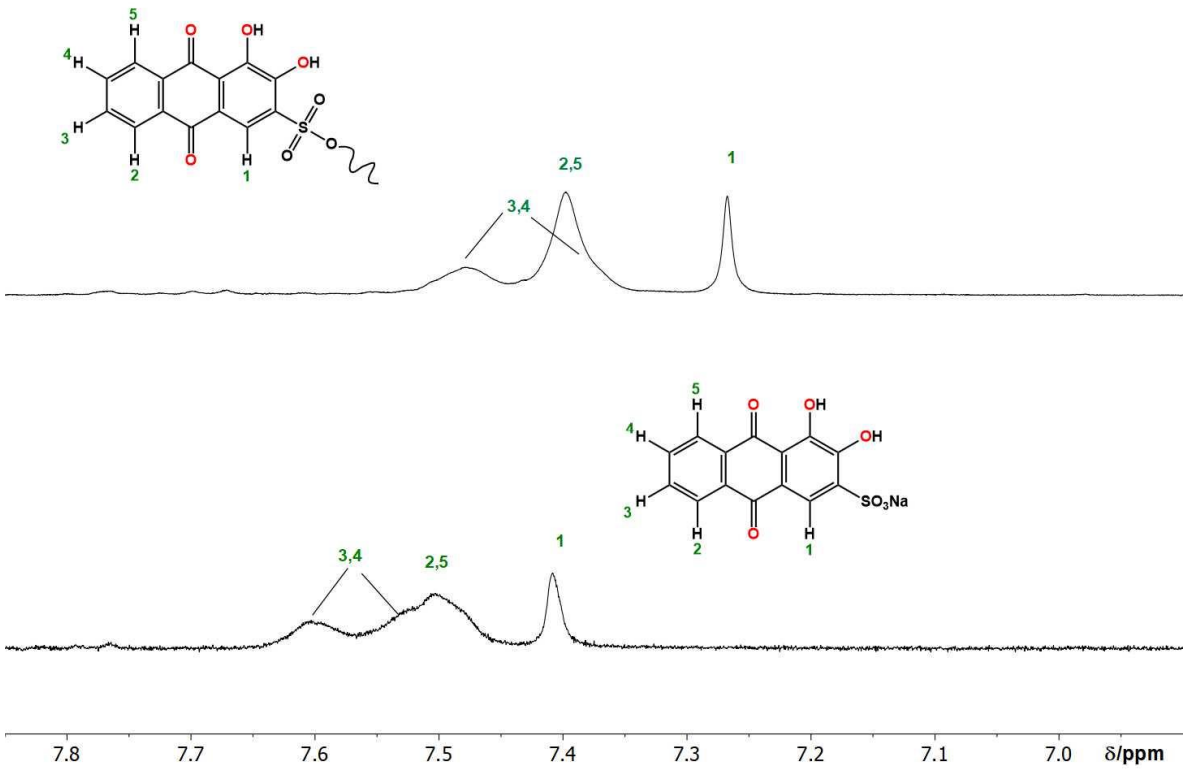

Figure 28: Aromatic section of ^{1}H NMR spectrum of the (up) G-A derivative and (down) ARS in D_2O (300 MHz, 298 K)

Helpful insights may be gained by Figure 29, viewing the aliphatic sections of the ^{1}H NMR spectra of G-A and the starting GPTMS. As expected, the protons belonging to the epoxy ring are those most

affected by the ring-opening reactions. As a matter of fact, the methinic H_5 and the methylenic H_6 protons show a low-field shift after the ester bond formation with the ARS dye.

The occurred sol-gel reaction is also attested by the presence of hydrolysis/condensation reaction by-products of the GPTMS trimethoxysilane end, in agreement with already reported literature data [40, 43, 66]; in particular: (i) the matching formation of free methanol (CH_3OH/CH_3OD) at 3.15 ppm; (ii) the corresponding presence of Si-OH groups that give rise to a broad peak at 4.32 ppm (not shown) in exchange with water and other OH groups.

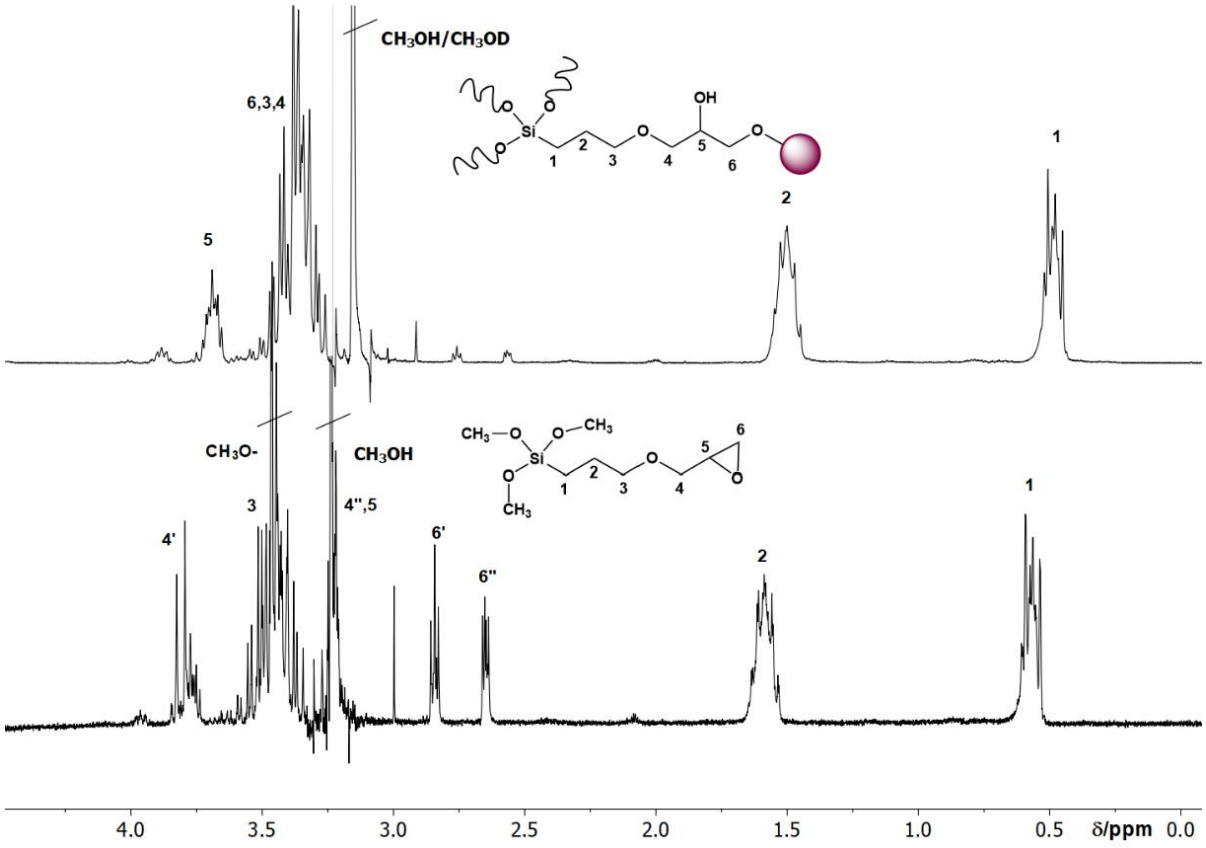

Figure 29: Aliphatic section of ^{1}H NMR spectrum of the (up) G-A derivative and (down) GPTMS in D_2O (300 MHz, 298 K)

4.4.3.2 Chemical composition of the G-A sol-gel coating

In Figure 30, ATR-FTIR spectra of ARS powder, G-A solution at zero time (G-A t_0), and final G-A sol (G-A t_f) are reported. As already explained in Chapter 2, the xerogel of G-A solution was obtained through thermal treatment to study the chemical composition of the hybrid halochromic coating without the interference of the high intense absorption bands of textile fabrics, both cotton and polyester.

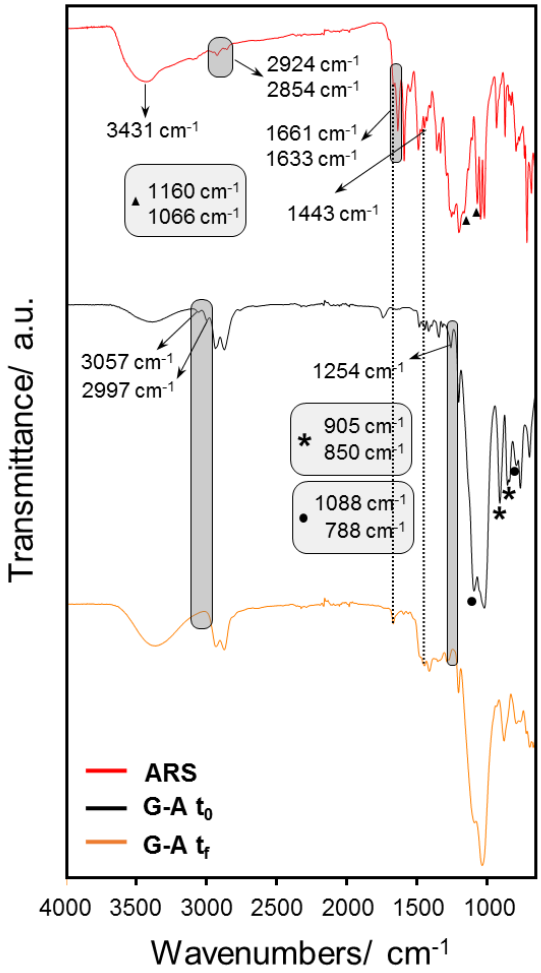

Figure 30: ATR-FTIR spectra of ARS powder, and G-A sol at time zero (t_0) and after reaction ends (t_f)

As clearly evident in Figure 30, and according to literature data [40, 41], the reaction carried out in the presence of BF_3OEt_2 leads to the epoxy ring-opening of GPTMS followed by the covalent bond with the SO_3^- group of ARS. Indeed, in the spectra of G-A t_0, collected immediately after the addition of the catalyst, the main FTIR peaks assigned to epoxy ring functionality of GPTMS are highlighted: asymmetric and symmetric C-H stretching (3057 and 2997 cm^{-1}, respectively), ring breathing (1254 cm^{-1}), and asymmetric and symmetric ring deformation (905 and 850 cm^{-1}, respectively) [40, 41]. The same absorption bands are no longer visible in the spectra of the G-A solution after reaction ending (G-A t_f), thus confirming the effectiveness of the catalyst action on the epoxy ring opening. Other main peaks relative to the silica matrix are assigned to the asymmetric and symmetric Si-O-Si stretching (1088 cm^{-1} and 788 cm^{-1}, respectively) and its bending mode (875 cm^{-1}) [40, 41, 44]. Moreover, other peaks are visible in G-A t_f spectra and assigned to the ARS chemical structure. These bands are highlighted in ARS spectra, and the most relevant are listed in Table 6 [67, 68].

FTIR bands	Literature data	Experimental data
O-H stretching	3487 cm^{-1} [67, 68]	3431 cm^{-1}
Aromatic C-H stretching	2925 cm^{-1} 2853 cm^{-1} [67, 68]	2924 cm^{-1} 2854 cm^{-1}
C=O carbonyl stretching	1666 cm^{-1} 1635 cm^{-1} [67, 68]	1661 cm^{-1} 1633 cm^{-1}
C=C stretching	1441 cm^{-1} [67, 68]	1443 cm^{-1}
SO_2 asymmetric stretching	1160 cm^{-1} [69, 70]	1160 cm^{-1}
SO_2 symmetric stretching	1060 cm^{-1} [69, 70]	1066 cm^{-1}

Table 6: Main FTIR vibrational mode of alizarin red S

By comparing spectra of ARS powder and functionalized ARS (G-A t_f), both the OH and CH stretching overlapped with the same vibrational mode of GPTMS groups and the SO_2 asymmetric and symmetric stretching, which are completely covered by the Si-O-Si symmetric stretching. The presence of ARS in the G-A coating can be confirmed thanks to C=O and C=C stretching modes, which are still visible in the G-A t_f spectrum.

4.4.3.3 FTIR characterization and washing fastness of halochromic ARS-based textile fabrics

Cotton and polyester fabrics were analyzed through ATR-FTIR spectroscopy before and after the application of both ARS and G-A solutions. Treated fabric samples were also analyzed after 1 and 5 washing cycles. In Figure 31, a comparison between untreated cotton (CO_UT), treated cotton with ARS (dashed curves) and G-A solution (solid curves) before (CO_ARS) and after 1 and 5 washing cycles are reported (CO_ARS 1w and CO_ARS 5w). Although the treatment, in each FTIR spectrum of the treated cotton sample, the typical absorption bands of cellulose moiety are still observed: 3500 – 3100 cm^{-1} (O-H stretching), 3000 - 2800 cm^{-1} (C-H stretching), 1400 - 1200 cm^{-1}(C-H wagging and deformation mode), 1200 - 800 cm^{-1} (asymmetric stretching of C-O-C, in-plane ring and C-O stretching) [71].

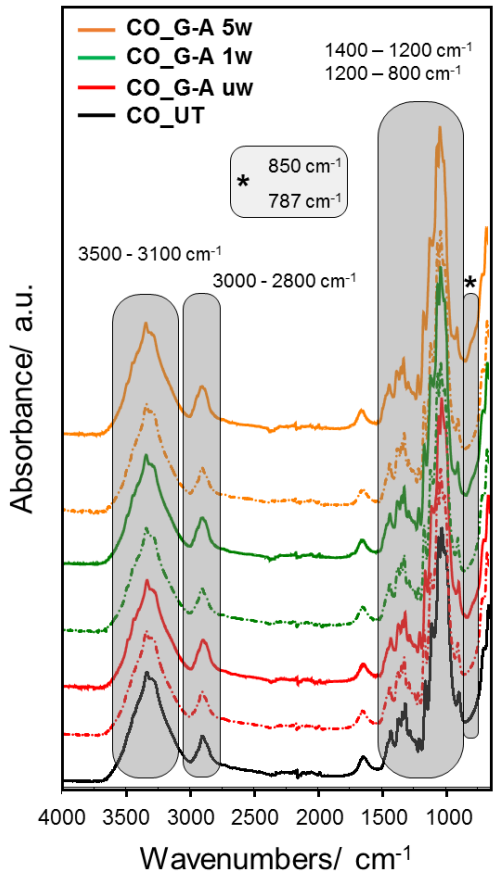

Figure 31: ATR-FTIR spectra of untreated cotton fabric (CO_UT) and cotton fabrics treated with pure ARS (dashed curves) and G-A sol (solid curves), before and after 1 and 5 washing cycles

The presence of the pure ARS on cotton fabrics does not provide significant changes in the O-H and C-H stretching spectral zone because of the high intensity of cellulose peaks that cover the main absorption peaks of ARS (Figure 32a). A slight increase of absorption bands intensity in the range 1200 - 800 cm^{-1} is observed due to the overlapping of the SO_2 stretching mode (Figure 32c). Contrary, in spectra of cotton treated with G-A sol, the coating deposition on cotton fabrics provides a slight decrease of O-H and C-H stretching bands intensity due to the presence of the coating, and an increase of the FTIR peaks intensities in the spectral region 1200 - 800 cm^{-1} due to Si-O-Si vibration mode and overlapping of asymmetric stretching of C-O-C and C-O stretching of GPTMS (Figure 32b-d). Moreover, the presence of the hybrid silica matrix is evident thanks to the comparison of low intense peaks at 850 cm^{-1} and 787 cm^{-1} referred to the bending and stretching of Si-O-Si silica moiety [40, 41], which are still visible also after washing cycles (Figure 32d).

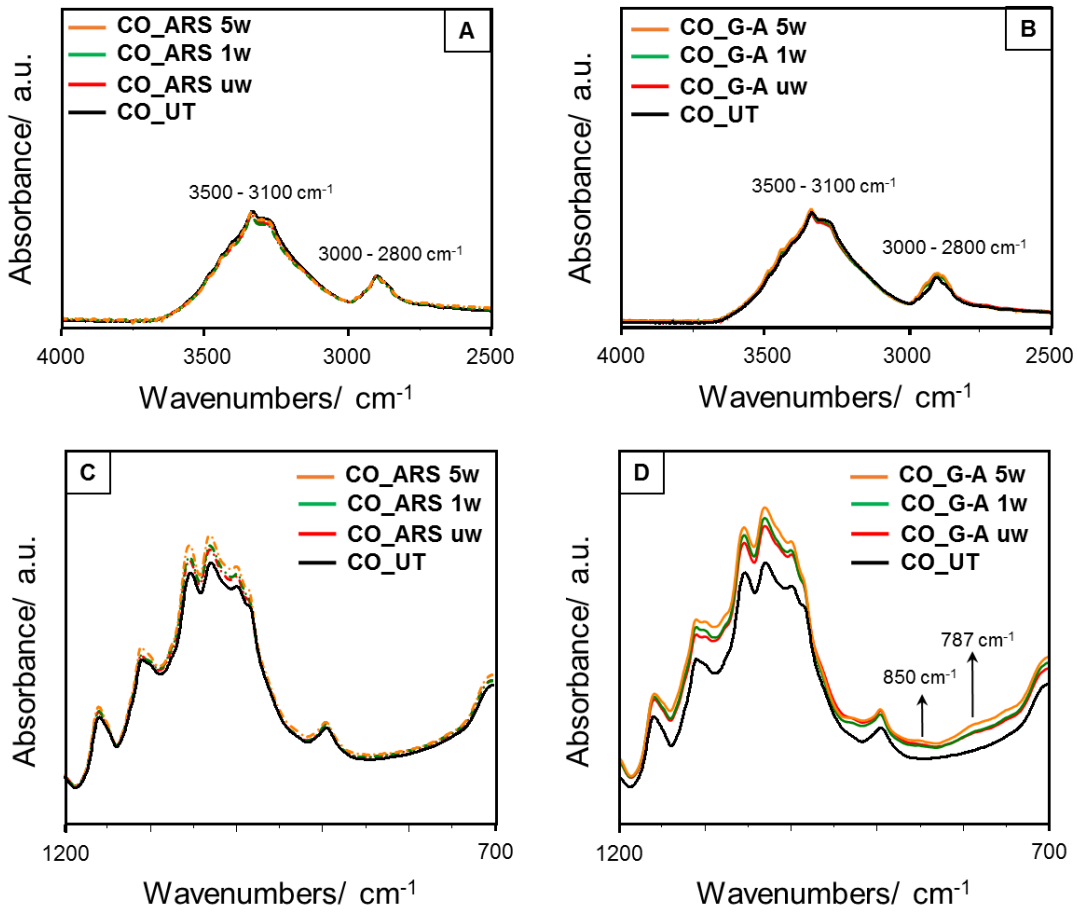

Figure 32: ATR-FTIR spectra of untreated cotton fabric (CO_UT) and cotton fabrics treated with pure ARS (dashed curves) and G-A sol (solid curves), before and after 1 and 5 washing cycles in the range between 4000 – 2500 cm^{-1} (A and B) and 1200 – 700 cm^{-1} (C and D)

As already observed in the cotton treated FTIR curve, the presence of pure ARS is no clearly visible in the spectra of polyester samples due to the high-intensity peaks of polyester functional groups (Figure 33).

In Table 7, the main absorption peaks of polyester fabric are reported.

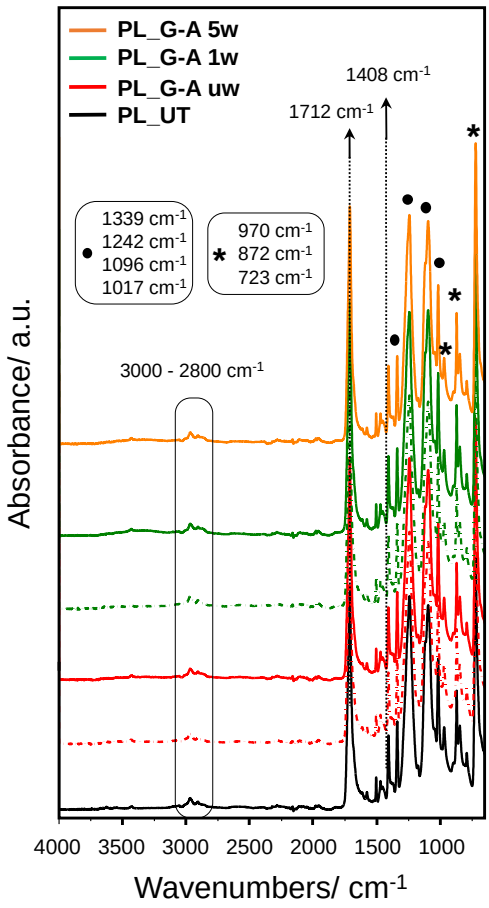

Figure 33: ATR-FTIR spectra of untreated polyester fabric (PL_UT) and polyester fabrics treated with pure ARS (dashed curves) and G-A sol (solid curves), before and after 1 and 5 washing cycles

FTIR peaks	Literature data	Experimental data
C=O stretching in ester	1710 cm^{-1} [72]	1712 cm^{-1}
C=C stretching in benzene	1408 cm^{-1} [72, 73]	1408 cm^{-1}
C-O stretching in ester and carboxylic acid	1016 cm^{-1} [72, 74] 1094 cm^{-1} [72, 74] 1240 cm^{-1} [72, 74]	1017 cm^{-1} 1096 cm^{-1} 1242 cm^{-1}
C-H bending	723 cm^{-1} [72, 75]	723 cm^{-1}
C-H (out of plane CH=CH bending)	871 cm^{-1} [72, 75]	872 cm^{-1}
C-H (in plane CH=CH bending)	968 cm^{-1} [72, 75]	970 cm^{-1}

Table 7: Main FTIR vibrational mode of untreated polyester fabric

The presence of G-A sol on polyester fabrics is confirmed by the increased intensity of the absorption peaks in the spectral region ranging from 3100 cm^{-1} to 2800 cm^{-1} ascribed to C-H stretching of polyester, ARS, and silica network (Figure 34A and 34B). A similar increase in intensity is observed in the range 1750 – 750 cm^{-1} due to the overlapping of carbonyl, SO_2, and silica vibrational mode (Figure 34C and 34D). Such differences from untreated polyester are also visible after washing cycles, thus confirming, as for cotton, the durability of the coating.

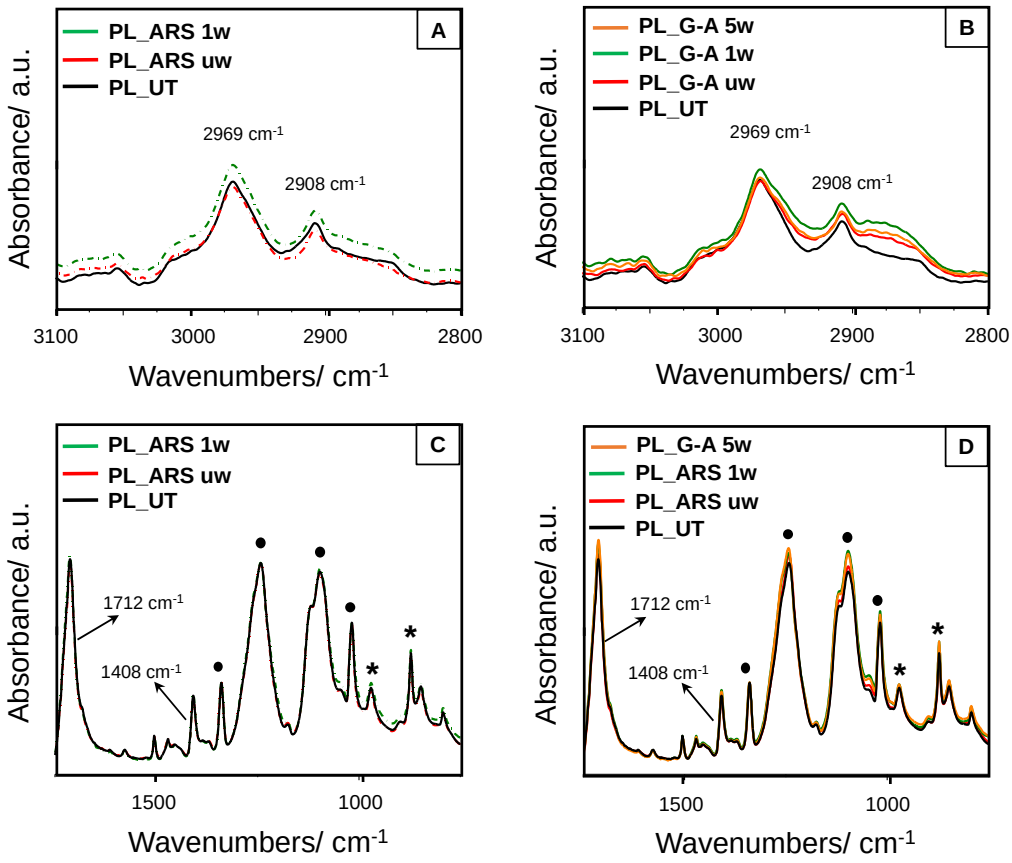

Figure 34: ATR-FTIR spectra of untreated polyester fabric (PL_UT) and polyester fabrics treated with pure ARS (dashed curves) and G-A sol (solid curves), before and after 1 and 5 washing cycles in the range between 4000 – 2500 cm^{-1} (A and B) and 1200 – 700 cm^{-1} (C and D)

To better evaluate the effect of the washing cycles on the durability of the G-A coating on textiles surfaces, both add-on (wt%) and weight loss (WLW, wt%) were calculated by following Eq. 1 and 2 reported in Chapter 2, respectively. CO_ARS and CO_G-A samples were washed 1 and 5 times by following the procedure described in Chapter 2, and measured add-on (wt%) and WLW (wt%) are reported in Table 8. The effectiveness of the functionalized ARS immobilization through the hybrid silica network is confirmed by the higher add-on obtained for sample CO_G-A and PL_G-A than that of CO_ARS and PL_ARS, respectively. In particular, the higher values obtained for cotton textiles

than that of polyester one demonstrated that the designed halochromic silica network is more suitable for cellulose fabric than polyester textiles due to their chemical structure. After one washing cycle, the treated cotton fabrics (CO_G-A) provide a weight loss of 1.06 % that remains unchanged after 5 washing cycles. The obtained data underlined the unique dye leaching after one washing cycle and the stable and durable coating after further washing laundering. Contrary, polyester fabrics (PL_G-A) reveal a low weight loss after one washing cycle and a significant dye leaching after 5 washing laundering, thus confirming the unstable and no durable coating functionalization.

On the other side, the low add-on % obtained for textile samples treated with pure ARS confirmed the weak linkage of the dyestuff with textile surfaces that lead to a significant dye leaching as a consequence of the washing cycle. For this reason, only images of the CO_ARS and PL_ARS samples after 1 washing cycle are reported in Table 8, while the images of the same samples after 5 washing cycles are not reported because they result completely uncolored by the naked eye. Moreover, due to the high weight loss observed after washing cycles, the WLW (wt%) values are not reported in Table 8 for both CO_ARS and PL_ARS samples. According to these experimental findings, the low efficiency of the conventional dyeing technique was confirmed for both cotton and polyester fabrics.

Sample	Add-on (%)	WLW %
CO_ARS	0.35	1W - -
CO_G-A	7.15	1W 1.06 5W 1.05
PL_ARS	0.27	1W - -
PL_G-A	4.44	1W 0.91 5W 2.33

Table 8: Add-on (wt%) and weight loss (WLW, wt%) of cotton and polyester fabrics with both pure ARS and G-A sol

4.4.3.4 XPS characterization of treated cotton samples

The surface chemical composition of both cotton and polyester fabrics, untreated and treated with pure ARS and G-A solutions, was investigated by XPS (Table 9 and 10 for cotton and polyester samples, respectively). The XPS analysis reveals the presence of C, O and Si in the treated samples. In all samples, the C 1s signal was fitted adding three synthetic peaks, positioned at BE = 285.0 eV, 286.6 and 288.9 eV and assigned to C-C, C-O, C=O and COOR bonds, respectively [76]. The O 1s signal is characterized by a single broad peak, including all oxygen species present on the surface (-OH, C=O and Si-O). Regarding the Si 2p signal, in CO_G-A samples, it is characterized by a peak positioned at BE = 102.7 eV, indicating that the adhesion of the coating to the cotton is favored by the C – Si - O bond in the R-SiO_3 configuration (Table 9).

Moreover, XPS data reveal a slight increase in the Si percentage following the first washing cycle and a further decrease in this value after 5 launderings. Considering even the C atomic percentages of each sample, this apparently abnormal behavior could be ascribed to the leaching of unbounded ARS dyestuff entrapped in the sol-gel matrix after the first washing cycle and to the following partial removal of silica-coating after several launderings. However, according to the absolute values given by the ratio of Si to C atomic percentage, the atomic ratios of such elements present on the cotton surface are quite similar before and after washing cycles, thus meaning no significant differences among unwashed and washed samples. The same behavior is shown by XPS data referred to polyester fabrics (Table 10).

	Chemical composition (%)				
BE (eV)	285.0	286.8	288.9	102.7	
	C – C	**C – O, C=O**	**COOR**	**SiO_2, O – Si – C**	**Si/C**
CO_UT	24.2 ± 2.42	35.2 ± 3.52	6.3 ± 0.63		
CO_ARS uw	23.7 ± 2.37	33.2 ± 3.32	6.5 ± 0.65		
CO_ARS 1w	22.9 ± 2.29	34.7 ± 3.47	6.5 ± 0.65		
CO_ARS 5w	15.6 ± 1.56	39.9 ± 3.99	6.5 ± 0.65		
CO_G-A uw	29.3 ± 2.93	28.5 ± 2.85	6.2 ± 0.62	4.5 ± 0.45	0.07
CO_G-A 1w	26.3 ± 2.63	29.0 ± 2.90	5.5 ± 0.55	5.7 ± 0.57	0.09
CO_G-A 5w	21.4 ± 2.14	33.0 ± 3.30	5.8 ± 0.58	4.7 ± 0.47	0.08

Table 9: Surface chemical composition of cotton samples by XPS

Chemical composition (%)					
BE (eV)	285.0	286.8	288.9	102.7	
	C – C	**C – O, C=O**	**COOR**	**SiO_2, O – Si – C**	**Si/C**
PL_UT	52.0 ± 5.20	13.1 ± 1.31	10.9 ± 1.09		
PL_ARS uw	45.5 ± 4.55	13.8 ± 1.38	11.3 ± 1.13		
PL_ARS 1w	42.6 ± 4.26	14.3 ± 1.43	10.8 ± 1.08		
PL_G-A uw	43.9 ± 4.39	15.3 ± 1.53	9.6 ± 0.96	2.8 ± 0.28	0.04
PL_G-A 1w	41.4 ± 4.14	16.7 ± 1.67	10.7 ± 1.07	2.9± 0.29	0.04
PL_G-A 5w	41.9 ± 4.19	16.4 ± 1.64	10.8 ± 1.08	2.8 ± 0.28	0.04

Table 10: Surface chemical composition of polyester samples by XPS

4.4.3.5 pH-dependent properties of hybrid G-A sol: UV-Vis study in solutions

Pure ARS and G-A solutions were investigated through UV-Vis spectroscopy to assess the halochromic behavior of ARS with and without the presence of the silica matrix in the pH range between 2 and 8. In this regard, the pH of diluted ARS and G-A solution was corrected with a specific amount of phosphate buffer ($Na_2HPO_4 \cdot 12\ H_2O$/ $NaH_2PO_4 \cdot 2\ H_2O$) at different pH, and the obtained buffer solutions were analyzed. The addition of phosphate buffer to both pure ARS and G-A sol provides a color change from yellow (pH 2) to red (pH 8), with very slight color differences between pure and functionalized dyestuff visible by the naked eye.

UV-vis spectra of buffered ARS solutions (Figure 35) reveal two maxima absorbance peaks at 423 nm for acidic pH (2 – 4) and 522 nm for slight alkaline pH (6 - 8) corresponding to the neutral and mono-anionic form, respectively, in accordance with literature data [61, 77]. For acidic pH, the pure dye exists in the protonated form, while at increasing pH (above 6), the deprotonation of one of the hydroxyl groups takes place, thus leading to intramolecular hydrogen bonding between other OH groups and ketonic oxygen by forming a six-membered ring. So, UV-Vis spectra of ARS at pH 6 are characterized by the absorption band at 522 nm, which are due to $n \rightarrow \pi^*$ transitions of p-benzoquinone group condensed between two rings [60]. For alkaline pH values, the observed large bathochromic shift from 423 nm to 522 nm is mainly due to the high delocalization of electrons that reduce the required energy for transition, thus shifting the absorption band towards higher wavelengths [60]. Similar behavior and the same maxima absorbance peaks were showed by the UV-Vis spectra of

buffered G-A solutions (Figure 35) by revealing slight differences in intensities with respect to pure ARS curves.

Indeed, the main differences are in the absorbance changes of the maximum wavelength at 522 nm of G-A solution, as clearly evident in Figure 35, even if the color changes of both ARS and G-A solutions appear quite similar to the naked eye. However, at increasing pH values, both solutions present the same bathochromic shift of the peak at 423 nm to 522 nm (pure ARS) and 519 nm (G-A sol), and similar hyper- and hypo-chromic shift of the peaks at 423 nm and 522 nm, respectively (Figure 35).

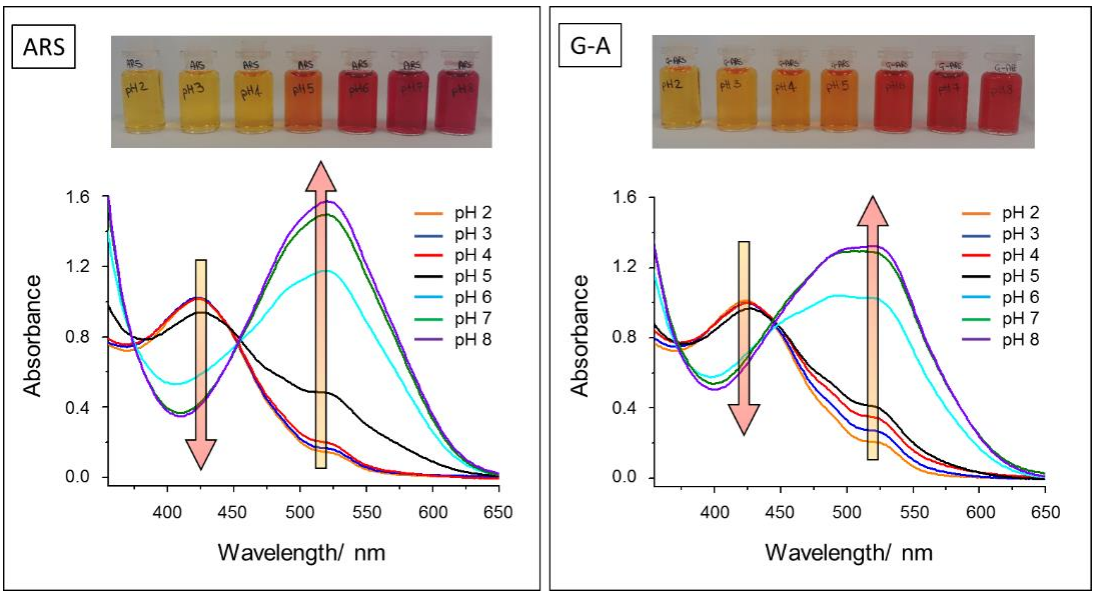

Figure 35: UV-Vis spectra of pure ARS and G-A solutions at different pH with the corresponding images of solutions

To confirm the halochromic behavior of ARS in the silica matrix, absorbance values at maxima wavelengths as a function of pH for both ARS and G-A solutions were reported in Figure 36. As confirmed by spectra, the ARS halochromic response between pH 2 and 8 is similar to that exhibited by G-A solutions despite the covalent linkages of ARS with GPTMS molecules through epoxy ring-opening, thus confirming that the pH response of G-A solutions is in accordance with ARS halochromic properties. Moreover, for pH ranging from 5 to 8, the G-A solution reveals lower, and higher absorbance values than that of the ARS curves for 522 nm and 423 nm maxima wavelength, respectively, which agrees with the slight color difference observed for pure ARS and G-A solutions.

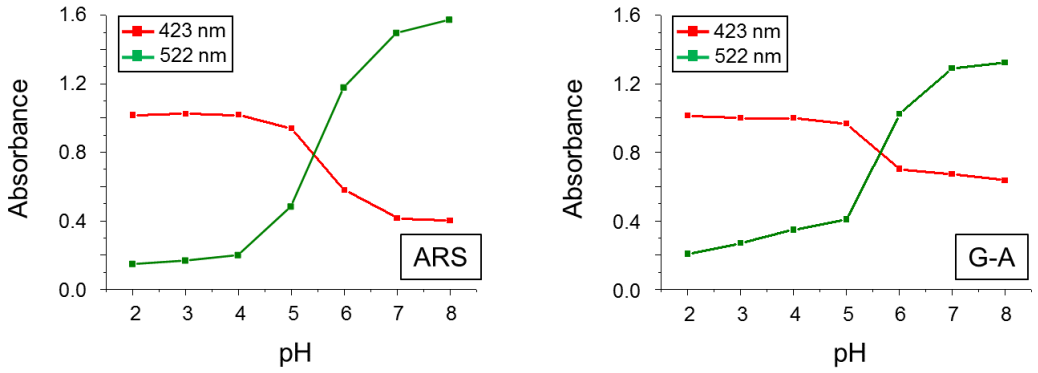

Figure 36: UV-Vis spectra of buffered ARS and G-A solutions at maxima wavelengths

4.4.3.6 Diffuse reflectance measurements: textile pH-response

Different halochromic behavior could be provided by dyestuffs if in buffered solution or on textile substrates because of the interaction between the dye and the textile fibers, as well as slightly different color changes can be observed depending on the nature of the textile fabrics. UV-Vis reflectance spectroscopy in CIELAB color space was employed to study the pH-response of treated cotton samples after washing cycles. All textiles treated with pure ARS and G-A sol, after 1 and 5 washing cycles, were soaked separately in pH buffer solutions ranging from 2 to 8, and the R% values were obtained for each sample and used in the Kubelka-Munk equation (Eq. 3, Chapter 2). The Kubelka-Munk diffuse reflectance UV-Vis spectra of cotton and polyester samples are reported in Figure 37, 38, 39, and 40.

The halochromic response of cotton dyed with pure ARS is coherent with that observed for the corresponding solution (Figure 37). According to this evidence, the interaction between the pure dye and the cotton fiber does not affect the halochromic behavior of ARS significantly. Cotton samples at different pH values provide a slight bathochromic shift of maxima wavelength from 423 nm (in solution) to 430 nm (on textiles) and from 522 nm (in solution) to 525 nm (on cotton for pH 8). A different response was obtained for the same cotton samples washed five times: for each pH, a significant K-M decrease was observed. The two absorbance maxima are no longer clearly discernible, thus confirming the loss of the pH response CO_ARS after 5 washing cycles.

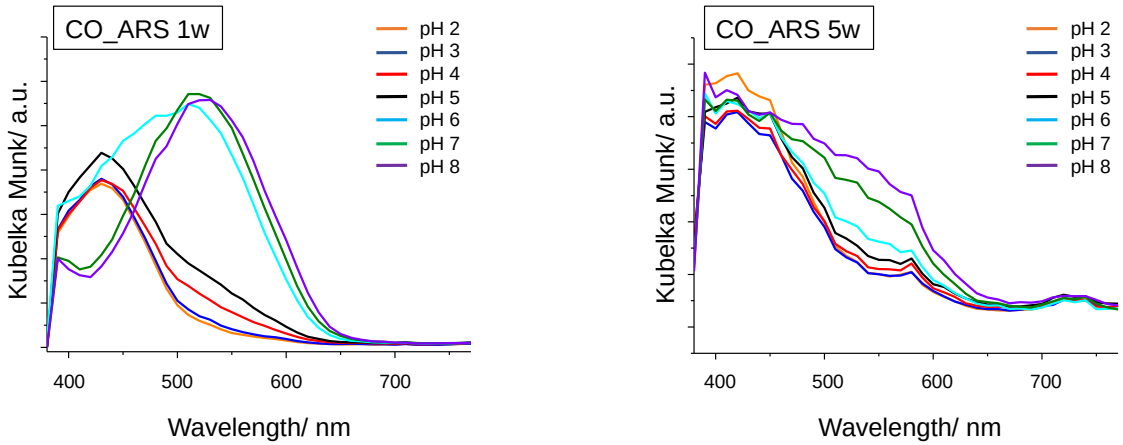

Figure 37: Kubelka-Munk spectra of CO_ARS at different pH values after 1 and 5 washing cycles

In Figure 38, K-M spectra of cotton treated with the hybrid dye silica coating after 1 and 5 washing cycles (CO_G-A 1w and CO_G-A 5w) are reported. As expected, CO_ARS 1w and CO_G-A 1w samples show a slightly different halochromic behavior due to the sol-gel covalent immobilization of the dye. In particular, the CO_G-A sample reveals higher K-M values than that of CO_ARS, and main differences are observed for pH 4 and 5. At these pH values, the maxima absorbance curves of CO_G-A 1w undergone a bathochromic shift from 423 nm to 481 nm (pH 4) and 503 nm (pH 5) due to covalent immobilization of the dyestuff with GPTMS sol precursor that provides a change in the surroundings of the chromophore. Similar bathochromic shifts were observed for pH 6, 7 and 8 from 519 nm (in solution) to 517 and 539 nm (on cotton). However, according to the obtained Kubelka-Munk curves, both treated cotton fabrics (CO_ARS and CO_G-A) show color changes in the pH ranging from yellow to red as previously observed from the solutions reported in Figure 35.

As clearly evident in Figure 38, compared to CO_G-A 1w curves, the CO_G-A 5w sample reveals a decrease in the 423 nm maximum absorbance peak for acidic pH, while no significant changes in the intensity of alkaline maximum wavelength are found. The latter evidence confirms the efficiency in the pH-response of the cotton fabrics treated with the silica-immobilized ARS even after 5 washing cycles.

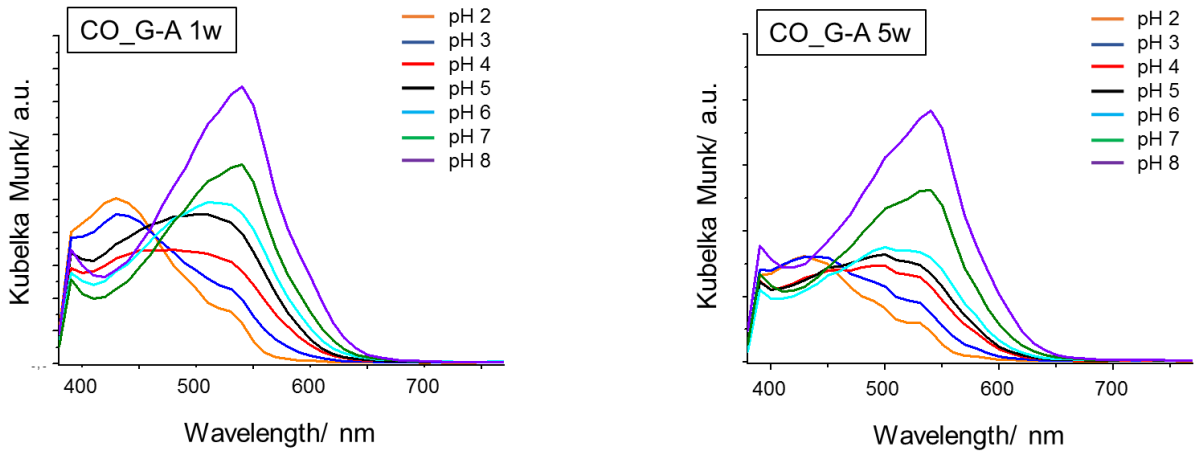

Figure 38: Kubelka-Munk spectra of CO_G-A at different pH values after 1 and 5 washing cycles

Kubelka Munk curves of polyester treated with pure ARS and G-A sol are reported in Figure 39 and Figure 40, respectively. As expected, K-M curves confirm the low pH response of the polyester fabrics treated with pure ARS, thus highlighting that no bathochromic shift occurs for alkaline pH. As a consequence of these results, K-M curves of PL_ARS 5w are not reported since the dye release was otherwise too high to allow for a halochromic study.

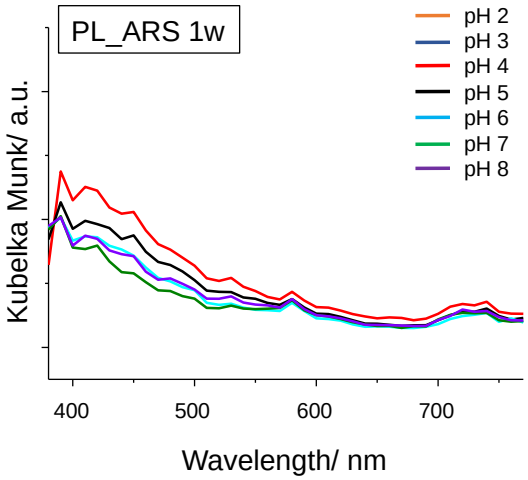

Figure 39: Kubelka-Munk spectra of PL_ARS at different pH values after 1 and 5 washing cycles

Kubelka-Munk curves of polyester samples treated with G-A sol are reported in Figure 40, notwithstanding they are no clearly defined and homogeneous. Maybe their aspect can be due to the low affinity of ARS with polyester fabric, as previously hypothesized by the obtained add-on (wt %). However, the typical halochromic response of ARS seems slightly different from that of cotton fabrics, maybe due to the interaction of dyestuff and polyester fabrics. No significant information can

be obtained from these spectra, thus confirming that the designed synthesis for the immobilization of ARS on textile fabrics is more suitable for cellulose ones.

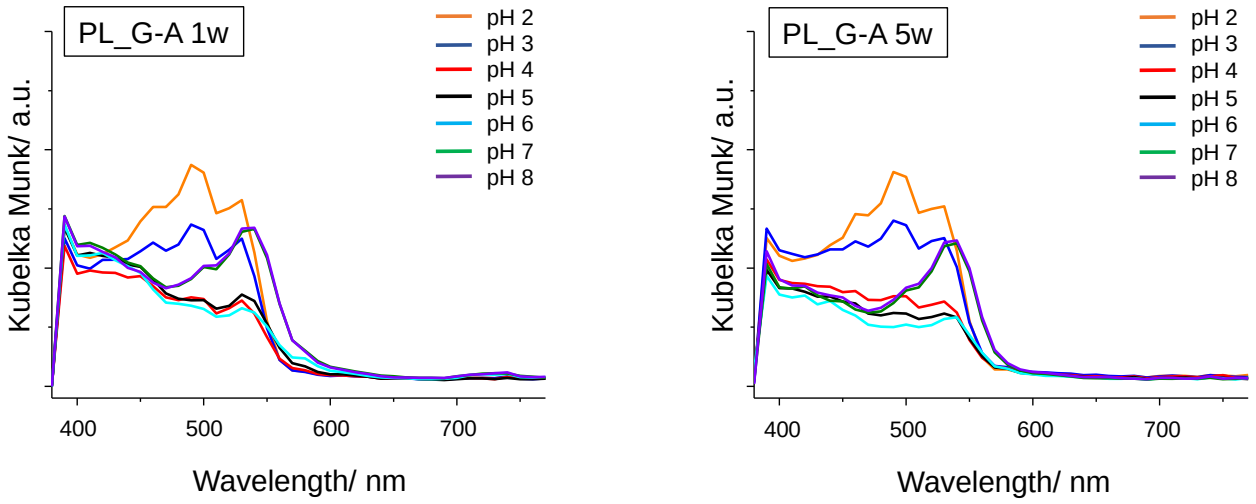

Figure 40: Kubelka-Munk spectra of PL_G-A at different pH values after 1 and 5 washing cycles

The time response of the halochromic textiles was fully established within 5 minutes for all samples. The pH response of treated cotton fabrics after 1 and 5 washing cycles was further evaluated through color changes in CIELAB color space (ΔE*). With this aim, ΔE* color changes with respect to pH 2 as a function of pH variations are reported in Figure 41 for both washed CO_ARS and CO_G-A samples. All samples show a distinct color variation between pH 2 and 8. Lower ΔE* for CO_ARS samples at each pH value was obtained. More in detail, the CO_ARS 5w sample provides ΔE* values significantly lower than that of CO_ARS 1w and CO_G-A samples due to the dye leaching. On the contrary, the CO_G-A 5w sample provides ΔE* values almost similar to those obtained for CO_G-A 1w. These experimental findings confirm both the good washing fastness of the G-A coated cotton fabrics and the consistent halochromic response of the G-A solution with the ARS dyestuff.

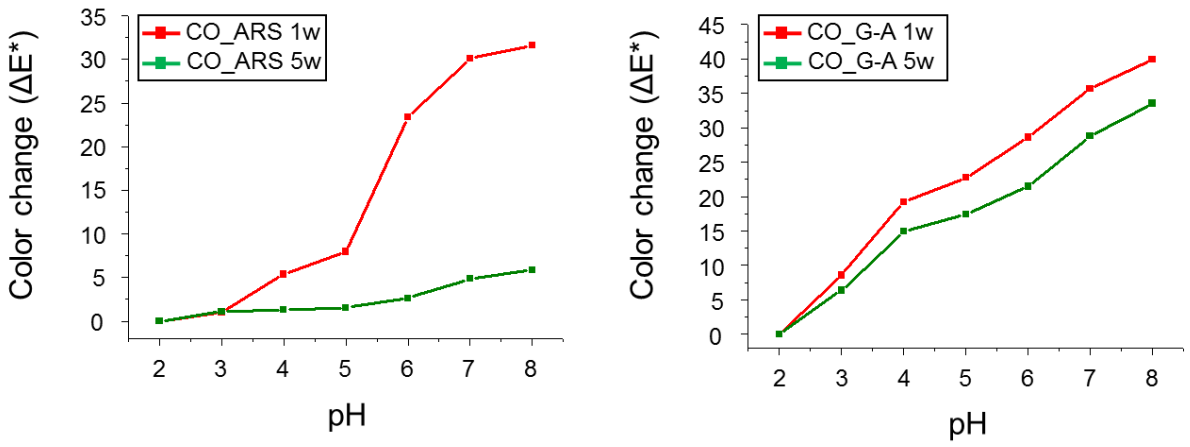

Figure 41: ΔE* color change with respect to pH 2 of both CO_ARS and CO_G-A after 1 and 5 washing cycles as a function of pH variations

4.5 Conclusions

The development of halochromic wearable sensors provides several advantages in healthcare, medicine, fitness, and diagnostic fields. The relevant aspects of these wearable sensors consist of their potentiality for real-time and continuous monitoring of patients' physiological conditions. The research studies explained in this Chapter highlight the advantages of covalent immobilization of a halochromic dye, nitrazine yellow and alizarin red S, specifically chosen for their color change in the pH scale of the human sweat, according to grafting or sol-gel approaches. The main advantage of these techniques consists of the reduced dye leaching due to laundering cycles and the stable immobilization of the dye without the loss of its halochromic response compared to conventional dyeing techniques. Furthermore, the use of non-toxic dyestuff is an important issue in this research field, and examples are reported in the literature with the immobilization of litmus and resorufin in the sol-gel polymer networks. In this scenario, even if nitrazine yellow and alizarin red S could be harmful, the low concentration needed to develop the halochromic textiles ensures their no-toxicity for human health. However, further investigations will be conducted to evaluate both the environmental impact and the consequence on the human health of the used halochromic dyestuffs.

Experimental findings, particularly based on UV-Vis studies, evidenced a slight alteration in the maxima wavelength of treated textiles compared to the reference solutions and the low influence of cotton fabrics in the halochromic response of both dyes. Conversely, the polyester fabrics significantly affect the pH-response of alizarin red S, thus resulting in a not suitable substrate for the development of ARS-based pH sensors. This behavior could be ascribed to fabrics nature and, consequently, to the presence of functional groups on the surface of the fabrics. Indeed, these functionalities affect both the hydrophilicity degree of the textile itself and the reactiveness toward

applied coatings. As demonstrated in the experiments carried out with the sol-gel ARS-based films, the different chemical structures of the fabric substrates (cotton and polyester) provide different chemical interactions with the hybrid film and dyestuff, thus influencing the dye leaching.
Finally, wearable pH-sensors are of great interest in health monitoring, and their development can be only a part of multidisciplinary research also involving electronic and engineering science through the integration of non-invasive electronic devices, thus providing useful, easy to use and low-cost wearable sensors. Moreover, previous research confirmed that sol-gel based coatings do not reveal cytotoxic effects on human skin cells. Therefore, halochromic textiles, realized through the sol-gel technique, are safe for use in contact with the skin and, thanks to their low environmental impact, such silica films could be considered interesting materials for the development of smart textiles for sensing and protective end-uses.

4.6 Development of prototype: “Health Belt”

The promising experimental findings obtained from both halochromic textiles realized through the covalent immobilization of nitrazine yellow and alizarin red S dyestuffs paved the way for the development of a prototype for the real-time monitoring of sweat pH, named “Health Belt”. As described in Chapter 2, “Health Belt" is an elastic textile integrated with microelectronics (Figure 42): the elastic strip consists of a textile fabric as a sweat pH-sensing element and a miniaturized electronic device for data detection, conditioning and transmission. In particular, the coating has been realized by immobilizing molecules with halochromic properties (in the sweat pH range) through the sol-gel technology or grafting approach described in previous paragraphs. The employed technology ensures the adhesion of the film on the textile substrate implementing an environmentally friendly and safe application for human health. The electronic device is made up of a LED/photodiode system for the detection of colorimetric variations, powered by a rechargeable Lithium polymer battery.
Further evaluation, among which accuracy and resolution of the pH measurements, have been performed to develop the prototype “Health Belt”. With this aim, the pH-response of the halochromic textile, previously characterized by UV-vis spectroscopy also to obtain a pH estimation model, was tested simultaneously by an electronic device and a reference pH-meter. To test the performance of the smart textiles integrated with electronics, an exercise bike session was performed, obtaining pH values with a resolution and accuracy of about ±0.2 and ±0.5 pH units, respectively. The results obtained from Health Belt are in agreement with those obtained in previous studies by using similar electronics [41].

The product has been developed with the aim of integrating it with software for remote data processing. Indeed, besides acquiring the signal, the device removes any interference and transmits the remote data collected through a Bluetooth Serial Port Profile (SPP). It is possible to collect data simply and rapidly and evaluate an athlete's sweat pH variation during physical activity by using a specific app. "Health Belt" makes it possible to obtain, in real-time and in a non-invasive way, information regarding the athlete's level of hydration, the concentration of specific ions, but also data related to some skin diseases.

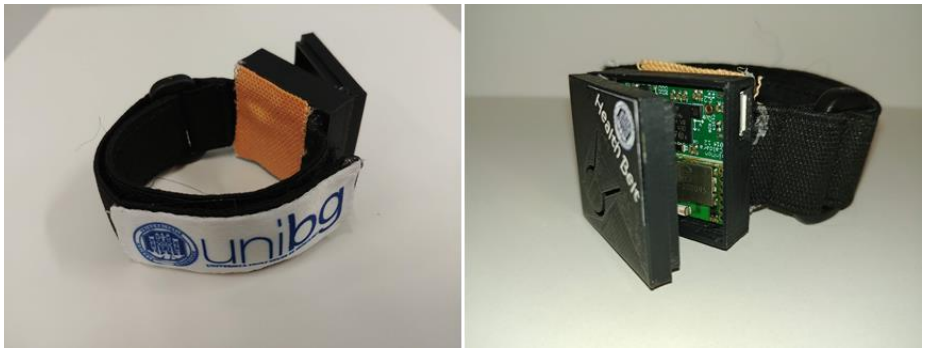

Figure 42: “Health Belt” realized by the integration of pH-sensitive textiles (on the left) and an electronic device (on the right). Adapted under the terms of the Creative Commons CC BY-NC-ND 4.0 license [5]. Copyright 2021, the Authors, Published by MDPI

References

1. Lin J (2000) Recent development and applications of optical and fiber-optic pH sensors. TrAC Trends Anal Chem 19:541–552. https://doi.org/10.1016/S0165-9936(00)00034-0
2. Tsai P-J, McIntosh J, Pearce P, et al (2002) Anthocyanin and antioxidant capacity in Roselle (Hibiscus Sabdariffa L.) extract. Food Res Int 35:351–356. https://doi.org/10.1016/S0963-9969(01)00129-6
3. Maciel VBV, Yoshida CMP, Franco TT (2012) Development of a prototype of a colourimetric temperature indicator for monitoring food quality. J Food Eng 111:21–27. https://doi.org/10.1016/j.jfoodeng.2012.01.037
4. Van der Schueren L, De Clerck K (2010) The Use of pH-indicator Dyes for pH-sensitive Textile Materials. Text Res J 80:590–603. https://doi.org/10.1177/0040517509346443
5. Ielo I, Giacobello F, Sfameni S, et al (2021) Nanostructured Surface Finishing and Coatings: Functional Properties and Applications. Materials (Basel) 14:2733. https://doi.org/10.3390/ma14112733
6. Robinson KL, Lawrence NS (2006) Redox-Sensitive Copolymer: A Single-Component pH Sensor. Anal Chem 78:2450–2455. https://doi.org/10.1021/ac051787k
7. Lobnik A, Turel M US (2012) Optical chemical sensors: design and applications. In: Prof. Wang W (ed) Advances in chemical sensors. pp 3–28
8. Nagl S, Wolfbeis OS Classification of Chemical Sensors and Biosensors Based on Fluorescence and Phosphorescence. In: Standardization and Quality Assurance in Fluorescence Measurements I. Springer Berlin Heidelberg, Berlin, Heidelberg, pp 325–346
9. Gründler P (2007) Chemical Sensors, An Introduction for Scientists and Engineers. Springer Berlin Heidelberg, Berlin, Heidelberg
10. Jeronimo P, Araujo A, Conceicao BSM Montenegro (2007) Optical sensors and biosensors based on sol–gel films. Talanta 72:13–27. https://doi.org/10.1016/j.talanta.2006.09.029
11. Seitz WR, Sepaniak MJ (1988) Chemical Sensors Based on Immobilized Indicators and Fiber Optics. C R C Crit Rev Anal Chem 19:135–173. https://doi.org/10.1080/10408348808542810
12. Trovato V, Colleoni C, Castellano A, Plutino MR (2018) The key role of 3-glycidoxypropyltrimethoxysilane sol–gel precursor in the development of wearable sensors for health monitoring. J Sol-Gel Sci Technol 87:27–40. https://doi.org/10.1007/s10971-018-4695-x

13. Wencel D, Abel T, McDonagh C (2014) Optical Chemical pH Sensors. Anal Chem 86:15–29. https://doi.org/10.1021/ac4035168
14. Lukowiak A, Strek W (2009) Sensing abilities of materials prepared by sol–gel technology. J Sol-Gel Sci Technol 50:201–215. https://doi.org/10.1007/s10971-009-1952-z
15. Van der Schueren L, de Clerck K (2012) Halochromic Textile Materials as Innovative pH-Sensors. Adv Sci Technol 80:47–52. https://doi.org/10.4028/www.scientific.net/AST.80.47
16. Mattila HR (2006) Intelligent textiles and clothing. Woodhead Publishing Limited
17. Van der Schueren L (2012) Halochromic fibrous materials for sensor applications Halochrome vezelmaterialen voor sensorapplicaties Lien Van der Schueren
18. Bamfield P (2001) Chromic Phenomena, Technological Applications of Color Chemistry. Royal Society of Chemistry, Cambridge
19. Nanda D, Tung K-L, Li Y-L, et al (2010) Effect of pH on membrane morphology, fouling potential, and filtration performance of nanofiltration membrane for water softening. J Memb Sci 349:411–420. https://doi.org/10.1016/j.memsci.2009.12.004
20. Van Geluwe S, Braeken L, Van der Bruggen B (2011) Ozone oxidation for the alleviation of membrane fouling by natural organic matter: A review. Water Res 45:3551–3570. https://doi.org/10.1016/j.watres.2011.04.016
21. Kobayashi O, Higuchi K, Miwa E, Tadano T (2010) Growth injury induced by high pH in rice and tomato. Soil Sci Plant Nutr 56:407–411. https://doi.org/10.1111/j.1747-0765.2010.00470.x
22. Murata MR, Hammes PS, Zharare GE (2003) Effect of Solution pH and Calcium Concentration on Germination and Early Growth of Groundnut. J Plant Nutr 26:1247–1262. https://doi.org/10.1081/PLN-120020368
23. Stefaniak AB, Harvey CJ (2006) Dissolution of materials in artificial skin surface film liquids. Toxicol Vitr 20:1265–1283. https://doi.org/10.1016/j.tiv.2006.05.011
24. Shirreffs SM, Maughan RJ (1997) Whole body sweat collection in humans: an improved method with preliminary data on electrolyte content. J Appl Physiol 82:336–341. https://doi.org/10.1152/jappl.1997.82.1.336
25. Patterson MJ, Galloway SD, Nimmo MA (2000) Variations in regional sweat composition in normal human males. Exp Physiol 85:869–875. https://doi.org/10.1111/j.1469-445X.2000.02058.x

26. Patterson MJ, Galloway SDR, Nimmo MA (2002) Effect of induced metabolic alkalosis on sweat composition in men. Acta Physiol Scand 174:41–46. https://doi.org/10.1046/j.1365-201x.2002.00927.x
27. Hayden G, Milne HC, Patterson MJ, Nimmo MA (2004) The reproducibility of closed-pouch sweat collection and thermoregulatory responses to exercise?heat stress. Eur J Appl Physiol 91:748–751. https://doi.org/10.1007/s00421-004-1057-x
28. Morgan RM, Patterson MJ, Nimmo MA (2004) Acute effects of dehydration on sweat composition in men during prolonged exercise in the heat. Acta Physiol Scand 182:37–43. https://doi.org/10.1111/j.1365-201X.2004.01305.x
29. Jacobi U, Gautier J, Sterry W, Lademann J (2005) Gender-Related Differences in the Physiology of the Stratum Corneum. Dermatology 211:312–317. https://doi.org/10.1159/000088499
30. Robinson S, Robinson AH (1954) Chemical Composition of Sweat. Physiol Rev 34:202–220. https://doi.org/10.1152/physrev.1954.34.2.202
31. Curto VF, Coyle S, Byrne R, et al (2012) Concept and development of an autonomous wearable micro-fluidic platform for real time pH sweat analysis. Sensors Actuators B Chem 175:263–270. https://doi.org/10.1016/j.snb.2012.02.010
32. Schmid-Wendtner M-H, Korting HC (2006) The pH of the Skin Surface and Its Impact on the Barrier Function. Skin Pharmacol Physiol 19:296–302. https://doi.org/10.1159/000094670
33. Harvey CJ, LeBouf RF, Stefaniak AB (2010) Formulation and stability of a novel artificial human sweat under conditions of storage and use. Toxicol Vitr 24:1790–1796. https://doi.org/10.1016/j.tiv.2010.06.016
34. Staneva D, Betcheva R, Chovelon J-M (2007) Optical sensor for aliphatic amines based on the simultaneous colorimetric and fluorescence responses of smart textile. J Appl Polym Sci 106:1950–1956. https://doi.org/10.1002/app.26724
35. Billah SMR, Christie RM, Shamey R (2008) Direct coloration of textiles with photochromic dyes. Part 1: Application of spiroindolinonaphthoxazines as disperse dyes to polyester, nylon and acrylic fabrics. Color Technol 124:223–228. https://doi.org/10.1111/j.1478-4408.2008.00145.x
36. Broadbent AD (2001) Basic principles of textile coloration. Society of Dyers and Colourists, England

37. Van der Schueren L, De Clerck K, Brancatelli G, et al (2012) Novel cellulose and polyamide halochromic textile sensors based on the encapsulation of Methyl Red into a sol?gel matrix. Sensors Actuators B Chem 162:27–34. https://doi.org/10.1016/j.snb.2011.11.077
38. Greiner A, Wendorff JH (2007) Electrospinning: A Fascinating Method for the Preparation of Ultrathin Fibers. Angew Chemie Int Ed 46:5670–5703. https://doi.org/10.1002/anie.200604646
39. Fantini D, Costa L (2009) Dye, fluorophores and pigment coloration of nanofibers produced by electrospinning. Polym Adv Technol 20:111–121. https://doi.org/10.1002/pat.1283
40. Guido E, Colleoni C, De Clerck K, et al (2014) Influence of catalyst in the synthesis of a cellulose-based sensor: Kinetic study of 3-glycidoxypropyltrimethoxysilane epoxy ring opening by Lewis acid. Sensors Actuators B Chem 203:213–222. https://doi.org/10.1016/j.snb.2014.06.126
41. Caldara M, Colleoni C, Guido E, et al (2016) Optical monitoring of sweat pH by a textile fabric wearable sensor based on covalently bonded litmus-3-glycidoxypropyltrimethoxysilane coating. Sensors Actuators, B Chem 222:213–220. https://doi.org/10.1016/j.snb.2015.08.073
42. Caldara M, Colleoni C, Guido E, et al (2012) Development of a textile-optoelectronic pH meter based on hybrid xerogel doped with Methyl Red. Sensors Actuators B Chem 171–172:1013–1021. https://doi.org/10.1016/j.snb.2012.06.024
43. Plutino MR, Guido E, Colleoni C, Rosace G (2017) Effect of GPTMS functionalization on the improvement of the pH-sensitive methyl red photostability. Sensors Actuators B Chem 238:281–291. https://doi.org/10.1016/j.snb.2016.07.050
44. Rosace G, Guido E, Colleoni C, et al (2017) Halochromic resorufin-GPTMS hybrid sol-gel: Chemical-physical properties and use as pH sensor fabric coating. Sensors Actuators B Chem 241:85–95. https://doi.org/10.1016/j.snb.2016.10.038
45. Rosace G, Colleoni C, Trovato V, et al (2017) Vinylphosphonic acid/methacrylamide system as a durable intumescent flame retardant for cotton fabric. Cellulose 24:3095–3108. https://doi.org/10.1007/s10570-017-1294-x
46. Waring DR, Hallas G (1990) The Chemistry and Application of Dyes. Springer US, Boston, MA
47. Kianfar P, Abate MT, Trovato V, et al (2020) Surface Functionalization of Cotton Fabrics by Photo-Grafting for pH Sensing Applications. Front Mater 7:. https://doi.org/10.3389/fmats.2020.00039

48. Trovato V, Vitale A, Bongiovanni R, et al (2021) Development of a Nitrazine Yellow-glycidyl methacrylate coating onto cotton fabric through thermal-induced radical polymerization reactions: a simple approach towards wearable pH sensors applications. Cellulose. https://doi.org/10.1007/s10570-021-03733-w
49. Ngwabebhoh FA, Erdem A, Yildiz U (2016) Synergistic removal of Cu(II) and nitrazine yellow dye using an eco-friendly chitosan-montmorillonite hydrogel: Optimization by response surface methodology. J Appl Polym Sci 133:. https://doi.org/10.1002/app.43664
50. Viscardi G, Quagliotto P, Barolo C, et al (2003) Structural characterisation of Nitrazine Yellow by NMR spectroscopy. Dye Pigment 57:87–95. https://doi.org/10.1016/S0143-7208(02)00164-X
51. Van der Schueren L, Hemelsoet K, Van Speybroeck V, De Clerck K (2012) The influence of a polyamide matrix on the halochromic behaviour of the pH-sensitive azo dye Nitrazine Yellow. Dye Pigment 94:443–451. https://doi.org/10.1016/j.dyepig.2012.02.013
52. Pavlović G, Racané L, Čičak H, Tralić-Kulenović V (2009) The synthesis and structural study of two benzothiazolyl azo dyes: X-ray crystallographic and computational study of azo–hydrazone tautomerism. Dye Pigment 83:354–362. https://doi.org/10.1016/j.dyepig.2009.06.002
53. Bredereck K (1993) Structure Reactivity Correlations of Azo Reactive Dyes Based on H-acid I. NMR Chemical Shift Values, pKa Values, Dyestuff Aggregation and Dyeing Behaviour. Dye Pigment 21:23–43. https://doi.org/10.1016/0143-7208(93)85003-I
54. Kr R, Singh AP, Chauhan GS (2014) Grafting of GMA and some comonomers onto chitosan for controlled release of diclofenac sodium. Int J Biol Macromol 64:368–376. https://doi.org/10.1016/j.ijbiomac.2013.12.028
55. Xu T, Tang Z, Zhu J (2012) Synthesis of polylactide-graft-glycidyl methacrylate graft copolymer and its application as a coupling agent in polylactide/bamboo flour biocomposites. J Appl Polym Sci 125:E622–E627. https://doi.org/10.1002/app.36808
56. Jenkins DW, Hudson SM (2001) Review of vinyl graft copolymerization featuring recent advances toward controlled radical-based reactions and illustrated with chitin/chitosan trunk polymers. Chem Rev 101:3245–3273. https://doi.org/10.1021/cr000257f
57. Khalil MI, Mostafa KM, Hebeish A (1993) Graft polymerization of acrylamide onto maize starch using potassium persulfate as initiator. Die Angew Makromol Chemie 213:43–54. https://doi.org/10.1002/apmc.1993.052130106

58. Rosace G, Massafra MR (2008) Marking of Cellulose Yarn by Vinyl Monomer Grafting. Text Res J 78:28–36. https://doi.org/10.1177/0040517507082187
59. Steyaert I, Vancoillie G, Hoogenboom R, De Clerck K (2015) Dye immobilization in halochromic nanofibers through blend electrospinning of a dye-containing copolymer and polyamide-6. Polym Chem 6:2685–2694. https://doi.org/10.1039/C5PY00060B
60. Sharma R, Kamal A, Mahajan RK (2016) A quantitative appraisal of the binding interactions between an anionic dye, Alizarin Red S, and alkyloxypyridinium surfactants: a detailed micellization, spectroscopic and electrochemical study. Soft Matter 12:1736–1749. https://doi.org/10.1039/C5SM02667A
61. Lemlikchi W, Sharrock P, Fiallo M, et al (2014) Hydroxyapatite and Alizarin Sulfonate ARS Modeling Interactions for Textile Dyes Removal from Wastewaters. Procedia Eng 83:378–385. https://doi.org/10.1016/j.proeng.2014.09.032
62. Kubo Y, Ishida T, Kobayashi A, James TD (2005) Fluorescent alizarin–phenylboronic acid ensembles: design of self-organized molecular sensors for metal ions and anions. J Mater Chem 15:2889. https://doi.org/10.1039/b501243k
63. Faouzi AM, Nasr B, Abdellatif G (2007) Electrochemical degradation of anthraquinone dye Alizarin Red S by anodic oxidation on boron-doped diamond. Dye Pigment 73:86–89. https://doi.org/10.1016/j.dyepig.2005.10.013
64. Zucca P, Vinci C, Sollai F, et al (2008) Degradation of Alizarin Red S under mild experimental conditions by immobilized 5,10,15,20-tetrakis(4-sulfonatophenyl)porphine–Mn(III) as a biomimetic peroxidase-like catalyst. J Mol Catal A Chem 288:97–102. https://doi.org/10.1016/j.molcata.2008.04.001
65. Zaggout FR, Qarraman AE-FA, Zourab SM (2007) Behavior of immobilized Alizarin Red S into sol–gel matrix as pH sensor. Mater Lett 61:4192–4195. https://doi.org/10.1016/j.matlet.2007.01.080
66. Gabrielli L, Connell L, Russo L, et al (2014) Exploring GPTMS reactivity against simple nucleophiles: chemistry beyond hybrid materials fabrication. RSC Adv 4:1841–1848. https://doi.org/10.1039/C3RA44748K
67. El-Nahass MM, Zeyada HM, El-Ghamaz NA, Awed AS (2018) Structural investigation, thermal analysis and AC conduction mechanism of thermally evaporated alizarin red S thin films. Optik (Stuttg) 170:304–313. https://doi.org/10.1016/j.ijleo.2018.05.130

68. Ranjitha S, Aroulmoji V, Mohr T, et al (2014) Structural and Spectral Properties of 1,2-dihydroxy-9,10-anthraquinone Dye Sensitizer for Solar Cell Applications. Acta Phys Pol A 126:833–840. https://doi.org/10.12693/APhysPolA.126.833
69. Zang L, Liu Q, Yang C, et al (2018) Alizarin red: a reactive dye to enhance nanoengineered polypyrrole with high electrochemical energy storage. Polym Bull 75:3311–3323. https://doi.org/10.1007/s00289-017-2211-z
70. Moriguchi T, Yano K, Nakagawa S, Kaji F (2003) Elucidation of adsorption mechanism of bone-staining agent alizarin red S on hydroxyapatite by FT-IR microspectroscopy. J Colloid Interface Sci 260:19–25. https://doi.org/10.1016/S0021-9797(02)00157-1
71. Chung C, Lee M, Choe E (2004) Characterization of cotton fabric scouring by FT-IR ATR spectroscopy. Carbohydr Polym 58:417–420. https://doi.org/10.1016/j.carbpol.2004.08.005
72. Küçük M, Öveçoğlu ML (2018) Surface modification and characterization of polyester fabric by coating with low temperature synthesized ZnO nanorods. J Sol-Gel Sci Technol 88:345–358. https://doi.org/10.1007/s10971-018-4817-5
73. da Silva RCL, Alves C, Nascimento JH, et al (2012) Surface Modification of Polyester Fabric by Non-Thermal Plasma Treatment. J Phys Conf Ser 406:012017. https://doi.org/10.1088/1742-6596/406/1/012017
74. Allahyarzadeh V, Montazer M, Nejad NH, Samadi N (2013) In situ synthesis of nano silver on polyester using NaOH/Nano TiO_2. J Appl Polym Sci 129:892–900. https://doi.org/10.1002/app.38907
75. Kale KH, Palaskar SS (2012) Plasma enhanced chemical vapor deposition of tetraethylorthosilicate and hexamethyldisiloxane on polyester fabrics under pulsed and continuous wave discharge. J Appl Polym Sci 125:3996–4006. https://doi.org/10.1002/app.36601
76. Shang S-M, Li Z, Xing Y, et al (2010) Preparation of durable hydrophobic cellulose fabric from water glass and mixed organosilanes. Appl Surf Sci 257:1495–1499. https://doi.org/10.1016/j.apsusc.2010.08.081
77. Jamal MM, Mousaoui AM, Naoufal DM, et al (2014) Effect of Operating Parameters on Electrochemical Degradation of Alizarin Red S on Pt and BDD Electrodes. Port Electrochim Acta 32:233–242. https://doi.org/10.4152/pea.201403233

Chapter 5. Controlled drug release textiles

In this chapter, a research study for the development of a sol-gel 3D network for controlled drug release will be deeply reported. Before describing the experimental part and discussing the main results, an introduction dealing with controlled release systems, methods, and substances commonly employed for this aim will be provided. Materials, general methods, and instrumentation for characterization were previously reported in Chapter 2.

The research was realized with the valuable contribution of Prof. F. Puoci, Prof. C. Saturnino, Dr. D. Iacopetta, Dr. E. Piperopoulos, Dr. C. Triolo, Prof. M. G. Bonomo, Prof. D. Drommi, Dr. O. I. Parisi, Prof. C. Milone, Prof. M. S. Sinicropi, Prof. G. Rosace and Dr. M. R. Plutino.

Part of this chapter was published on:

- *Puoci F, Saturnino C, Trovato V, et al (2020) Sol–Gel Treatment of Textiles for the Entrapping of an Antioxidant/Anti-Inflammatory Molecule: Functional Coating Morphological Characterization and Drug Release Evaluation. Appl Sci 10:2287. https://doi.org/10.3390/app10072287*

5.1 Introduction

Thanks to the innovative medical and well-being applications, textile-based drug delivery systems have aroused much interest in the last years. In particular, since the 1970s, the controlled drug delivery systems have been thoroughly studied until their growth, and they are diversified during recent times, thus providing important benefits in health care and representing a large market segment [1]. As a matter of fact, the controlled drug release principle is the main factor of an efficient drug therapy [1,2] that reflect in several advantages, among which the improvement of therapeutic activity, reduction of the number of drug administrations, as well as of the intensity of side effects, and elimination of specialized drug administrations [3]. The interest in this research field has led to innovative controlled release systems for diversified application sectors such as cosmetics [4], agriculture [5], and textile [6, 7]. The latter, thanks to the already described properties, mainly for their breathability, biocompatibility, and absorptive capacity, are considered substrates (for ex-vivo applications) of great interest and comfortability for the controlled release of several substances: active principles, fragrances, aroma, essential oils, drugs and so on [8]. The transdermal patches or textiles costumes

deserve to be mentioned among the most common ones, mainly consisting of different layers in which the release of a substance is generated by specific stimuli (e.g., enzyme, humidity, temperature, friction, or perspiration types) [9].

Textile-based delivery systems (e.g., patches, bandages) can be developed through several methodologies that ensure the main characteristics, such as biocompatibility, that these systems must satisfy. These methodologies are based on the use of host-guest molecules (cyclodextrins [10], aza-crown, ethers, fullerenes) or doping functional molecules (drug-loaded hollow, nanoparticles, ion-exchange, bioactive) [8, 11]. Several C-C polymer heteroatoms containing (e.g., N, P, Si) backbones for controlled release applications have been tested for improving the effectiveness of the drug therapy [3]. The generic action mechanism of these polymeric release systems is mainly based on temporal controlled release (e.g., diffusion control, drugs solution flow control, drug-delayed dissolution) as a function of skin stimuli or interaction with environmental water. Encapsulation or inclusion techniques of drugs or active principles in the polymer matrix are the most common process carried out for the design of drug-controlled release textiles. Essential characteristics of a controlled release system that must be monitored are represented by controllability, biocompatibility, toxicity, carcinogenicity, mutagenicity, and teratogenicity [8, 12].

Compared to conventional controlled release systems (e.g., oral administration), those based on textiles present both advantages and disadvantages. The former is represented by: i) the efficacy of therapy since the released drugs avoid the digestive apparatus and the hepatic metabolism that could reduce the molecule concentration; ii) the use of low dosages thanks to the high diffusion through tissues, which correspond to lower social costs of therapies [9]. These advantages make the textile-based controlled release systems an easy and attractive treatment for patients. On the other hand, a disadvantage of these systems mainly consists of drug diffusion rate as a function of its molecular structure and body surface administration [9].

Among several technologies, the sol-gel technique represents an interesting approach for developing functional nanostructure coatings by combining the entrapment or encapsulation of biomolecules and bioactive compounds and their controlled release [13].

As already explained in Chapter 1, the sol-gel method is a synthetic strategy useful for the preparation of functional nano-hybrid networks in which it is possible to encapsulate molecules with different properties and functions (e.g., antimicrobial [14], dye [15–21], hydrophobic [22–24] or flame-retardant molecules [25, 26]).

In the following paragraphs, the mechanisms of release, the main approaches for developing textile-based controlled release systems, and commonly employed active substances for encapsulation will

be described. An in-depth description of the development of a textile-based controlled release system by sol-gel encapsulation of an antioxidant/anti-inflammatory molecule will be further provided.

5.1.1 Controlled release

The primary function of a controlled release system is to make an active substance (commonly drugs, fragrances, vitamins, essential oils, enzyme and so on) available in response to a stimulus or at a specific time, rate or situation (mechanical pressure, moisture, heat and so on) or at a particular site, to produce the desired effect [27].

A generic controlled release system is characterized by the active agent and the carrier, often a polymer able to transport the active substances to a specific site in the human body. Depending on the nature of the substances to be released, the mechanism can be considered different. If it is a drug to be released, the controlled release refers to its concentration in blood plasma that should be at least as effective level and as low as the toxic one. On the other hand, the controlled release of a drug entails reproducibility of release rate over a longer time.

5.1.1.1 Controlled release mechanisms

In controlled release systems, active agents are embedded and protected by an external shell that prevents the diffusion and mass loss of the encapsulated active molecule. Based on the design of controlled release devices, both physical and chemical mechanisms are common.

Diffusion of active substances (e.g., drugs) through a polymer matrix, osmotic pressure, ion exchange, or dissolution/degradation of the polymer matrix are the main physical mechanisms involved in controlled release systems [28]. On the other hand, the chemical mechanisms provide modifications of active molecules: chemical or enzymatic degradation occurs on the chemical bonds between drugs and carriers, thus breaking them.

Controlled release systems can be classified into four groups:

- diffusion controlled (reservoir matrix);
- water penetration controlled (swelling systems);
- chemically controlled;
- regulated systems.

The already mentioned carrier is commonly represented by a polymer that mainly influences the drug release rate [29]. Indeed, drugs can diffuse through polymers pores or passing in between polymer chains. The most common mechanism of controlled release is the diffusion of an active agent. In

matrix diffusion-controlled systems, the drug can be dissolved or dispersed throughout the polymer. Contrary, reservoir diffusion-controlled systems generate a drug core covered by a polymer membrane and separated from the external environment.

When structural polymers have hydrophilic nature, they can swell partially or throughout the matrix, and the controlled release of drugs is defined as swelling-controlled. This mechanism is typical of hydrogels, 3D polymer networks, and it refers to dry hydrogels doped with drug molecules that swell when they are in contact with water or biological fluids. Due to the swelling, the systems result in an inner glassy phase and an outer swollen rubbery.

The chemical controlled release is driven by chemical reactions consisting of the degradation of the polymer to release drugs. Another chemical mechanism is represented by the hydrolytic or enzymatic degradations that provide the breaking of established polymer chains between the drug and the polymer matrix [30].

Another type of polymers used for the design of controlled release systems is the stimuli-sensitive polymers able to change their physical properties depending on environmental changes (stimuli). Both the controlled release rate and the diffusion of active substances out of polymer strictly depend on these stimuli [31].

5.1.1.2 Textile-based controlled release systems

As already mentioned, the most diffused method of drug delivery is the oral administration characterized by several disadvantages, among which: drug permeability only in the gastrointestinal regions, poor dissolution rate in intestinal fluids, drug degradation before absorption due to the drug instability in the gastrointestinal areas [32]. As an alternative to oral administration, intestinal patches represent an efficient drug delivery method thanks to their capability to release active molecules in the intestinal mucosa without undesired losses in other sites. In contrast, transdermal drug applications avoid blood level troughs and undesired early metabolism of the drug.

In this scenario, textile materials are considered useful supports for the application of active agents to anybody area thanks to their flexible structure [33]. Transdermal applications, sutures, small diameter vascular grafts and stents, nerve regeneration and tissue, are the potential application of textile-based drug delivery systems [27].

Several methods are available for the incorporation of active agents in textile fibers: (i) fibers could be spun and woven, and the drug could be incorporated by impregnation, coating, yarn-dying, ion-exchanging, and so on [34]; (ii) the drug could be incorporated in the shell/core fibers structure by coating and melt-spun fiber [35]; (iii) the active agent and the filament-forming materials can be

blending (co-blending) and then, the spinning liquids are spun into fibers [34]. Moreover, active agents loaded in thin films can be applied on textiles surfaces by coating or impregnation, and they result beneficial in wound healing and treating skin disease and injuries. Active agents can also be encapsulated in microparticles, thus obtaining microcapsules and microspheres. The latter are homogeneous mixtures of polymer and active agents, while microcapsules are spherical particles that have at least one discrete domain of active agent [36]. Microcapsules refer to the core/shell structure and dispersion in solid matrices (dimensions between 50 and 2 mm). Thanks to their large surfaces, microcapsules form uniform and continuous coatings both on the textile surfaces and between the textile fibers [37], and they are of great importance for their reproducibility in molecules release [36].

5.1.1.3 Microencapsulation of substances and their incorporation into textile structures

Microencapsulation is a technology employed to realize systems for protection, structuration, and controlled release of active agents. Indeed it is widely used for the protection of substances sensitive to moisture, light, oxygen, or to create a structure for substances with volatile, insoluble or high reactive properties. It is an interesting technology also for the realization of controlled release systems. Several methods are available to microencapsulate active substances, mainly based on mechanical, physicochemical, and chemical approaches. In general, through microencapsulation, the stability and high efficiency of encapsulation of substances, the reproducibility and the easy scalability of designed systems, should be ensured. An in-depth overview of all available approaches goes beyond the aim of this thesis; thus, only a schematic representation of such methods is reported in Table 11.

Mechanical	Physicochemical	Chemical
Spray drying	Supercritical fluid technology	Solvent evaporation
Spinning disk microencapsulation	Polyelectrolyte complexation	In situ polymerization
Fluid bed coating	Ionotropic gelation	Matrix polymerization
Centrifugal extrusion	Coacervation – phase separation	Interfacial polycondensation
Vibrating nozzle		Interfacial cross-linking

Table 11: Microencapsulation approaches, according to mechanical, physicochemical, and chemical classifications

Depending on the nature of the active substance (drug, fragrance, moisturizer, vitamin, and so on), the controlled release system should be suitably designed by choosing the adequate polymer and technology for the efficient encapsulation of the molecule. In the textile field, the most commonly employed technique for substances encapsulation is represented by coacervation (physicochemical method). Several approaches are useful for embedding microcapsules into textiles structures, including immersion, padding, printing, spraying coating, or direct incorporation in artificial fibers [33, 38–42].

Usually, for textile application of microcapsules, a binder is necessary to fix them on fabric surfaces by forming a film characterized by long-chain macromolecules arranged in a 3D linked network [43]. Carboxymethylcellulose, polyvinyl acetate, starches, styrene-butadiene, silicons, amino aldehyde resins, polyvinyl alcohol, xanthenes are some of the commonly employed binders for embed microcapsules on textiles. Such binders ensure the water and wearing resistance of the capsules and, sometimes, they avoid the release of the substances. It is possible to covalently bond the microcapsules to the textiles by employing cross-linking agents, thus overcoming release problems. One example is melamine-formaldehyde resin, a cross-linking agent interesting for its high hardness, excellent heat resistance, mechanical robustness, unlimited colorability, and water resistance [44]. Depending on the nature of textile fabrics, microcapsules can be completely wrapped by the binder or bonded with it, and linked between the fibers, while for the washing fastness, no elevated concentrations of both capsules and binders are necessary. However, due to their toxicity, formaldehyde-based cross-linkers are nowadays avoided while environmentally friendly chemicals are employed, such as formaldehyde-free cross-linkers and polycarboxylic acids [45], which acts through the formation of ester bonds between cross-linker, active substances, and the textile substrate. In general, the covalent immobilization of the controlled release systems on textiles surfaces ensures good washing fastness. In this regard, several application techniques are efficient for stable immobilization of such systems, including UV-grafting, impregnation, bath exhaustion, depending on the nature of both cross-linkers employed and textiles nature. The size of the microcapsules is another essential parameter in designing controlled release systems for ensuring the correct penetration between the fibers space and the efficient grafting on the fibers [37].

The average fibers diameter influences the diameter of microcapsules that, in the case of cotton applications, it should be between 1 and 20 μm. On the other hand, the woven structure of fabrics (e.g., plain weave, honeycomb, and so on) affects the adhesion of microcapsules on textile fibers. Several parameters must be considered to achieve effective and durable embedding microcapsules in textiles: functionalities and architecture of textiles fabrics, microcapsule shell composition, the

chemical structure of binders/cross-linking agents. In this regard, pretreatments of textiles can be useful for obtaining active sites on textile fibers according to plasma technology or water treatments [46, 47].

The optimal formulation of microcapsules should satisfy several aspects such as good abrasion resistance, high loading per fabric surface weight, controlled substance release without undesired hinder and harmless to human health.

5.1.1.4 Active substances for microencapsulation for textile-based controlled release systems

As previously mentioned, drugs are the most common substances for controlled release in medical fields, even if other agents can be encapsulated for different end-use, such as vitamins, fragrances, or insect repellents. The drug release strictly depends on the polymer wall in which it is encapsulated and on the nature of the drug itself.

The microencapsulation of drugs for textile-based controlled release systems is of great interest and useful for transdermal delivery. Such systems are advantageous for their ability to interrupt drug delivery by removing the textile transdermal system and avoiding early drug metabolism. Several examples are reported in literature dealing with efficient systems for controlled drug release from textiles.

Ma et al. reported the realization of microcapsules of Tamoxifen, a drug for breast cancer treatment, according to complex coacervation using gelatine and acacia gum and glutaraldehyde as a cross-linker for transdermal delivery from cotton twill fabric [41]. An adhesive was used for the application of the coating. A high burst effect and steady states were showed by in vitro tests during the first hours and for the time of incubation increased, respectively. Moreover, the rate of tamoxifen release is affected by the polymer concentration, drug/polymer ratio, and stirring rate in the preparation of microcapsules.

For transdermal drug delivery, also biopolymers are of great interest for biomedical applications. One example is Chitosan, a biodegradable and biocompatible polymer used to develop microcapsules for oral and topical medications.

Cyclodextrins play an important role in the realization of microcapsules for dispersed drug delivery systems [48]. They are cyclic oligosaccharides based on glucopyranose and characterized by a lipophilic central cavity and a hydrophilic outer surface with the capability to increase the availability of hydrophobic drugs from dispersed systems. The development of core/shell fibers is also of great interest, as demonstrated by Yu et al. [49], which uses electrospinning and UV-graft polymerization to produce the poly(ε-caprolactone)/polyethylene glycol core/sheath fibers loaded with salicylic acid.

Also, these systems showed the initial burst followed by sustained drug release depending on fiber thickness.

Besides drug molecules, fragrances, flavors, and essential oils are also important for designing controlled release systems for textile applications in food, agriculture, and pharmaceutical fields [50]. In particular, textiles with embedded fragrances microencapsulation are used for active sportswear, gloves, socks, business suits, woman's hosiery, bedding, towels, shoe liners, and so on [51, 52]. However, due to their poor stability, these classes of volatile molecules need to be encapsulated, and the controlled release and their long-lasting perception is a significant challenge [53].

In this regard, small microcapsules can be greater uniformly dispersed, thus giving prolonged-release performances [54]. Several characterization techniques can be employed to investigate the structure and properties of microcapsules, such as FTIR spectroscopy, X-ray diffraction, gas chromatography-mass spectrometry, transmission electron microscopy, dynamic light scattering, and electronic noise. The dimension of microcapsules influences the washing resistance of treated cotton fabrics, and smaller capsules provide better washing fastness than fragrances alone. Moreover, the smaller microcapsules release lower fragrances amount from cotton fabrics than bigger microcapsules. As already mentioned, the process used for the preparation of microcapsules could also affect the average size and morphology of capsules.

Another important class of active agents to be microencapsulated in textiles is cosmetic molecules, among which vitamin E is interesting for its strong antioxidant properties and moisturizing effects and, for these reasons, widely employed in the cosmetotextile industry. Moreover, smart textiles of great interest are realized through microencapsulation of molecules with insect repellency properties, useful in particular in tropical areas because insects are vectors for several human diseases, such as malaria, dengue fever, yellow fever, chikungunya, filariasis, and so on [55]. Important challenges in the development of insect repellent textiles are resistance to sweating, rubbing and friction, and no toxicity of residual active agents [55]. Many efforts have been made in the design of this textile-based controlled release system by employing plant-based insect repellents like extract of citronella genus, essential oils, neem, lemon eucalyptus, pine tar. Being essential oils, they are characterized by high volatility and poor longevity if applied topically. On the other hand, the efficiency of the controlled release of essential oils is difficult to be evaluated.

Textile fabrics embedding microcapsules loaded with active substances have aroused much interest in several application fields, among which cosmetics, medicine, wellness. Nowadays, they are attractive also for textiles engineering, material sciences, and pharmaceutical engineering.

Based on what has been described in this chapter, several challenges should be addressed, such as the employment of sustainable substances, both polymers and active agents, and biodegradation of textile structures for intra-body delivery.

5.2 Controlled drug release textiles by sol-gel encapsulation of active molecules

A research study aimed at developing functional sol-gel coatings for the controlled release of drug molecules for medical application was conducted and thoroughly described in the following subparagraphs.

As a cross-linked silica precursor, *3*-glycidoxypropyltriethoxysilane (GPTES) was employed in an acid-catalyzed sol-gel reaction for the realization of a polyethylene oxide (PEO) network in whose holes, an *N*-palmitoyl-ethanolamine derivative (PEA), the *N*-palmitoyl-(*4*-nitro-phenyl)-amine (PNPA), was stably immobilized. The PNPA molecule was previously synthesized according to an optimized strategy, and its antioxidant and anti-inflammatory properties have been already established [56]. In the absence of external stimuli (e.g., variable pH conditions), the PNPA molecule results stably encapsulated into the 3D hybrid PEO through weak interactions (e.g., hydrogen bonds and van der Waals interactions) between the non-polar active molecule and the alkoxysilane hosting network.

The obtained GPTES-PNPA sol was applied on cotton fabrics, thus obtaining a uniform coating on textile surfaces after thermal treatments as confirmed by the performed morphological studies. In vitro diffusion tests were performed on treated cotton fabrics to evaluate their ability to release in a controlled manner the synthesized PEA derivative compared to a standard solution of the molecule. Experimental findings demonstrated that the developed cotton fabrics are suitable for controlled drug release for medical applications, thus showing interesting potentiality in the fields of medical textiles [57].

5.2.1 PEA derivatives

Since the late 1950s, *N*-palmitoyl-ethanolamine (PEA), fatty acid amides belonging to *N*-acylethanolamines (NAEs), was known as the anti-inflammatory component of egg yolk and employed in the prevention of viral infection of the respiratory apparatus [58, 59]. In particular, palmitoyl-ethanolamide (PEA) are of great interest due to their elevated presence in the central nervous system. Indeed, studies have been conducted to assess the therapeutic efficacy in some central nervous system disorders related to inflammation [60]. However, even if experimental models have demonstrated the efficient anti-inflammatory and analgesic effects according to different

mechanisms, few experimental data about the use of PEA derivatives in animals or humans are present until now [61]. Several mechanisms have been suggested to demonstrate the analgesic and anti-inflammatory effects of PEA molecules. One of them is based on the protective endogenous mediation "on-demand" of PEA molecules to hinder inflammation or neuronal damage. Moreover, PEA is involved in the endogenous mechanism of protection of in-body response to several kinds of damage, where a decrease in PEA concentration generates an inflammatory reaction. Scientific research underlined the possibility to prepare novel drugs related to natural sources, and in this regard, PEA derivatives or analogues with potential anti-inflammatory and antioxidant activities were obtained [56].

5.2.2 Experimental Part

25 mg of PNPA was solubilized in methanol (40 ml) through ultrasonication and stirring. To obtain clear methanol dispersion, 2 ml of an aqueous sol-gel solution of GPTES 1 M were added slowly (drop by drop), thus obtaining a final GPTES concentration of 0.05 M (1:0.034 molar ratio with respect to PNPA). A sol GPTES-PNPA was obtained, ultrasonicated, and then left under stirring at room temperature for 90 minutes.

A similar synthetic procedure was followed to prepare the reference GPTES sol without the presence of the antioxidant molecule.

Both the GPTES sol and the GPTES-PNPA sol were applied separately on light and heavy cotton textiles (CO_L and CO_H, respectively) according to the padding procedure described in Chapter 2 by obtaining CO_L-GPTES, CO_H-GPTES, CO_L-GPTES-PNPA, and CO_H-GPTES-PNPA for cotton treated with GPTES and GPTES-PNPA sol, respectively.

5.2.3 Results and discussion

In the following subparagraphs, a detailed discussion of the most important experimental findings according to characterization techniques described in Chapter 2 is reported.

5.2.3.1 Synthetic strategy and coating composition

The antioxidant and anti-inflammatory molecule PNPA was employed as a drug molecule for the design of controlled drug release fabrics realized through the sol-gel technique [56]. With this aim, GPTES was used as the sol-gel precursor to immobilize PNPA molecules thanks to the interesting and simultaneous presence of both an epoxy group and triethoxysilane functionalities. These chemical

moieties are responsible for the crosslinking between GPTES molecules, the entrapment of the antioxidant PNPA, and the immobilization of the obtained doped matrix on cotton surfaces.

As described before, aqueous GPTES sol was synthesized by adding a slight amount of catalyst, HCl, and then a specific amount of the sol was added to the methanol dissolved PNPA solution. According to previous evidence [15–21], a hybrid polymeric 3D network was formed as a consequence of the catalyzed epoxy ring-opening of GPTES and the interaction of triethoxysilane ends by creating a polyethylene oxide network (PEO) [20]. In this PEO structure, the PNPA molecule has filled the holes by being physically entrapped in a stable configuration (Scheme 12a). After deposition on the cotton fabric of the GPTES-PNPA sol through padding technique and thermal curing, a nano-hybrid coating for the realization of controlled drug release textiles was obtained as schematically reported in Scheme 12b.

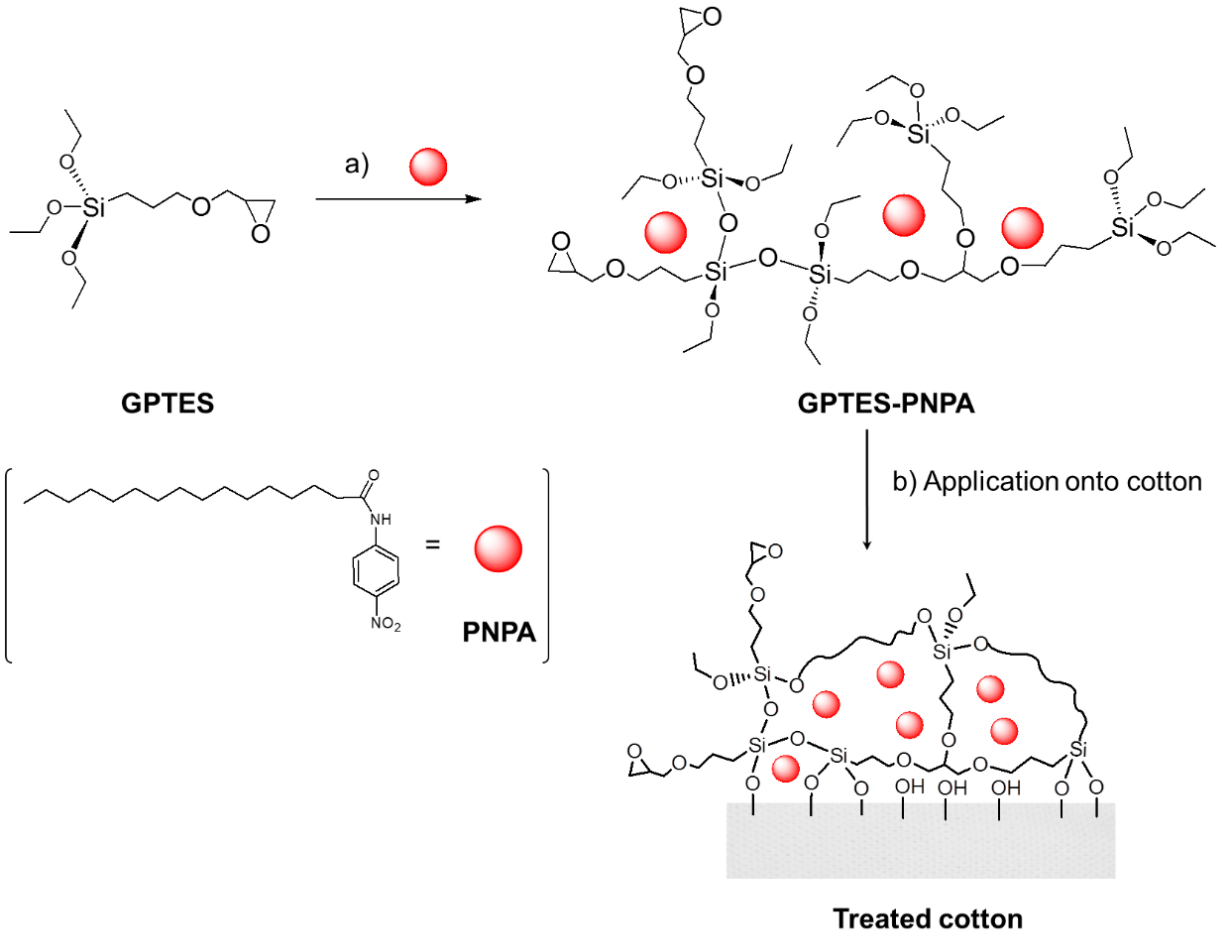

Scheme 12: a) Schematic representation of the physical entrapment of PNPA molecules in the PEO network; b) Deposition of GPTES-PNPA sol on cotton surfaces. Adapted under the terms of the Creative Commons CC BY-NC-ND 4.0 license [57]. Copyright 2020, the Authors, Published by MDPI

5.2.3.2 NMR characterizations

For ^{1}H mono- and bidimensional NMR characterizations, a reaction mixture of GPTES-PNPA sol was prepared in situ (1:0.1 = [GPTES]:[PNPA] molar ratio) in methanol-d_4. The ^{1}H NMR spectra were recorded at time zero and after 24 hours (methanol-d_4 at 298 K, 300 MHz). The collected ^{1}H NMR spectra at different times reveal, in the aliphatic region, the presence of the protonic pattern typical of diol/PEO silylated derivatives and the starting GPTES (Figure 43 green and yellow circles respectively) [20]. More in detail, the aliphatic regions of the ^{1}H NMR spectra clearly show: (i) the presence of the expected protonic pattern for the GPTES open ring derivative, bringing a hydroxyl and an ether group bonded to two vicinal carbon C_e and C_f atoms (δ = 0.68, CH_{2a}; 1.71, CH_{2b}; 3.48, CH_{2c}+CH_{2d}+CH_{2f}; 3.88 CH_{2e}, green circles in the lower spectrum); (ii) the proton peaks relative to the starting GPTES in a decreased concentration (δ = 0.67, CH_{2a}; 1.68, CH_{2b}; 2.61+2.78, CH_{2f}; 3.16, CH_{2e}; 3.32 + 3.76, CH_{2d}; 3.49, CH_{2c}, yellow circles in the upper spectrum); (iii) the presence of the upper-field methylene and the methyl proton resonances relative to free ethanol moieties, compared to those relative to the ethylic groups of GPTES (δ = 3.63, CH_2, 1.19, CH_3 *vs* 3.84, CH_2, 1.22, CH_3; cut signals in both spectra).

Due to the higher molar ratio of GPTES than PNPA, the NMR signal of the long penta-decanoic protonic chain is masked under GPTES signals, while the aromatic region shows the expected and unchanged pattern for the *para*-substituted phenyl ring of the PNPA molecule.

According to the ^{1}H NMR data, neither the nucleophilic attack by PNPA molecule on GPTES epoxy ring and the formation of a resulting ether covalent bond did not occur. On the other hand, the stable encapsulation of PNPA molecules in the PEO network occurs through the formation of weak bonds (e.g., electrostatic or van der Waals) between the polymerized GPTES and the PNPA molecules, as also demonstrated in previous studies [20]. Such weak bonds are established between the hydroxyl groups or ether oxygen of polymerized GPTES and the nitrogen, oxygen, long alkyl chain, or phenyl groups of PNPA molecules.

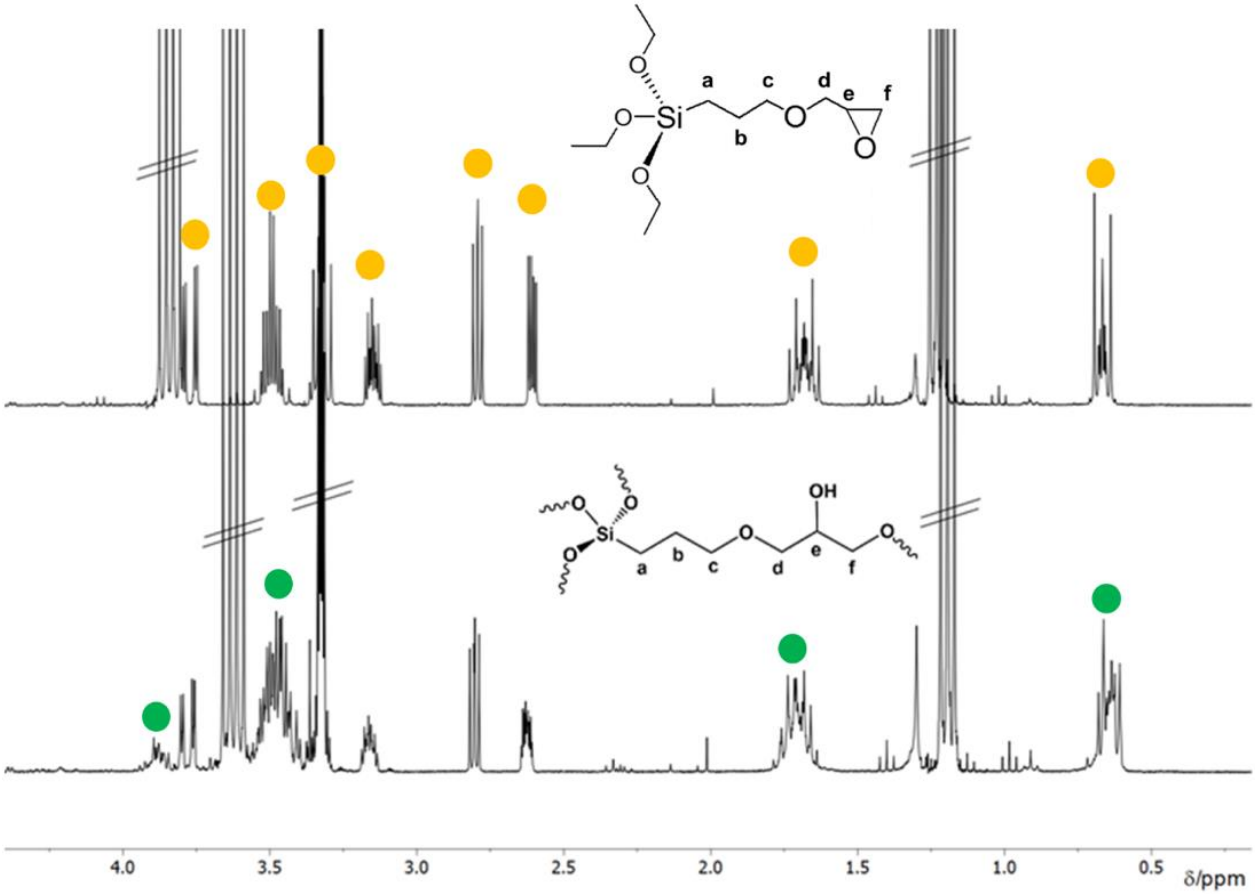

Figure 43: ^{1}H NMR spectra of the GPTES-PNPA sol (in methanol-d_4 at 298 K, 300 MHz) at time zero (upper spectrum) and after 24 hours reaction time in the presence of a slight amount of HCl (lower spectrum). Adapted under the terms of the Creative Commons CC BY-NC- ND 4.0 license [57]. Copyright 2020, the Authors, Published by MDPI

5.2.3.3 ATR-FTIR characterizations

Before investigating the coating presence on cotton surfaces, the chemical structure of the synthesized hybrid network and its interactions with PNPA molecules were assessed by comparing the ATR - FTIR spectra obtained from the three xerogels (PNPA, GPTES sol, and GPTES-PNPA sol) obtained through the procedure described in Chapter 2. The FTIR spectra of GPTES sol (Figure 44 black curve) reveal the typical absorption bands of the inorganic silica network and the epoxy group. The former is confirmed by bands at 1093-1010 cm^{-1} , 756 cm^{-1} (asymmetric and symmetric stretching of Si-O-Si, respectively) and 850 cm^{-1} (Si-O-Si bending) [17, 18, 20]. The epoxy functionality was confirmed by the peaks relative to the asymmetric and symmetric C-H stretch (3072 – 3000 cm^{-1}), ring breathing (1255 cm^{-1}), and asymmetric and symmetric ring deformation (906 – 850 cm^{-1}) [17, 18]. ATR - FTIR curve of PNPA (Figure 44 yellow curve) is characterized by the following peaks: 2916 and 2849 cm^{-1} (asymmetric and symmetric CH_2 stretching mode of the

alkyl chain, respectively), 1470 – 1458 cm^{-1} (bending of CH_2), 1737 and 3075 cm^{-1} (the C=O and C-N stretching of the secondary amide, respectively) and 1596 cm^{-1} (C-N stretching mode) [62]. The same peaks, attributable to GPTES sol, are also present in the spectra of GPTES-PNPA sol together with the already described absorption peaks of the PNPA molecule (Figure 44 green curve).

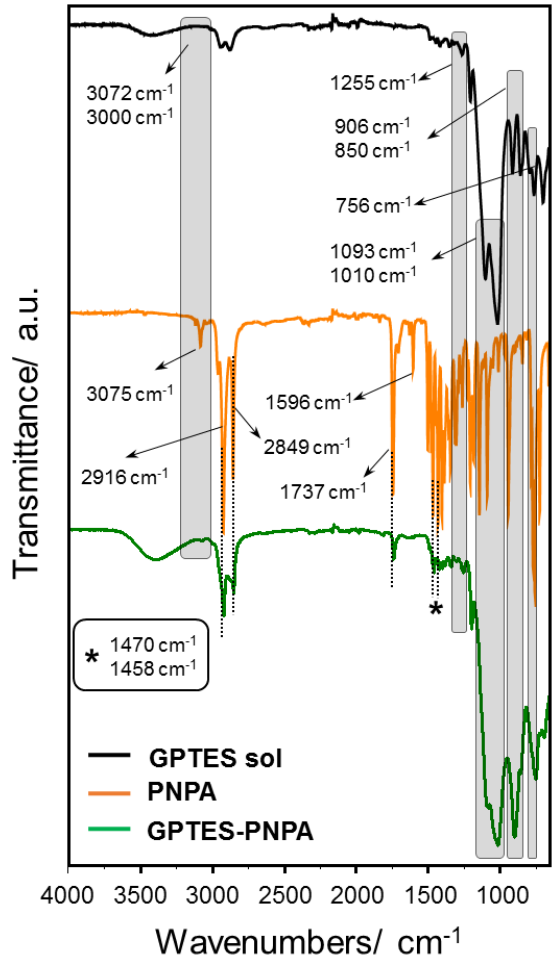

Figure 44: ATR – FTIR spectra of GPTES sol (black curve), PNPA molecule (yellow curve), and GPTES-PNPA sol (green curve)

ATR-FTIR spectra of both untreated and treated cotton fabrics are reported in Figure 45 after normalization at 1362 cm^{-1} (C-H bending of cellulose). For better clarity, spectra relative to CO_L and to CO_H samples are reported separately by comparing the untreated cotton (CO_L_UT and CO_H_UT), the cotton treated with GPTES sol (CO_H_GPTES and CO_L_GPTES), and the cotton treated with GPTES-PNPA sol (CO_H_GPTES-PNPA and CO_L_GPTES-PNPA).

In all mentioned FTIR spectra, the typical absorption bands of cellulose are evident. In particular, the peaks evidenced in Figure 45b and Figure 45c: 3331 cm^{-1} and 2894 cm^{-1} (stretching mode of O-

H and C-H, respectively) and the absorption bands between 1097 cm^{-1} and 895 cm^{-1} (asymmetric in-plane ring stretch, C-O stretch, and asymmetric out-of-phase ring stretch (C_1-O- C_4)) [63]. Furthermore, the increase in the intensity of absorption bands in the range between 1145 cm^{-1} and 895 cm^{-1} (asymmetric stretching of Si-O-Si) for the treated CO_L and peaks at 852 cm^{-1} (Si-O-Si absorption bending) and 790 cm^{-1} (stretching Si-O-Si) for the CO_H confirms the presence of the silica GPTES matrix.

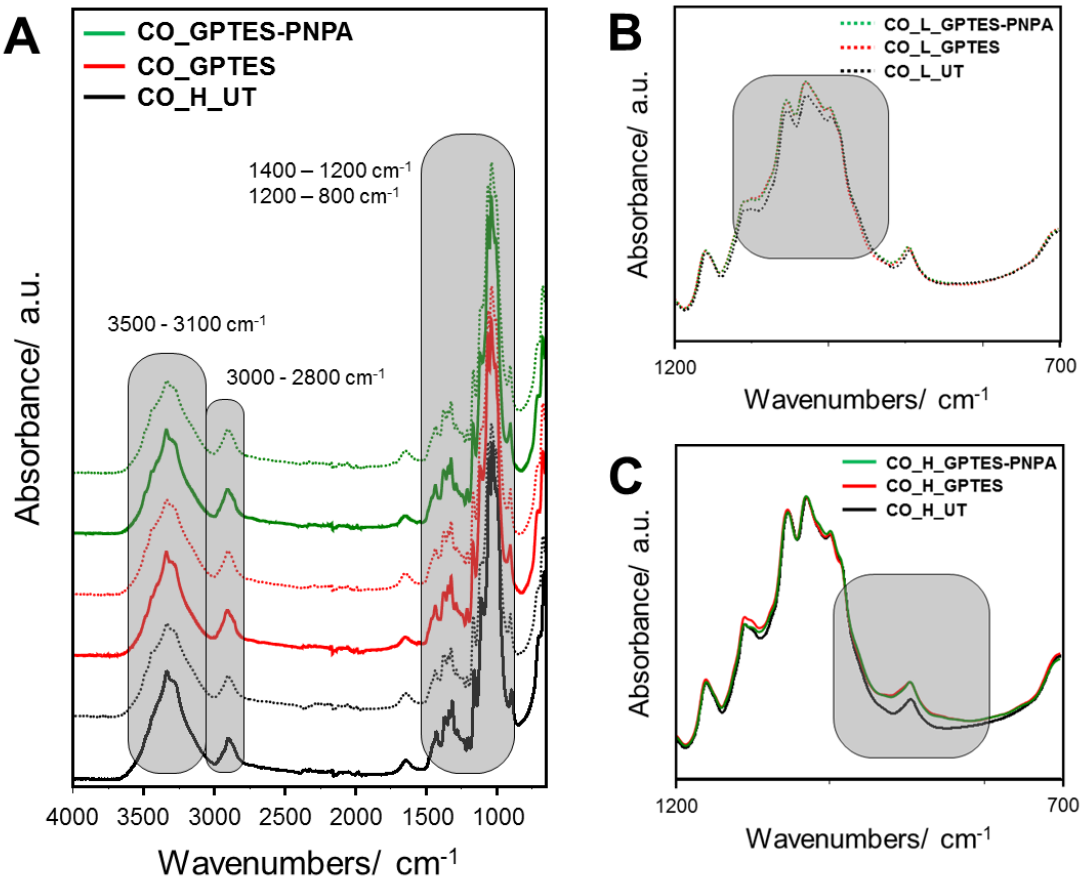

Figure 45: A) ATR-FTIR spectra of untreated cotton fabric (CO_L_UT dashed black curve and CO_H_UT solid black curve) and cotton fabrics treated with pure GPTES (red dashed and solid curves for CO_L and CO_H, respectively) and GPTES-PNPA (green dashed and solid curves for CO_L and CO_H, respectively). B) ATR-FTIR spectra of untreated and treated cotton fabrics, CO_L in the range 700 – 1200 cm^{-1}. C) ATR-FTIR spectra of untreated and treated cotton fabric, CO_H in the range 700 – 1200 cm^{-1}

5.2.3.4 Morphological characterizations

The morphology of untreated and treated cotton fabrics with both GPTES and GPTES-PNPA sols was assessed through SEM and AFM characterization techniques as already described in Chapter 2. Besides the morphology of textiles, the same analysis underlined structural differences between

untreated and treated cotton fabrics, as well as differences between cotton treated with GPTES and GPTES-PNPA sols.

Both CO_L_UT and CO_H_UT reveal different weaves as observed in SEM images (Figure 46 and Figure 47, respectively). More in detail, CO_H_UT is characterized by a larger weave with fibers less ordered than that of CO_L_UT. The morphology of both cotton samples does not show modification after coating deposition as confirmed by SEM images of treated textiles, thus proving that no changes at the micrometer scale occur.

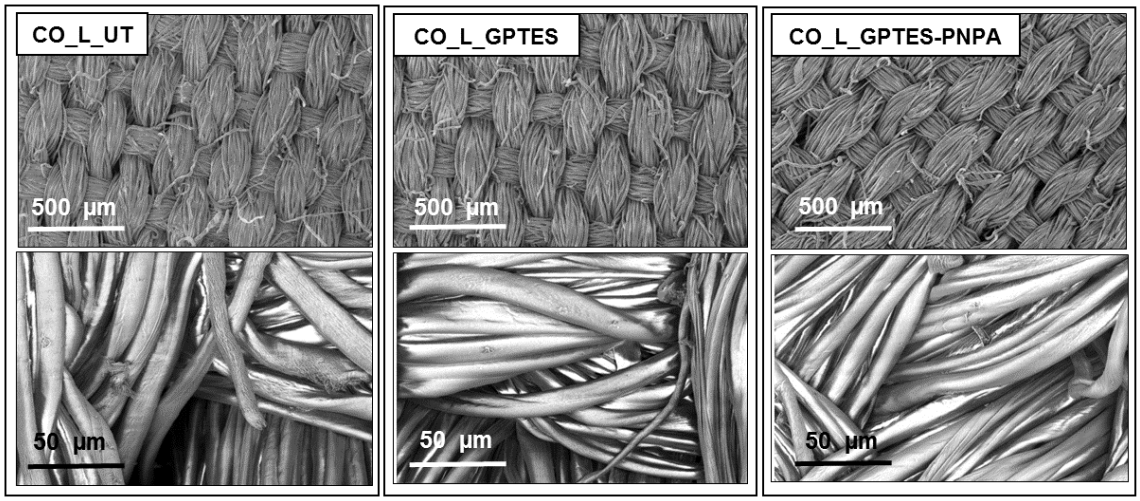

Figure 46: SEM images of CO_L, untreated and treated with both GPTES and GPTES-PNPA sol at increasing magnifications (up to down). Adapted under the terms of the Creative Commons CC BY-NC-ND 4.0 license [57]. Copyright 2020, the Authors, Published by MDPI

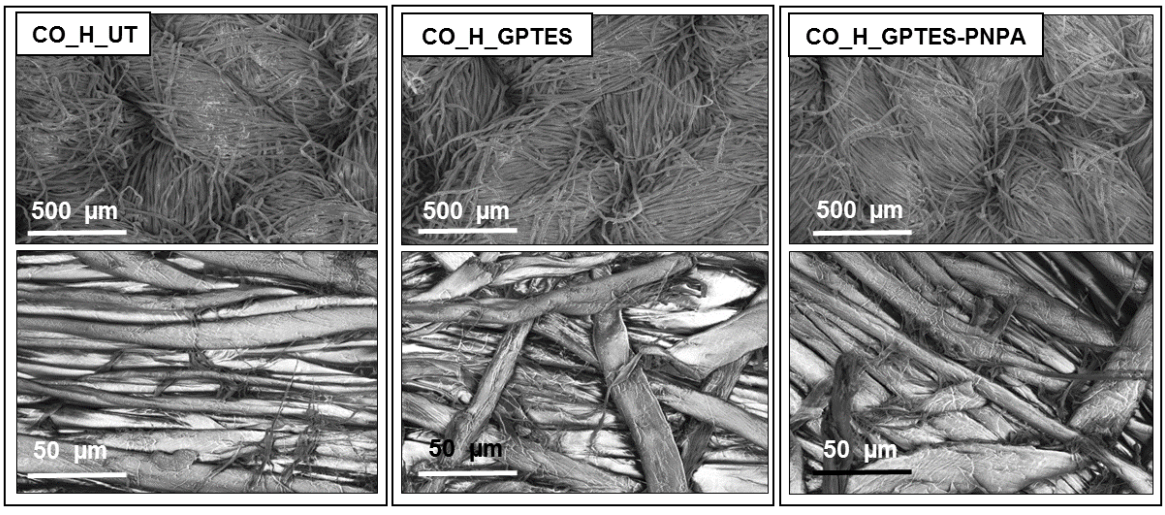

Figure 47: SEM images of CO_H, untreated and treated with both GPTES and GPTES-PNPA sol at increasing magnifications (up to down). Adapted under the terms of the Creative Commons CC BY-NC-ND 4.0 license [57]. Copyright 2020, the Authors, Published by MDPI

Moreover, EDS analysis reveals the presence of Si in samples treated with both sols (CO_L_GPTES, CO_L_GPTES-PNPA, CO_H_GPTES, and CO_H_GPTES-PNPA). Other peaks observed are referred to carbon (present in fabrics and the graphite adhesive used for SEM analysis), oxygen (present in fabrics and the vapor-low vacuum atmosphere), and aluminum (present in SEM stub). The Si distribution appears very uniform without phase separation, as observed in mapping in Figure 48.

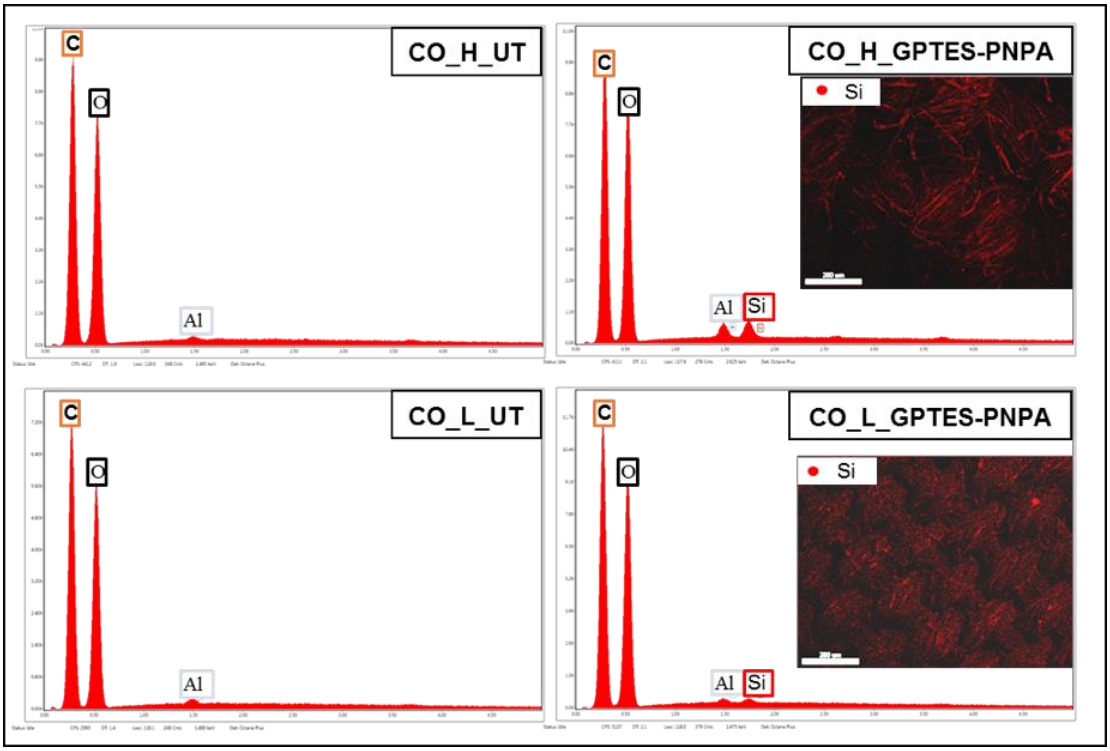

Figure 48: EDS mapping of both CO_L and CO_H untreated and treated with GPTES-PNPA sol and Si distribution of treated textiles. Adapted under the terms of the Creative Commons CC BY-NC-ND 4.0 license [57]. Copyright 2020, the Authors, Published by MDPI

In agreement with EDS Si mapping, both GPTES and GPTES-PNPA sols wrap homogeneously and intimately the cotton fibers as observed from AFM micrographs (Figure 49). The latter evidenced a higher roughness of treated samples compared with untreated cotton, which results characterized by the typical filamentary structure of fibers on the nanoscale. Moreover, by analyzing a sample area in which there is a lack of coating, it was possible to evaluate the coating thickness in the range of 2.5 and 4 nm.

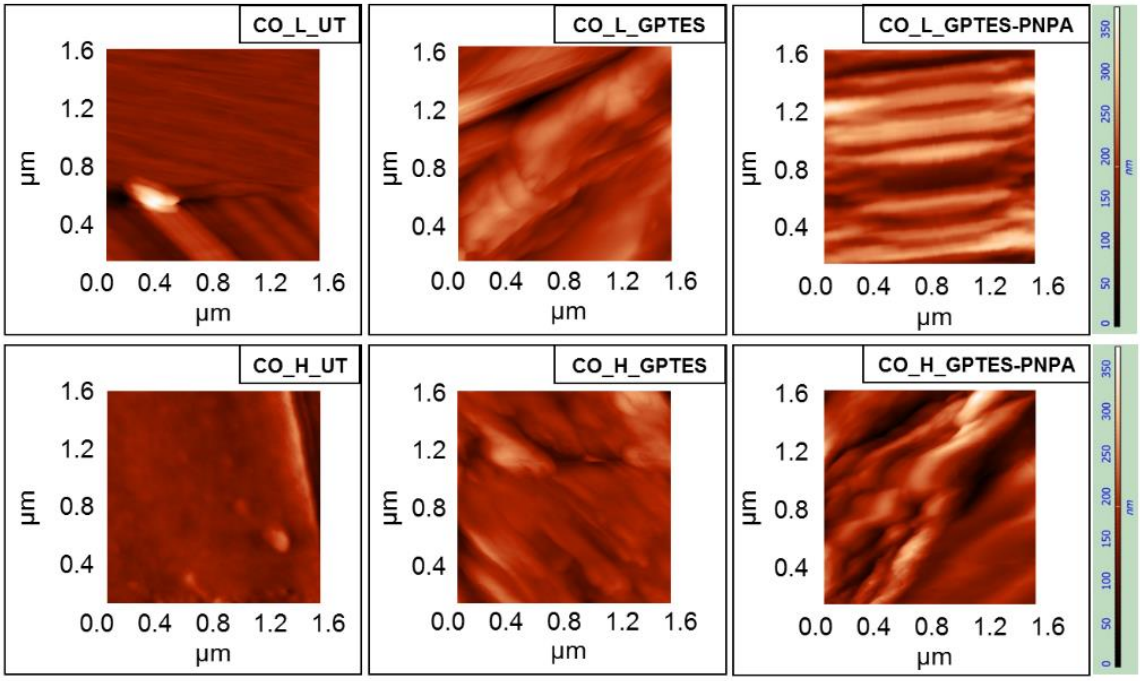

Figure 49: AFM micrographs of untreated and treated CO_L and CO_H samples. Adapted under the terms of the Creative Commons CC BY-NC-ND 4.0 license [57]. Copyright 2020, the Authors, Published by MDPI

5.2.3.5 In vitro diffusion tests

The controlled release properties of the treated cotton fabrics were assessed through in vitro diffusion studies as described in Chapter 2. With this aim, the controlled release capability of the realized PNPA network was compared with a standard solution of the molecule.

To predict the diffusion process occurring through human skin, the synthetic alternative Strat-M® membranes were used. Both CO_L_GPTES-PNPA and CO_H_GPTES-PNPA were studied, and obtained results were expressed as the cumulative diffused amount (%), and the corresponding diffusion profiles are reported in Figure 50.

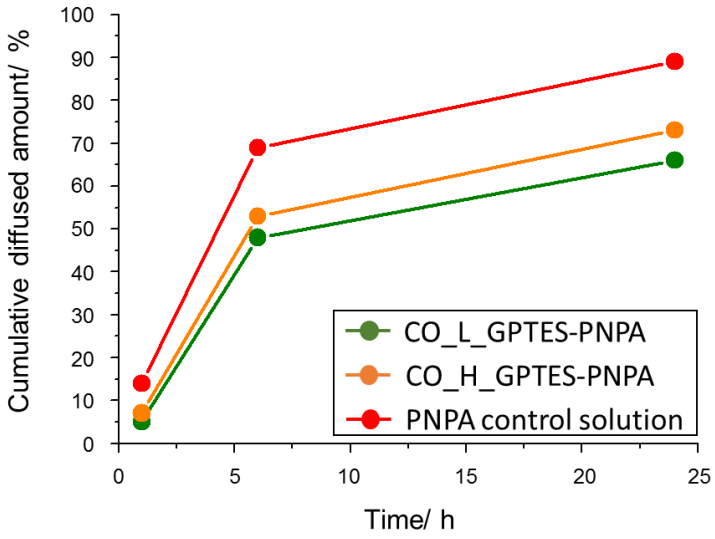

Figure 50: Cumulative diffused amount (%) data provided by both CO_L and CO_H fabrics treated with GPTES-PNPA and comparison with PNPA control solution at different times

Both samples show similar results in the in vitro diffusion tests, and diffused amount (%) of PNPA from both textiles and a control solution is reported in Table 12.

Sample	Diffused amount (%)		
	1 h	6 h	24 h
CO_L_GPTES-PNPA	5	48	66
CO_H_GPTES-PNPA	7	53	73
PNPA control solution	14	69	89

Table 12: Diffused amount (%) at a different time of PNPA drug molecule for the cotton samples treated with GPTES-PNPA sol and of a PNPA control solution

The obtained results can be compared to the rate-limiting steps in drug release reported in the literature and confirm the capability of the developed cotton textiles to release the PNPA molecule in a controlled manner [41, 64].

The controlled drug release observed in this research study is probably mainly due to the weak interaction of the PNPA molecules within the 3D sol-gel network. Depending on the presence of sweat, simulated with the buffer solution in contact with the PNPA-treated fabric, the weak interactions between the treated fabric and the anti-inflammatory/antioxidant molecule disappear, and the drug is completely released. The presence of the sol-gel matrix has increased the bonding interactions between the network and the drug, slowing down its release.

5.2.4 Conclusions

The synthesized PEA derivative, PNPA (*N*-palmitoyl-(*4*-nitro-phenyl)-amine) with known anti-inflammatory and antioxidant properties, was employed as a drug molecule to develop a GPTES-based sol-gel matrix for controlled release. The synthesis of a polyethylene oxide 3D network in which the PNPA molecule is entrapped was confirmed by NMR and FTIR spectroscopy that evidenced the GPTES epoxy ring opening and the subsequent polymerization of the PEO network. The uniform distribution of the GPTES-PNPA coating on cotton fabrics, with both high and low mass per unit area, was confirmed by SEM and AFM characterizations.

The realized treated cotton fabrics were screened for the in vitro diffusion test to evaluate the controlled release of the PNPA molecule from fabrics compared to that from a standard molecule solution. Experimental findings demonstrated the efficiency of the developed textiles in the PEA derivative release through the medium, thanks to the weak bonding of the molecule in the sol-gel matrix. Moreover, the sol-gel functionalized matrix ensures biocompatibility, PNPA reservoir and its release under the action of cutaneous stimuli and represents a suitable technique for designing a functional hybrid network for controlled drug release in biomedical application fields. Furthermore, the system could be tuned in terms of release in time or concentration depending on the patient's health conditions. With this perspective, future studies will be conducted to develop a very smart textile for biomedical applications.

References

1. Langer R (1998) Drug delivery and targeting. Nature 392:5–10
2. Brouwers JRBJ (1996) Advanced and controlled drug delivery systems in clinical disease management. Pharm World Sci 18:153–162. https://doi.org/10.1007/BF00820726
3. Uhrich KE, Cannizzaro SM, Langer RS, Shakesheff KM (1999) Polymeric Systems for Controlled Drug Release. Chem Rev 99:3181–3198. https://doi.org/10.1021/cr940351u
4. Brannon-Peppas L (1993) Controlled Release in the Food and Cosmetics Industries. pp 42–52
5. Levy R, Nichols MA, Miller TW (1993) Encapsulated Systems for Controlled Release and Pest Management. pp 202–212
6. Radu CD, Parteni O (2015) Comparative Study of a Drug Release from a Textile to Skin. J Pharm Drug Deliv Res 04: https://doi.org/10.4172/2325-9604.1000134
7. Hashemikia S, Hemmatinejad N, Ahmadi E, Montazer M (2016) A novel cotton fabric with anti-bacterial and drug delivery properties using SBA-15-NH 2 /polysiloxane hybrid containing tetracycline. Mater Sci Eng C 59:429–437. https://doi.org/10.1016/j.msec.2015.09.092
8. Ten Breteler MR, Nierstrasz VA, Warmoeskerken MMCG (2002) Textile slow-release systems with medical applications. Autex 2 (4):175–189
9. Cezar-Doru R, Marcel P, Oana P, et al (2014) Achievements and Limits on the Controlled Release of a Drug from a Textile Fabric to Dermis. Open Conf Proc J 5:1–8. https://doi.org/10.2174/2210289201405010001
10. Radu C-D, Parteni O, Ochiuz L (2016) Applications of cyclodextrins in medical textiles — review. J Control Release 224:146–157. https://doi.org/10.1016/j.jconrel.2015.12.046
11. Ielo I, Giacobello F, Sfameni S, et al (2021) Nanostructured Surface Finishing and Coatings: Functional Properties and Applications. Materials (Basel) 14:2733. https://doi.org/10.3390/ma14112733
12. Plutino MR, Colleoni C, Donelli I, et al (2017) Sol-gel 3-glycidoxypropyltriethoxysilane finishing on different fabrics: The role of precursor concentration and catalyst on the textile performances and cytotoxic activity. J Colloid Interface Sci 506:504–517. https://doi.org/10.1016/j.jcis.2017.07.048
13. Mahltig B, Haufe H, Böttcher H (2005) Functionalisation of textiles by inorganic sol–gel coatings. J Mater Chem 15:4385. https://doi.org/10.1039/b505177k

14. Poli R, Colleoni C, Calvimontes A, et al (2015) Innovative sol–gel route in neutral hydroalcoholic condition to obtain antibacterial cotton finishing by zinc precursor. J Sol-Gel Sci Technol 74:151–160. https://doi.org/10.1007/s10971-014-3589-9
15. Caldara M, Colleoni C, Guido E, et al (2012) Development of a textile-optoelectronic pH meter based on hybrid xerogel doped with Methyl Red. Sensors Actuators B Chem 171–172:1013–1021. https://doi.org/10.1016/j.snb.2012.06.024
16. Van der Schueren L, De Clerck K, Brancatelli G, et al (2012) Novel cellulose and polyamide halochromic textile sensors based on the encapsulation of Methyl Red into a sol?gel matrix. Sensors Actuators B Chem 162:27–34. https://doi.org/10.1016/j.snb.2011.11.077
17. Guido E, Colleoni C, De Clerck K, et al (2014) Influence of catalyst in the synthesis of a cellulose-based sensor: Kinetic study of 3-glycidoxypropyltrimethoxysilane epoxy ring opening by Lewis acid. Sensors Actuators B Chem 203:213–222. https://doi.org/10.1016/j.snb.2014.06.126
18. Caldara M, Colleoni C, Guido E, et al (2016) Optical monitoring of sweat pH by a textile fabric wearable sensor based on covalently bonded litmus-3-glycidoxypropyltrimethoxysilane coating. Sensors Actuators B Chem 222:213–220. https://doi.org/10.1016/j.snb.2015.08.073
19. Plutino MR, Guido E, Colleoni C, Rosace G (2017) Effect of GPTMS functionalization on the improvement of the pH-sensitive methyl red photostability. Sensors Actuators B Chem 238:281–291. https://doi.org/10.1016/j.snb.2016.07.050
20. Rosace G, Guido E, Colleoni C, et al (2017) Halochromic resorufin-GPTMS hybrid sol-gel: Chemical-physical properties and use as pH sensor fabric coating. Sensors Actuators B Chem 241:85–95. https://doi.org/10.1016/j.snb.2016.10.038
21. Trovato V, Colleoni C, Castellano A, Plutino MR (2018) The key role of 3-glycidoxypropyltrimethoxysilane sol–gel precursor in the development of wearable sensors for health monitoring. J Sol-Gel Sci Technol. https://doi.org/10.1007/s10971-018-4695-x
22. Avnir D, Coradin T, Lev O, Livage J (2006) Recent bio-applications of sol–gel materials. J Mater Chem 16:1013–1030. https://doi.org/10.1039/B512706H
23. Cardiano P (2008) Hydrophobic properties of new epoxy-silica hybrids. J Appl Polym Sci 108:3380–3387. https://doi.org/10.1002/app.27985
24. Cardiano P, Lo Schiavo S, Piraino P (2010) Hydrorepellent properties of organic–inorganic hybrid materials. J Non Cryst Solids 356:917–926. https://doi.org/10.1016/j.jnoncrysol.2009.12.025

25. Brancatelli G, Colleoni C, Massafra MR, Rosace G (2011) Effect of hybrid phosphorus-doped silica thin films produced by sol-gel method on the thermal behavior of cotton fabrics. Polym Degrad Stab 96:483–490. https://doi.org/10.1016/j.polymdegradstab.2011.01.013
26. Grancaric AM, Colleoni C, Guido E, et al (2017) Thermal behaviour and flame retardancy of monoethanolamine-doped sol-gel coatings of cotton fabric. Prog Org Coatings 103:174–181. https://doi.org/10.1016/j.porgcoat.2016.10.035
27. Petrusic S, Koncar V (2016) Controlled release of active agents from microcapsules embedded in textile structures. In: Smart Textiles and their Applications. Elsevier, pp 89–114
28. Acharya G, Park K (2006) Mechanisms of controlled drug release from drug-eluting stents. Adv Drug Deliv Rev 58:387–401. https://doi.org/10.1016/j.addr.2006.01.016
29. Wise DL (2000) Handbook of Pharmaceutical Controlled Release Technology. CRC Press
30. Peppas N (2000) Hydrogels in pharmaceutical formulations. Eur J Pharm Biopharm 50:27–46. https://doi.org/10.1016/S0939-6411(00)00090-4
31. Galaev I, Mattiasson B Smart Polymers - Applications in Biotechnology and Biomedicine, Second. CRC Press Taylor & Francis Group
32. Teutonico D, Ponchel G (2011) Patches for improving gastrointestinal absorption: an overview. Drug Discov Today 16:991–997. https://doi.org/10.1016/j.drudis.2011.05.013
33. Nierstrasz VA (2007) Textile-based drug release systems. In: Van Langenhove L (Ed. . (ed) Smart Textiles for Medicine and Healthcare: Materials, Systems and Applications. S. Woodhead Publishing Ltd., Cambridge, p 67
34. Zhu L-M, Yu DG (2013) Drug delivery systems using biotextiles. In: Biotextiles as Medical Implants. Elsevier, pp 213–231
35. Zilberman M (2007) Novel composite fiber structures to provide drug/protein delivery for medical implants and tissue regeneration. Acta Biomater 3:51–57. https://doi.org/10.1016/j.actbio.2006.06.008
36. Singh MN, Hemant KS., Ram M, Shivakumar HG (2010) Microencapsulation:a promising technique for controlled drug delivery. Res Pharm Sci 5 (2):65–77
37. Liu J, Liu C, Liu Y, et al (2013) Study on the grafting of chitosan–gelatin microcapsules onto cotton fabrics and its antibacterial effect. Colloids Surfaces B Biointerfaces 109:103–108. https://doi.org/10.1016/j.colsurfb.2013.03.040
38. Alonso D, Gimeno M, Sepúlveda-Sánchez JD, Shirai K (2010) Chitosan-based microcapsules containing grapefruit seed extract grafted onto cellulose fibers by a non-toxic procedure. Carbohydr Res 345:854–859. https://doi.org/10.1016/j.carres.2010.01.018

39. Anitha R, Ramachandran T, Rajendran R, Mahalakshmi M (2011) Microencapsulation of lemon grass oil for mosquito repellent finishes in polyester textiles. Elixir Bio Phys 40:5196–5200
40. Jaâfar F, Lassoued MA, Sahnoun M, et al (2012) Impregnation of ethylcellulose microcapsules containing jojoba oil onto compressive knits developed for high burns. Fibers Polym 13:346–351. https://doi.org/10.1007/s12221-012-0346-y
41. Ma Z-H, Yu D-G, Branford-White CJ, et al (2009) Microencapsulation of tamoxifen: Application to cotton fabric. Colloids Surfaces B Biointerfaces 69:85–90. https://doi.org/10.1016/j.colsurfb.2008.11.005
42. Monllor P, Bonet MA, Cases F (2007) Characterization of the behaviour of flavour microcapsules in cotton fabrics. Eur Polym J 43:2481–2490. https://doi.org/10.1016/j.eurpolymj.2007.04.004
43. Badulescu R, Vivod V, Jausovec D, Voncina B (2008) Grafting of ethylcellulose microcapsules onto cotton fibers. Carbohydr Polym 71:85–91. https://doi.org/10.1016/j.carbpol.2007.05.028
44. Fei X, Zhao H, Zhang B, et al (2015) Microencapsulation mechanism and size control of fragrance microcapsules with melamine resin shell. Colloids Surfaces A Physicochem Eng Asp 469:300–306. https://doi.org/10.1016/j.colsurfa.2015.01.033
45. Mohsin M, Farooq U, Iqbal T, Akram M (2014) Impact of high and zero formaldehyde crosslinkers on the performance of the dyed cotton fabric. Chem Ind Chem Eng Q 20:353–360
46. Chatterjee S, Salaün F, Campagne C (2014) Development of Multilayer Microcapsules by a Phase Coacervation Method Based on Ionic Interactions for Textile Applications. Pharmaceutics 6:281–297. https://doi.org/10.3390/pharmaceutics6020281
47. Salaün F, Vroman I, Elmajid I (2012) A novel approach to synthesize and to fix microparticles on cotton fabric. Chem Eng J 213:78–87. https://doi.org/10.1016/j.cej.2012.09.062
48. Loftsson T, Duchene D (2007) Cyclodextrins and their pharmaceutical applications. Int J Pharm 329:1–11. https://doi.org/10.1016/j.ijpharm.2006.10.044
49. Yu H, Jia Y, Yao C, Lu Y (2014) PCL/PEG core/sheath fibers with controlled drug release rate fabricated on the basis of a novel combined technique. Int J Pharm 469:17–22. https://doi.org/10.1016/j.ijpharm.2014.04.045

50. Xiao Z, Liu W, Zhu G, et al (2014) A review of the preparation and application of flavour and essential oils microcapsules based on complex coacervation technology. J Sci Food Agric 94:1482–1494. https://doi.org/10.1002/jsfa.6491
51. Holme I (2007) Innovative technologies for high performance textiles. Color Technol 123:59–73. https://doi.org/10.1111/j.1478-4408.2007.00064.x
52. Nelson G (2002) Application of microencapsulation in textiles. Int J Pharm 242:55–62. https://doi.org/10.1016/S0378-5173(02)00141-2
53. Peña B, Panisello C, Aresté G, et al (2012) Preparation and characterization of polysulfone microcapsules for perfume release. Chem Eng J 179:394–403. https://doi.org/10.1016/j.cej.2011.10.090
54. Hu J, Xiao Z, Zhou R, et al (2011) Properties of Aroma Sustained-release Cotton Fabric with Rose Fragrance Nanocapsule. Chinese J Chem Eng 19:523–528. https://doi.org/10.1016/S1004-9541(11)60016-5
55. Van Langenhove L, Paul R (2014) Insect repellent finishes for textiles. In: Paul R (ed) Functional Finishes for Textiles: Improving Comfort, Performance and Protection. Elsevier, Cambridge, pp 333–360
56. Saturnino C, Popolo A, Ramunno A, et al (2017) Anti-Inflammatory, Antioxidant and Crystallographic Studies of N-Palmitoyl-ethanol Amine (PEA) Derivatives. Molecules 22:616. https://doi.org/10.3390/molecules22040616
57. Puoci F, Saturnino C, Trovato V, et al (2020) Sol–Gel Treatment of Textiles for the Entrapping of an Antioxidant/Anti-Inflammatory Molecule: Functional Coating Morphological Characterization and Drug Release Evaluation. Appl Sci 10:2287. https://doi.org/10.3390/app10072287
58. Darmani NA, Izzo AA, Degenhardt B, et al (2005) Involvement of the cannabimimetic compound, N-palmitoyl-ethanolamine, in inflammatory and neuropathic conditions: Review of the available pre-clinical data, and first human studies. Neuropharmacology 48:1154–1163. https://doi.org/10.1016/j.neuropharm.2005.01.001
59. Petrosino S, Iuvone T, Di Marzo V (2010) N-palmitoyl-ethanolamine: Biochemistry and new therapeutic opportunities. Biochimie 92:724–727. https://doi.org/10.1016/j.biochi.2010.01.006
60. Mattace Raso G, Russo R, Calignano A, Meli R (2014) Palmitoylethanolamide in CNS health and disease. Pharmacol Res 86:32–41. https://doi.org/10.1016/j.phrs.2014.05.006

61. Lambert D, Vandevoorde S, Jonsson K-O, Fowler C (2002) The Palmitoylethanolamide Family: A New Class of Anti-Inflammatory Agents ? Curr Med Chem 9:663–674. https://doi.org/10.2174/0929867023370707
62. Peng Y-D, Wang F, Gao L, Dong W-K (2018) Structurally characterized dinuclear zinc(II) bis(salamo)-type tetraoxime complex possessing square pyramidal and trigonal bipyramidal geometries. J Chinese Chem Soc. https://doi.org/10.1002/jccs.201800038
63. Chung C, Lee M, Choe E (2004) Characterization of cotton fabric scouring by FT-IR ATR spectroscopy. Carbohydr Polym 58:417–420. https://doi.org/10.1016/j.carbpol.2004.08.005
64. Messaritaki A, Black SJ, van der Walle CF, Rigby SP (2005) NMR and confocal microscopy studies of the mechanisms of burst drug release from PLGA microspheres. J Control Release 108:271–281. https://doi.org/10.1016/j.jconrel.2005.08.010

Conclusions and future perspectives

In recent years, textile fibers and fabrics have aroused great interest as substrates for the design of advanced materials with innovative properties besides the conventional ones of textiles. The unique characteristics of textile fabrics and their structure provide a useful and commonly available starting point for the realization of miniaturizing sensors characterized by lightweight, flexibility, stretchability, wearability, breathability, biocompatibility (when employed natural fibers or fabrics), and re-use thanks to the possibility to be washed. Moreover, the growing interest in real-time monitoring of both environmental parameters but especially those related to human health, as well as the synergistic approach of different scientific disciplines, including nanotechnology and textile engineering, has contributed to the development of this new class of sensors, smart textiles. These are defined as smart fabrics capable of actions such as sensing, calculation, and communication.

Initially, smart textiles were used in very limited areas, but after scientific efforts and development, nowadays, they are of great social and scientific interest and are considered as the future of the textile industry.

Thanks to scientific research, conventional textiles have been integrated with electronic components to produce wearable diagnostics and therapeutic systems to monitor physiological parameters for both medical and protective textile-based applications such as for the simultaneous detection of volatile organic compounds (VOCs), gas, temperature, pH, ions, and much more. The combination of fabrics and microelectronics also allows innovative applications in continuous evolution, which use fabrics often based on conductive fibers as the main element. Many examples of smart textiles concern the design and development of coating nanomaterials, consisting of micro- and nano-sized thin films, for textile polymers and the integration of microelectronic components in fabrics. In this regard, several chemical substances, able to sense and react to specific analytes, are nowadays available. On the other side, the miniaturization and flexibility of the electronic systems integrated into fabrics are fundamental to guarantee smart textiles operation even in conditions of wear. Through the available technologies, it is possible to integrate electroconductive or stimuli-responsive coatings in textiles, thus obtaining advanced functionalities. In this thesis, electroconductive and halochromic coatings have been introduced in cotton textiles according to sol-gel and grafting polymerization, thus providing stable and durable smart textiles materials for both environmental and medical applications. The unique properties of the sol-gel matrix, among which its biocompatibility, make such technology attractive and suitable also for the development of controlled release systems of drug molecules from

textiles realized through the stable immobilization of antioxidant/anti-inflammatory molecules into the 3D silica network.

Electrically conductive coatings for environmental monitoring were realized by dispersing carbon nanotubes (CNTs) into a polymeric matrix, thus resulting in their good homogeneity distribution and alignment. These features ensure the conductive properties of the obtained coatings, thanks to which it is possible to detect concomitant variations of environmental humidity and temperature levels through electrical resistance changes of the coating itself. Moreover, the flexibility showed by the CNT-coating allows their interesting application for textiles fields and their employment as flexible, adaptable material in innovative wearable sensors.

By employing carbon nanotubes with a high aspect ratio, conductive textiles through the sol-gel technique were developed for heart rate monitoring. Indeed, sol-gel precursors contribute to the dispersion of conductive particles, such as carbon nanotubes, and the coating adhesion on textiles. The coated cotton fabrics seem not to be affected significantly by the presence of the CNT-based sol-gel coatings in terms of comfortability. Coated textiles were found to make the transmission of biomedical data reliable and efficient for the development of wearable smart textiles for sports, healthcare, and military applications, also due to their properties consisting of comfort and non-invasive compared to the conventional conductive systems in long-term monitoring applications.

Among the stimuli-responsive coatings, halochromic textiles have been developed aimed at the colorimetric detection of sweat pH variation to assess the health status of the human body. Controlled release textiles have also been realized to control the release from textiles of an antioxidant/anti-inflammatory molecule under cutaneous stimuli.

Two halochromic molecules, nitrazine yellow and alizarin red S, were covalently functionalized by epoxy ring-opening of specific precursors (glycidyl methacrylate (GMA) and *3*-glycidoxypropyltrimethoxysilane (GPTMS), respectively), and the resulting modified-dyestuffs were immobilized on cotton textiles through grafting polymerization and sol-gel process, respectively. UV-Vis spectroscopic characterizations of buffer solutions containing the functionalized dyestuffs confirmed the typical pH-response of both pure dyes at different pH, although the changes in their chromophore surroundings due to the covalent functionalization. UV-Vis diffuse reflectance spectroscopy and CIELAB color space highlighted the pH-response of the treated cotton fabrics even after washing cycles, thus confirming the efficacy of both the grafting of nitrazine yellow and sol-gel immobilization of alizarin red S on textile substrates compared to conventional dyeing techniques. In particular, all experimental findings confirmed the reversibility and the reliability of the grafted nitrazine yellow wearable sensor to pH changes even after 4 exposure cycles. The research studies

highlight the advantages of covalent immobilization of a halochromic dye, nitrazine yellow and alizarin red S, specifically chosen for their color change in the pH scale of the human sweat according to grafting or sol-gel approaches. The main advantages of these techniques consist of the reduced dye leaching consequently to laundering cycles and the immobilization of the dye without the loss of its halochromic response, compared to conventional dyeing techniques. The development of halochromic wearable sensors provides several advantages in healthcare, medicine, fitness, and diagnostic fields. The relevant aspects of these wearable sensors consist of their potential for real-time and continuous monitoring of patients' physiological conditions.

The sol-gel approach allows developing a porous 3D silica matrix in which cavities, an antioxidant/anti-inflammatory molecule (*N*-palmitoyl-(*4*-nitro-phenyl)-amine (PNPA)) was successfully and stably entrapped for the controlled release from textiles.

The sol-gel functionalized matrix ensures biocompatibility, PNPA reservoir, and its release under the action of cutaneous stimuli and represents a suitable technique for the design of functional hybrid networks for controlled drug release in biomedical application fields.

With the sol-gel approach, it is possible to obtain organic-inorganic hybrid thin films doped with halochromic molecules, active molecules, or carbon nanotubes and efficiently adhered to the cotton surfaces.

Thanks to the obtained results, two prototypes have been developed, "ELECT" and "Health Belt". The former is a T-shirt realized by the deposition of CNT-electroconductive tracks integrated with an electronic device for the monitoring of heart rate rhythm through electrocardiogram. The latter, a belt realized through a halochromic textile integrated with an electronic device for the monitoring of sweat pH.

The reported studies are a step forward for the integration between electronics and textile materials by real application processes, industrially scalable, usable for the development of high-performance wearable e-textiles.

Despite their innovation and the added value lead by smart textiles to daily life, several challenging aspects be still addressed, some of them consisting of the lack of standards and cost of fabrication. Moreover, mechanical and electrical connections should be washable and resistant to water, torsion, bending, and all types of typical body deformations, as well as new materials, should be the result of innovation in technology manufactory.

Smart textile applications greatly performant can be reached thanks to the development of a future generation of electrically conductive and stimuli-responsive coatings. An important challenge will be the total integration of electronics in the textile structure mainly focused on advanced fields, such as

wound monitoring and healing as well as in surgery. The continuous evolution of scientific research with a multidisciplinary approach will allow increasing advantages to the smart textile sector, thus obtaining greater innovative, intelligent materials able to satisfy the main requirements of the end-user in the most common application fields related to health, sport, fitness (health monitoring, clinical applications, sportswear), safety (workwear), and automotive.

Appendix 1

List of abbreviations

AFM	Atomic Force Microscopy
ARS	Alizarin Red S
ATR - FTIR	Attenuated Total Reflection Fourier Transform Infrared spectroscopy
BF_3OEt_2	Boron trifluoride diethyl etherate
BTCA	*1,2,3,4*-butanetetracarboxylic acid
CNTs	Carbon Nanotubes
EDAES	N-[*3*-(triethoxysilyl)propyl]ethylenediamine
EDS	Energy Dispersive X-ray Spectroscopy
F_{dye}	Dye Fixation ratio
F-MWCNTs	Functionalized Multiwalled Carbon Nanotubes
GMA	Glycidyl methacrylate
GPTES	(*3*-Glycidyloxypropyl)triethoxysilane
GPTMS	(*3*-Glycidyloxypropyl)trimethoxysilane
HCl	Hydrochloric acid
HRSEM	High-Resolution Scanning Electron Microscopy
HRTEM	High-Resolution Transmission Electron Microscopy
K-M	Kubelka Munk
KPS	Potassium persulfate
l-CNTs	Long Carbon Nanotubes
MWCNTs	Multiwalled Carbon Nanotubes
NMR	Nuclear Magnetic Resonance
NY	Nitrazine Yellow
P-MWCNTs	Pristine Multiwalled Carbon Nanotubes
PNPA	*N*-palmitoyl-(*4*-nitro-phenyl)-amine
PPG	Photoplethysmography
PVA	Poly(vinyl alcohol)
Rs	Surface Resistance
s-CNTs	Short Carbon Nanotubes
SHP	Sodium hypophosphite monohydrate
SEM	Scanning Electron Microscopy

TEM	Transmission Electron Microscopy
UV-Vis	Ultraviolet - Visible spectroscopy
VACNTs	Vertical Aligned Carbon Nanotubes
WLW	Weight Loss after Washing cycles
XPS	X-ray Photoelectron spectroscopy

Appendix 2

List of Peer-Reviewed publications

- Ielo, F. Giacobello, S. Sfameni, G. Rando, M. Galletta, V. Trovato, G. Rosace, M.R. Plutino, Nanostructured Surface Finishing and Coatings: Functional Properties and Applications, Materials (Basel). 14 (2021) 2733. doi:10.3390/ma14112733.
- V. Trovato, A. Vitale, R. Bongiovanni, A. Ferri, G. Rosace, M.R. Plutino, Development of a Nitrazine Yellow-glycidyl methacrylate coating onto cotton fabric through thermal-induced radical polymerization reactions: a simple approach towards wearable pH sensors applications, Cellulose. (2021). doi:10.1007/s10570-021-03733-w.
- V. Trovato, E. Teblum, Y. Kostikov, A. Pedrana, V. Re, G.D. Nessim, G. Rosace, Electrically conductive cotton fabric coatings developed by silica sol-gel precursors doped with surfactant-aided dispersion of vertically aligned carbon nanotubes fillers in organic solvent-free aqueous solution, J. Colloid Interface Sci. 586 (2021) 120–134. doi:10.1016/j.jcis.2020.10.076.
- P. Kianfar, M.T. Abate, V. Trovato, G. Rosace, A. Ferri, R. Bongiovanni, A. Vitale, Surface Functionalization of Cotton Fabrics by Photo-Grafting for pH Sensing Applications, Front. Mater. 7 (2020). doi:10.3389/fmats.2020.00039.
- F. Puoci, C. Saturnino, V. Trovato, D. Iacopetta, E. Piperopoulos, C. Triolo, M.G. Bonomo, D. Drommi, O.I. Parisi, C. Milone, M.S. Sinicropi, G. Rosace, M.R. Plutino, Sol–Gel Treatment of Textiles for the Entrapping of an Antioxidant/Anti-Inflammatory Molecule: Functional Coating Morphological Characterization and Drug Release Evaluation, Appl. Sci. 10 (2020) 2287. doi:10.3390/app10072287.
- V. Trovato, E. Teblum, Y. Kostikov, A. Pedrana, V. Re, G.D. Nessim, G. Rosace, Sol-gel approach to incorporate millimeter-long carbon nanotubes into fabrics for the development of electrical-conductive textiles, Mater. Chem. Phys. 240 (2020) 122218. doi:10.1016/j.matchemphys.2019.122218.
- G. De Luca, P. Bonaccorsi, V. Trovato, A. Mancuso, T. Papalia, A. Pistone, M.P. Casaletto, A. Mezzi, B. Brunetti, L. Minuti, A. Temperini, A. Barattucci, M.R. Plutino, Tripodal tris-disulfides as capping agents for a controlled mixed functionalization of gold nanoparticles, New J. Chem. 42 (2018) 16436–16440. doi:10.1039/C8NJ03086C.
- V. Trovato, C. Colleoni, A. Castellano, M.R. Plutino, The key role of 3-glycidoxypropyltrimethoxysilane sol–gel precursor in the development of wearable sensors for health monitoring, J. Sol-Gel Sci. Technol. (2018). doi:10.1007/s10971-018-4695-x.

- G. Rosace, A. Castellano, V. Trovato, G. Iacono, G. Malucelli, Thermal and flame retardant behaviour of cotton fabrics treated with a novel nitrogen-containing carboxyl-functionalized organophosphorus system, Carbohydr. Polym. 196 (2018) 348–358. doi:10.1016/j.carbpol.2018.05.012.
- G. Rosace, V. Trovato, C. Colleoni, M. Caldara, V. Re, M. Brucale, E. Piperopoulos, E. Mastronardo, C. Milone, G. De Luca, M.R. Plutino, Structural and morphological characterizations of MWCNTs hybrid coating onto cotton fabric as potential humidity and temperature wearable sensor, Sensors Actuators B Chem. 252 (2017) 428–439. doi:10.1016/j.snb.2017.05.175.
- G. Rosace, C. Colleoni, V. Trovato, G. Iacono, G. Malucelli, Vinylphosphonic acid/methacrylamide system as a durable intumescent flame retardant for cotton fabric, Cellulose. 24 (2017) 3095–3108. doi:10.1007/s10570-017-1294-x.

List of figures

List of tables

List of schemes